SENSOR MANAGEMENT FOR SURVEILLANCE AND TRACKING

AN OPERATIONAL PERSPECTIVE

SENSOR MANAGEMENT FOR SURVEILLANCE AND TRACKING

AN OPERATIONAL PERSPECTIVE

Proefschrift

ter verkrijging van de graad van doctor
aan de Technische Universiteit Delft,
op gezag van de Rector Magnificus prof. ir. K. C. A. M. Luyben,
voorzitter van het College voor Promoties,
in het openbaar te verdedigen op 5 maart 2015 om 12:30 uur

door

Fotios KATSILIERIS

Master of Science of Kungliga Tekniska Högskolan, Sweden
geboren te Amarousio, Attica, Griekenland.

Dit proefschrift is goedgekeurd door de promotor:

Prof. DSc. A. Yarovoy

Copromotor: Dr. ir. J. N. Driessen

Samenstelling promotiecommissie:

Rector Magnificus,	voorzitter
Prof. DSc. A. Yarovoy,	Technische Universiteit Delft, promotor
Dr. ir. J. N. Driessen,	Thales Nederland B.V., copromotor
Prof. F. Le Chevalier,	Technische Universiteit Delft
Prof. G. Leus,	Technische Universiteit Delft
Prof. H. Blom,	Technische Universiteit Delft
Dr. W. Koch,	Fraunhofer FKIE

The research described in Chapters 1 through (part of) 3 was undertaken at Thales Nederland B.V. in partnership with the department of Applied Mathematics, Faculty of Electrical Engineering, Mathematics and Computer Science, University of Twente. This research work was carried out in the MC IMPULSE project: https://mcimpulse.isy.liu.se. Funding for this research project was provided by the EU's Seventh Framework Program under grant agreement n° 238710.

The research described in Chapters 3 through 5 was undertaken at the Microwave Sensing, Signals and Systems (MS3) group, department of Microelectronics, Faculty of Electrical Engineering, Mathematics and Computer Science, Delft University of Technology. This research was conducted as part of the Sensor Technology Applied in Reconfigurable systems for sustainable Security (STARS) project. For further information: www.starsproject.nl.

Keywords: Sensor management, resource allocation, radar beam-pointing, threat assessment, area surveillance

Typeset with: LaTeX, TU Delft dissertation template
Printed by: Ipskamp Drukkers
Front cover: Patrouille Acrobatique de France at Luchtmachtdagen 2013, photo by F. Katsilieris.

ISBN 978-94-6186-429-1

An electronic version of this dissertation is available at
http://repository.tudelft.nl/.

To my family, friends,
and all the countries that have welcomed me.

ACKNOWLEDGEMENTS

The first acknowledgements go to my daily supervisors at Thales Nederland B.V.: Dr. Hans Driessen and Dr. Yvo Boers. Their advice and support during the last four years are immensely appreciated. Furthermore, I would like to thank my academic supervisors at the Delft Institute of Technology and the University of Twente: Prof. Alexander Yarovoy and Prof. Arun Bagchi. Your comments and suggestions for improving my academic work and writing have had a major impact on this thesis.

Except for my formal supervisors, I thank Dr. Martin Podt, Dr. Pranab Mandal, Dr. Oleg Krasnov and Dr. Victor Paashuis for the discussions that we had and for their support.

I would like to thank the members of my defense committee: Prof. François Le Chevalier, Prof. Geert Leus, Prof. Henk Blom, Dr. Wolfgang Koch, and Prof. ir. K. C. A. M. Luyben for their reviews, comments and suggestions for improving my dissertation.

In the last four years I have made lots of new friends, especially as a member of the MC IMPULSE project. I have had a great time working, discussing, and traveling in several countries and continents with Dr. Edson Aoki, Dr. Mélanie Bocquel, Dr. Francesco Papi, Dr. Nikolay Petrov, Marek Syldatk, and Katerina Tzavela. Similarly, I would like to thank my friends and office-mates at TU Delft: Dr. Teun de Groot, Alexey Narykov and Dr. Shenario Valavan who made my experience at TU Delft even better.

My quality of life while away from Greece has been immensely improved due to the new friends that I made while living in Hengelo. Jonathan, Patrick S., Óscar, Nuno, Kiri, Anne-Marie, Patrick M., Grégoire, Anton, Nelson, Pierre-Olivier, and Germain thank you for your friendship and the time that we spent together in and out of the Netherlands.

I would like to thank my housemates at Delft: Silvan, Remko and Bastiaan. Not only have I had a great time living with you but you have also helped me improve my Dutch language skills. Furthermore, I would like to thank the Delft Fencing Club for helping me stay healthy and keep my mind sharp.

A special acknowledgement goes to Dr. Alexander Charlish and Dr. Paolo Braca. You were both great hosts during my research visits and I have learned a lot from you.

On a personal note, I would like to thank my family and my friends in Greece for their constant support and encouragement in pursuing this PhD. Without your support I would have never made this step.

Last but not least, I would like to thank Dr. Maaike Beliën for her advice on writing this dissertation and Minke van der Put for making sure that people of the MS3 group only have to worry about their academic work.

The first part of this research work was carried out in the MC IMPULSE project: https://mcimpulse.isy.liu.se. Funding for this research project was provided by the EU's Seventh Framework Program under grant agreement n° 238710. The second part of this research work was conducted as part of the Sensor Technology Applied in Reconfigurable systems for sustainable Security (STARS) project. For further information: www.starsproject.nl.

Fotios Katsilieris
Delft, March 2015

CONTENTS

LIST OF FIGURES

List of Tables

List of Acronyms

(C)PHD (Cardinalized) Probability Hypothesis Density

AIS Automatic Identification System

C-LRT Clairvoyant Likelihood Ratio Test

CB-MeMBer Cardinality-Balanced Multi-target Multi-Bernoulli

CDAPS Continuous Double Auction Parameter Selection

CPA Closest Point of Approach

CPHD Cardinalized Probability Hypothesis Density

DTD *"Detected Targets"* Density

Fraunhofer FKIE Fraunhofer-Institut fur Kommunikation, Informationsverarbeitung und Ergonomie

G-LRT Generalized Likelihood Ratio Test

JDL Joint Directors of Laboratories

JoM Joint Multitarget

JPDA Joint Probabilistic Data Association

k-NN *k*th Nearest Neighbour

KLD Kullback-Leibler Divergence

LRT Likelihood Ratio Test

MaM Marginal Multi-target

MAP Maximum A Posteriori

MFR Multi-Function Radar

MHT Multiple Hypothesis Tracking

NATO-STO CMRE NATO-STO Centre for Maritime Research and Experimentation

OLFC Open Loop Feedback Control

OODA Object, Orient, Decide and Act

OSPA Optimal Sub-Pattern Assignment

PCR Pulse Compression Ratio [%]

PDF Probability Density Function

PENT Posterior Expected Number of Targets

PENTI Posterior Expected Number of Targets of Interest

PHD Probability Hypothesis Density

POMDP Partially Observed Markov Decision Processes

PRF Pulse Repetition Frequency

RCS Radar Cross-Section

RFS Random Finite Set

ROC Receiver Operating Characteristic

SIR Sampling Importance Resampling

SLRT Sequential Likelihood Ratio Test

SMC Sequential Monte Carlo

SNR Signal-to-Noise Ratio

unDTD *"undetected Targets"* Density

1

INTRODUCTION

1.1. THE SENSOR MANAGEMENT PROBLEM IN THE RADAR DOMAIN

Since their conception, radars have gained increased popularity as sensing devices due to their unique sensing capabilities. Radars can be used for detecting and classifying objects of interest, also called targets, at very long distances, during day or night and without being severely limited by weather conditions. Moreover, radars can measure (directly or indirectly) several attributes of targets, such as their Radar Cross-Section (RCS) and Doppler spectrum of the reflected (scattered) signal. The specific problem of using (radar) measurements sequentially for estimating the state of a moving target is called *target tracking*, see [Bar-Shalom and Li, 1995, Ch. 1]. Typical examples where radars are used can be found in several domains, both civilian and military. Air-traffic-control radars are used for preventing collisions between aircrafts, weather-radars for observing clouds and tornadoes, and fire-control radars for guiding missiles.

Advances in technology have led to incredible improvements in the measurement performance of radars. It is now possible not only to have better detection statistics and measurement accuracy but also to choose the sensing parameters of a radar in order to further improve its performance. For instance, the parameters of the transmitted waveform can be optimized online. Such controllable parameters are the waveforms' bandwidth, Pulse Repetition Frequency (PRF) and carrier frequency among others. Especially in the class of radars that employ active phased array technology, the radar-beam direction can also be controlled, see Skolnik [2002]. The beam was controlled almost always in the early days mechanically but now this can be done electrically.

Active phased array technology is most commonly employed in Multi-Function Radars (MFRs) along with digital waveform generators. These two key components give MFRs significant advantages over conventional, rotating radars with horn-fed reflector antennas. Most notably, MFRs can be used for performing several tasks, such as *a*) *searching* for targets that have not yet been detected; *b*) *tracking* the detected ones; *c*) guiding missiles or fire control; and *d*) various communication functions, instead of using a dedicated sensor per task. These tasks are integral to the operation of most radar systems

1

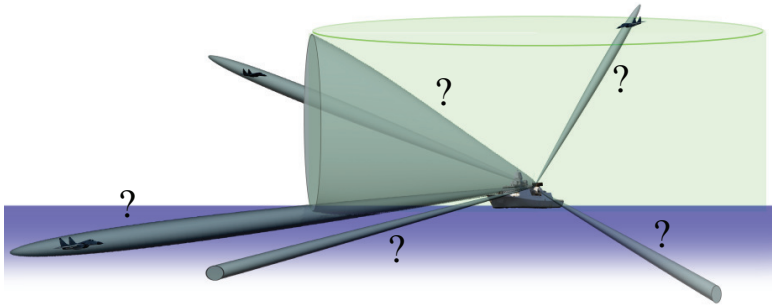

Figure 1.1: The radar beam pointing problem. Which target should be observed and when should it be observed? Where and when should the radar search for targets that have not been detected yet? Image courtesy of Christian Wolff, http://www.radartutorial.eu/.

and are all competing for the limited resources of an MFR, i.e. time and energy. This problem is illustrated in Figure 1.1.

The capabilities of MFRs can be exploited via the development of adaptive strategies for finding the best task to be performed and the best task-related parameters at each time instance. The challenge of choosing the best task and its corresponding parameters at each time instance is commonly known as the *sensor management* or *resource allocation* problem.

In sensor management, sensor parameters are controlled adaptively such that the performance of a system is improved in some sense, as compared to using fixed parameters or naive (non-adaptive) methods. Lower power consumption and better estimation performance are the two most common goals of sensor management in literature. Sensor management is present in several domains, as diverse as radars, wireless sensor networks, medical applications and robotics. An overview can be found in Hero and Cochran [2011] for example.

The control of sensing tasks, such as searching for and tracking of targets, and the estimation of target quantities, such as position and velocity, via the received measurements are independent problems but closely coupled in a radar system. In this case, sensor management can be seen as the component that closes the control loop in the estimation process, see the discussion in Hero and Cochran [2011]. This can also be seen in Fig. 1.2, where a block diagram of a generic estimation process is shown. In practice, a user can also intervene in the sensor management process by selecting different options or parameters depending on the operational context for instance. Intelligent sensor control can lead to improved estimation results whereas bad sensor control can exacerbate the estimation performance. As a result, sensor management algorithms are of paramount importance in processes such as target detection, tracking and classification.

Even though several approaches to sensor management have been proposed, for example in Blackman and Popoli [1999]; Yang et al. [2012]; Kalandros [2002]; Manyika and Durrant-Whyte [1995]; Mahler [2003]; Kreucher et al. [2005a]; Boers et al. [2010]; Katsilieris et al. [2012a]; Charlish et al. [2011]; Bolderheij et al. [2005]; Papageorgiou and Raykin [2007], many challenges have not been addressed yet, see Castañón et al. [2006].

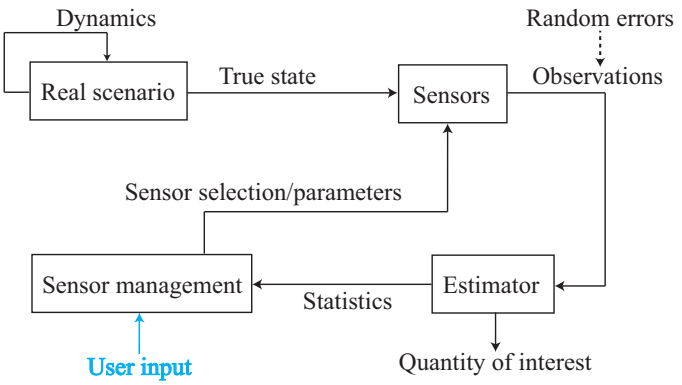

Figure 1.2: Block diagram of an estimation process. Sensors observe a real scenario and a signal processing algorithm uses the received measurements for estimating the quantities of interest. Sensor management can be used for controlling the sensor(s) parameters and improving the estimation results. Original image courtesy of Dr. Edson Hiroshi Aoki with the addition of "User input".

Some prominent questions that are still open are *a*) The management of sensors with multiple operational modes/functions. Which function/mode of such a sensor should be used at each time instance for accomplishing its task(s)? A prominent example of such sensor are the MFRs. *b*) The management of multiple sensors. How can sensors with overlapping field of view be optimally managed? Is it better to observe each target by one or multiple sensors? Can the management algorithms be implemented in a decentralized fashion while still attaining good performance? What is the best way to combine/fuse measurements from several sensors? *c*) Optimizing myopically or over long horizons? For how long horizons does it make sense to optimize the sensing actions? Can the computational complexity of non-myopic optimization be reduced without significant performance loss? *d*) The definition of objective functions. How can we describe mathematically what a user really wants to achieve? How can we take into account several non-commensurate performance metrics; *e*) Taking into account the operational context. How can a sensor be controlled such that a mission is accomplished successfully? This is closely related to the previous point and implies that, for succeeding in a mission, optimizing the probability of detection (for instance) might not be the best strategy. Furthermore, different objective functions might be better suited to different missions or operational contexts.

Especially in the radar domain, when considering MFRs - as in this thesis, the context-adaptive trade-off among different tasks to be performed is of special importance, see Castañón et al. [2006]. Among all these tasks, two sensing tasks receive most attention, i.e. *a*) *searching* for targets that have not yet been detected; and *b*) *tracking* the detected ones. Accordingly, an important open question is the definition of objective functions that take into account non-commensurate performance metrics and that address explicitly the operational goal of a radar system. For example, how can the probability of detecting a target be aggregated with a measure of tracking accuracy? And how do these relate to the situation awareness of a radar operator in different operational contexts? Thus the aim of this dissertation is *to investigate how the limited radar resources can be*

1

distributed among the different radar sensing tasks in a Bayes-optimal way, taking into account the operational goal of the radar system.

1.2. OVERVIEW OF EXISTING SENSOR MANAGEMENT APPROACHES

1.2.1. HEURISTICS

The early approaches to balancing search and tracking were *rule-based*, also called *heuristics*. Heuristics refer to a set of rules (or ad-hoc adjustments to an otherwise optimal result) that dictate the behavior of a sensor/resource manager. For several years, heuristics have been the workhorse of sensor management, also in radar systems, as discussed in Blackman and Popoli [1999].

A set of rules is created and tuned such that a sensor demonstrates the desired performance. These rules are usually dictated by the operational context and the operational needs of the sensor itself. For example, when using an MFR, a maximum revisit interval per target can be defined such that the track uncertainty does not exceed a specified threshold. This serves two purposes, the track uncertainty stays bounded such that *a*) a user can rely on it; and *b*) the radar beam can be pointed to a target without needing to re-acquire it. An example from the radar domain where different sensing tasks are scheduled using rules can be found in Butler [1998].

Rules can also be defined after observing the behavior of an objective function. These rules try to imitate the behavior of an objective function and they select the sensing action to be performed at a much lower computational cost than optimizing an objective function. Examples of such rule definitions can be found in Charlish et al. [2012] and also in this thesis.

Finally, heuristics also refer to manually adjusting an otherwise Bayes-optimal result by allowing a user to interfere with it. Such examples can be found in Romero and Goodman [2013] and White et al. [2008], where the end-result of the optimization process can be adjusted by means of a scaling factor. Moreover, if such an approach is followed, the system might end up offering several scaling factors that an end-user can set, e.g. a different scaling factor per search area or target.

1.2.2. TASK-BASED SENSOR MANAGEMENT

In order to produce Bayes-optimal sensor management results, it has been suggested to optimize quantities that are relevant to the sensing tasks and to the operational goal of a system, hence the name *task-based* sensor management. For example, when area surveillance is performed using radar measurements, one could *a*) maximize the expected probability of detecting a target; *b*) maximize the expected Signal-to-Noise Ratio (SNR) of a measurement; and/or *c*) minimize the expected uncertainty in the position estimate of a target.

One of the most common approaches when tracking a target is to select the sensing action such that a covariance-based measure is optimized, see Yang et al. [2012]; Kalandros [2002]. The trace of the covariance matrix is usually considered when tracking a target using a Kalman Filter and a sensing action is selected such that its expected value is minimized. The trace is preferred because it is simple to evaluate and intuitive to explain what it practically represents, see the discussion in Yang et al. [2012]. In this way, the uncertainty in the estimated Probability Density Function (PDF) is managed,

assuming that it can be described sufficiently well by a covariance matrix.

Under this class, one can also obtain non-myopic solutions given certain assumptions that allow the problem to be formulated as a Partially Observed Markov Decision Processes (POMDP). Examples of POMDP problem formulations for multitarget tracking can be found in Krishnamurthy and Evans [2001]; Wintenby and Krishnamurthy *IEEE Fellow* [2006].

In multitarget tracking, when the true number of targets is not known, the trace of the covariance matrix (or any of the other commonly used covariance-based schemes) cannot be used as measure of uncertainty because the state space is not Euclidean, see [Mahler, 2007, pp.65]. This is due to the existence variable of each track taking values in $[0,1]$ instead of $\mathbb{R}$. To overcome this problem and to take into account the limited field of view of a sensor, the Posterior Expected Number of Targets (PENT) criterion was proposed in Mahler and Zajic [2004] as an objective function for sensor management.

More applications of task-based sensor management can be found in van Keuk and Blackman [1993]; Charlish et al. [2012]; Zwaga et al. [2003].

1.2.3. INFORMATION-DRIVEN SENSOR MANAGEMENT

More recently, a novel approach suggested using information theoretic measures of uncertainty, hence the name *information-driven* sensor management. This approach is characterized by a measure of the information-theoretic notion of uncertainty, i.e. the Shannon entropy and its generalization the Rényi (also called α-) entropy. In this way, the uncertainty in the estimated PDF is managed via its information-theoretic description. Accordingly, a sensor manager selects the sensing action that minimizes the conditional or the Rényi entropy of the estimated PDF $p(x_k|\mathbf{Z}_{1:k})$ at time k given by Eq. (1.1) and (1.2) respectively.

$$H(X_k|\mathbf{Z}_{1:k}) = -\int p(z_k) \int p(x_k|\mathbf{Z}_{1:k}) \log\big(p(x_k|\mathbf{Z}_{1:k})\big)\, \mathrm{d}x_k\, \mathrm{d}z_k \tag{1.1}$$

$$H_\alpha(X_k|\mathbf{Z}_{1:k}) = -\frac{1}{\alpha-1} \int p(z_k) \log\left(\int p^\alpha(x_k|\mathbf{Z}_{1:k})\, \mathrm{d}x_k\right) \mathrm{d}z_k \tag{1.2}$$

where X_k is a random variable denoting the state at time k, (x_k, z_k) are the state and measurement realizations at time k, $\mathbf{Z}_{1:k}$ is the measurement history until and including time k, and $\alpha \in (0,1)$. For $\alpha \to 1$ the Rényi entropy becomes equivalent to the Shannon entropy, see Bialynicki-Birula [2007]; van Erven and Harremos [2014].

Another popular information-theoretic utility function is the Kullback-Leibler Divergence (KLD), presented in Manyika and Durrant-Whyte [1995]; Mahler [2003] and given by Eq. (1.3).

$$\mathrm{KLD}\left[p(X_k|Z_k)||p(X_k)\right] = \int p(x_k|z_k) \log\left(\frac{p(x_k|z_k)}{p(x_k)}\right) \mathrm{d}x_k \tag{1.3}$$

where $p(X_k)$ denotes the predicted PDF before the measurement update step. KLD represents the information gain from updating $p(X_k)$ with a measurement z_k whose distribution is $p(Z_k)$, see the discussion in Aoki et al. [2011]. Similarly, the Rényi (also called α-) divergence can be used:

$$D_\alpha\left[p(X_k|Z_k)||p(X_k)\right] = \frac{1}{\alpha-1}\log\left(\int p^\alpha(x_k|z_k)p^{1-\alpha}(x_k)\,\mathrm{d}x_k\right) \tag{1.4}$$

and for $\alpha \to 1$ Rényi divergence becomes equal to KLD, see van Erven and Harremos [2014].

For sensor management purposes, the sensing action that maximizes the expected KLD or α-divergence is used, the expectation taken with respect to the measurement PDF. It has been shown that for sensor management purposes, using the conditional entropy or the expected KLD leads to the same myopic sensor selection, see Aoki et al. [2011], but KLD induces a lower computational cost, see the particle approximations in Doucet et al. [2002] and Boers et al. [2010]. A similar result has not been obtained yet for the Rényi entropy and divergence.

Rényi entropy and divergence are of interest because the choice of α gives an extra degree of freedom during the design process of a sensor management algorithm, see Kreucher et al. [2005b]. Different values of α can give emphasis to different parts of a distribution but that might or might not be desirable, see Aughenbaugh and La Cour [2008]; Aoki [2013].

Applications of information-driven sensor management can be found in Boers et al. [2010]; Cole [2009]; Katsilieris et al. [2012a,b]; Romero and Goodman [2013]; Kreucher et al. [2005a]; Aughenbaugh and LaCour [2011]; Mahler [2007]; Ristic and Vo [2010].

1.2.4. RISK-BASED SENSOR MANAGEMENT

Risk-based methods aim to taking into account explicitly the operational goals of a radar system by allocating the radar resources according to the risk that is posed to mission success. In this approach, the notion of operational risk is used for performing sensor management, hence the name *risk-based* sensor management[1]. The risk-based approach to sensor management appeared as a result of attempts to *a*) consider quantities that are directly of interest to the operational goal of the system; and *b*) obtain better situational awareness within a given operational context. Risk-based sensor management is motivated by the threat assessment process that is an integral part of defence applications.

For example, in an asset-defence mission, a radar operator might not be directly interested in knowing the exact position of an aircraft but instead in having a clear idea of whether this aircraft is a threat to a specific asset and then take actions accordingly.

Risk-based sensor management can also be categorized under the heuristics/rules-based approaches, as in Bolderheij et al. [2005], or it can be Bayes-optimal, as in Papageorgiou and Raykin [2007]. In Bolderheij et al. [2005]; Papageorgiou and Raykin [2007] more sensor resources are allocated to targets that are considered to be more threatening to executing a mission or to an asset. Nevertheless, risk-based sensor management is considered as a separate class due to the novelty in considering higher-level quantities that are defined according to the operational context.

In-between the task-based and the risk-based approaches lies an extension of PENT, namely the Posterior Expected Number of Targets of Interest (PENTI), presented in Mahler

[1] Unfortunately, this already coined name can be misleading due to the conflict between operational risk and Bayes risk.

[2004], that also considers the tactical significance of any targets present in the considered scenario.

More applications of risk-based sensor management can be found in Bush et al. [2012]; Flint et al. [2003]; Vanheeghe et al. [2001]; Barbaresco [2007].

1.3. PROPOSED APPROACH

From the state of the art overview above, one can conclude that the existing resource management approaches are not simultaneously *a*) Bayes-optimal; *b*) directly related to the operational goals of a radar system; and *c*) easy for an operator to adjust the parameters of an MFR to a particular mission and operational scenario.

To overcome the aforementioned shortcomings of the existing schemes, this thesis proposes managing the uncertainty in higher-level quantities that are *directly of interest to the operator* and directly related to the operational goal of the radar system. In this way an operator can make better decisions with lower operational risk [Roux and van Vuuren, 2007, Ch. 3,5,8] and eventually complete the assigned mission successfully. The novelty of this approach is that it can be adapted to the *operational context* at hand, be that military or civilian, by redefining these higher-level quantities based on the given operational context or the assigned mission.

The proposed approach is motivated by the threat assessment process and it can be explained with the use of the Joint Directors of Laboratories (JDL) data fusion model, explained in Steinberg and Bowman [2004] and shown in Fig. 1.3. As discussed in Steinberg and Bowman [2004], the JDL model has five levels of data fusion: **Level 0** - Signal assessment: estimation of states of sub-object entities (e.g. SNR); **Level 1** - Object assessment: estimation of states of discrete physical objects (e.g. position of vehicles); **Level 2** - Situation assessment: estimation of relationships among entities (e.g. aggregates, cuing, intent, acting on); **Level 3** - Impact assessment: estimation of impacts (e.g. consequences of threat activities on one's own assets and goals); and **Level 4**- Performance Assessment: estimation and prediction of a system's performance as compared to given desired states and measures of effectiveness. The Level 4 *Process Refinement* function has been substituted by *Performance Assessment* because Process Refinement falls within the Resource Management model levels, see Steinberg and Bowman [2004].

For sensor management purposes, formal dual Resource Management process levels have been defined, see Steinberg and Bowman [2004]. These are: **Level 0** - Resource Signal Management: control of specific resource response actions (e.g., signals, pulses, waveforms, etc.); **Level 1** - Resource Response Management: control of continuous and discrete resource responses (e.g., radar modes, countermeasures, maneuvering, communications); **Level 2** - Resource Relationship Management: control of relationships (e.g., aggregation, coordination, conflict) among resource responses; **Level 3** - Mission Objective Management: establish/modify the objective of level 0, 1, 2 action, response, or relationship states; and **Level 4** - Design Management: task/control the system engineering (e.g. problem-to-solution space algorithm/model design mapping, model discovery and generalization).

It must be noted that processing at these Levels is not necessarily performed sequentially, and any one Level can be processed on their own given their corresponding inputs, see Llinas et al. [2004] and Steinberg and Bowman [2004].

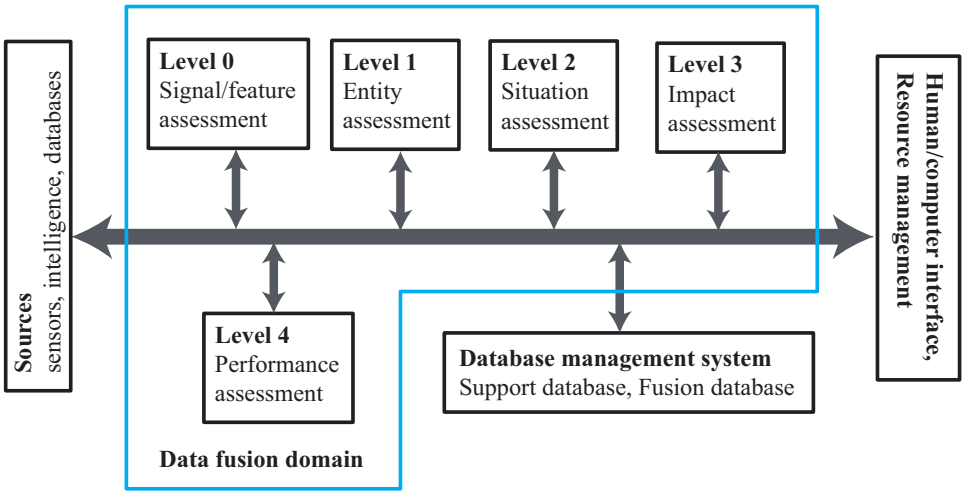

Figure 1.3: The JDL data fusion model. Reproduction of Fig. 2 from Steinberg and Bowman [2004].

While moving from Level 0 to Level 4 more complex attributes are encountered and the higher the Level the closer these attributes are to the operational goal or the mission of a system. This leads to the idea that if context-adaptive management of sensors is required then it is necessary to move to higher levels of the JDL model. In other words, instead of optimizing waveform parameters such that the expected SNR is optimized, it might be more beneficial to optimize waveform parameters such that better threat estimation is achieved.

Considering the JDL model, the task-based and information driven schemes constitute Level 0/1 based sensor management. The risk-based approach to sensor management represents a shift from Level 0/1 based sensor management to Level 2/3 based sensor management. This shift brings the sensor management objective closer to what a user is interested in, see the discussion in Blasch et al. [2008]. This also motivates the term “higher-level" quantities. In the JDL model, quantities such as SNR, probability of detection and track uncertainty are considered Level 0 (Signal assessment) or Level 1 (Object assessment) quantities whereas threat-level and risk are considered Level 2/3 (Situation Assessment / Impact Assessment or Threat Refinement) quantities.

An example of a commonly used higher-level quantity is the *threat-level* of a target. The process of estimating the threat-level of a target is an integral part of missions performed in the defence domain and it is known as *threat assessment*. Threat assessment is performed by radar operators based on their experience and the operational context. Using these tools, an operator can estimate the threat-level of a target, or in other words, if a target is friendly or hostile. Similarly, in a civilian context, air traffic controllers decide, based on their experience and the current set of aviation rules, whether there is high collision probability and instruct the pilots accordingly. This process can be seen as the counterpart of threat assessment in civilian scenarios. Threat-assessment will play a key role in this thesis as a sensor management algorithm will be proposed such that threat assessment is performed with minimum uncertainty.

The key challenges in implementing a scheme that allocates the radar resources such that the uncertainty in the threat-level is managed are *a*) the mathematical definition of threat with respect to the mission goals of a system; and *b*) the calculation of the corresponding threat probability density function. In other words, an implementation of the proposed approach requires a solution to the following problems:

1. how can the threat be mathematically modeled;
2. how can the threat probability density function of a target be calculated; and
3. how can a sensing action be chosen based on the uncertainty in the threat probability density function?

Up to now, the attempts to mathematically quantify the threat-level of a target have led to an *estimate of the threat-level* of a target, according to which the sensing resources are allocated, see for example Bolderheij et al. [2005]; Papageorgiou and Raykin [2007], instead of producing an estimate of the *threat probability density function* of a target. This happens because of the complexity of the rules and the difficulty to translate them in mathematical functions using a *meaningful* and *systematic* approach.

In order to attain the aim specified above, first some key questions must be addressed:

1. What are the advantages and disadvantages of the existing approaches to sensor management in light of the considered problem formulation?
2. How the problem of sensor management for area surveillance (including search and multitarget tracking) has to be formulated in order to avoid the limitations of the existing approaches?
3. How can the beam of an MFR be controlled for tracking multiple targets while taking into account the operational context?
4. How can the beam of an MFR be controlled for area surveillance, i.e. integrated search and multitarget tracking, while taking into account the operational context?

1.4. OUTLINE AND CONTRIBUTIONS

In order to aid the reader, this section discusses the outline of the dissertation and highlights the corresponding peer-reviewed publications. Finally, two more publications on work that is appended to this dissertation are mentioned.

Chapter 2 presents two case-studies where the behavior of existing sensor management schemes is explored and compared. The goal of this chapter is to demonstrate that controlling an MFR based on JDL Level 0/1 quantities is extremely difficult, if not impossible, when the operational context must also be taken into account. Accordingly, Chapter 2 serves as a motivation for the idea proposed in Chapter 3. The discussion is based on a literature review and on results reported in

Katsilieris et al. [2012b] Fotios Katsilieris, Yvo Boers, and Hans Driessen. Sensor management for PRF selection in the track-before-detect context. In *Proceedings of the IEEE Radar Conference*, pages 360–365, 2012.

Katsilieris et al. [2012a] Fotios Katsilieris, Yvo Boers, and Hans Driessen. Optimal search: a practical interpretation of information-driven sensor management. In *Proceedings of the 15th International Conference on Information Fusion*, pages 439–446, 2012.

Chapter 3 discusses in detail the novel idea for overcoming the shortcomings of the existing sensor management schemes. The proposed sensor management approach, i.e. the threat-based approach is presented. It is explained how threat can be mathematically modeled and how the threat probability density function can be calculated. Additionally, it is discussed how the uncertainty in the threat probability density function can be quantified. Finally, simple examples are given where the feasibility and the versatility of the proposed approach are demonstrated. This chapter is based on research reported in

Katsilieris et al. [2014] Fotios Katsilieris, Hans Driessen, and Alexander Yarovoy. Radar resource management for improved situation awareness. Accepted for publication to the International Radar Conference, Lille, France, 2014.

Katsilieris et al. [2015a] Fotios Katsilieris, Hans Driessen, and Alexander Yarovoy. Threat-based sensor management for target tracking. Under review for IEEE Transactions on Aerospace and Electronic Systems.

Chapter 4 presents an application of the threat-based approach to multiple target tracking with an MFR. The proposed approach is used in combination with a state-of-the-art signal processing algorithm (i.e. a Cardinality-Balanced Multi-target Multi-Bernoulli (CB-MeMBer) filter, see Vo et al. [2009a]) in order to take into account an imperfect detection process. This chapter is based on

Katsilieris et al. [2015a] Fotios Katsilieris, Hans Driessen, and Alexander Yarovoy. Threat-based sensor management for target tracking. Submitted to the IEEE Transactions on Aerospace and Electronic Systems.

Chapter 5 discusses how the threat-based approach to sensor management can be used for area surveillance, i.e. for integrated search and multitarget tracking. The chapter starts by discussing how the search for undetected targets can be performed in an optimal way. Subsequently, it is shown how the two tasks can be tackled simultaneously without using heuristics. Simulated examples are shown where the threat PDF is evaluated based on quantities of state-of-the-art signal processing algorithms (i.e. a Probability Hypothesis Density (PHD) filter, presented in Mahler [2007], and a CB-MeMBer filter). This chapter is based on

Katsilieris et al. [2015b] Fotios Katsilieris, Hans Driessen, and Alexander Yarovoy. Adaptive radar beam-pointing for area surveillance. To be submitted to the IEEE Transactions on Aerospace and Electronic Systems.)

Chapter 6 concludes this dissertation by summarizing the research results and suggesting possible topics for future research.

ADDITIONAL RESULTS

While being a Marie Curie fellow in the MC Impulse project[2], I visited two research institutes.

First, during a research visit at Fraunhofer-Institut fur Kommunikation, Informationsverarbeitung und Ergonomie (Fraunhofer FKIE), I worked on merging the research presented in Chapter 2 and in Katsilieris et al. [2012a] with the research of Dr. Alexander Charlish on optimization and scheduling for MFRs. The results of this collaboration are discussed in Appendix A and were reported in

Katsilieris et al. [2012c] Fotios Katsilieris, Alexander Charlish, and Yvo Boers. Towards an online, adaptive algorithm for radar surveillance control. In *Future Security - Security Research Conference 2012: Sensor Data Fusion Workshop*, Bonn, Germany, 2012.

Secondly, during a research visit at the NATO-STO Centre for Maritime Research and Experimentation (NATO-STO CMRE), I collaborated with Dr. Paolo Braca on using radar measurements for detecting the malicious spoofing of the Automatic Identification System (AIS) reports. The results of this collaboration are discussed in Appendix B and were presented in

Katsilieris et al. [2013] Fotios Katsilieris, Paolo Braca, and Stefano Coraluppi. Detection of malicious AIS position spoofing by exploiting radar information. In *Proceedings of the 16th International Conference on Information Fusion*, pages 1–7, 2013.

[2]More information about the MC Impulse project can be found at `http://mcimpulse.isy.liu.se`

2

CASE-STUDY-BASED ANALYSIS OF EXISTING SENSOR MANAGEMENT CRITERIA

In the previous chapter, the problem of sensor management was introduced in the context of multitarget tracking using an MFR. Furthermore, the existing approaches to sensor management were presented. This chapter presents two case studies where existing approaches are compared for *a*) waveform selection for tracking a single-target; and *b*) for radar-beam control for searching for a target. The goal is to understand the behavior of existing criteria and obtain insight into their advantages and disadvantages.

Section 2.1 presents a case-study of the behavior of task-based and information driven criteria when the PRF of a radar must be controlled for tracking a target. Section 2.2 presents a case-study of the behavior of task-based and information driven criteria when searching for a target. Section 2.3 compares the existing approaches to sensor management with respect to their behavior, optimality and flexibility to account for the user needs. Finally, Section 2.4 concludes the chapter.

2.1. CASE-STUDY A: PRF SELECTION FOR TARGET TRACKING

The first case-study considers an application where the estimated PDF can be multimodal. The goal is to explore the behavior of task-based and information-driven criteria in such a case. This case-study was also published in Katsilieris et al. [2012b].

2.1.1. THE PRF SELECTION PROBLEM

Consider a scenario where a target is tracked by a radar and the radar can utilize several PRFs, of which only one can be used at each time of transmission.

The fact that the radar transmits pulses with a given frequency causes the following problems, also discussed in Skolnik [2002]:

- blind (range) zones exist where the target cannot be detected. This happens because the radar antenna cannot receive any echoes while transmitting a pulse.
- range ambiguities exist due to a PRF. Assume for example that there have been transmitted n pulses and then the radar starts receiving an echo. How can it be sure from which pulse the echo was received and therefore, where exactly is the target?
- velocity ambiguities exist because it is not possible to directly measure the pulse duration difference due to the Doppler effect. For this reason, the phase difference between the transmitted and the received pulses is measured. The phase shift is subject to a modulo 2π operation and therefore aliasing can happen.
- conflicting PRF requirements for resolving range and velocity ambiguities. In order to avoid range ambiguities low PRFs must be used whereas, in order to avoid velocity ambiguities high PRFs must be used.

2.1.2. SYSTEM SETUP

The system under consideration can be mathematically described by the following (discrete time) state and measurement equations:

$$\mathbf{x}_k = f(\mathbf{x}_{k-1}, \mathbf{w_k}) \tag{2.1}$$
$$\mathbf{z}_k = h(\mathbf{x}_k, PRF_k, \mathbf{v_k}) \tag{2.2}$$
$$\mathbf{x}_0 \sim p(\mathbf{x}_0) \tag{2.3}$$

where $k = 1,2,\ldots$ is the time index, $\mathbf{x}_k = [x \;\; v_x \;\; y \;\; v_y \;\; \rho]^\top \in \mathbb{R}^5$ is the 5 dimensional state of the system describing the position and velocity of a target in Cartesian coordinates and the amplitude of its echo, $\mathbf{w_k}$ is the 5 dimensional process noise with probability density $p_w(\mathbf{w_k})$, PRF_k is the chosen PRF at time k, $\mathbf{z}_k \in \mathcal{Z} = \mathbb{R}^{N_r \cdot N_d \cdot N_b}$ is the received radar measurement, meaning the reflected power level of the target in the $N_r \times N_d \times N_b$ sensor cells, N_r, N_d, N_b are the number of range, Doppler, and bearing cells respectively, $\mathbf{v_k}$ is the 3 dimensional measurement noise with probability density $p_v(\mathbf{v_k})$, $\mathbf{x}_0$ is the initial state of the system with probability density $p(\mathbf{x}_0)$. The vector and possibly non-linear function $f(\cdot) : \mathbb{R}^5 \mapsto \mathbb{R}^5$ describes the dynamics of the system. Similarly, the vector and possibly non-linear function $h(\cdot) : \mathbb{R}^5 \mapsto \mathbb{R}^{N_r \cdot N_d \cdot N_b}$ describes how the measurement $\mathbf{z}_k$ is related to the system state $\mathbf{x}_k$ and the chosen PRF PRF_k.

The considered problem amounts to finding the optimal, in the sense of the proposed criteria, sequence of PRF_k of the pulses to be transmitted.

The chosen sequence of PRFs will then be used for solving the attached filtering problem of determining the posterior probability density function $p(\mathbf{x}_k|\mathbf{Z}_{1:k}, \mathbf{U}_{1:k})$ that describes the kinematic properties and the amplitude of the target. The measurement history is denoted by $\mathbf{Z}_{1:k} = \{\mathbf{z}_1, ..., \mathbf{z}_k\}$ and the chosen PRF history by $\mathbf{U}_{1:k} = \{PRF_1, ..., PRF_k\}$.

DYNAMICAL MODEL

A target with simple dynamics is considered and therefore a linear Gaussian nearly constant velocity motion model, as presented in Li and Jilkov [2003], is employed:

$$\mathbf{x}_k = f(\mathbf{x}_{k-1}, w_k) = F\mathbf{x}_{k-1} + \mathbf{w_k} \tag{2.4}$$

where:

$$\mathbf{w_k} \sim \mathcal{N}(\mu, \Sigma)$$

$$F = \begin{bmatrix} 1 & T & 0 & 0 & 0 \\ 0 & 1 & 0 & 0 & 0 \\ 0 & 0 & 1 & T & 0 \\ 0 & 0 & 0 & 1 & 0 \\ 0 & 0 & 0 & 0 & 1 \end{bmatrix}, \quad \Sigma = \begin{bmatrix} b_x T^3/3 & b_x T^2/2 & 0 & 0 & 0 \\ b_x T^2/2 & b_x T & 0 & 0 & 0 \\ 0 & 0 & b_y T^3/3 & b_y T^2/2 & 0 \\ 0 & 0 & b_y T^2/2 & b_y T & 0 \\ 0 & 0 & 0 & 0 & b_\rho \end{bmatrix}$$

and $b_x = b_y$ are the power spectral densities of the acceleration noise in the $x-y$ direction, T is the sampling time, $\mu = [0\ 0\ 0\ 0\ 0]^\intercal$ is the mean of the Gaussian noise and b_ρ is the variance of the increment in the echo's amplitude.

THE ROLE OF PRF IN THE RADAR MEASUREMENT MODEL

Firstly, the choice of PRF affects the maximum unambiguous range (r_{fold}) and velocity (d_{fold}), see Eq. (2.5). If the range (or velocity) of the target is higher than r_{fold} (or d_{fold}) then a radar cannot be sure what is the correct range (velocity) of the target because any target echo from $r + n\frac{c}{2 \cdot PRF}$ would give the same measurement, where $r \in (0, \frac{c}{2 \cdot PRF})$, c is the speed of light and $n = 0, 1, 2 \ldots$. A similar relationship holds for the velocity domain. In other words, the target PDF has *multiple modes both in range and in velocity*.

Secondly, the range and velocity resolution (Δr, Δd) depend on the chosen PRF, Pulse Compression Ratio [%] (PCR) and number of transmitted pulses n_P, see Eq. (2.6).

Thirdly, the length of the blind zones (r_{blind}) depends on the pulse width PW and the location of the blind velocities (d_{blind}) depends on the chosen PRF and the wavelength of the waveform carrier λ, see Eq. (2.7) where $n = 0, 1, 2, \ldots$.

$$r_{fold} = \frac{c}{2 \cdot PRF} \quad , \quad d_{fold} = \frac{\lambda \cdot PRF}{2} \tag{2.5}$$

$$\Delta r = \text{PCR}\frac{c \cdot \text{PW}}{2} \quad , \quad \Delta d = \frac{\lambda \cdot PRF}{2 \cdot n_P} \tag{2.6}$$

$$r_{blind} = \text{PW} \cdot c \quad , \quad d_{blind} = n\frac{\lambda \cdot PRF}{2} \tag{2.7}$$

By using the equations for r_{fold} and r_{blind}, it is possible to derive an expression for the blind zones where the target cannot be detected:

$$r_k \in \left[n\frac{c}{2PRF_k},\ n\frac{c}{2PRF_k} + (c\text{PW}) \right], n = 0, 1, 2 \ldots \tag{2.8}$$

where r_k is the distance between the radar and the target at time k.

MEASUREMENT MODEL

The considered application deals with tracking a target in the *track-before-detect* context. This means that the received measurements are not thresholded in order to obtain plot measurements. On the contrary, all the $N_r \times N_d \times N_b$ sensor cells are considered. The approach presented in Boers and Driessen [2004] is followed, with the difference that in the considered scenario there is only one target and no target birth or death.

In each cell, the measurement is:

$$\begin{aligned} \mathbf{z}_k^{ijl}(\mathbf{x}_k, PRF_k) &= |\mathbf{z}_{A,k}^{ijl}(\mathbf{x}_k, PRF_k)|^2 \\ &= |A_k h_A^{ijl}(\mathbf{x}_k, PRF_k) + \mathbf{v_k}|^2 \end{aligned} \tag{2.9}$$

where $\mathbf{z}_{A,k}^{ijl}(\mathbf{x}_k, PRF_k)$ is the complex amplitude data of the target in the cell ijl, $A_k = \rho_k e^{i\varphi_k}$ is the complex amplitude of the target, $\varphi \in (0, 2\pi)$, $h_A({}^{ijl}\mathbf{x}_k, PRF_k)$ is the reflection form and $\mathbf{v_k}$ is complex Gaussian noise with zero mean and covariance σ^2.

The reflection form $h_A^{ijl}(\mathbf{x}_k, PRF_k)$ is given by:

$$h_A^{ijl}(\mathbf{x}_k, PRF_k) = e^{-\frac{(r_i - r_k)^2}{2R} - \frac{(d_j - d_k)^2}{2D} - \frac{(b_l - b_k)^2}{2B}} \tag{2.10}$$

where $i = 1, \ldots, N_r$, $j = 1, \ldots, N_d$, $l = 1, \ldots, N_b$, $R = (\Delta r_k)^2, D = (\Delta d_k)^2, B = (\Delta b_k)^2$ are constants related to the size of a range, a Doppler and a bearing cell respectively. $\Delta r_k, \Delta d_k, \Delta b_k$ are the range, Doppler and bearing resolutions of the radar and

$$r_k = \sqrt{x_k^2 + y_k^2} \left(\text{mod } \frac{c}{2 \cdot PRF_k} \right) \tag{2.11}$$

$$d_k = \dot{r}_k = \frac{x_k v_x + y_k v_y}{\sqrt{x_k^2 + y_k^2}} \left(\text{mod } \frac{\lambda \cdot PRF_k}{2} \right) \tag{2.12}$$

$$b_k = \arctan(y_k / x_k) \tag{2.13}$$

are the apparent target range, velocity and bearing respectively.

These measurements, conditioned on the states $\mathbf{x}_k$ of the target, are assumed to be exponentially distributed and therefore the likelihood function $p(\mathbf{z}_k^{ijl} | \mathbf{x}_k, PRF_k)$ is:

$$p(\mathbf{z}_k^{ijl} | \mathbf{x}_k, PRF_k) = \frac{1}{\mu^{ijl}} \cdot e^{-\frac{1}{\mu^{ijl}} \mathbf{z}_k^{ijl}(\mathbf{x}_k, PRF_k)} \tag{2.14}$$

where

$$\mu^{ijl} = \mathrm{E}[\mathbf{z}_k^{ijl}(\mathbf{x}_k, PRF_k)] = \rho_k^2 h_P^{ijl}(\mathbf{x}_k, PRF_k) + 2\sigma^2 \tag{2.15}$$

$$h_P^{ijl}(\mathbf{x}_k, PRF_k) = \left[h_A^{ijl}(\mathbf{x}_k, PRF_k) \right]^2 = e^{-\frac{(r_i - r_k)^2}{R} - \frac{(d_j - d_k)^2}{D} - \frac{(b_l - b_k)^2}{B}} \tag{2.16}$$

As it can be noticed from Eq. (2.15,2.16) and (2.11,2.12,2.13) the received measurement depends both on the target states (position, velocity, amplitude) and on the PRF that is chosen.

Therefore,

$$\mathbf{z}_k^{ijl} = \begin{cases} \mathbf{v_k}, & \text{if no target in cell } ijl \\ & \text{or Eq. (2.8) is true} \quad (2.17a) \\ h^{ijl}(\mathbf{x}_k, PRF_k, \mathbf{v_k}), & \text{if target in cell } ijl \\ & \text{and Eq. (2.8) is false} \quad (2.17b) \end{cases}$$

where $h^{ijl}(\mathbf{x}_k, PRF_k, \mathbf{v_k})$ is given by Eq. (2.9).

This means that if the choice of PRF is poor, the target can be placed in a blind zone and therefore, it can be made undetectable. This is especially important in the track-before-detect context, where targets usually have low SNR and no measurements should be wasted.

2.1.3. PROPOSED SOLUTION

The described target tracking problem is solved by employing sensor management criteria for choosing the best PRF and the recursive Bayesian estimation theory for recursively estimating the posterior density $p(\mathbf{x}_k|\mathbf{Z}_{1:k}, \mathbf{U}_{1:k})$.

RECURSIVE BAYESIAN ESTIMATION

Given a probability density function $p(\mathbf{x}_{k-1}|\mathbf{Z}_{1:k-1}, \mathbf{U}_{1:k-1})$, in the recursive Bayesian estimation context the prediction step is performed using the Chapman-Kolmogorov equation:

$$p(\mathbf{x}_k|\mathbf{Z}_{1:k-1}, \mathbf{U}_{1:k-1}) = \int p(\mathbf{x}_k|\mathbf{x}_{k-1})\ p(\mathbf{x}_{k-1}|\mathbf{Z}_{1:k-1}, \mathbf{U}_{1:k-1})\, d\mathbf{x}_{k-1} \quad (2.18)$$

where $p(\mathbf{x}_k|\mathbf{x}_{k-1})$ is usually determined by the kinematics model of the target.

Then the predictive density $p(\mathbf{x}_k|\mathbf{Z}_{1:k-1}, \mathbf{U}_{1:k-1})$ is updated with the received measurement $\mathbf{z}_k$ using Bayes' rule

$$p(\mathbf{x}_k|\mathbf{Z}_{1:k}, \mathbf{U}_{1:k}) = \frac{p(\mathbf{z}_k|\mathbf{x}_k, PRF_k)\ p(\mathbf{x}_k|\mathbf{Z}_{1:k-1}, \mathbf{U}_{1:k-1})}{p(\mathbf{z}_k|\mathbf{Z}_{1:k-1}, \mathbf{U}_{1:k})} \quad (2.19)$$

where $p(\mathbf{z}_k|\mathbf{x}_k, PRF_k)$ is the likelihood function and

$$p(\mathbf{z}_k|\mathbf{Z}_{1:k-1}, \mathbf{U}_{1:k}) = \int p(\mathbf{z}_k|\mathbf{x}_k, PRF_k)\ p(\mathbf{x}_k|\mathbf{Z}_{1:k-1}, \mathbf{U}_{1:k-1})\, d\mathbf{x}_k \quad (2.20)$$

is a normalizing constant which in practice does not have to be calculated if a particle filter is employed. Therefore, it holds that

$$p(\mathbf{x}_k|\mathbf{Z}_{1:k}, \mathbf{U}_{1:k}) \propto p(\mathbf{z}_k|\mathbf{x}_k, PRF_k)\ p(\mathbf{x}_k|\mathbf{Z}_{1:k-1}, \mathbf{U}_{1:k-1}) \quad (2.21)$$

and Eq. (2.18,2.19) can be easily approximated using a standard Sampling Importance Resampling (SIR) particle filter, see Ristic et al. [2004], with N particles $\mathbf{x}_k^i$ and corresponding weights q_k^i such that the approximation converges to the true posterior distribution $p(\mathbf{x}_k|\mathbf{Z}_{1:k}, \mathbf{U}_{1:k})$ as $N \to \infty$, see Hu et al. [2008].

SENSOR MANAGEMENT CRITERIA

As it is discussed in the introduction of this case-study, criteria from two classes are used. From the information-driven class, the expected KLD is used. From the task-based class, the trace of the expected covariance matrix of the posterior density is used.

2

MAXIMUM EXPECTED KULLBACK-LEIBLER DIVERGENCE

When using the expected KLD, the best PRF at each time instance is given by:

$$\widehat{PRF_k} = \underset{PRF}{\arg\max}\, \mathrm{E}_{\mathcal{Z}} \left\{ \mathrm{KLD} \left[p(\mathbf{X}_k|\mathbf{z}_k, \mathbf{Z}_{1:k-1}, PRF, \mathbf{U}_{1:k-1}) || p(\mathbf{X}_k|\mathbf{Z}_{1:k-1}, \mathbf{U}_{1:k-1}) \right] \right\} \tag{2.22}$$

where $\mathbf{X}_k$ is the random variable that denotes the state of the target at time k.

A particle approximation of the expected KLD is used, given by Eq. 2.23, similar to the equation presented in Doucet et al. [2002]. In the following formulas, $(\mathbf{x}_k, \mathbf{z}_k)$ are the state and measurement realizations at time k, $\mathbf{z}_k^p$ denotes the simulated measurement at time k, using particle $\mathbf{x}_k^p$ with weight q_{k-1}^p and PRF_k.

$$\begin{aligned}
&\mathrm{E}_{\mathcal{Z}} \left\{ \mathrm{KLD} \left[p(\mathbf{X}_k|\mathbf{z}_k, \mathbf{Z}_{1:k-1}, PRF_k, \mathbf{U}_{1:k-1}) || p(\mathbf{X}_k|\mathbf{Z}_{1:k-1}, \mathbf{U}_{1:k-1}) \right] \right\} \\
&\quad = \int p(\mathbf{z}_k|\mathbf{x}_k, PRF_k) \int p(\mathbf{x}_k|\mathbf{Z}_{1:k-1}, \mathbf{U}_{1:k-1}) \log \left(\frac{p(\mathbf{z}_k|\mathbf{x}_k, PRF_k)}{p(\mathbf{z}_k|\mathbf{Z}_{1:k-1}, \mathbf{U}_{1:k-1}, PRF_k)} \right) \mathrm{d}\mathbf{x}_k \, \mathrm{d}\mathbf{z}_k \\
&\quad \approx \sum_{p=1}^{P} q_{k-1}^p \left\{ \log \left(\frac{p(\mathbf{z}_k^p|\mathbf{x}_k^p, PRF_k)}{\hat{p}_M(\mathbf{z}_k^p|\mathbf{Z}_{1:k-1}, \mathbf{U}_{1:k-1}, PRF_k)} \right) \right\}
\end{aligned} \tag{2.23}$$

where

$$\hat{p}_M(\mathbf{z}_k^p|\mathbf{Z}_{1:k-1}, \mathbf{U}_{1:k-1}, PRF_k) = \sum_{m=1}^{M} \left\{ q_{k-1}^m \; p(\mathbf{z}_k^p|\mathbf{x}_k^m, PRF_k) \right\} \tag{2.24}$$

In Eq. (2.23), P is the number of simulated measurements. In Eq. (2.24), M denotes the number of particles used within the criterion.

This evaluation is repeated K times (1 time per PRF) and then the PRF for which Eq. (2.23) attains its highest value is chosen. Accordingly, the computational complexity of this criterion is $\mathcal{O}(MPK)$ and the corresponding computational complexity of the equivalent conditional entropy would be $\mathcal{O}(M^2PK)$.

MINIMUM TRACE OF THE EXPECTED COVARIANCE MATRIX

Under the assumption that the uncertainty about the target's attributes (position, velocity and amplitude) is sufficiently represented by the mean and the covariance of the corresponding probability density function, it is intuitive to choose a criterion that selects the PRF that leads to the minimum trace of the expected covariance matrix of the posterior density.

In this case, the corresponding sensor management criterion is:

$$\widehat{PRF_k} = \underset{PRF}{\arg\min}\, \mathrm{tr} \left[\mathrm{E}_{\mathcal{Z}} \left\{ \mathrm{Cov} \left[p(\mathbf{x}_k|\mathbf{z}_k, \mathbf{Z}_{1:k-1}, PRF, \mathbf{U}_{1:k-1}) \right] \right\} \right] \tag{2.25}$$

Eq. (2.25) is approximated as follows:

$$\begin{aligned}
&\mathrm{E}_{\mathcal{Z}}\left\{\mathrm{Cov}\left[\ p(\mathbf{x}_k|\mathbf{z}_k,\mathbf{Z}_{1:k-1},PRF_k,\mathbf{U}_{1:k-1})\right]\right\}\\
&\quad=\int p(\mathbf{z}_k|\mathbf{Z}_{1:k-1},PRF_k,\mathbf{U}_{1:k-1})\int(\mathbf{x}_k-\mu_{\mathbf{x}_k})(\mathbf{x}_k-\mu_{\mathbf{x}_k})^{\mathsf{T}}\\
&\qquad\times p(\mathbf{x}_k|\mathbf{z}_k,\mathbf{Z}_{1:k-1},PRF_k,\mathbf{U}_{1:k-1})\,\mathrm{d}\mathbf{x}_k\,\mathrm{d}\mathbf{z}_k\\
&\quad\approx\sum_{p=1}^{P}q_{k-1}^{p}\left\{\sum_{m=1}^{M}q_{k-1}^{m}(\mathbf{x}_k^m-\mu_{\mathbf{x}_k}^p)(\mathbf{x}_k^m-\mu_{\mathbf{x}_k}^p)^{\mathsf{T}}\right\} \qquad (2.26)\\
\text{where}\quad&\mu_{\mathbf{x}_k}^p=\int\mathbf{x}_k\ p(\mathbf{x}_k|\mathbf{z}_k^p,\mathbf{Z}_{1:k-1},PRF_k,\mathbf{U}_{1:k-1})\,\mathrm{d}\mathbf{x}_k\approx\sum_{n=1}^{M}\left(q_k^m\,\mathbf{x}_k^m\right)\\
&\mathbf{x}_k^m\sim p(\mathbf{x}_k|\mathbf{z}_k^p,\mathbf{Z}_{1:k-1},PRF,\mathbf{U}_{1:k-1}) \qquad (2.27)
\end{aligned}$$

which is evaluated using $\mathbf{z}_k^p$ in Eq. (2.18) and (2.19). The reader is reminded that $\mathbf{z}_k^p$ denotes the simulated measurement at time k, using particle $\mathbf{x}_k^p$ with weight q_{k-1}^p and PRF_k. The updated weight q_k^m is evaluated using the simulated measurement $\mathbf{z}_k^p$ in Eq. (2.14) followed by a normalization step. In Eq. (2.26), M denotes the number of particles used within the criterion and P is the number of simulated measurements.

Again, this evaluation is repeated K times (1 time per PRF) and then the PRF for which Eq. (2.26) attains its highest value is selected. The computational complexity of the covariance based criterion is $\mathcal{O}[(M+1)PK]$, which is between $\mathcal{O}(MPK)$ and $\mathcal{O}(M^2PK)$.

2.1.4. SIMULATIONS

Figure 2.1 depicts the scenario under consideration. In Fig. 2.1 the position of the radar, the trajectory of the target and the blind zones caused by each PRF can be seen. The radar is assumed to be at the origin of the axes. The target to be tracked starts at $k=0$ from $[x_0^{true},y_0^{true}]=[74.2,74.2]$ km and moves with constant velocities $v_x^{true}=v_y^{true}=-300$ m/s for 60 sec towards the radar. Its SNR is assumed to be 11 dB.

The chosen PRFs along with the corresponding pulse widths (PW), PCRs and number of transmitted pulses (n_P) are given by Eq. (2.28) through (2.31). They were chosen such that the range and velocity resolutions and the duty cycle (given by PRF · PW) are constant. These conditions make sure that no PRF is favored due to better resolution or more covered area.

$$\mathrm{PRF}=[1.4,\ 4,\ 5,\ 5.5,\ 23.5]\ \mathrm{kHz} \qquad (2.28)$$
$$\mathrm{PW}=[53,\ 18.9,\ 15.1,\ 13.7,\ 3.2]\ \mu\mathrm{sec} \qquad (2.29)$$
$$\mathrm{PCR}=[0.013,\ 0.036,\ 0.045,\ 0.05,\ 0.21] \qquad (2.30)$$
$$n_P=[3,\ 8,\ 10,\ 11,\ 47] \qquad (2.31)$$

The $N=10^4$ particles are initially distributed uniformly such that: $r_0\in[0,115]$ km, $b_0\in[0.75,0.85]$ rad, $d_0\in[-500,0]$ m/s; $SNR_0\in[4,16]$ dB; $\rho_0=\sqrt{2\sigma^2\cdot10^{SNR/10}}\in[1.58,6.31]$ Watts; $\varphi_{0:k}$ is considered random and does not affect the results.

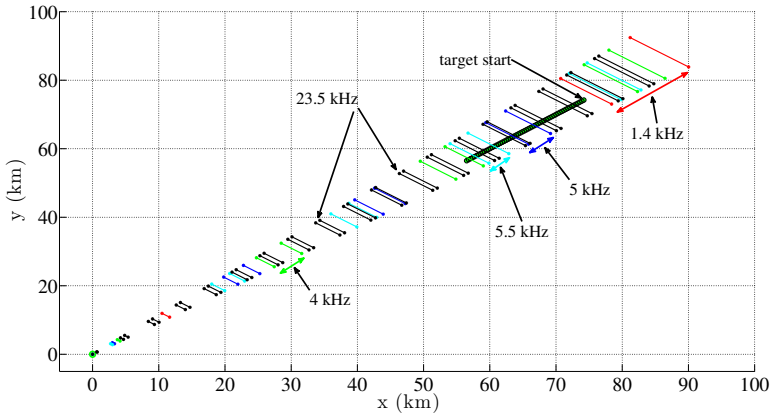

Figure 2.1: The scenario considered in our simulations. The blind zones for each PRF are the areas between the two closest lines of same color, as denoted by the arrows of same color in the corresponding examples.

It is assumed that a highly maneuverable target is tracked, such as a fighter or a missile, and therefore high process noise is used. The dynamical model parameters are: $b_x = b_y = 400$ m^2/s^4 and $b_\rho = 10^{-3}$ Watts^2; $T = 1$ sec and $k = 1,\ldots,60$ sec.

The parameters for the measurement model are: $\lambda = 0.03$ m, $c = 3 \cdot 10^8$ m/s and $\sigma^2 = 1/2$; beam width $\Delta b = 0.1$ rad $\simeq 5.7^o$; $\Delta r, \Delta d$ according to Eq. (2.11, 2.12) and (2.28) through (2.31).

Due to high computational load involved in the experiments, only 100 out of $N = 10^4$ particles are selected and 1 measurement per chosen particle is simulated for the evaluation of the criteria, meaning 100 measurements in total. The choice of 100 particles is performed by a multinomial resampling step. This procedure is repeated 5 times because 5 different PRFs are employed. According to the notation in Doucet et al. [2002], $M = 100$ particles, $P = 100$ simulated measurements (1 from each particle) and $K = 5$ (due to 5 PRFs) are used for evaluating the criteria.

Figures 2.2 and 2.3 show a characteristic example of the obtained sensor management results for the two criteria. In Fig. 2.2, higher KLD represents better PRF choice. Therefore, PRFs that would put the target in a blind zone are avoided because they lead to lower KLD. On the contrary, in Fig. 2.3, lower trace of the covariance matrix represents better PRF choice. Therefore, PRFs that would put the target in a blind zone are avoided because they lead to higher trace of the covariance matrix.

Figures 2.4a and 2.4b show the sequence of chosen PRFs produced by the two criteria. It can be noticed that the highest PRF is preferred. This can be explained by the fact that a high process noise is used for tracking a highly maneuverable target. This leads to ambiguities being created at every time instance in the velocity domain and therefore the highest PRF must be chosen for resolving them. The aforementioned explanation was verified by a new set of experiments with lower process noise where the medium PRFs were also chosen, provided that they would not place the target in a blind zone.

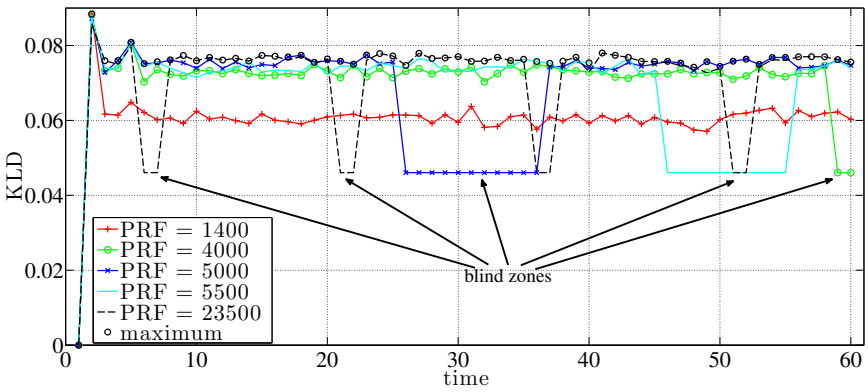

Figure 2.2: The expected KLD between the predictive and the posterior density for each PRF. PRFs that put the target in a blind zone result in a lower KL divergence and therefore they are not chosen.

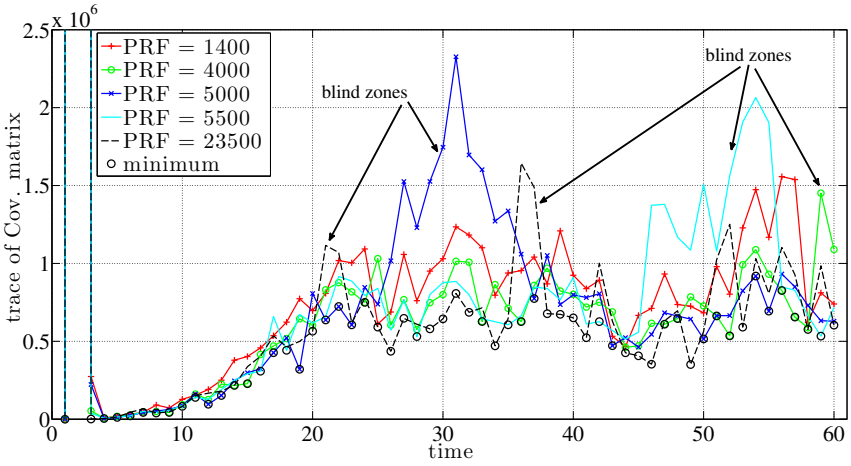

Figure 2.3: The trace of the expected covariance matrix of the posterior density for each PRF. PRFs that put the target in a blind zone result in a higher covariance and therefore they are not chosen.

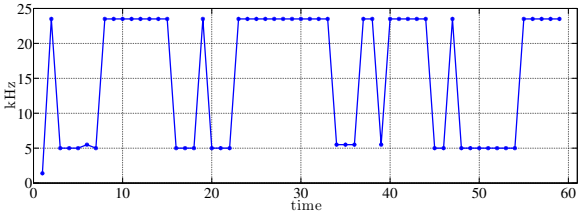

(a) KLD-based criterion

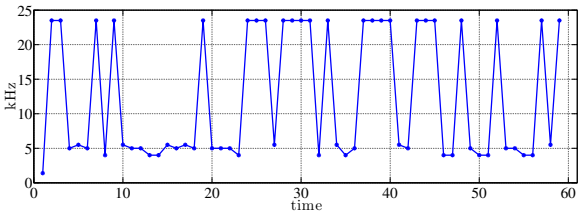

(b) Covariance-based criterion

Figure 2.4: The sequence of chosen PRFs by each criterion. Notice that the highest PRF is preferred by both criteria.

2.1.5. CONCLUSIONS

The proposed criteria were found to produce similar results in the sense that *a*) both criteria resolve the ambiguities; and *b*) avoid choosing a PRF that would place the target in a blind zone. In other words, both criteria eliminate the multiple modes in the posterior PDF, given that there is such a sensing option.

Furthermore, both criteria produced an unexpected but interesting result, namely the highest PRF would be preferred by both criteria unless its selection would place the target in a blind zone. The selection of the highest available PRF depends on the maneuverability of the target to be tracked, as verified by a second series of experiments (not shown here) where tracking targets with lower maneuverability did not lead to high PRF preference.

The fact that both criteria managed to detect that the motion model creates problems in the tracking process by constantly introducing velocity ambiguities and they managed to tackle this problem automatically is an extra advantage over the classical solutions. In the considered scenario, PRF staggering would have addressed this problem every 5 sec, when the lowest PRF would be used, and PRF jittering would have addressed it at random time instances.

The obtained results are also applicable when plot measurements, resulting from a detection process, are used instead of the unthresholded.

An interesting and partially open question is to explore how the results obtained by the KLD-based criterion perform in the context of the covariance based criterion and vice versa. According to the discussion in Boers et al. [2010] about the representation of uncertainty in unimodal distributions, it is expected that the aforementioned comparison would indicate that the criteria would produce very similar results. A more practical explanation is that the criteria have similar behaviors because both resolve the ambigu-

ities and try to avoid the blind zones.

2.2. CASE-STUDY B: SEARCH FOR UNDETECTED TARGETS

The second case-study considers an application where search for undetected targets is performed. The goal is to compare the behavior of a task-based and an information-driven criterion in such a case. This case-study was also published in Katsilieris et al. [2012a] and, as a memorandum, in Katsilieris and Boers [2012].

2.2.1. THE TARGET SEARCH PROBLEM

The problem of performing search emerges when the available sensor resources have to be utilized in an efficient way such that the search for an object or a feature is successful.

The challenges are to find the object as soon as possible while spending as few resources as possible. Towards this goal, sensor management criteria can be utilized. The main advantage of using such criteria over the simple approaches of periodic or random search is that they can take into account any available external information and as a result demonstrate adaptive behavior. For instance, if the object is expected to be with higher probability in a specific region, the periodic or random search approaches would not take this information into account. On the other hand, a carefully chosen or designed criterion would produce search patterns that leverage this information in order to find the object faster and/or by using less resources. If the external information is updated at each iteration, like in this case, then the problem amounts to performing one-step ahead (or myopic) optimal search.

Some examples where these challenges appear are: target detection, discussed in Danskin [1968]; Koopman [1957] and search for wreckages or survivors, discussed in Kratzke and Frost [2010]; Stone et al. [2011]. In the robotics community the search problem is usually referred to as the 'pursuit-evasion problem' and has been studied under different assumptions and solved using different approaches, see for example Suzuki and Yamashita [1992]; Gerkey et al. [2004].

This case-study considers the scheduling of an agile sensor for efficiently searching for a target. A characteristic example of such a sensor is a MFR. MFRs have received a lot of attention from the research community as an attempt to schedule efficiently their tasks, one of which is to perform search for undetected targets.

In Bolderheij and Van Genderen [2004] the track and search functions of an MFR were scheduled according to a threat-based criterion. For scheduling search functions, the authors used ghost targets that dictate volume or horizon search instead of tracking a target.

In Koch [1999] the revisit intervals, radar beam positions, and energy per dwell were controlled for improving track quality and energy efficiency. Especially in the case of searching, the use of negative information has been suggested for updating the predictive densities of the targets and obtaining a search pattern by searching the region where the maximum of the predictive density was located. An updated version is Koch [2007].

In White et al. [2008] the authors used a user-defined *search-to-track* ratio. The sensor manager scheduled the corresponding tasks of the radar according to this ratio. When the search task was considered, an estimate of the spatial density of previously undetected targets was utilized. The sensing action that maximized the expected num-

ber of newly detected targets was chosen whenever a search function was scheduled. A disadvantage of this approach is that the search-to-track ratio is user-defined and not automatically determined by the scheduling algorithm according to the optimization of a criterion. A similar scheduling approach was presented in Boers et al. [2008] where the scheduling criterion suggested selecting recursively those sensors that cover the most probability mass of the predictive density.

In Matthiesen [2010] an approach similar to the one proposed in this case-study was presented. An a priori probability distribution of the target to be detected was specified by a set of discrete target position probabilities corresponding to each search beam. Immediately after the increment of search effort was applied, the target position probability density was updated using Bayes' rule. The presented solution suggested making the next look in the search cell that provided the maximum value of the incremental search energy and S/N payoff ratios (target cumulative probability of detection increase divided by search effort expenditure increase) for all cells and maximizing the duty factor of each cell.

In Charlish et al. [2011] the authors introduced the Continuous Double Auction Parameter Selection (CDAPS) which managed the MFR resources by utilizing an auction mechanism to select parameters for individual radar tasks. The authors showed that their algorithm performed better than periodic search.

The approach presented in this case-study builds on the approaches described in the literature and the specific novelties are:

- The construction of a probability density function of the undetected target and its implementation using a particle filter.
- The use of two sensor management criteria based on the aforementioned density: a criterion based on KLD and a criterion based on the expected probability of detection.
- It is proven that the two aforementioned criteria are equivalent, in the sense that they lead to the same sensor selection sequence, under certain conditions.

The importance of the latter result lies in the connection that is established between an information-driven criterion (whose practical meaning is difficult to explain) and a criterion that has straightforward practical meaning, i.e. choosing the action that will yield the maximum probability of detecting a target.

2.2.2. SYSTEM SETUP AND PROBLEM FORMULATION

Consider a scenario where an agile sensor searches for one target. This system can be described mathematically by the following (discrete time) state and measurement equations:

$$\mathbf{x}_k = f(\mathbf{x}_{k-1}, \mathbf{w_k}) \tag{2.32}$$

$$\mathbf{x}_0 \sim p(\mathbf{x}_0) \tag{2.33}$$

$$\mathbf{z}_k = \begin{cases} \{\emptyset\} & \text{if no target is present} \\ h(\mathbf{x}_k, u_k, \mathbf{v_k}) & \text{if one target is present} \end{cases} \tag{2.34}$$

where

- $k = 1, 2, \ldots$ is the time index;
- $\mathbf{x}_k \in \mathbb{R}^{N_s}$ is the state of the system at time k and $\mathbf{x}_0$ is the initial state of the system with probability density $p(\mathbf{x}_0)$;
- $\mathbf{w_k} \in \mathbb{R}^{N_s}$ is the process noise with probability density $p_w(\mathbf{w_k})$;
- $u_k \in \mathscr{U}$ is the chosen sensing action, with $\mathscr{U}$ being the set of the available sensing actions. Sensing actions can correspond for example to areas (as in this section) or targets to be observed;
- $\mathbf{z}_k \in \mathbb{R}^{N_z}$ is the received measurement with dimensionality N_z. If there is no target, then there will be no measurement and therefore $\mathbf{z}_k = \{\emptyset\}$, see Eq. (2.34);
- $\mathbf{v_k}$ is the N_z-dimensional measurement noise with probability density $p_v(\mathbf{v_k})$;
- the vector and possibly non-linear function $f(\cdot) : \mathbb{R}^{N_s} \mapsto \mathbb{R}^{N_s}$ describes the dynamics of the system;
- similarly, the vector and possibly non-linear function $h(\cdot) : \mathbb{R}^{N_s} \mapsto \mathbb{R}^{N_z}$ relates the measurement $\mathbf{z}_k$ to the system state $\mathbf{x}_k$ and the sensing action u_k.

The considered problem amounts to finding the best sensing action u_k by optimizing a user-defined criterion. Subsequently, the chosen sensing action is used for solving the attached filtering problem of determining the posterior probability density function $p(\mathbf{x}_k|\mathbf{Z}_{1:k}, \mathbf{U}_{1:k})$ that describes where the target might be. The measurement history is denoted by $\mathbf{Z}_{1:k} = \{\mathbf{z}_1, ..., \mathbf{z}_k\}$ and the sensing action history by $\mathbf{U}_{1:k} = \{u_1, ..., u_k\}$.

2.2.3. PROPOSED SOLUTION

The described problem is solved by employing the recursive Bayesian estimation approach implemented by a particle filter and using quantities of the running particle filter for evaluating the criterion to be optimized.

RECURSIVE BAYESIAN ESTIMATION

Given a probability density function $p(\mathbf{x}_{k-1}|\mathbf{Z}_{1:k-1}, \mathbf{U}_{1:k-1})$, in the recursive Bayesian estimation context the prediction step is performed using the Chapman-Kolmogorov equation:

$$p(\mathbf{x}_k|\mathbf{Z}_{1:k-1}, \mathbf{U}_{1:k-1}) = \int p(\mathbf{x}_k|\mathbf{x}_{k-1})\, p(\mathbf{x}_{k-1}|\mathbf{Z}_{1:k-1}, \mathbf{U}_{1:k-1})\, \mathrm{d}\mathbf{x}_{k-1} \tag{2.35}$$

where $p(\mathbf{x}_k|\mathbf{x}_{k-1})$ is determined by the kinematic model of the target.

Then the predictive density $p(\mathbf{x}_k|\mathbf{Z}_{1:k-1}, \mathbf{U}_{1:k-1})$ is updated with the received measurement $\mathbf{z}_k$ using Bayes' rule

$$p(\mathbf{x}_k|\mathbf{Z}_{1:k}, \mathbf{U}_{1:k}) = \frac{p(\mathbf{z}_k|\mathbf{x}_k, u_k) \cdot p(\mathbf{x}_k|\mathbf{Z}_{1:k-1}, \mathbf{U}_{1:k-1})}{p(\mathbf{z}_k|\mathbf{Z}_{1:k-1}, \mathbf{U}_{1:k})} \tag{2.36}$$

$$\propto p(\mathbf{z}_k|\mathbf{x}_k, u_k) \cdot p(\mathbf{x}_k|\mathbf{Z}_{1:k-1}, \mathbf{U}_{1:k}) \tag{2.37}$$

where $p(\mathbf{z}_k|\mathbf{x}_k, u_k)$ is the likelihood function and

$$p(\mathbf{z}_k|\mathbf{Z}_{1:k-1}, \mathbf{U}_{1:k}) = \int p(\mathbf{z}_k|\mathbf{x}_k, u) \cdot p(\mathbf{x}_k|\mathbf{Z}_{1:k-1}, \mathbf{U}_{1:k-1})\, \mathrm{d}\mathbf{x}_k \tag{2.38}$$

is a normalizing constant which in practice does not have to be calculated if a particle filter is used.

A standard SIR particle filter, see Ristic et al. [2004], is used for approximating Equations (2.35) and (2.36) with N particles $\mathbf{x}_k^i$ and corresponding weights q_k^i such that the approximation converges to the true posterior distribution $p(\mathbf{x}_k|\mathbf{Z}_{1:k}, \mathbf{U}_{1:k})$ as $N \to \infty$, see Hu et al. [2008].

DYNAMICAL MODEL

The state of the system is assumed to be 4-dimensional, describing the position and velocity of the target in Cartesian coordinates

$$\mathbf{x} = [x \;\; v_x \;\; y \;\; v_y]^\mathsf{T} \in \mathbb{R}^4 \tag{2.39}$$

The following target dynamics are also assumed:

$$\mathbf{x}_k = f(\mathbf{x}_{k-1}, \mathbf{w_k}) = F\mathbf{x}_{k-1} + \mathbf{w_k} \tag{2.40}$$

where:

$$\mathbf{w_k} \sim \mathcal{N}(\mu, \Sigma)$$

$$F = \begin{bmatrix} 1 & T & 0 & 0 \\ 0 & 1 & 0 & 0 \\ 0 & 0 & 1 & T \\ 0 & 0 & 0 & 1 \end{bmatrix}, \qquad \Sigma = \begin{bmatrix} b_x T^3/3 & b_x T^2/2 & 0 & 0 \\ b_x T^2/2 & b_x T & 0 & 0 \\ 0 & 0 & b_y T^3/3 & b_y T^2/2 \\ 0 & 0 & b_y T^2/2 & b_y T \end{bmatrix}$$

and $b_x = b_y$ are the power spectral densities of the acceleration noise in the $x-y$ direction, T is the sampling time and $\mu = [0\ 0\ 0\ 0]^\mathsf{T}$ is the mean of the Gaussian noise.

MEASUREMENT MODEL AND ITS USE IN THE UPDATE STEP

This case-study considers the search for an undetected target. This implies that no targets have been detected or equivalently that the measurement (i.e. detections) vector $\mathbf{z}_k$ is *always* an empty set (see Eq. 2.34) and the measurement history is a vector of empty sets. Furthermore, it is assumed that no false alarms are present:

$$\mathbf{Z}_{1:k-1} = \{\emptyset, \emptyset, \ldots\} \tag{2.41}$$

Therefore, if the probability of detecting the target when performing sensing action u_k is defined as $P_D(\mathbf{x}_k, u_k) \in (0, 1)$ then the likelihood function becomes

$$p(\mathbf{z}_k|\mathbf{x}_k, u_k) = p(\mathbf{z}_k = \emptyset|\mathbf{x}_k, u_k) = 1 - P_D(\mathbf{x}_k, u_k) \tag{2.42}$$

This form of likelihood function is referred to in the literature as *Negative Information*, see Koch [2007].

From now on $\mathbf{z}_k = \emptyset$ and $\mathbf{Z}_{1:k-1} = \{\emptyset, \emptyset, \ldots\}$ will be skipped in the notation for simplicity reasons and $p(\mathbf{x}_k|\mathbf{U}_{1:k})$ will be used.

Given the aforementioned simplification, the prediction step in Eq. (2.35) becomes:

$$p(\mathbf{x}_k|\mathbf{U}_{1:k-1}) = \int p(\mathbf{x}_k|\mathbf{x}_{k-1})\ p(\mathbf{x}_{k-1}|\mathbf{U}_{1:k-1})\,\mathrm{d}\mathbf{x}_{k-1} \tag{2.43}$$

and the update step in Eq. (2.36) becomes:

$$p(\mathbf{x}_k|\mathbf{U}_{1:k}) = \frac{[1-P_D(\mathbf{x}_k,u_k)]\ p(\mathbf{x}_k|\mathbf{U}_{1:k-1})}{\mathscr{C}} \tag{2.44}$$

$$\propto [1-P_D(\mathbf{x}_k,u_k)]\ p(\mathbf{x}_k|\mathbf{U}_{1:k-1}) \tag{2.45}$$

where $\mathscr{C} = \int [1-P_D(\mathbf{x}_k,u_k)]\ p(\mathbf{x}_k|\mathbf{U}_{1:k-1})\,\mathrm{d}\mathbf{x}_k$ is a normalizing constant that does not need to be calculated because a particle filter is used.

SENSOR MANAGEMENT CRITERIA

Any knowledge about the location of the undetected target is represented by a probability density function and consequently, the uncertainty about this knowledge (or the information gain by means of performing search) can be conveniently described in the information theory context.

The expected KLD is used in order to contribute to the ongoing discussion on whether task-based or information-driven criteria should be used in sensor management and what the practical interpretation of the latter is (a more elaborate discussion on this subject can be found in Aoki et al. [2011]). The maximum expected KLD is compared to a practical (task-based) criterion that selects the search action that yields the maximum expected probability of detecting the target.

In all the following formulas for the particle approximations it holds that the weights of all particles $\mathbf{x}_k^i$ are $q_k^i = 1/N$, where N is the number of particles, because resampling is performed at every time step and that particles $\mathbf{x}_k^i, \mathbf{x}_k^j$ are distributed according to $p(\mathbf{x}_k|\mathbf{U}_{1:k-1})$, i.e. $\mathbf{x}_k^i, \mathbf{x}_k^j \sim p(\mathbf{x}_k|\mathbf{U}_{1:k-1})$.

MAXIMUM EXPECTED KULLBACK-LEIBLER DIVERGENCE

In this case-study, the maximum expected KLD is chosen instead of the conditional entropy because its computation is less expensive, see discussion in Subsec. 1.2.3. The sensor management criterion is:

$$\begin{aligned} u_k &= \arg\max_u \mathrm{E}_{\mathcal{Z}}\left\{\mathrm{KLD}\left[p(\mathbf{X}_k|u,\mathbf{U}_{1:k-1})||p(\mathbf{X}_k|\mathbf{U}_{1:k-1})\right]\right\} \\ &= \arg\max_u \left\{\mathrm{KLD}\left[p(\mathbf{X}_k|u,\mathbf{U}_{1:k-1})||p(\mathbf{X}_k|\mathbf{U}_{1:k-1})\right]\right\} \end{aligned} \tag{2.46}$$

where $\mathbf{X}_k$ is the random variable that denotes the state of the target at time k.

The expectation over the measurement space $\mathcal{Z}$ is trivial and not shown in Eq. (2.46) because of the assumption that the measurement is always an empty set, see Eq. (2.34).

With some manipulations, the expression for the KLD in this case-study becomes:

$$\begin{aligned} &\mathrm{KLD}\left[p(\mathbf{X}_k|u,\ \mathbf{U}_{1:k-1})||p(\mathbf{X}_k|\mathbf{U}_{1:k-1})\right] \\ &\quad = \int \frac{1-P_D(\mathbf{x}_k,u)}{\mathscr{C}} \log\left(\frac{1-P_D(\mathbf{x}_k,u)}{\mathscr{C}}\right) p(\mathbf{x}_k|\mathbf{U}_{1:k-1})\,\mathrm{d}\mathbf{x}_k \end{aligned} \tag{2.47}$$

where $\mathbf{x}_k$ is the state realization at time k. The particle approximation of Eq. (2.47) is given by:

$$\begin{aligned}\mathrm{KLD}\left[p(\mathbf{X}_k|u,\mathbf{U}_{1:k-1}) \;||p(\mathbf{X}_k|\mathbf{U}_{1:k-1})\right] \\ \approx \frac{1}{N}\sum_{i=1}^{N}\left\{\frac{1-P_D(\mathbf{x}_k^i,u)}{\hat{\mathscr{C}}}\log\left(\frac{1-P_D(\mathbf{x}_k^i,u)}{\hat{\mathscr{C}}}\right)\right\} \qquad (2.48)\end{aligned}$$

$$\begin{aligned}\text{where}\quad \mathscr{C} = \int\left[1-P_D(\mathbf{x}_k,u)\right]\cdot p(\mathbf{x}_k|\mathbf{U}_{1:k-1})\,\mathrm{d}\mathbf{x}_k \\ \approx \frac{1}{N}\sum_{j=1}^{N}\left\{1-P_D(\mathbf{x}_k^j,u)\right\} = \hat{\mathscr{C}} \qquad (2.49)\end{aligned}$$

and $\mathbf{x}_k^i, \mathbf{x}_k^j \sim p(\mathbf{x}_k|\mathbf{U}_{1:k-1})$.

MAXIMUM EXPECTED PROBABILITY OF DETECTION

Even though the use of a criterion based on the KLD is motivated by its equivalence to the conditional entropy (for sensor management purposes), it is not easy to explain its practical meaning, see the discussion in Subsec. 1.2.3. For this reason, the usage of criteria that have practical operational meaning is explored. The criterion chosen from this set of criteria suggests performing the sensing action that yields the maximum expected probability of detecting the target. The choice of this specific criterion has been motivated by the works presented in White et al. [2008]; Boers et al. [2008].

Given a probability density function $q(\mathbf{x})$ that describes where the target might be and the probability of detection function $P_D(\mathbf{x},u)$ that depends on the states $\mathbf{x}$ of the target and the sensing action u, the probability of detecting the target when action u is performed is given by:

$$\hat{P}_D = \int P_D(\mathbf{x},u)\; q(\mathbf{x})\,\mathrm{d}\mathbf{x} \qquad (2.50)$$

In the considered scenario, the predictive density $p(\mathbf{x}_k|\mathbf{U}_{1:k-1})$ is used in order to define a criterion that selects the sensing action u_k that yields the maximum probability of detecting the target:

$$u_k = \arg\max_u\left[\int P_D(\mathbf{x}_k,u)\; p(\mathbf{x}_k|\mathbf{U}_{1:k-1})\,\mathrm{d}\mathbf{x}_k\right] \qquad (2.51)$$

and its particle approximation is:

$$u_k \approx \arg\max_u\left[\frac{1}{N}\sum_{i=1}^{N}P_D(\mathbf{x}_k^i,u)\right]\;,\;\; \mathbf{x}_k^i \sim p(\mathbf{x}_k|\mathbf{U}_{1:k-1}) \qquad (2.52)$$

2.2.4. PROOF OF EQUIVALENCE OF THE TWO CRITERIA

In the simplest scenario, where the probability of detecting the target is constant, it can be proven that the two criteria produce the same sensor management results. The sensor management results depend on the probability of detection and the probability mass in each sector but not on the number of the sensing actions or the size of the

search area. The mathematical proof can be found in Katsilieris and Boers [2012] and only a graphical explanation of the proof is provided here.

In a scenario where the probability of detection is constant, the sensor would only have to choose the direction towards where to perform search. Because a particle filter is used, each direction (or sector) $u \in U$ contains a certain number of particles n_u such that $\sum_{u=1}^{N_U} n_u = N$. Another interpretation of n_u is that it represents the percentage of probability mass that is located in each sector u, assuming that all particles have equal weights.

The particle approximations of the two criteria can then be simplified by splitting the sums in two parts: a part where the probability of detection is P_D (i.e. in the chosen sector) and a part where it is zero (i.e. in all the other sectors).

The KLD is then given by:

$$\begin{aligned}
&\mathrm{KLD}\left[p(\mathbf{X}_k|u,\mathbf{U}_{1:k-1}) \;||p(\mathbf{X}_k|\mathbf{U}_{1:k-1})\right] \\
&\qquad \approx \frac{1}{N}\sum_{j=1}^{N}\frac{1-P_D(\mathbf{x}_k^j,u_k)}{\hat{\mathscr{C}}}\log\left(\frac{1-P_D(\mathbf{x}_k^i,u_k)}{\hat{\mathscr{C}}}\right) \\
&\qquad = \frac{1}{N}\left\{\sum_{j=1}^{n_U}\frac{1-P_D}{\hat{\mathscr{C}}}\log\left(\frac{1-P_D}{\hat{\mathscr{C}}}\right)+\sum_{j=1}^{N-n_U}\frac{1}{\hat{\mathscr{C}}}\log\left(\frac{1}{\hat{\mathscr{C}}}\right)\right\} \\
&\qquad \cdots \\
&\qquad = \frac{n_u(1-P_D)\log(1-P_D)}{N-n_uP_D}+\log(N)-\log(N-n_uP_D)
\end{aligned} \tag{2.53}$$

and the sector that maximizes Eq. (2.53) is chosen.

Accordingly, the second criterion can be simplified as

$$u_k \approx \arg\max_u\left[\frac{1}{N}\sum_{i=1}^{N}P_D(\mathbf{x}_k^i,u)\right] = \arg\max_u\left[\frac{1}{N}\sum_{i=1}^{n_u}P_D+\frac{1}{N}\sum_{i=1}^{N-n_u}0\right] = \arg\max_u\left[\frac{n_u}{N}P_D\right] \tag{2.54}$$

Figure 2.5a shows the behavior of the maximum probability of detection based criterion as a function of n_u for various values of the probability of detection. It can be easily noticed that the criterion is a monotonically increasing function of n_u for any value of P_D. This means that the sector that contains the most particles, or equivalently the most probability mass, is always chosen. This can also be inferred by Eq. (2.54) because N, P_D are constants (known in advance) and therefore they do not affect the sensor management results.

Figure 2.5b shows the behavior of the KLD-based sensor management criterion as a function of n_u for various values of the probability of detection. It is easy to see that it is a monotonically increasing function of n_u for any value of P_D up to a maximum point maxKLD that actually depends on P_D. To be more precise, maxKLD is assumed for $n_u^{max} \in (N/2, N)$ and the exact value of n_u^{max} depends on P_D.

Therefore, if n_u is lower than n_u^{max} for every $u \in U$ then the two criteria are equivalent because they are both monotonically increasing functions of n_u for any value of P_D. This can be noticed at Fig. 2.5a and Fig. 2.5b.

On the other hand, if n_u is greater than n_u^{max} then the value of $\mathrm{KLD}(n_u, P_D)$ must be compared to the worst case scenario value of $\mathrm{KLD}(N-n_u, P_D)$ and it actually holds that

$$\mathrm{KLD}(n_u, P_D) > \mathrm{KLD}(N-n_u, P_D) \ , \ n_u \in (n_u^{max}(P_D), N) \tag{2.55}$$

Therefore, the two criteria are still equivalent.

The claim that Eq. (2.55) refers to the worst case scenario can be explained by the fact that $N-n_u \in (0, N/2)$ holds. Therefore, it also holds that

$$\mathrm{KLD}(N-n_u, P_D) > \mathrm{KLD}(n, P_D) \tag{2.56}$$

for any number of particles n that satisfies $N-n_u > n$ because KLD is a monotonically increasing function for any $n \in (0, N/2)$ and for any P_D.

The conclusion that can be drawn is that both criteria choose the sector that contains the highest probability mass. Equivalently, if a particle filter approximation is used, they both choose to search the sector with the largest number of particles.

2.2.5. SIMULATIONS

CONSTANT P_D

The theoretical results are illustrated by performing 50 Monte Carlo simulations where the sensor searches in 8 sectors with constant $P_D \in (0,1)$ for $k = 1, \ldots, 160$ sec.

An example of such a scenario, where a particle filter approximates the posterior density, is depicted in Fig. 2.6. The sensor is located at the origin of the axes and it has to choose one of the 8 sectors for performing search. Therefore, the set of sensing actions is equal to set of sectors (8 sectors in this example): $\mathscr{U} = \{1, 2, .., 8\}$. The probability of detection in the chosen sector is P_D and in all the other sectors is zero. The physical interpretation of this assumption is that the target cannot be detected in sectors that are not searched.

The density is initialized at $k = 0$ by uniformly distributing particles in an disk of 100 km radius. The velocities v_x and v_y are chosen such that the radial speed of the targets is uniformly distributed in [0, 400] m/s and they move towards the radar. This initialization process resembles a real life scenario of the moment when the sensor is turned on and there is no information about the target's location, meaning that the target might be anywhere.

For the motion model, $b_x = b_y = 2\ (\mathrm{m/s^2})^2$ are chosen as the power spectral densities of the acceleration noise in the $x-y$ direction and $T = 1$ sec as the sampling time.

Furthermore, target birth is modeled at the border of the field of view of the sensor in order to take into account the fact that the target might have not entered the area yet.

In the simulations, the number of particles is varied such that $N = (5, 10, \ldots, 100) \cdot 10^3$ in order to study the influence of using limited number of particles. The ranking of the sensing actions (in this case sectors) and the percentage of same chosen sensing actions (top ranked sensing actions) of the two criteria are compared.

Figure 2.7 shows that as the number of particles increases, the percentage of same chosen sensing actions by both criteria approaches 100%. Figure 2.8 shows that the percentage of differently ranked sensing actions approaches 0% as the number of particles increases. Therefore, the experimental results support the theoretical result that the two sensor management criteria are equivalent.

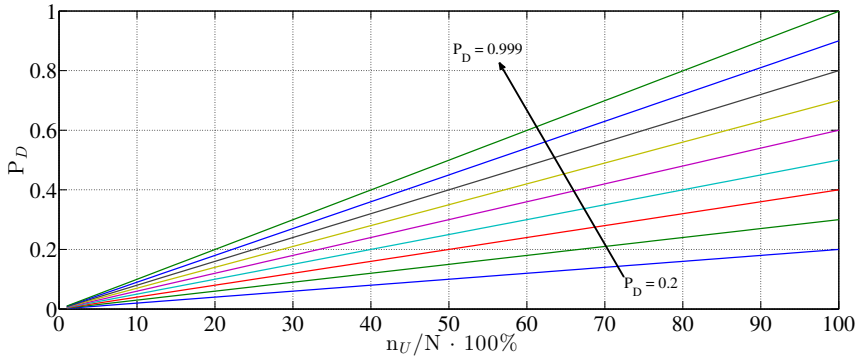

(a) Maximum probability of detecting the target.

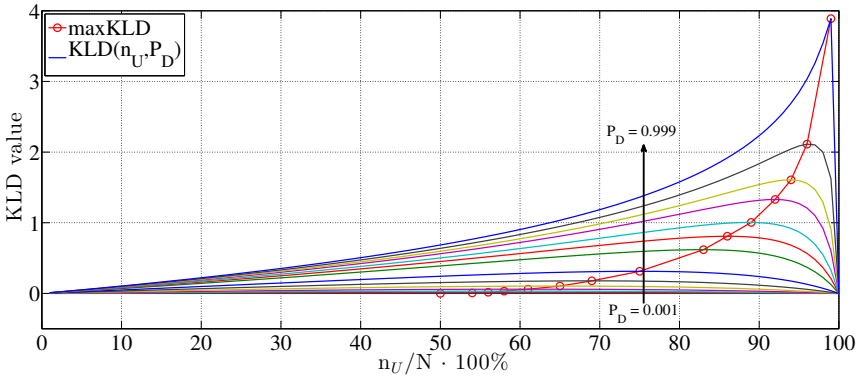

(b) Maximum expected KLD.

Figure 2.5: The behavior of the proposed criteria as a function of n_u for different values of P_D.

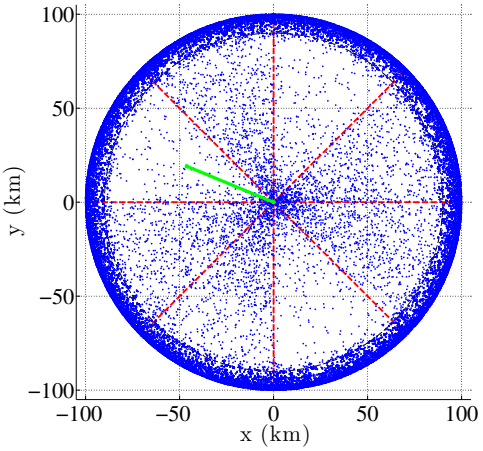

Figure 2.6: An example of the density that describes where the undetected target might be. A radar searches with constant $P_D < 1$ an area of 100 km radius divided in 8 sectors.

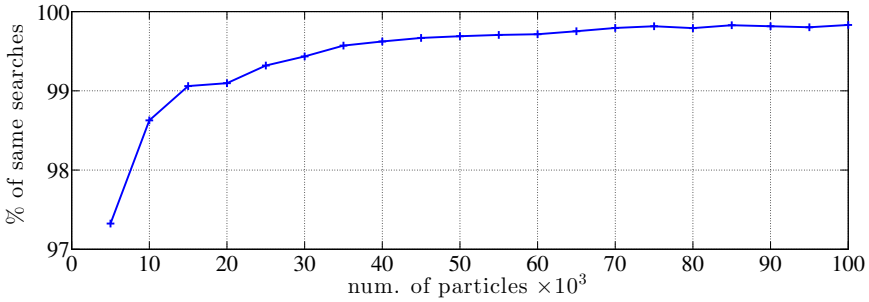

Figure 2.7: The percentage of same chosen sensing actions as a function of the number of particles used in the simulations. The results are averaged over 50 Monte Carlo runs and over the duration of each simulated scenario (160 sec).

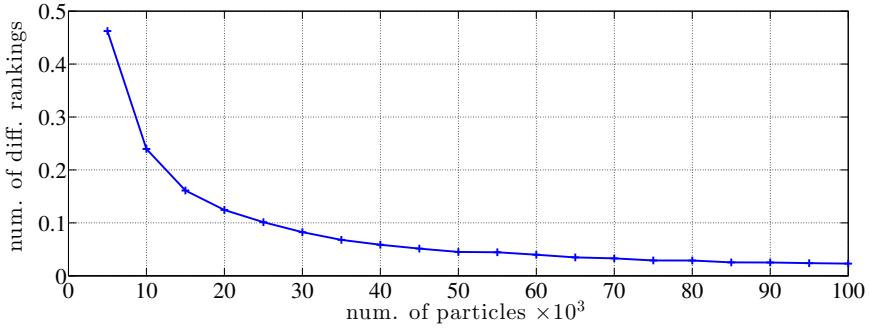

Figure 2.8: The percentage of differently ranked sensing actions as a function of the number of particles used in the simulations. The results are averaged over 50 Monte Carlo runs and over the duration of each simulated scenario (160 sec).

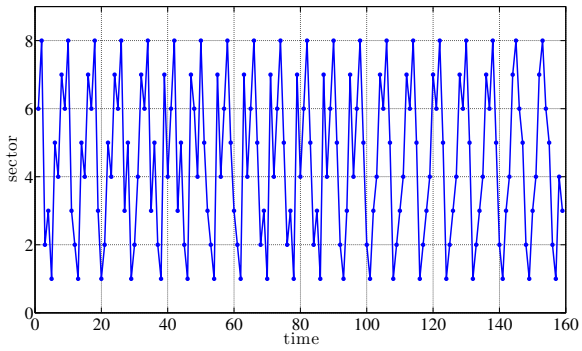

Figure 2.9: The search pattern produced by the KLD-based criterion for a scenario with constant P_D. It can be noticed that there are several repetitive sub-patterns.

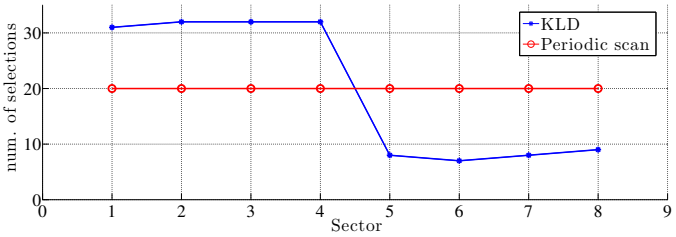

Figure 2.10: Search time per sector when the target is expected from the north with 80% probability.

An interesting point is that both criteria produce search patterns that are somehow repetitive and this becomes more obvious as the number of particles used in the simulations increases. Figure 2.9 shows an example of a search pattern where this phenomenon can be observed. A reason for the search pattern not to be totally repetitive is the randomness induced by the particle filter itself. There is no measurement-induced uncertainty because of the assumption that the measurements indicate that no target has been detected, see subsection 2.2.3.3.

TAKING INTO ACCOUNT EXTERNAL INFORMATION

Consider now a scenario where the target is expected to be in the 4 northern sectors with 80% probability and in the 4 southern with 20%. All the other parameters in the simulation are the same as the ones used in the previous example.

Figure 2.10 demonstrates the adaptiveness of the KLD-based criterion that focuses on the 4 northern sectors. The task based criterion has (but is not shown) exactly the same behavior because the probability of detection is assumed to be constant. On the other hand, the simple approach of periodic search wastes time and resources in sectors where the target is not expected to be found with high probability. This is an improvement because the target would be detected faster if the presented criteria are used instead of periodic search since they spend more search effort on sectors with higher probability of target existence.

NONCONSTANT P_D

In the case of nonconstant P_D, it can be assumed that the sensor models the behavior of an MFR. Consequently, P_D depends on the RCS of the target and on its distance from the radar.

The rest of the parameters of the scenario are the same, meaning that the radar performs search in 8 sectors and that a particle filter is employed with the same dynamical model for the target.

For each particle in the sector to be searched, first the radar equation is used for evaluating the SNR_i:

$$\begin{aligned} SNR_i \text{ (dB)} = {} & 10\log(P_{peak}) + 10\log(T_{pulse}) + 20\log(\lambda) + 10\log(RCS_i) + G_{tx} + G_{rx} \\ & - 10\log(k_{Boltzman}) - 10\log(Temp) - F\cdot L - 10\log[r_i^4(4\pi)^3] \end{aligned} \tag{2.57}$$

and then the Swerling I case is used for evaluating the corresponding $P_D(i)$, as given in Skolnik [2002]:

$$P_D(i) = P_{FA}^{1/(1+SNR_i)} \tag{2.58}$$

where: $r_i = \sqrt{x_i^2 + y_i^2}$, $\lambda = 0.03$ m, $P_{peak} = 100$ kWatts, $T_{pulse} = 162$ μsec, $G_{tx} = G_{rx} = 35$ dB, $k_{Boltzman} = 1.37\cdot 10^{-23}$, $Temp = 300$ Kelvin, $F\cdot L = 1.1$ dB losses, probability of false alarms $P_{FA} = 1.4\cdot 10^{-9}$ and $i = 1,2,\ldots,N$.

Then Eq. (2.46), (2.48) and (2.49) are used for the KLD-based criterion and Eq. (2.52) for the maximum probability of detection criterion.

In the experiment, the number of particles is varied such that $N = (5,10,\ldots,100)\cdot 10^3$ and the target's RCS is varied such that $RCS = [1\ 10\ 10^2\ 10^3\ 10^4\ 10^5]$ m^2. The ranking of sensing actions (again: sectors) and the percentage of same chosen sensing actions (top ranked sectors) of the two criteria are compared.

In Fig. 2.11a through 2.12c it can be noticed that as the number of particles and the RCS increase, the percentage of different rankings approaches 0% and the percentage of same chosen sensing actions approaches 100%. These results indicate that the two criteria are equivalent for high RCS targets and as the number of particles increases in this more involved scenario. Furthermore, the existence of repetitive search sub-patterns was noticed again.

Figure 2.13 shows how the computation time difference between the two criteria scales as a function of the number of particles that are used for approximating the density that describes where the undetected target can be. It can be observed that the KLD-based criterion requires linearly more computation time than the task-based criterion, which seeks to maximize the probability of detecting the target.

2.2.6. CONCLUSIONS

Two fundamentally different sensor management criteria for performing search for a target have been compared and actually shown to be equivalent, under certain conditions. This result has two interesting and important implications:

1. a practical interpretation of an information-driven criterion, i.e. maximizing the expected KLD between the predictive and the posterior density, can be given in

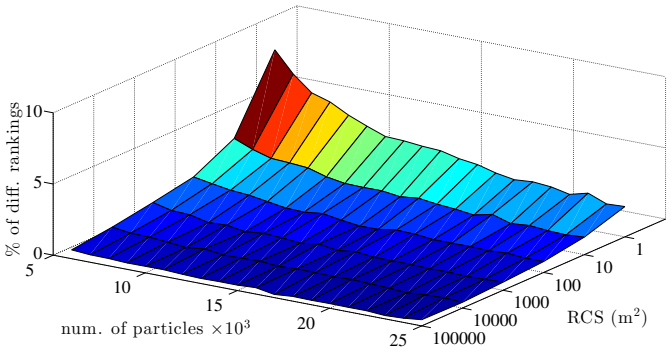

(a) 3D view

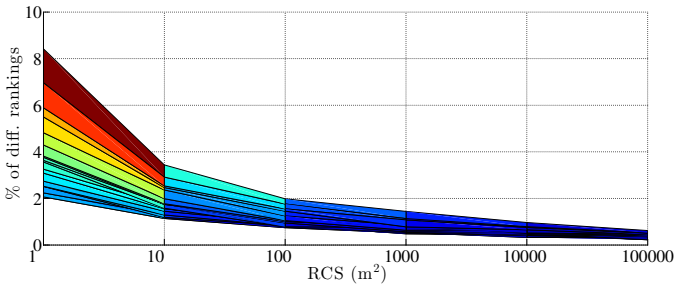

(b) X-view

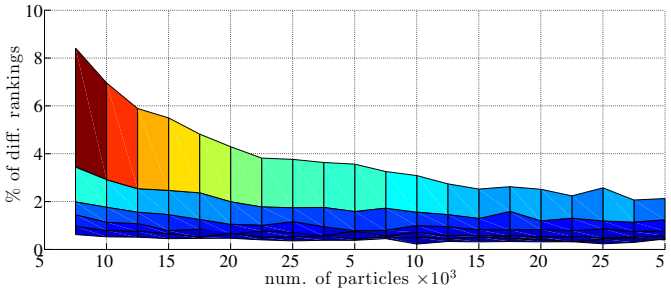

(c) Y-view

Figure 2.11: The percentage of differently ranked sensing actions as a function of the number of particles used for simulation and of the RCS. The results are averaged over 20 Monte Carlo runs and over the duration of each simulated scenario (160 sec).

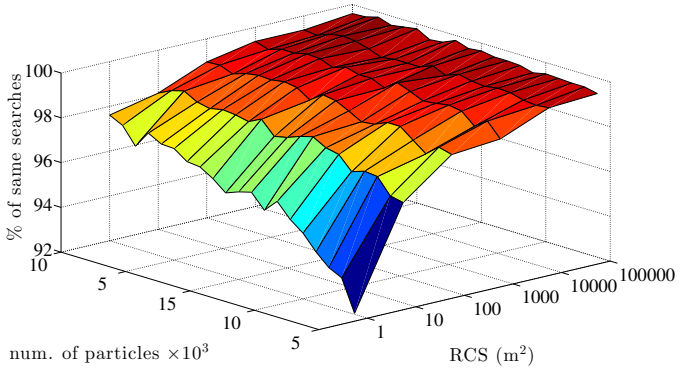

(a) 3D view

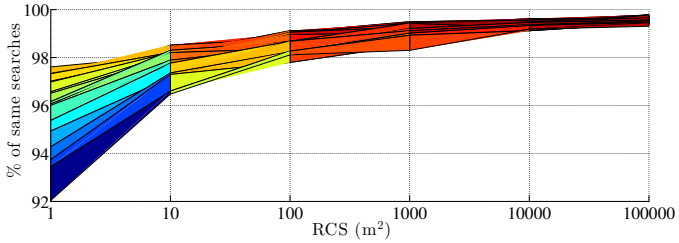

(b) X-view

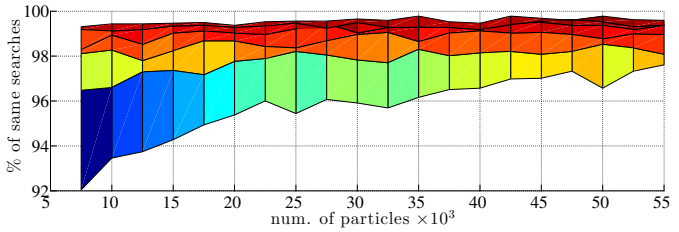

(c) Y-view

Figure 2.12: The percentage of same chosen sensing actions as a function of the number of particles used for simulation and of the RCS. The results are averaged over 20 Monte Carlo runs and over the duration of each simulated scenario (160 sec).

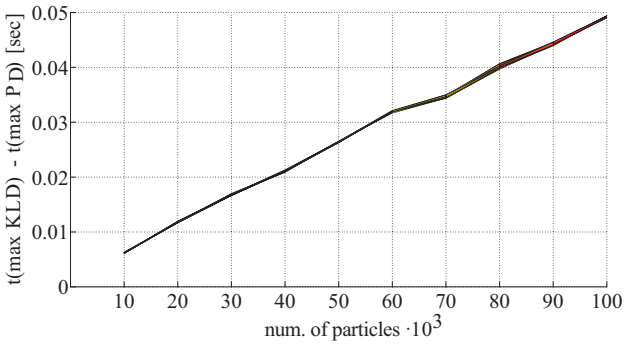

Figure 2.13: The computation time difference between the two compared criteria plotted as a function of the number of particles used.

the search context. Performing the search action that maximizes the KLD is the same as performing the search action that yields the maximum expected probability of detecting the target, when the probability of detection is constant.

2. the criterion which is based on the highest probability of detection not only has practical meaning but it is also computationally less expensive to implement, see Eq. (2.48) and (2.52). Eq. (2.54) means that the implementation of the criterion boils down to just performing a particle count for determining n_u, since N, P_D are constant and known in advance.

From this case-study it can be concluded that even when it is possible to explain what it means practically to maximize the expected KLD, its use is not always justified. For instance, in the presented examples the KLD has higher computational complexity than the intuitive task-based criterion.

Nevertheless, the compared criteria appear to give different results for low RCS targets. This implies that the criteria are not in general equivalent when the probability of detection varies and this phenomenon worths further attention.

2.3. COMPARISON OF EXISTING SENSOR MANAGEMENT SCHEMES

When selecting a sensor management scheme, several aspects must be considered. Within the context considered in this thesis, a sensor management scheme should provide Bayes-optimal selections, take into account explicitly the user-needs within different operational contexts and have reasonable computational complexity.

Bayes-optimality is a very important aspect of sensor management algorithms. It guarantees that the best solution is obtained given a user-defined loss or reward function that models the operational needs of an operator, also see the discussion in Berger [1980]. Therefore, this thesis focuses on Bayes-optimal approaches.

Similarly, taking into account the user needs is of paramount importance. Ideally, a sensor management algorithm should be adaptive not only with respect to the environment but also with respect to changes in the operational requirements. Consider for example the use of an MFR in an asset-defence context and in an air-traffic-control

context. Does a user have the same operational goals in these two contexts? If not, why would the sensor management algorithm not take that into account?

The requirement on computational complexity arises from practical, implementation considerations. In this thesis, computational complexity is not considered as the driving requirement for selecting a specific scheme but nevertheless, it is taken into account.

Given the requirements discussed above, one can conclude the following for the existing approaches:

HEURISTICS

Heuristics have low computational complexity and take into account both practical and operational aspects. Their main disadvantages are that they do not produce Bayes-optimal solutions and that their behavior can become unpredictable in situations that were not taken into account during design.

TASK-BASED SENSOR MANAGEMENT

Task-based schemes result in Bayes-optimal solutions. Their main disadvantage is that most commonly they optimize quantities that are relevant to the operational goal but not explicitly what the user really needs. Consider for example an air-traffic-control scenario. Minimizing the uncertainty in position and velocity of all aircrafts is beneficial but what an operator is really interested in is whether two aircrafts are going to collide.

Furthermore, it is not straightforward how to aggregate several objectives in a meaningful and mathematically rigorous manner. Consider for example area surveillance. In area surveillance, search for and tracking of multiple targets are performed simultaneously. In this case, how can objectives that are related to either/both search and tracking be aggregated? For instance, how can tracking accuracy (task-based objective function in subsec. 2.1), be aggregated with the probability of detecting new targets in a given region (task-based objective function in Subsec. 2.2)? If a multiobjective optimization problem is formed, then several solutions are obtained that are all equivalent and optimal. Therefore, one still has to solve a decision problem of which sensing action to perform. If, on the other hand, one tries to form a weighted sum, then how can the weights of tracking accuracy and probability of detection be defined in a meaningful manner? This problem arises because probability of detection and track accuracy are non-commensurate.

INFORMATION-DRIVEN SENSOR MANAGEMENT

Information-driven schemes are Bayes-optimal. Nevertheless, they suffer from similar disadvantages as the task-based approaches. That is, how can different objectives functions be aggregated in this context?

Moreover, if information-driven objective functions are used based on the probability density function of the states of a system, e.g. of an aircraft, it is not clear on which aspect of the probability density function the emphasis is placed, see the discussion in Aughenbaugh and La Cour [2008]. And even if an explanation can be found, as in Subsec. 2.2, the computational complexity of the considered information-driven criterion can be higher than the equivalent task-based criterion.

An additional challenge arises when considering objective functions for different operational contexts. For instance, why would the conditional entropy be the best objective function both for air-traffic-control and asset protection[1]?

RISK-BASED SENSOR MANAGEMENT

Risk-based approaches can be either Bayes-optimal, as in Papageorgiou and Raykin [2007], or not, as in Bolderheij [2007]. Their main advantage is that they take into account explicitly the operational goal of a system. Their disadvantage is that they do not focus on managing the uncertainty in the quantities of interest such that an operator can make decisions under lower uncertainty. In Bolderheij [2007], priorities are assigned to tasks and in Papageorgiou and Raykin [2007], the reduction of operational risk is considered. Risk cannot be reduced by the sensor itself but rather with the use of an actuator.

CONCLUSIONS

It can be seen from the comparison above that there is not a single approach that has all the desired properties described in the beginning of Sec. 2.3. This creates a research opportunity for devising a scheme that *a*) is Bayes-optimal; *b*) takes into account explicitly the user requirements in different operational contexts; and *c*) has reasonable computational complexity.

2.4. SUMMARY

This chapter aimed at providing a better insight to the existing sensor management criteria. Special attention was paid to gaining better understanding of the behavior of task-based and information-driven criteria and identifying any differences and similarities that they have. This was of special interest because of the ongoing discussion on whether information-driven criteria can be used as objective functions that can incorporate in a meaningful manner several aspects of interest to the user.

For this reason, objective functions motivated from these two classes were compared in two case-studies. The first case-study focused on PRF selection when tracking a target. The important aspect of this case-study was that the estimated PDF can be multimodal, depending on the motion of the target and the sequence of PRF selections. The second case-study considered the search for an undetected target. The important aspect of this case-study was the update with negative information and the use of the estimated PDF for performing optimal search for targets.

From these case-studies it was concluded that criteria from the task-based and information-driven classes can have very similar behavior and in some cases they can lead to identical sensor selections. The latter result, presented in the second case-study, provided a practical explanation of an information theoretic criterion, albeit in the specific experimental setting. Furthermore, in both case-studies it was verified that using sensor management can lead to improved estimation results as compared to using non-adaptive methods.

The results obtained from the two case-studies were also used in order to compare the task-based and information-driven approaches to other existing approaches to sen-

[1] This question was originally posed to the author by Dr. Hans Driessen and Dr. Yvo Boers.

sor management. The aspects of interest were Bayes-optimality, adaptiveness to different operational contexts and computational complexity of the existing approaches. From the comparison it was concluded that the existing sensor management criteria lack the combination of three desirable properties, i.e. the *Bayes-optimal* allocation of resources *among diverse tasks* while *taking into account explicitly the user-needs* within a given operational context.

The latter conclusions practically means that the existing approaches do not allow for a systematic and mathematically rigorous method to form objective functions that take into account several quantities of interest. Motivated by this conclusion, I developed a novel approach to sensor management that is presented in the following chapter.

3

THREAT-BASED SENSOR MANAGEMENT

The previous chapter presented in detail the existing approaches to sensor management along with two case-studies. These approaches were shown to have certain disadvantages, with the most prominent being that it is not straightforward how to take into account user-needs in different operational contexts. This chapter presents a novel idea for constructing objective functions that directly take into account user-needs according to the operational context at hand and in a Bayes-optimal way.

Section 3.1 presents the threat assessment process and how it is connected to sensor management. Section 3.2 explains how threat can be mathematically modeled depending on the operational context, how the uncertainty in a threat probability density function can be measured and and how it can be used for allocating sensor resources. Section 3.3 presents simulated examples for demonstrating the feasibility and flexibility of the proposed approach. Finally, Section 3.4 concludes this chapter.

3.1. THE THREAT ASSESSMENT PROCESS AND ITS CONNECTION TO SENSOR MANAGEMENT

It is very common in a defense context to assign labels to all present targets according to the threat that they pose to own assets or to mission success[1]. For instance, this set of labels can be defined as $\mathscr{L} = \{\ell_1, \ldots, \ell_{n_D}\}$, where ℓ_i can be “friendly", “neutral" or “hostile". An operator estimates the threat label of each target by observing the overall target behavior and considering the operational context and mission goals. This process is called *threat assessment* and is an integral part of missions in the defense domain. Figures 3.1a and 3.1b demonstrate a threat assessment example. In the presented example,

[1] In order to avoid the confusion between *threat* and *risk*, the terminology used in Romberg [2000] is followed. In Romberg [2000] Romberg describes an approach where objects are sought that threaten valuable assets. Romberg denominates such an object as *threat* and defines *risk* as the expected loss of value due to a possible event caused by a threat. Also see the discussion in [Bolderheij, 2007, Ch. 4.7]

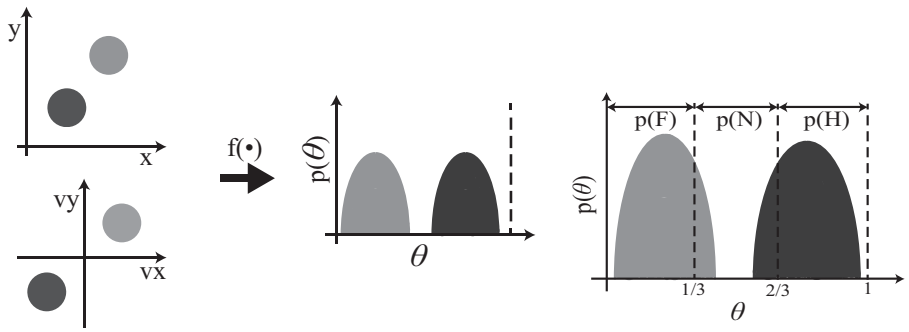

(a) The operator observes the behavior of the targets via their state estimates. The uncertainty in the states is translated in uncertainty in the threat-level θ.

(b) The estimated threat-level θ can be used for labeling the targets with a certain probability.

Figure 3.1: Demonstration of the threat assessment process for two targets, one incoming and one receding.

an operator observes the position and velocity of two targets, estimates their threat-level and assigns a threat label to each target according to the operational context and goals.

In practice, threat assessment is performed based not only on kinematic information but also on additional contextual information. Such contextual information can be, for instance, intelligence about expected threat types and their capability and intent, see for example the discussion and models in Roux and van Vuuren [2007]; Bolderheij et al. [2005]. Here threat is modeled based only on observable kinematic properties of targets. This simplification is motivated by the limitations in modeling all aspects of interest but nevertheless gives a proof of concept of performing sensor management based on the threat-level of targets. In other words, the method proposed in this thesis can be seen as a first step towards JDL level 2/3 sensor management.

In terms of mathematics, the threat that a target poses can be seen as an added state, estimated along with the standard state vector that usually includes target's position and velocity. A threat function $f : \mathscr{X} \mapsto \mathscr{T}$ is defined as a map from the conventional elements of the single target state space (typically 2D/3D position and velocity) $\mathscr{X} = \mathbb{R}^n$ to the elements of single target threat space $\mathscr{T} = [0,1]$ according to an operational context. Minimum threat is denoted by 0 and maximum threat by 1. In multitarget scenarios, each individual target state space is mapped to its individual threat space.

A threat function is the mathematical translation of what an operator classifies as threat. Because threat is a function of random variables, such as the position and velocity of a target, threat θ is also a random variable, whose PDF $p(\theta)$ is found by utilizing the user-defined threat function(s). The threat PDF is important because it can be used for assigning a threat label to a target and for suggesting a course of action to a system operator. In an asset-defense scenario an operator can use the threat PDF in order to decide whether to engage a target or not. In a civilian, air-traffic-control scenario, an operator can use the threat PDF in order to instruct the pilot of an aircraft to change its trajectory such that a collision is avoided. Threat functions for these specific scenarios are presented in the following subsection.

Motivated by the threat assessment process, *I propose selecting the best sensing action such that the uncertainty in the threat-level of targets is managed* instead of allocat-

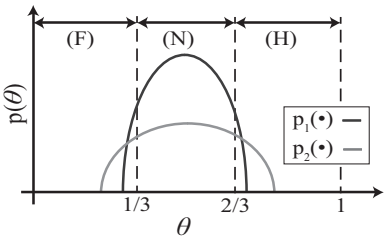

Figure 3.2: An example of why lower uncertainty leads to better decisions.

ing the resources proportionally to the threat-level of each target or managing the uncertainty in the target states. The novelties of the proposed approach are that it can *a*) be adapted to different operational contexts by proper definition of the threat function $f(\cdot)$; and *b*) lead to an operator taking decisions with less uncertainty and consequently with lower operational and Bayesian risk.

In order to demonstrate the importance of managing the uncertainty in threat-level, let us consider a simple example. Two possible threat distributions for a target are shown in Fig. 3.2 and one of the following three labels can be assigned to the target: {friendly (F), neutral (N), hostile (H)}. Each label also implies that a certain course of action will be followed according to the operational context. The label probabilities are $p_i(F) = \int_0^{1/3} p_i(\theta)\,\mathrm{d}\theta$, $p_i(N) = \int_{1/3}^{2/3} p_i(\theta)\,\mathrm{d}\theta$, $p_i(H) = \int_{2/3}^{1} p_i(\theta)\,\mathrm{d}\theta$ where $i = 1,2$. In both cases the label (N) would be chosen because $p_i(N) > \{p_i(F), p_i(H)\}$. Nevertheless, it is obvious that an operator would prefer to assign a threat-label or take an action based on the first threat distribution due to its lower intrinsic uncertainty.

The importance of managing the uncertainty in the threat PDF, as per the proposed approach, is also evident when the Object, Orient, Decide and Act (OODA) loop is considered in a defense context. As discussed in the review paper [Roux and van Vuuren, 2007, Ch. 3,5,8] and the references therein, reduced uncertainty in threat leads to a better OODA loop, which in turn gives a significant advantage over an adversary.

At this point, it is important to point out that the uncertainty in threat can also be scaled in light of its expected value. In many practical applications a slightly uncertain high threat might require more sensor resources than a more uncertain but less threatening target. In this thesis, this effect is acknowledged but for practical purposes it will not be considered.

3.2. MATHEMATICAL MODELING OF THREAT

3.2.1. THREAT DEFINITIONS AND HOW TO AGGREGATE THEM

The mathematical formulation of threat must in principle take into account what an operator classifies as threat in a given operational context and by definition it must hold that $\theta \in [0,1]$.

In order to motivate the proposed approach, three threat functions are given for two examples: one drawn from the defense domain and one from the civilian domain. In both examples, the notions of range to the Closest Point of Approach (CPA) and time to the CPA, see Bolderheij et al. [2005], are utilized. Time and range to CPA are two

quantities that can be used for modeling several aspects of threat, as threat is described in the bibliography. In Bolderheij [2007]; Nilsson et al. [2008] for example, it is stated that when a target approaches another target or an asset of interest then the operator must be notified because this is an event of interest, or in other words, one of the targets is a potential threat. In Roy et al. [2002], time and range to CPA are parts of the situation geometry, situation projection and timing analysis.

The specific examples are intentionally simple but sufficient for demonstrating the versatility of the proposed threat-based approach. Ideally, the system operator can select the modeled aspects of threat, possibly from a library, to be taken into account according to the operational needs. Finally, it is demonstrated how different threat functions can be aggregated in a meaningful manner.

The time and range to CPA for two targets i and j with corresponding state vectors $\mathbf{x}^{(i)} = [x^{(i)} \;\; v_x^{(i)} \;\; y^{(i)} \;\; v_y^{(i)}]^\top$ and $\mathbf{x}^{(j)} = [x^{(j)} \;\; v_x^{(j)} \;\; y^{(j)} \;\; v_y^{(j)}]^\top$ are given by:

$$t_{CPA}^{ij} = -\frac{\Delta_x^{ij}\Delta_{v_x}^{ij} + \Delta_y^{ij}\Delta_{v_y}^{ij}}{\sqrt{\left(\Delta_{v_x}^{ij}\right)^2 + \left(\Delta_{v_y}^{ij}\right)^2}} \tag{3.1}$$

$$d_{CPA}^{ij} = \sqrt{\left(\Delta_x^{ij} + t_{CPA}\Delta_{v_x}^{ij}\right)^2 + \left(\Delta_y^{ij} + t_{CPA}\Delta_{v_y}^{ij}\right)^2} \tag{3.2}$$

where

$$\Delta_{\text{pos}}^{ij} = [\Delta_x^{ij} \;\; \Delta_y^{ij}]^\top = [x^{(i)} \;\; y^{(i)}]^\top - [x^{(j)} \;\; y^{(j)}]^\top \tag{3.3}$$

$$\Delta_{\text{vel}}^{ij} = [\Delta_{v_x}^{ij} \;\; \Delta_{v_y}^{ij}]^\top = [v_x^{(i)} \;\; v_y^{(i)}]^\top - [v_x^{(j)} \;\; v_y^{(j)}]^\top \tag{3.4}$$

Consider an example from the defense domain first, where an operator wants to protect asset j. It is assumed that the threat that is posed by target i to asset j depends on how close and how fast target i can come to asset j. In order to move from the time and range domain to the threat domain, a sigmoid function can be utilized for example[2]:

$$\theta_t^{ij}\left(\mathbf{x}^{(i)};\mathbf{x}^{(j)}\right) = \begin{cases} 1 & \text{if } |t_{CPA}^{ij}| \le t_1 \\ 1 - 2\left(\frac{|t_{CPA}^{ij}| - t_1}{t_0 - t_1}\right)^2 & \text{if } t_1 < |t_{CPA}^{ij}| \le t_{0.5} \\ 2\left(\frac{|t_{CPA}^{ij}| - t_0}{t_0 - t_1}\right)^2 & \text{if } t_{0.5} < |t_{CPA}^{ij}| \le t_0 \\ 0 & \text{if } t_0 < |t_{CPA}^{ij}| \end{cases} \tag{3.5}$$

[2] The specific choice of sigmoid functions is only for demonstration purposes. Any other convenient function could be used by the system designer and the operator.

$$\theta_d^{ij}\left(\mathbf{x}^{(i)};\mathbf{x}^{(j)}\right)=\begin{cases}1 & \text{if } d_{CPA}^{ij}\le d_1\\ 1-2\left(\frac{d_{CPA}^{ij}-d_1}{d_0-d_1}\right)^2 & \text{if } d_1<d_{CPA}^{ij}\le d_{0.5}\\ 2\left(\frac{d_{CPA}^{ij}-d_0}{d_0-d_1}\right)^2 & \text{if } d_{0.5}<d_{CPA}^{ij}\le d_0\\ 0 & \text{if } d_0<d_{CPA}^{ij}\end{cases} \tag{3.6}$$

where $t_1<t_{0.5}<t_0$ and $d_1<d_{0.5}<d_0$ are the points where threat is equal to 1, 0.5 and 0.

Consider now an example from the civilian domain, e.g. an air traffic control application. The operator monitors the behavior of the targets and is interested in whether any two targets will collide with each other. The time and range to CPA can be utilized again in this example since they model conveniently whether and when two targets might collide, also see the discussion in Gore and Corker [2000]; Kastelein [2012] about measures of effectiveness when performing air traffic management. The time and range to CPA among all pairs of targets (i,j), where $i,j=1,\ldots,N$ and $i\neq j$, are considered rather than between each target and an asset. From the $N-1$ different threat values for a target i, the threat value j^* can be selected such that:

$$\theta^*\left(\mathbf{x}^{(i)}\right):=\theta\left(\mathbf{x}^{(i)};\mathbf{x}^{(j^*(i))}\right) \tag{3.7}$$

$$\text{where } j^*(i)=\arg\max_{j(\ldots)}\hat{\theta}\left(\mathbf{x}^{(i)};\mathbf{x}^{(j)}\right)$$

$$\forall i,j\in[1,\ldots,N],\ i\neq j \tag{3.8}$$

$$\text{with}\quad \hat{\theta}(\mathbf{x}^{(i)};\mathbf{x}^{(j(i)})=\int\theta(\mathbf{x}^{(i)};\mathbf{x}^{(j(i)})p\left(\theta(\mathbf{x}^{(i)};\mathbf{x}^{(j(i)})\right)\mathrm{d}\theta(\mathbf{x}^{(i)};\mathbf{x}^{(j(i)}) \tag{3.9}$$

N is the number of targets in the scenario and $p\left(\theta(\mathbf{x}^{(i)};\mathbf{x}^{(j^*(i))})\right)$ is obtained by using Eq. (3.5), (3.6) and the states' PDF. Eq. (3.7) can be evaluated in a Monte Carlo fashion by using samples from the corresponding states' PDFs $p\left(\mathbf{x}^{(i)}\right)$ and $p\left(\mathbf{x}^{(j)}\right)$.

When anomaly detection is of interest, deviation from trajectories or shipping lanes is an important quantity to be taken into account, as discussed in Ristic et al. [2008]; Riveiro and Falkman [2010]. If one would like to model the deviation of a target i from a given trajectory $\mathscr{C}$, then a similar mathematical approach can be followed. A sigmoid function can be used and the three distances $d_0^{\mathscr{C}}<d_{0.5}^{\mathscr{C}}<d_1^{\mathscr{C}}$ from the axis of a trajectory $\mathscr{C}$ must be defined where threat is equal to 0, 0.5 and 1 respectively. Then

$$\theta_{d^{\mathscr{C}}}^{i}\left(\mathbf{x}^{(i)};\mathscr{C}\right)=\begin{cases}1 & \text{if } d_1^{\mathscr{C}}<d_{min}^{i\mathscr{C}}\\ 1-2\left(\frac{d_{min}^{i\mathscr{C}}-d_1^{\mathscr{C}}}{d_0^{\mathscr{C}}-d_1^{\mathscr{C}}}\right)^2 & \text{if } d_{0.5}^{\mathscr{C}}<d_{min}^{i\mathscr{C}}\le d_1^{\mathscr{C}}\\ 2\left(\frac{d_{min}^{i\mathscr{C}}-d_0^{\mathscr{C}}}{d_0^{\mathscr{C}}-d_1^{\mathscr{C}}}\right)^2 & \text{if } d_0^{\mathscr{C}}<d_{min}^{i\mathscr{C}}\le d_{0.5}^{\mathscr{C}}\\ 0 & \text{if } d_{min}^{i\mathscr{C}}\le d_0^{\mathscr{C}}\end{cases} \tag{3.10}$$

where $d_{min}^{i\mathscr{C}}$ is the minimum distance between target i and trajectory $\mathscr{C}$.

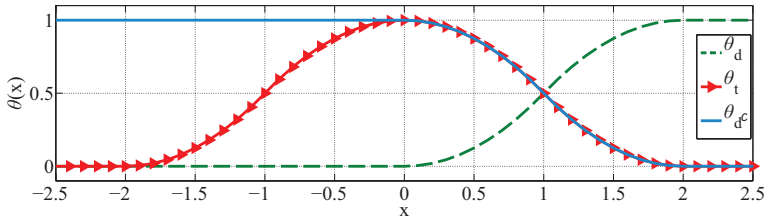

Figure 3.3: Plots of the defined threat functions, for gaining intuition about their shape.

Figure 3.3 demonstrates the plots of the defined threat functions for $[t_1 \;\; t_{0.5} \;\; t_0] = [d_1 \;\; d_{0.5} \;\; d_0] = [d_0^{\mathscr{C}} \;\; d_{0.5}^{\mathscr{C}} \;\; d_1^{\mathscr{C}}] = [0,1,2]$.

Following the procedure described above, all quantities of interest (time and range to CPA, deviation from a given trajectory) have been mapped to the same domain, i.e. threat. In other words, it has been demonstrated how to model mathematically the aspects of threat that are of interest. Moreover, it is meaningful to aggregate them using a weighted sum in order to evaluate the threat-level of a target i:

$$\theta^{i\cdot}\left(\mathbf{x}^{(i)};\cdot\right) = \sum_{l=1}^{M} m_l \theta_l^{ij}\left(\mathbf{x}^{(i)};\cdot\right) \tag{3.11}$$

where m_l is the weight assigned by the operator to $\theta_l^{ij}\left(\mathbf{x}^{(i)};\cdot\right)$ such that $\sum_{l=1}^{M} m_l = 1$. In this way, what would have been a multiobjective optimization problem has been simplified to a simpler but still meaningful single objective problem. The single objective function is the weighted sum of the different aspects of threat. In other words, instead of managing the uncertainty in non-commensurate quantities, such as the time/range to CPA and deviation from a given trajectory, the uncertainty in the threat-level is managed.

Equation (3.11) means that, in principle, a database of different aspects of threat can be created. The operator can then select the necessary aspects of threat $\theta_l^{ij}\left(\mathbf{x}^{(i)};\cdot\right)$ and their corresponding weights m_l such that different needs in different operational contexts are satisfied. The threat definitions that are given here can be combined such that asset protection, air traffic control and maritime surveillance can be performed, to name a few different operational contexts. Furthermore, this is an improvement over the conventional weighted sum approaches because now commensurate quantities, i.e. aspects of threat, are summed.

When multiple targets are present in a scenario, each target has its own threat PDF. In the Random Finite Set (RFS) context, the multitarget threat RFS variable Θ can have the same cardinality distribution $p(|\mathbf{X}|)$, $|\mathbf{X}| \in [0,\ldots,N]$ as the RFS multitarget state variable $\mathbf{X}$, depending on the mathematical definition of threat.

3.2.2. EVALUATING THE UNCERTAINTY IN A THREAT PROBABILITY DENSITY FUNCTION

As discussed in the previous sections, threat can be seen as an added state of each target and has a PDF that can depend, among others, on a target state's PDF and the considered operational context. Therefore, the uncertainty in a threat PDF can be evaluated

using any of the popular approaches: for example, via its covariance or via its entropy (or equivalently for myopic sensor management purposes, the KLD). The best choice remains an open question, as explained in the introduction.

The key difference is that the commonly used measures of uncertainty in a PDF are not applied to the estimated target states' PDF but rather in the estimated threat PDF that takes into account the operational needs of an operator.

As a reminder, *a*) when a task-based approach is used, the best sensing action can be given, for example, by the trace of the target states' PDF covariance matrix; and *b*) when an information-driven approach is used, the best sensing action can be given by the conditional entropy of the target states' PDF or by the expected KLD between the posterior and the predicted target states' PDFs. The term "sensing action" can refer to the target to be observed (as in this chapter), the area to be observed and/or specific sensing parameters, such as PRF.

On the other hand, when the proposed threat-based approach is used, the best sensing action can be given by Eq. (3.12), (3.13) or (3.14) for example. In these equations, choosing sensing action i corresponds to observing target i.

$$i_k = \arg\min_i \left\{ \mathrm{E}_{\mathcal{Z}} \left[\sum_{n=1}^{N} \left(\sigma_{k|k}^{(n)}(i) \right)^2 \right] \right\} \tag{3.12}$$

$$i_k = \arg\max_i \mathrm{E}_{\mathcal{Z}} \left\{ \mathrm{KLD} \left[p\left(\Theta_k(i)|\mathbf{z}_k\right) \middle| \middle| p\left(\Theta_k\right) \right] \right\} \tag{3.13}$$

$$i_k = \arg\min_i \mathrm{E}_{\mathcal{Z}} \left\{ H\left[p\left(\Theta_k(i)|\mathbf{z}_k\right) \right] \right\} \tag{3.14}$$

where $\left(\sigma_{k|k}^{(n)}(i)\right)^2$ is the variance of single target threat $\theta_k^{(n)}(i)$ of target n, $\Theta_k(i)$ is the multitarget threat, $H\left[p\left(\Theta_k(i)\right)\right]$ is the entropy of $p\left(\Theta_k(i)\right)$ and $\sigma_{k|k}^{(n)}(i)$, $p\left(\Theta_k(i)|\mathbf{z}_k\right)$ depend on the target i that is observed.

If an analytical expression cannot be found for Eq. (3.12), (3.13) and (3.14), they can be implemented in a Monte Carlo fashion by sampling from the PDF of the corresponding target. In this case, Eq. (3.13) can be evaluated using the *k*th Nearest Neighbour (k-NN) method presented in Chou et al. [2011] and Eq. (3.14) can be evaluated using the k-NN method presented in Ajgl and Šimandl [2011].

3.3. SIMULATED EXAMPLES

In the following subsections, it is demonstrated that the proposed approach is easy to adapt to operational requirements and that it gives meaningful sensor selections. This is done by taking into account different aspects of threat in different contexts and discussing the corresponding sensor management results in a single- and in a multi-target scenario.

The threat-based approach is also compared to a task-based approach to sensor management. For both approaches, the trace of the covariance matrix is used as measure of uncertainty because it is intuitively easier to understand than KLD or entropy. The chosen task-based approach selects the sensing action that minimizes the expected trace of the (multi)target *states'* covariance matrix whereas, the threat-based approach

selects the sensing action that minimizes the expected trace of the (multi)target *threat* covariance matrix.

3.3.1. ASSUMPTIONS

The threat-based sensor management approach is presented in a target tracking context. In order to focus on the sensor management instead of the filtering problem, the following assumptions are made:

- the targets are well separated and for simplicity, their PDFs are treated as decoupled such that one filter per target can be used;
- the multitarget state vector $\mathbf{X}$ is the concatenation of single target state vectors $\mathbf{x}$ and the multitarget covariance matrix is a block-diagonal matrix whose elements are single-target covariance matrices P;
- the targets move in the 2-dimensional $(x-y)$ space;
- there is one sensor that provides range and bearing measurements of the selected target and/or of the selected accuracy;
- there are no false alarms and there is no detection uncertainty, i.e. the probability of detection is one.

These assumptions are rather limiting but necessary for providing a proof of concept of the proposed approach. In the following chapters, these assumptions are relaxed and the proposed approach is applied in more challenging multitarget scenarios with detection uncertainty and presence of spurious measurements.

3.3.2. FILTERING PARAMETERS AND SENSOR SELECTION

The motion of each target[3] in the Cartesian coordinates is modeled using a nearly constant velocity model, as presented in Li and Jilkov [2003]:

$$\mathbf{x}_k = F\mathbf{x}_{k-1} + \mathbf{w}_k \tag{3.15}$$

$$\text{where } \mathbf{x}_{k-1} = \begin{bmatrix} x \\ v_x \\ y \\ v_y \end{bmatrix}, \; F = \begin{bmatrix} 1 & T & 0 & 0 \\ 0 & 1 & 0 & 0 \\ 0 & 0 & 1 & T \\ 0 & 0 & 0 & 1 \end{bmatrix}, \tag{3.16}$$

$$\mathbf{w}_k \sim \mathcal{N}(\mu_w, \Sigma_w), \; \mu_w = \begin{bmatrix} 0 \\ 0 \\ 0 \\ 0 \end{bmatrix}, \; \Sigma_w = \begin{bmatrix} \sigma_x^2 T^3/3 & \sigma_x^2 T^2/2 & 0 & 0 \\ \sigma_x^2 T^2/2 & \sigma_x^2 T & 0 & 0 \\ 0 & 0 & \sigma_y^2 T^3/3 & \sigma_y^2 T^2/2 \\ 0 & 0 & \sigma_y^2 T^2/2 & \sigma_y^2 T \end{bmatrix}, \tag{3.17}$$

σ_x^2, σ_y^2 are the power spectral densities of the acceleration noise and T is the sampling time.

[3] For simplicity, the target index is omitted in this section.

A sensor provides range and bearing measurements of a target with states $\mathbf{x}_k$ according to:

$$\mathbf{z}_k = \begin{bmatrix} \sqrt{x^2+y^2} \\ \text{atan2}(y,x) \end{bmatrix} + \mathbf{v}_k \tag{3.18}$$

$$\text{where } \mathbf{v}_k \sim \mathcal{N}(\mu_v, \Sigma_v) \ , \ \mu_v = \begin{bmatrix} 0 \\ 0 \end{bmatrix} \ , \ \Sigma_v = \begin{bmatrix} \sigma_r^2 & 0 \\ 0 & \sigma_b^2 \end{bmatrix}, \tag{3.19}$$

atan2 is the four-quadrant inverse tangent function and σ_r^2, σ_b^2 are the variances of the range and bearing measurements respectively.

Each target is tracked using an Extended Kalman filter, see Bar-Shalom et al. [2011]. First, the time prediction step is performed:

$$\hat{\mathbf{x}}_{k|k-1} = F\hat{\mathbf{x}}_{k-1} \tag{3.20}$$

$$P_{k|k-1} = FP_{k-1}F^\top + \Sigma_w \tag{3.21}$$

where P_{k-1} is the covariance matrix of the system states estimate $\hat{\mathbf{x}}_{k-1}$ at time $k-1$ and $P_{k|k-1}$ is the predicted covariance matrix of the predicted system states estimate $\hat{\mathbf{x}}_{k|k-1}$ at time k.

Then, the measurement update step is performed:

$$\hat{\mathbf{x}}_{k|k} = \hat{\mathbf{x}}_{k|k-1} + K(\mathbf{z}_k - \hat{\mathbf{z}}_k) \tag{3.22}$$

$$P_{k|k} = (I_{4\times 4} - KH)P_{k|k-1} \tag{3.23}$$

where

$$\hat{\mathbf{z}}_k = \begin{bmatrix} \hat{r} \\ \hat{\alpha} \end{bmatrix} = \begin{bmatrix} \sqrt{\hat{x}_{k|k-1}^2 + \hat{y}_{k|k-1}^2} \\ \text{atan2}(\hat{y}_{k|k-1}, \hat{x}_{k|k-1}) \end{bmatrix} \tag{3.24}$$

$$H = \begin{bmatrix} \cos(\hat{\alpha}) & 0 & \sin(\hat{\alpha}) & 0 \\ -\sin(\hat{\alpha})/\hat{r} & 0 & \cos(\hat{\alpha})/\hat{r} & 0 \end{bmatrix} \tag{3.25}$$

$$K = P_{k|k-1}H^\top(HP_{k|k-1}H^\top + \Sigma_v)^{-1} \tag{3.26}$$

Due to the assumption that the targets' PDFs are decoupled and well-separated, each sensing action only affects the PDF of the corresponding target. In other words, during the measurement update only the corresponding estimate $\hat{\mathbf{x}}_{k|k-1}$ and covariance matrix $P_{k|k-1}$ are updated. This also holds when sensor management is performed.

In the following examples, the trace of the covariance matrix is used as measure of uncertainty because it is intuitive to understand what it represents.

Accordingly, when a task-based approach is used the sensing action (i.e. target to be observed) is given by

$$\begin{aligned} i_k &= \arg\min_i \left\{ \mathrm{E}_{\mathcal{Z}} \left[\text{trace}\left(P_{k|k}^{(i)}\right) \right] + \sum_{\substack{n=1 \\ n\neq i}}^{N} \text{trace}\left(P_{k|k-1}^{(n)}\right) \right\} \\ &= \arg\min_i \left\{ \text{trace}\left(P_{k|k}^{(i)}\right) + \sum_{\substack{n=1 \\ n\neq i}}^{N} \text{trace}\left(P_{k|k-1}^{(n)}\right) \right\} \end{aligned} \tag{3.27}$$

and $P^{(i)}_{k|k}$ depends on target i to be observed. The expectation over the measurement space $\mathcal{Z}$ is trivial because $P^{(i)}_{k|k}$ does not depend on the measurement realization. Eq. (3.27) seeks to minimize the uncertainty in the (multi)target pdf, measured by the trace of its covariance matrix.

When the proposed threat-based approach is used, Eq. (3.12) is simplified to

$$i_k = \arg\min_i \left\{ \mathrm{E}_{\mathcal{Z}} \left[\left(\sigma^{(i)}_{k|k} \right)^2 \right] + \sum_{\substack{n=1 \\ n \neq i}}^{N} \left(\sigma^{(n)}_{k|k-1} \right)^2 \right\} \tag{3.28}$$

where $\left(\sigma^{(i)}_{k|k} \right)^2$ is the variance of $\theta^{(i)}_{k|k}$ and depends on target i to be observed.

3.3.3. SINGLE TARGET EXAMPLE: AGGREGATION OF SEVERAL THREAT FUNCTIONS

In the first example, a single target is considered that is supposed to stay within a given corridor of 1 km total width along a predefined trajectory. This scenario is typically found in maritime-/air- traffic management where ships or aircrafts are expected to move within shipping lanes or follow specific trajectories.

The target is observed by a radar that can use two different sensing modes: $\Sigma_1 = \mathrm{diag}\left(30^2\ \mathrm{m}^2, 1^2\ \mathrm{deg}^2\right)$ and $\Sigma_2 = \mathrm{diag}\left(10^2\ \mathrm{m}^2, 3^2\ \mathrm{deg}^2\right)$. The first mode has much better angular accuracy, whereas the second mode has much better range accuracy in order to strongly emphasize the differences between the two sensor management approaches. Depending on the relative position and velocity of a target to the radar, one of these two modes might be more favorable for tracking the target.

Figure 3.4 demonstrates the geometry of the considered example for three different target trajectories. In all cases the target starts at $[-4.5, 6]$ km.

Trajectory 1: Incoming target, leaving the corridor. The target has constant $x-y$ velocity of $[20, -20]$ m/s.

Trajectory 2: Target moving in the corridor. The target has constant $x-y$ velocity of $[20, 0]$ m/s.

Trajectory 3: Receding target, leaving the corridor. The target has constant $x-y$ velocity of $[20, 20]$ m/s.

The target is tracked using an Extended Kalman filter with a nearly constant velocity motion model where $T = 1$ sec and $\sigma_x^2 = \sigma_y^2 = 5$ m/s. The filter is initialized with the correct target position/velocity and with covariance matrix defined as

$$P = \mathrm{diag}(20^2\ \mathrm{m}^2,\ 2^2\ (\mathrm{m/s})^2\ 20^2\ \mathrm{m}^2,\ 2^2\ (\mathrm{m/s})^2)$$

The duration of the considered scenario is 500 seconds.

It is assumed that an operator wants to take into account three aspects of threat: time to CPA, range to CPA (both with respect to the radar location - representing the mission of defending the location of the radar) and target distance from the center of the corridor around a predefined trajectory. The mathematical form of these threat

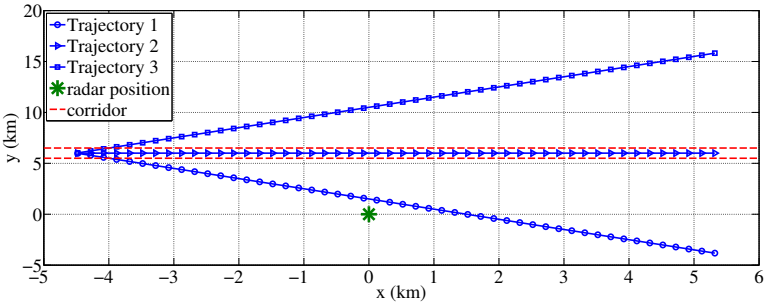

Figure 3.4: The geometry of the example, along with the three different target trajectories that are considered.

definitions and their aggregation are the same as in Subsec. 3.2.1, with equal weights $m_1 = m_2 = m_3 = 1/3$ and $[t_1 \quad t_{0.5} \quad t_0] = [0 \quad 5 \quad 10]$ min, $[d_1 \quad d_{0.5} \quad d_0] = [0 \quad 5 \quad 10]$ km, $[d_0^{\mathscr{C}} \quad d_{0.5}^{\mathscr{C}} \quad d_1^{\mathscr{C}}] = [500 \quad 750 \quad 1000]$ m.

Firstly, it is verified that the aforementioned threat functions are reasonable. Figures 3.5a through 3.5c demonstrate how the mean value of the threat evolves for each target trajectory. As expected, threat attains its highest value for the incoming target. The target that remains in the corridor has the lowest threat values. The threat values of the receding target are somewhere in-between. It can also be noticed that the threat-level increases when the target approaches the radar or leaves the corridor.

Secondly, the differences in sensor selection between the threat-based approach and the task-based approach are highlighted. Figures 3.6a through 3.6c demonstrate how the trace of the covariance matrix of the target $x-y$ position estimate evolves over time when using each of the two different sensor management approaches. Table 3.1 shows the sensor selections for the two different approaches along with the expected logarithm of the squared error in threat estimation, the expectation taken with respect to the scenario time. In other words, it is examined how the threat-based approach performs in the context of the task-based approach and vice versa.

By comparing Fig. 3.6a through 3.6c to Table 3.1, the first advantage of the threat-based approach can be seen. The two approaches provide comparable threat estimation errors but the threat-based approach uses much less sensor resources, see Table 3.1. A consequence of the lower resource consumption is that the target is tracked with less accuracy, especially when the target is close to the radar and the uncertainty in the threat is minimal. Here it must be pointed out that good tracking accuracy was not the objective of the threat-based approach as opposed to the task-based approach. The threat-based approach assumes that the uncertainty in the threat-level of the target is important and that once the uncertainty is low enough the operator will take a proper action. If tracking accuracy is also of interest, then a corresponding threat function must be (re)defined.

The preference of each sensor management approach for a given sensing mode depends on the geometry of the scenario at hand and the specific choice of the measurement noise covariance matrices. For different geometries, different sensing mode preferences have been observed but the threat-based approach always used less resources than the task-based approach.

The second advantage of the threat-based approach, which is its flexibility to be

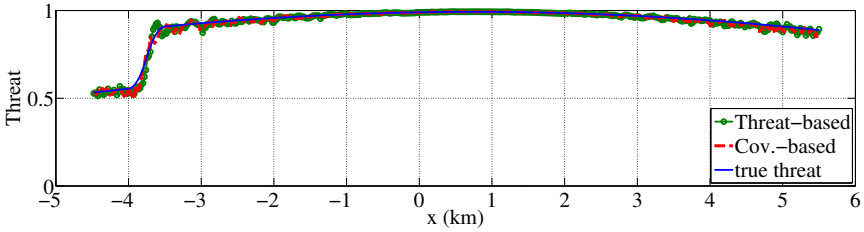

(a) Incoming target, leaving the corridor (trajectory 1 in Fig. 3.4).

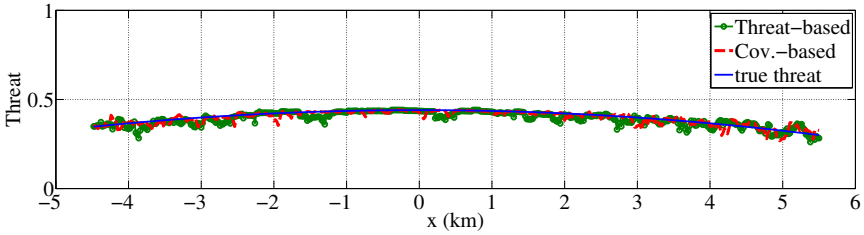

(b) Target moving in the corridor (trajectory 2 in Fig. 3.4).

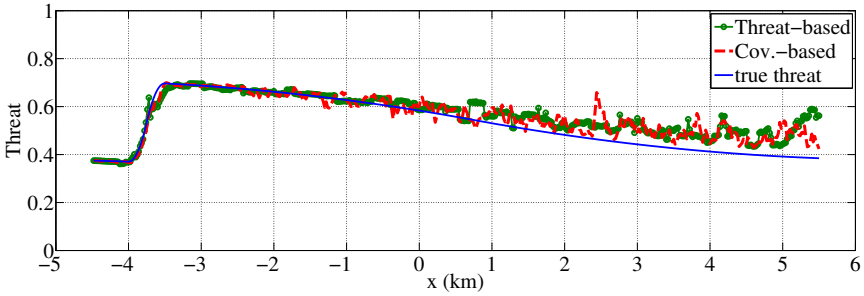

(c) Receding target, leaving the corridor (trajectory 3 in Fig. 3.4).

Figure 3.5: The threat evolution for the three different trajectories.

Table 3.1: Sensor mode selection results and threat estimation squared error (T.S.E.)

(a) Incoming target, leaving the corridor

	Threat-based	**Task-based**
no meas. [selections / Total time]	110/500	0/500
mode 1 [selections / Total time]	138/500	439/500
mode 2 [selections / Total time]	252/500	61/500
E_t[log(T.S.E.)]	-12.01	-11.768

(b) Target moving in the corridor

	Threat-based	**Task-based**
no meas. [selections / Total time]	161/500	0/500
mode 1 [selections / Total time]	33/500	494/500
mode 2 [selections / Total time]	306/500	6/500
E_t[log(T.S.E.)]	-9.509	-10.263

(c) Receding target, leaving the corridor

	Threat-based	**Task-based**
no meas. [selections / Total time]	331/500	0/500
mode 1 [selections / Total time]	67/500	493/500
mode 2 [selections / Total time]	102/500	7/500
E_t[log(T.S.E.)]	-7.898	-8.064

adapted to different operational contexts, is demonstrated in the following subsection.

3.3.4. MULTITARGET EXAMPLE: ADAPTING THE THREAT DEFINITION TO THE OPERATIONAL CONTEXT

In the second example, three targets are considered that are observed by a radar with a single sensing mode. The radar can observe only one target per time instance and the problem is to decide which target must be observed at each time instance. This is a simplified version of the beam-pointing problem for multiple target tracking that is considered later on in this thesis.

EXPERIMENTAL SETUP

Figures 3.7a and 3.7b show the two different scenarios that are considered:

Scenario 1: One receding and two incoming targets, with initial $x-y$ positions $[5,0]$ km, $[10,0]$ km, $[15,0]$ km and constant $x-y$ velocities $[30,0]$ m/s, $[-30,0]$ m/s, $[-30,0]$ m/s respectively.

Scenario 2: Three incoming targets, with initial $x-y$ positions $[5,0]$ km, $[10,0]$ km, $[15,0]$ km and constant $x-y$ velocities $[-30,0]$ m/s, $[-30,0]$ m/s, $[-30,0]$ m/s respectively.

The duration of each scenario is 75 seconds.

The targets are tracked using three Extended Kalman filters with nearly constant velocity motion models where $T = 1$ sec, $\sigma_x^2 = 2$ m/s and $\sigma_y^2 = 0.1$ m/s. The measurement noise covariance matrix is $\Sigma = \text{diag}\left(10^2 \text{ m}^2, 1^2 \text{ deg}^2\right)$. The filters are initialized with the

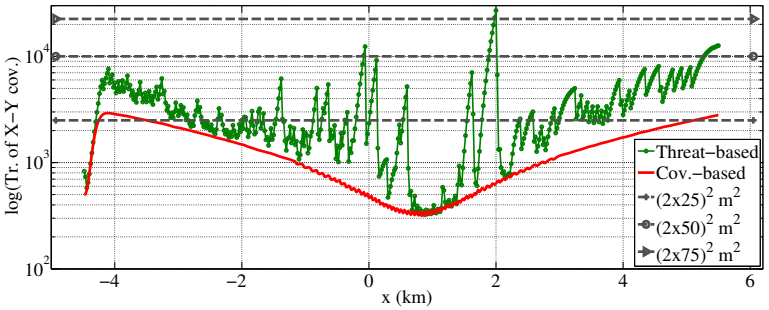

(a) Incoming target, leaving the corridor (trajectory 1 in Fig. 3.4).

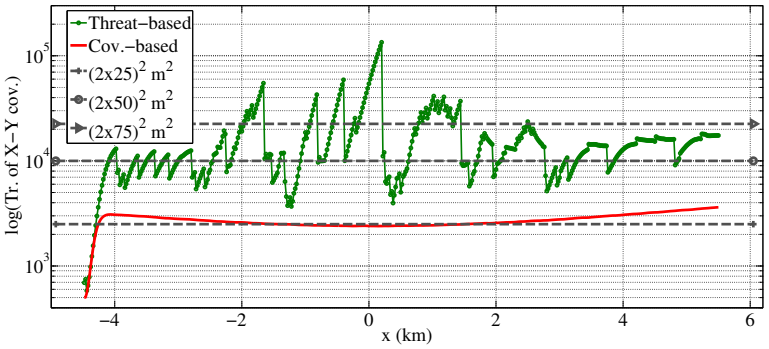

(b) Target moving in the corridor (trajectory 2 in Fig. 3.4).

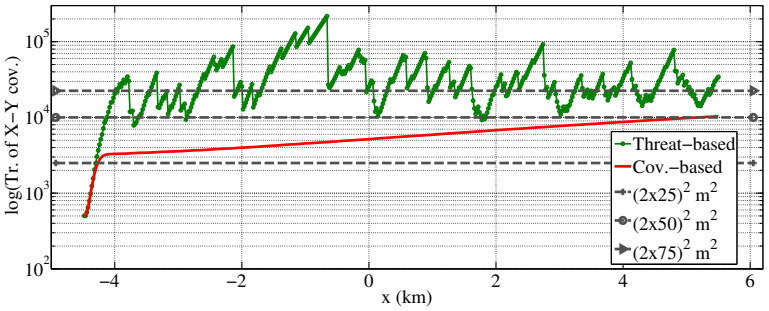

(c) Receding target, leaving the corridor (trajectory 3 in Fig. 3.4).

Figure 3.6: The evolution of the trace of the X-Y covariance matrix for the three different trajectories. Notice that logarithmic scale is used for the Y-axis.

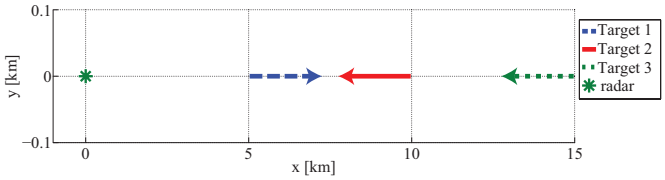

(a) Scenario 1: One receding and two incoming targets.

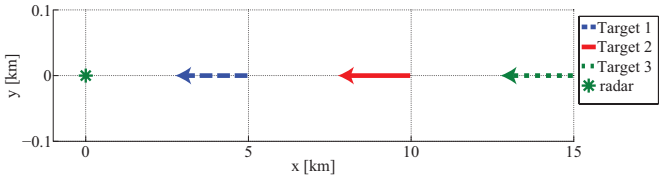

(b) Scenario 2: Three incoming targets.

Figure 3.7: The target trajectories for the two considered scenarios.

correct target positions/velocities and with covariance matrices

$$\begin{aligned} P^{(1)} &= \text{diag}(20^2\ \text{m}^2,\ 2^2\ (\text{m/s})^2,\ 20^2\ \text{m}^2,\ 2^2\ (\text{m/s})^2) \\ P^{(2)} &= 1.2P^{(1)} \\ P^{(3)} &= 1.5P^{(1)} \end{aligned} \tag{3.29}$$

Two different contexts are considered:

Defense: An operator wants to protect the asset where the radar is located. Accordingly, the operator takes into account two aspects of threat: the time and range to CPA with respect to the radar location.

Civilian: An operator performs traffic control and is interested in avoiding collisions between targets. Accordingly, the operator takes into account two aspects of threat: the time and range to CPA among all pairs of targets.

The mathematical form of these threat definitions and their aggregation are the same as in Subsec. 3.2.1, with equal weights $m_1 = m_2 = 0.5$ and $[t_1 \quad t_{0.5} \quad t_0] = [0 \quad 3 \quad 6]$ min, $[d_1 \quad d_{0.5} \quad d_0] = [0 \quad 6 \quad 12]$ km.

The sensor selections at each time instance are evaluated using three control schemes:

- myopic control, i.e., optimization with horizon of one time instance;
- Open Loop Feedback Control (OLFC) with optimization horizon of two time instances (OLFC-2), i.e. optimize for two time instances but only apply the sensing action for the first time instance; and
- OLFC with optimization horizon of five time instances (OLFC-5), i.e. optimize for five time instances but only apply the sensing action for the first time instance.

The OLFC-2 and OLFC-5 schemes are used as better approximations to the optimal, closed-loop sensor management [Huber, 2009, Subsec. 2.4.2] and are presented for reasons that become evident in the following subsections.

Table 3.2: Sensor selection results

(a) Myopic control

	Scenario 1			Scenario 2		
	mean number of selections			mean number of selections		
Method	**Targ. 1**	**Targ. 2**	**Targ. 3**	**Targ. 1**	**Targ. 2**	**Targ. 3**
Task-based	21	25	29	20	25	30
Threat-based, defense	29.78	24.85	20.37	35.39	22.24	17.37
Threat-based, civilian	34.27	26.1	14.63	20.21	20.77	34.02

(b) OLFC-2

	Scenario 1			Scenario 2		
	mean number of selections			mean number of selections		
Method	**Targ. 1**	**Targ. 2**	**Targ. 3**	**Targ. 1**	**Targ. 2**	**Targ. 3**
Task-based	26.35	26.1	22.55	20.1	29.54	24.48
Threat-based, defense	27.26	24.58	23.16	14	35.85	25.15
Threat-based, civilian	4.85	65.15	5	6.95	47.48	20.57

(c) OLFC-5

	Scenario 1			Scenario 2		
	mean number of selections			mean number of selections		
Method	**Targ. 1**	**Targ. 2**	**Targ. 3**	**Targ. 1**	**Targ. 2**	**Targ. 3**
Task-based	32.27	17.98	24.78	24.26	21.64	29.1
Threat-based, defense	17.16	23	34.84	7.81	30.11	37.08
Threat-based, civilian	4.74	65.54	4.72	8.24	35.91	30.85

SIMULATION RESULTS AND DISCUSSION ON THE SENSOR SELECTIONS

The results obtained using *myopic* control in both contexts are summarized in Table 3.2a. The results were evaluated over 100 Monte Carlo runs using 500 simulated measurements for sensor management purposes and 1000 samples for approximating the threat PDFs.

The results for OLFC-2 and OLFC-5 schemes are summarized in Tables 3.2b and 3.2c respectively. These were evaluated over 100 Monte Carlo runs using 25 simulated measurements for sensor management purposes and 500 samples for approximating the threat PDFs due to the high computational load caused by the combinatorial complexity of the OLFC implementation.

When using myopic control, see Table 3.2, it can be concluded that:

- the qualitative behavior of the task-based criterion (sum of the traces of the covariance matrices of the three targets) is the same for the two scenarios and does not depend on the operational context;
- the task-based criterion assigns most sensor resources to the target that is located furthest away from the sensor, *irrespective of the operational context* and the target trajectories;

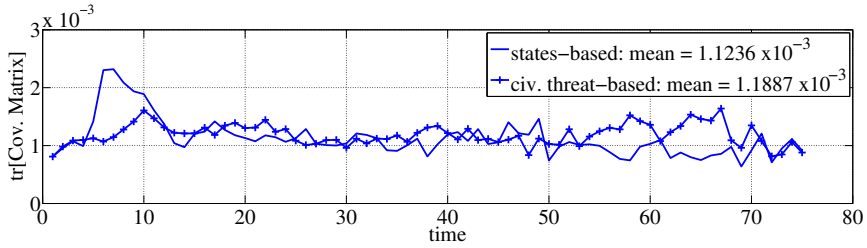

(a) Myopic control.

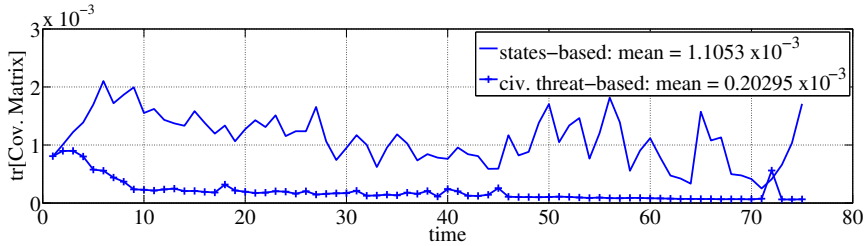

(b) OLFC-2.

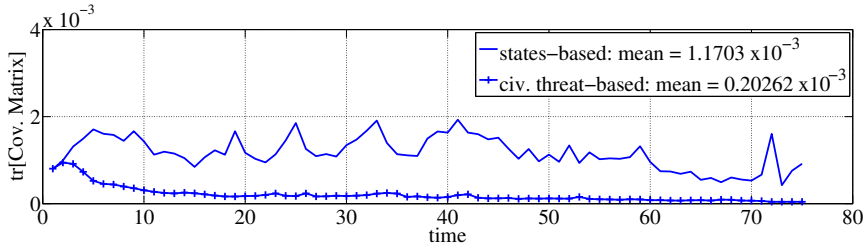

(c) OLFC-5.

Figure 3.8: Civilian context: Threat uncertainty evolution for scenario 1. The uncertainty in threat is measured by the trace of the multitarget threat covariance matrix.

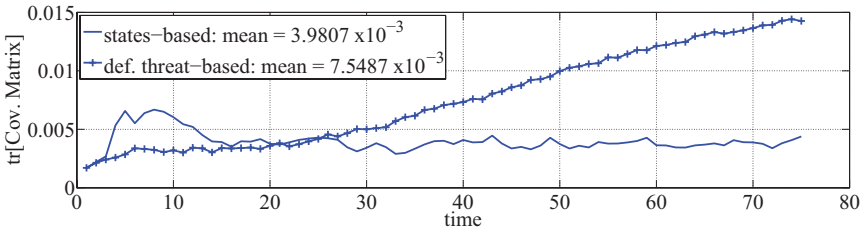

(a) Myopic control.

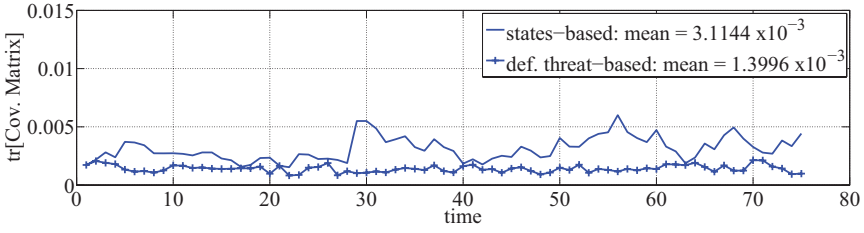

(b) OLFC-2.

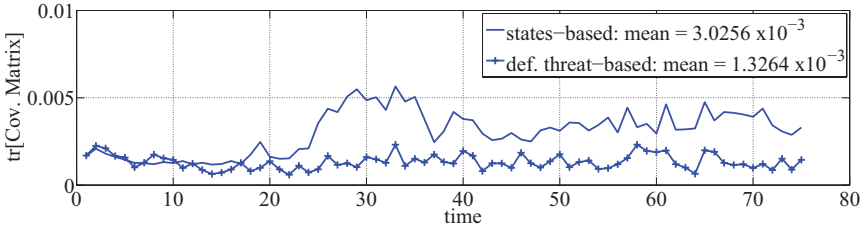

(c) OLFC-5.

Figure 3.9: Defense context: Threat uncertainty evolution for scenario 1. The uncertainty in threat is measured by the trace of the multitarget threat covariance matrix.

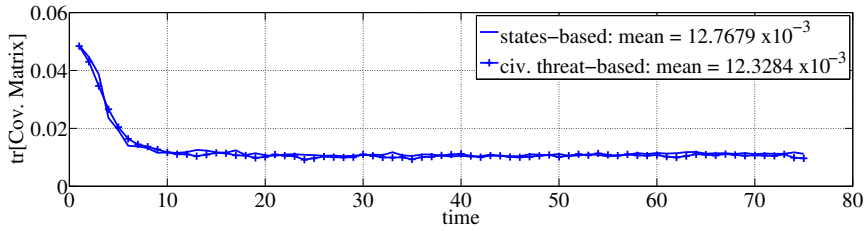

(a) Myopic control.

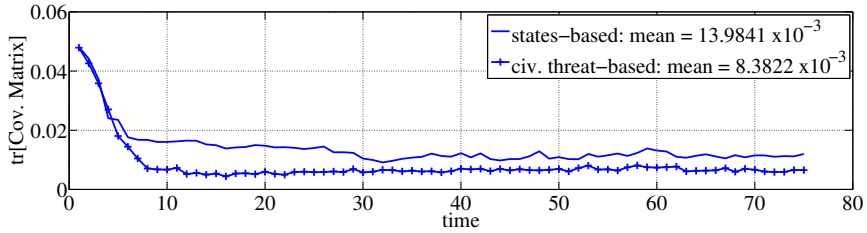

(b) OLFC-2.

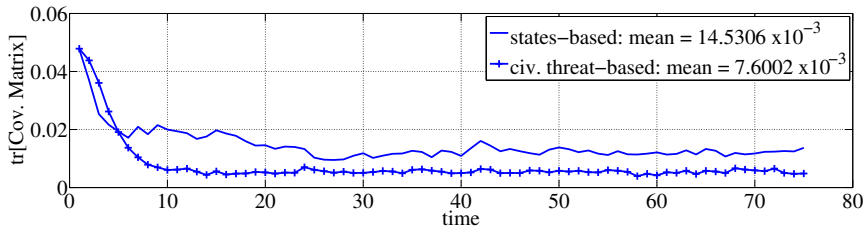

(c) OLFC-5.

Figure 3.10: Civilian context: Threat uncertainty evolution for scenario 2. The uncertainty in threat is measured by the trace of the multitarget threat covariance matrix.

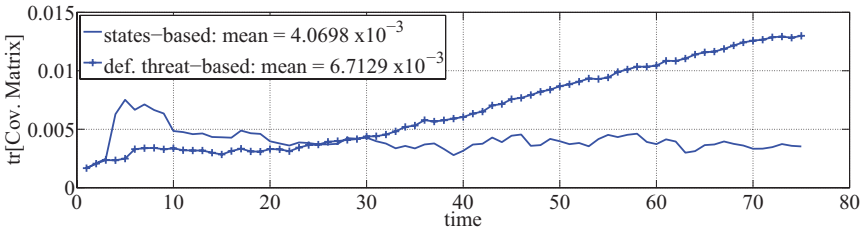

(a) Myopic control.

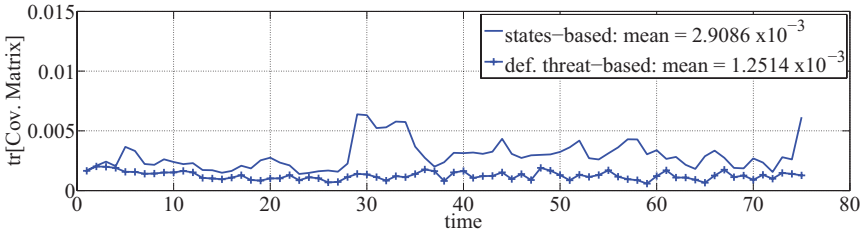

(b) OLFC-2.

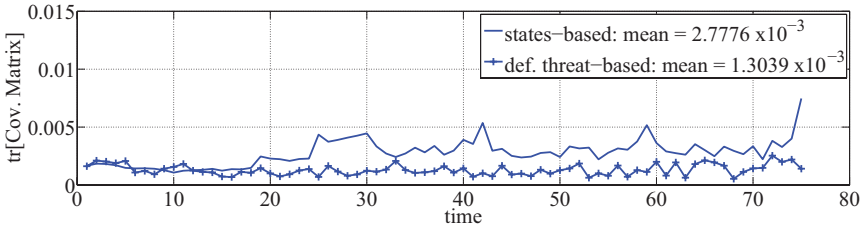

(c) OLFC-5.

Figure 3.11: Defense context: Threat uncertainty evolution for scenario2. The uncertainty in threat is measured by the trace of the multitarget threat covariance matrix.

- the threat-based approach offers *qualitatively different results that depend on the operational context* and on the behavior of the targets. Especially, when myopic optimization is used:
  - in the considered defense context, the threat-based approach focuses on the target that is closest to the radar, especially if it is incoming;
  - in the considered civilian context and in Scenario 1, the threat-based approach spends more resources to the targets that are about to collide;
  - in the considered civilian context and in Scenario 2, the threat-based approach focuses on the target at the longest range because the range effect is isolated and that target has the highest uncertainty in its threat-level. This happens because all the targets are equally spaced and move towards the radar with the same speed, which severely limits the collision probability.

When applying OLFC, the sensor selections become less intuitive, see for example Table 3.2c where the closest target is selected by the defense threat-based criterion only 8 times. Nevertheless, OLFC is of interest in this example. As it can be seen in Fig. 3.9a and 3.11a, even though the sensing action that minimizes the uncertainty in the threat is chosen by the threat-based approach, in the long run this might not lead to lower uncertainty in the threat-level than using the task-based approach. This phenomenon happens due to the suboptimal nature of myopic optimization, i.e. because the sensing action is selected by taking into account only the subsequent time instance.

If OLFC is used, it can be seen that the proposed threat-based method results in lower uncertainty in the threat-level than the task-based method also in the long run. Figures 3.8a through 3.11c verify this claim for the considered scenarios and contexts when using OLFC. As seen in Tables 3.2b and 3.2c, the conclusions drawn for the myopic sensor management selections are no longer valid when OLFC is used.

3.4. SUMMARY

This chapter aimed at addressing the disadvantages of the existing sensor management schemes that were documented in the previous chapter. For this reason, a novel threat-based approach to resource allocation was presented. The proposed approach was inspired by the threat assessment process, which is an integral part of missions executed in the defense domain. The key idea behind the proposed approach is to manage the uncertainty in higher-level quantities that describe in a better way what are the user-needs in a specific operational context. Accordingly, the proposed approach manages the uncertainty in the threat-level of all targets present in a scenario.

The proposed approach has the three desirable properties that were identified in the previous chapter and that the existing approaches do not have, i.e. the *Bayes-optimal* allocation of resources *among diverse tasks* while *taking into account explicitly the user-needs* within a given operational context. In other words, the objective function to be optimized is a measure of uncertainty of the threat-level of each target. The threat-level is a higher-level quantity that can be defined according to the operational context and the user needs. Moreover, it was shown how to model mathematically the threat-level in different contexts, both defense and civilian.

Via simulated examples, it was shown that using the proposed approach results in improved situation awareness in contexts as diverse as asset-defense and air-traffic-control. The improvement in situation awareness was measured by the reduction in the uncertainty in the threat-level of all targets. As a consequence, by using this method an operator can make decisions with lower uncertainty and lower operational risk.

In the presented examples, the proposed approach did not result in improved tracking accuracy but it is important to understand that this was not explicitly taken into account when modeling threat. Nevertheless, the proposed method has the potential to also address this problem by considering tracking accuracy as an aspect of threat.

4

THREAT-BASED MULTIPLE TARGET TRACKING USING AN MFR

The previous chapter presented the proposed approach to sensor management and demonstrated its feasibility and flexibility by means of examples. The presented examples were intentionally simple for demonstration purposes, which means that important aspects of multitarget tracking were ignored. The most prominent of these is the imperfect radar detection process. This chapter applies the proposed approach in complicated multitarget tracking scenarios where there is detection uncertainty, false alarms can arise and the true number of targets is unknown.

Section 4.1 presents the multitarget tracking problem and explains the difficulties that an imperfect detection process poses to resource management and signal processing algorithms. Section 4.2 presents the considered system setup and formulates the radar-beam pointing problem. Section 4.3 discusses the existing resource allocation approaches to radar beam-pointing. Section 4.4 explains how the proposed, threat-based approach can be applied to the radar beam-pointing problem. Section 4.5 shows simulated examples where the proposed approach is compared to existing approaches and is found to be superior. Finally, Section 4.6 concludes the chapter.

4.1. THE MULTITARGET TRACKING PROBLEM AND WHY IT IS DIFFICULT TO SOLVE

Multi-Function Radars (MFRs) receive an increasing amount of attention due to their unique capability to execute several diverse tasks such as area surveillance, communications and weapon control. Most commonly, they employ active phased array technology and digital waveform generators, which give them significant advantages over conventional, rotating radars with horn-fed reflector antennas. One of the key advantages of MFRs is their capability to steer their (narrow) antenna beam almost instantaneously to the desired direction. This capability offers an opportunity to use adaptive beam-pointing via a resource management algorithm in order to improve the performance of

MFRs.

An important application, where this capability is of interest, is the tracking of multiple targets, such as aircrafts, ships and missiles. In multitarget tracking, it is desired to estimate the number and kinematic states of all targets present in a scenario given a series of observations. The challenging nature of this problem is due to *a*) the presence of false alarms; *b*) detection uncertainty; and *c*) because targets can enter and leave the observation space. The aforementioned challenges not only hinder the localization of any observed targets, as discussed in the previous chapter, but also introduce uncertainty in the estimated number of targets that are present. In other words, both the *number of targets* and their *kinematic properties* must be estimated.

The control of beam-direction and the performance of the algorithm that uses any received measurements for estimating target quantities, such as their number, position and velocity, are closely coupled. In this case, radar resource management can be seen as the component that closes the control loop in the estimation process, see the discussion in Chapter 1. Good beam-direction control can lead to improved estimation results whereas bad beam-direction control can exacerbate the estimation results. Therefore, radar resource management algorithms are of paramount importance when tracking (multiple) targets using an MFR.

In this chapter, the aforementioned resource management problem for tracking multiple targets is considered. To be more specific, the focus is on the radar-beam pointing problem, that is, to determine at each time step the best direction for a narrow radar-beam such that multiple targets can be tracked. The problem must be considered under these two aspects: *a*) the selection of a suitable signal processing algorithm for estimating the number and states of all targets; and *b*) the selection of a resource management algorithm for using the best beam-direction at each time instance. Ideally, both selections produce Bayes-optimal results and do not make use of any heuristics.

For several years, the Multiple Hypothesis Tracking (MHT) and the Joint Probabilistic Data Association (JPDA) algorithms have been the workhorse of multitarget tracking, see Blackman and Popoli [1999]; Bar-Shalom et al. [2011]. A common characteristic of these approaches is the divide-and-conquer strategy employed for solving the data association problem, see [Mahler, 2007, Ch. 10]. In other words, several hypotheses for the measurement-to-track associations are formed and retained until a dominating hypothesis is found. Given a certain association hypothesis, a variant of the Kalman filter is applied for solving each of the multiple single-target filtering problems. Unfortunately, the approximations employed in these approaches result in a non-Bayes-optimal estimation process for the multitarget probability density function, see [Mahler, 2007, Ch. 10.7.2].

A new approach that has emerged in the last years is to use the Random Finite Set (RFS) theory in order to solve the multitarget tracking problem in a fully Bayesian manner. This means that approximations are not employed from the beginning but only when the filtering problem becomes intractable. Among the pioneers of this approach are Mahler [2007]; Vo et al. [2003, 2007, 2009a].

The most popular approximations to the optimal Bayesian multitarget filter that have been proposed are: *a*) the Probability Hypothesis Density (PHD) filter, where the number of targets is assumed to be distributed according to a Poisson distribution and therefore it is sufficient to propagate and update only its first moment, see Mahler [2007];

Vo et al. [2003]; *b*) the Cardinalized Probability Hypothesis Density (CPHD) filter that relaxes the Poisson assumption on the number of objects and additionally propagates the full distribution of the number of targets, see Mahler [2007]; Vo et al. [2007]; and *c*) the Cardinality-Balanced Multi-target Multi-Bernoulli (CB-MeMBer) filter that approximates the multitarget PDF as a multi-object multi-Bernoulli PDF, see Vo et al. [2009a].

The choice of a PHD or Cardinalized Probability Hypothesis Density (CPHD) filter appears to be unsuitable for addressing the beam-pointing problem. The reason is that, for beam-pointing, a reliable target position estimate is required but a (C)PHD filter suffers from unreliable state estimate extraction from the estimated multitarget density due to the error-prone clustering step, required in the case of moment approximations, as discussed in [Vo and Ma, 2006, Sec. III.C]. In particular, an inadequate matching between the expected number of targets and the number of natural clusters appearing in the running (C)PHD filter results in extraction of bad target position estimates. Obviously, using bad target position estimates leads to bad selection of beam direction and eventually bad tracking performance. Therefore, to tackle the aforementioned problem, a CB-MeMBer filter is used because the multi-Bernoulli representation of the posterior density allows direct and accurate state estimates extraction, see the discussion in Vo et al. [2009a].

The main criteria that have been proposed up to now for performing resource management in the RFS context are due to Mahler and have been implemented (most commonly) using quantities of a running PHD filter. The first scheme selects the sensing action that maximizes the expected number of targets, assuming that there are no false alarms and no measurement noise, and it is called Posterior Expected Number of Targets (PENT), see Mahler and Zajic [2004]. The second scheme is an extension of the first one such that the tactical importance of each target is taken into account and it is called Posterior Expected Number of Targets of Interest (PENTI), see Mahler [2004]. Another scheme that was proposed in the robotics context for path planning, but can also be of interest, is selecting the measurement that maximizes the Rényi or alpha divergence between the multi-object prior and the multi-object posterior densities, see Ristic and Vo [2010].

Lately, a new sensor management criterion has been proposed that is most suitable when the multitarget PDF is estimated using a CB-MeMBer filter. This criterion suggests minimizing the expected variance of the multi-Bernoulli cardinality, the expectation taken with respect to the measurement PDF. This criterion was proposed in Gostar et al. [2013a] and also used in different problem formulations in Gostar et al. [2013c,b, 2014]. A similar criterion, i.e. minimizing the expected variance of the Maximum A Posteriori (MAP) estimate of the multi-Bernoulli cardinality, was proposed in Hoang [2012]; Hoang and Vo [2014]. Both these criteria select sensing actions based only on the uncertainty in the cardinality of the estimated PDF but ignore the uncertainty in the kinematic states (e.g. position/velocity). Furthermore, they do not take into account the operational context.

In order to tackle the beam pointing problem, the threat-based approach presented in the previous chapter is used. In other words, the uncertainty in higher-level quantities that are directly relevant to the operational goal of a radar system is managed rather than the uncertainty in the estimated multitarget PDF.

4.2. SYSTEM SETUP AND PROBLEM FORMULATION

Consider a scenario where an MFR is tasked with tracking multiple targets. An MFR can have a narrow beam that can be steered almost instantaneously to the desired direction. The considered problem is: towards which direction $u \in [0, \pi/2]$ should the narrow radar-beam be pointed at each time instance? In other words, which target should be observed by the radar at each time instance?

For solving the multitarget filtering problem, a CB-MeMBer filter is used and the standard assumptions that pertain to it are made, see Vo et al. [2009a]. The assumptions behind the CB-MeMBer filter and its Sequential Monte Carlo (SMC) implementation are also summarized in Appendix C. A state estimate is extracted from the estimated multitarget PDF using the Marginal Multi-target (MaM) estimator, introduced in [Mahler, 2007, pp.497]. The MaM estimator first finds the MAP estimate $\hat{N}$ of the number of targets using the estimated cardinality distribution. Subsequently, a MAP state estimate is extracted from the $\hat{N}$ densities with the highest probability of existence.

For solving the beam-pointing problem, the sensing action that minimizes the uncertainty in higher level quantities that are directly related to the operational goal of the radar system is selected. Accordingly, a function that maps the states of the targets to the *threat* domain is considered, obtaining in this way the PDF of the threat that each target poses to an asset of interest. Then, the sensing action that minimizes the intrinsic uncertainty in the multitarget *threat* PDF is chosen. Moreover, an example drawn from the civilian domain is also presented.

Several approaches, both adaptive and naive, are compared to the proposed approach. The naive approaches amount to selecting the beam direction such that all the targets are observed sequentially or at random order. The adaptive approaches take into account the uncertainty in the estimated multitarget PDF and try to minimize it in some sense. The adaptive approaches, against which the proposed method is compared, are: *a*) selecting the action that maximizes PENT; *b*) selecting the action that minimizes the expected variance of the multi-Bernoulli cardinality; and *c*) selecting the action that minimizes the expected intrinsic uncertainty in the multitarget *states* PDF.

The conditional entropy is used as a means of quantifying the intrinsic uncertainty in the multitarget (states or threat) PDFs. The trace of the covariance is not defined in this context because the state space is not Euclidean, see [Mahler, 2007, pp.65].

4.3. EXISTING APPROACHES TO RADAR BEAM-POINTING FOR MULTITARGET TRACKING

As discussed in Section 4.1, the existing adaptive sensor management schemes are based on the Rényi or alpha divergence (between the multi-object prior and the multi-object posterior densities), the predicted expected number of targets (of interest) and also based on the variance of the multi-Bernoulli cardinality. These schemes are presented in the following subsections.

4.3.1. INFORMATION-DRIVEN SENSOR MANAGEMENT

In information theory, a measure of the intrinsic uncertainty in a PDF is its Shannon entropy (or its generalization, the Rényi or alpha entropy). In the case of myopic sen-

sor management, minimizing the conditional entropy gives the same sensor selection as maximizing the KLD between the posterior and the predicted PDFs, see Aoki et al. [2011]. Unfortunately, a similar result has not been proven for the generalizations of the conditional entropy and the KLD, i.e., for the Rényi or alpha entropy/divergence or within the RFS context. For this reason, the conditional entropy is used as a measure of uncertainty of a PDF in the RFS context. Accordingly, the radar-beam is pointed towards direction u_k, given by:

$$u_k = \arg\min_u \left[\int H(\mathbf{X}_k|\mathbf{Z})\, g(\mathbf{Z}|\mathbf{X}_k, u)\, \delta\mathbf{Z} \right] \tag{4.1}$$
$$u = \left\{ \text{atan2}(\hat{y}^j, \hat{x}^j) \right\} \quad , \quad \forall j \in [1, \ldots, N]$$

where $\mathbf{Z}$ is the set of measurements collected due to pointing the radar-beam at direction u given by the MAP estimate $\hat{\mathbf{x}}^{(j)} = [\hat{x}^j, \hat{v}_x^j, \hat{y}^j, \hat{v}_y^j]^\intercal$ of the distribution of component (j), $\mathbf{X}_k = \{\mathbf{x}^{(1)}, \ldots, \mathbf{x}^{(N)}\}$ is the predicted multitarget state at time k, N is the cardinality of $\mathbf{X}_k$, $g(\mathbf{Z}|\mathbf{X}_k, u)$ is the measurement likelihood and $H(\mathbf{X}_k|\mathbf{Z})$ is the entropy of $p(\mathbf{X}_k|\mathbf{Z})$.

The entropy of some basic RFS PDFs has been calculated in an unpublished paper, see Rezaeian and Vo [2000]. Eq. (17) in Rezaeian and Vo [2000] can be used for calculating the entropy $H(\mathbf{X})$ of a multi-Bernoulli RFS $\mathbf{X} \in \mathscr{X}$:

$$H(\mathbf{X}) = H(|\mathbf{X}|) + \mathrm{E}[H(p_n(\mathbf{x}))] - \mathrm{E}[\log(|\mathbf{X}|!)] - \mathrm{E}[|\mathbf{X}|]\log(\bar{K}) \tag{4.2}$$

where:

- $H(|\mathbf{X}|)$ is the entropy of the cardinality distribution $B(N)$. The cardinality distribution of a multi-Bernoulli RFS is given in [Mahler, 2007, pp.369] and the evaluation of its entropy is trivial. This term represents the uncertainty in the number of targets present in a considered scenario.
- $\mathrm{E}[H(p_n(\mathbf{x}))]$ is the expected entropy of the distribution of the Bernoulli components, the expectation taken w.r.t. the cardinality distribution. This term can be calculated by first reconstructing $p_n(\mathbf{x})$ for every possible cardinality $n = 1, \ldots, N$, then calculating each corresponding entropy and finally, calculating $\mathrm{E}[H(p_n(\mathbf{x}))]$. The PDFs $p_n(\mathbf{x})$ can be approximated by properly combining samples drawn from the PDF of each independent Bernoulli component (i). The entropies $H(p_n(\mathbf{x}))$ can be calculated using the sample approximations of the corresponding PDFs and the k-NN method proposed in Ajgl and Šimandl [2011]. This term represents the uncertainty in the states of targets present in a considered scenario. It also includes information about the ordering of targets, which is deducted using the following term.
- $\mathrm{E}[\log(|\mathbf{X}|!)]$ is the expected value of the factorial of the cardinality, the expectation taken w.r.t. the cardinality distribution. Its evaluation is also trivial. This term represents the uncertainty in the ordering of targets present in a scenario.
- $\mathrm{E}[|\mathbf{X}|]\log(\bar{K})$ is a term that compensates for the units in the $p_n(x)$. $\bar{K} = K/\alpha$ is a unitless quantity, where K represents the unit that the space is measured and α is the unit of the volume measure of $\mathbf{X}$.

4.3.2. PENT-BASED SENSOR MANAGEMENT

The Posterior Expected Number of Targets (PENT) scheme, presented in Mahler and Zajic [2004], has been devised in order to take into account the non-ideal field of view of a sensor. PENT selects the sensing action that maximizes the number of objects to be seen by the sensor. This scheme has also been extended such that it can take into account the tactical significance of a target, resulting in the Posterior Expected Number of Targets of Interest (PENTI), see Mahler [2004] scheme.

In order to reduce the computational complexity, it is assumed that an ideal set of measurements can be collected, i.e. no measurement noise and no false alarms but the probability of detection can be less than one, see the discussion in Mahler and Zajic [2004]. Given this ideal set of predicted measurements, the sensing action that maximizes the posterior expected number of targets is performed.

When a CB-MeMBer filter is used, the radar-beam direction, based on PENT, is given by

$$u_k = \arg\max_u \left[\int \left(\sum_{i=1}^{N(k)} r_{k|k}^{(i)}(\mathbf{Z}) \right) g(\mathbf{Z}|\mathbf{X}_k, u)\, \delta\mathbf{Z} \right] \tag{4.3}$$
$$\text{where } u = \left\{ \text{atan2}(\hat{y}^j, \hat{x}^j) \right\} \ , \ \forall j \in [1, \ldots, N]$$

where $r_{k|k}^{(i)}(\mathbf{Z})$ is the updated probability of existence of component (i) using the (multitarget) measurement Z that is simulated from $p(\mathbf{Z}|\mathbf{Z}_{1:k-1})$ without adding measurement noise and false alarms but only taking into account the detection uncertainty, as proposed in Mahler and Zajic [2004].

4.3.3. CARDINALITY-BASED SENSOR MANAGEMENT

This scheme, suggested in Gostar et al. [2013a], seeks to minimize the variance of the cardinality estimate. Accordingly, the radar beam position is given by:

$$u_k = \arg\min_u \left\{ \int \left[\sum_{i=1}^{N(k)} r_{k|k}^{(i)}(\mathbf{Z}) \left(1 - r_{k|k}^{(i)}(\mathbf{Z}) \right) \right] g(\mathbf{Z}|\mathbf{X}_k, u)\, \delta\mathbf{Z} \right\} \tag{4.4}$$
$$\text{where } u = \left\{ \text{atan2}(\hat{y}^j, \hat{x}^j) \right\} \ , \ \forall j \in [1, \ldots, N]$$

In order to reduce the computational complexity, in this thesis it is assumed that an ideal set of measurements can be collected Mahler and Zajic [2004], i.e. no measurement noise and no false alarms but the probability of detection can be less than one. The authors in Gostar et al. [2013a] do not make this assumption but it is reasonable, much like when PENT is used.

4.4. THREAT-BASED RADAR BEAM-POINTING FOR MULTITARGET TRACKING

As an alternative to the sensor management approaches presented in the previous section, the approach presented in Chapter 3 is used. In this chapter, two examples are given. One from the defense and one from the civilian domain.

From the defense domain, asset protection is considered. Accordingly, the threat that is posed by a target i to asset j depends on how close and how fast target i can come to asset j. These are measured by the time and range to Closest Point of Approach (CPA), as explained in Chapter 3.

In order to move from the time and range domain to the single-target threat domain $\mathcal{T} = [0,1]$, a sigmoid function can be utilized for example[1]:

$$\theta_t\left(\mathbf{x}^{(i)};\mathbf{x}^{(j)}\right) = \begin{cases} 1 & , \text{if } |t_{CPA}^{ij}| \le t_1 \\ 1-2\left(\frac{|t_{CPA}^{ij}|-t_1}{t_0-t_1}\right)^2 & , \text{if } t_1 < |t_{CPA}^{ij}| \le t_{0.5} \\ 2\left(\frac{|t_{CPA}^{ij}|-t_0}{t_0-t_1}\right)^2 & , \text{if } t_{0.5} < |t_{CPA}^{ij}| \le t_0 \\ 0 & , \text{if } t_0 < |t_{CPA}^{ij}| \end{cases} \tag{4.5}$$

$$\theta_d\left(\mathbf{x}^{(i)};\mathbf{x}^{(j)}\right) = \begin{cases} 1 & , \text{if } d_{CPA} \le d_1 \\ 1-2\left(\frac{d_{CPA}^{ij}-d_1}{d_0-d_1}\right)^2 & , \text{if } d_1 < d_{CPA}^{ij} \le d_{0.5} \\ 2\left(\frac{d_{CPA}^{ij}-d_0}{d_0-d_1}\right)^2 & , \text{if } d_{0.5} < d_{CPA}^{ij} \le d_0 \\ 0 & , \text{if } d_0 < d_{CPA}^{ij} \end{cases} \tag{4.6}$$

where $t_1 < t_{0.5} < t_0$ and $d_1 < d_{0.5} < d_0$ are the points where the threat is equal to 1, 0.5 and 0.

Since both time and range to CPA have been mapped to the same domain, i.e. threat, it is meaningful to aggregate them using a weighted sum in order to evaluate the total threat level of a target i with respect to asset j:

$$\theta\left(\mathbf{x}^{(i)};\mathbf{x}^{(j)}\right) = m_t\theta_t\left(\mathbf{x}^{(i)};\mathbf{x}^{(j)}\right) + m_d\theta_d\left(\mathbf{x}^{(i)};\mathbf{x}^{(j)}\right) \tag{4.7}$$

where m_i is the weight assigned by the operator to $\theta_i\left(\mathbf{x}^{(i)};\mathbf{x}^{(j)}\right)$ such that $m_t + m_d = 1$. In this way, a two-objective optimization problem is simplified to a still meaningful single objective problem that consists of the weighted sum of the two aspects of threat.

From the civilian domain, air traffic control is considered. Accordingly, threat is now defined by how close and how fast two aircrafts i, j can come to each other. In this case, the notions of time and range to CPA can be utilized again. The difference is that time and range to CPA are now evaluated among all pairs of targets (i,j), where $i,j = 1,\ldots,N$ and $i \neq j$ instead of between each target and an asset. From the $N-1$ different threat values for a target i, the threat value $\theta^*\left(\mathbf{x}^{(i)}\right)$ is selected such that:

$$\theta^*\left(\mathbf{x}^{(i)}\right) := \theta\left(\mathbf{x}^{(i)};\mathbf{x}^{(j^*(i))}\right) \tag{4.8}$$

$$\text{where } j^*(i) = \underset{j(\ldots)}{\arg\max}\ \hat{\theta}\left(\mathbf{x}^{(i)};\mathbf{x}^{(j)}\right),\ \forall i,j \in [1,\ldots,N],\ i \neq j \tag{4.9}$$

$$\text{with } \hat{\theta}\left(\mathbf{x}^{(i)};\mathbf{x}^{(j(i))}\right) = \int \theta\left(\mathbf{x}^{(i)};\mathbf{x}^{(j(i))}\right) p\left(\theta\left(\mathbf{x}^{(i)};\mathbf{x}^{(j(i))}\right)\right) \mathrm{d}\theta\left(\mathbf{x}^{(i)};\mathbf{x}^{(j(i))}\right) \tag{4.10}$$

[1] The specific choice of sigmoid functions is only for demonstration purposes. Any other convenient function could be used by the system designer and the operator.

and N is the number of targets in the scenario. The mean threat $\hat{\theta}\left(\mathbf{x}^{(i)};\mathbf{x}^{(j)}\right)$ can be evaluated in a Monte Carlo fashion using samples from the estimated single targets PDFs $p^{(i)}(\mathbf{x}^{(i)}), p^{(j)}(\mathbf{x}^{(j)})$.

In the multitarget tracking context, each target has its own threat PDF. Especially when a CB-MeMBer filter is used, the multitarget threat RFS variable Θ is a union of N independent Bernoulli RFSs $\Theta^{(c)}$ with corresponding existence probabilities $r^{(c)} \in [0,1]$ and probability density $p\left(\theta^{(c)}\right)$ defined on $\mathcal{T}$ for $c = 1,\ldots,N_c$. Accordingly, Θ is fully described by the corresponding multi-Bernoulli parameter set $\{r^{(c)}, p\left(\theta^{(c)}\right)\}_{c=1,\ldots,N_c}$, where $p\left(\theta^{(c)}\right) := p\left(\theta^{(c)}(\mathbf{x})\right) : \mathbf{x} \sim p^{(c)}(\mathbf{x})$. The multitarget threat Θ has the same cardinality distribution as the multitarget state RFS $\mathbf{X}$.

Therefore, the radar-beam direction is given by

$$u_k = \arg\min_{u} \left[\int H(\Theta|\mathbf{Z}) g(\mathbf{Z}|\mathbf{X}_k, u)\, \delta\mathbf{Z} \right] \tag{4.11}$$
$$\text{where } u = \left\{ \text{atan2}(\hat{y}^j, \hat{x}^j) \right\} \ , \ \forall j \in [1,\ldots,N]$$

where $\text{atan2}(\hat{y}^j, \hat{x}^j)$ is the four-quadrant inverse tangent function.

It holds that the single-target threat space $\mathcal{T}$ has volume 1 and that $\bar{K} = 1$ and $\log(\bar{K}) = 0$. Accordingly, the term $\mathrm{E}[|\mathbf{X}|]\log(\bar{K}^n)$ in Eq. (4.2) is equal to zero and can be ignored.

The main difference between the proposed threat-based sensor management and the PENTI scheme is that the uncertainty in the multitarget threat PDF is explicitly minimized, whereas in PENTI the threat level (or tactical significance) of each target is taken into account for modifying the PENT, which is the quantity to be maximized. Unfortunately, the authors were not able up to this point to implement the PENTI scheme using quantities from a running CB-MeMBer filter.

4.5. SIMULATED EXAMPLES

In this section, simulated examples are presented based on the definitions of threat explained in Section 4.4. Both asset protection and air-traffic-control are considered.

4.5.1. EXPERIMENTAL SETUP

Consider a scenario, shown in Figure (4.1), where an MFR is tasked with tracking an unknown number of targets. The radar can track targets in the sector defined by $[0,10]$ km in range and $[0,\pi/2]$ rad in bearing using its "pencil" beam. Three targets are present during the full duration of the scenario, which is 90 time instances. Their initial positions in $x-y$ are $[1,5]$ km, $[5,5]$ km and $[8,2.5]$ km respectively. Their initial velocities in $x-y$ are $[6,0]$ m/s, $[-5,-5]$ m/s and $[0,7]$ m/s respectively.

The motion of the targets follows a nearly constant velocity model with noise covariance matrix:

$$\Sigma_w = \begin{bmatrix} \sigma_x^2 T^3/3 & \sigma_x^2 T^2/2 & 0 & 0 \\ \sigma_x^2 T^2/2 & \sigma_x^2 T & 0 & 0 \\ 0 & 0 & \sigma_y^2 T^3/3 & \sigma_y^2 T^2/2 \\ 0 & 0 & \sigma_y^2 T^2/2 & \sigma_y^2 T \end{bmatrix} \tag{4.12}$$

where $T = 1$ sec and $\sigma_x^2 = \sigma_y^2 = 1$ $(\text{m/s})^2$. All the targets have RCS $= 10$ m^2.

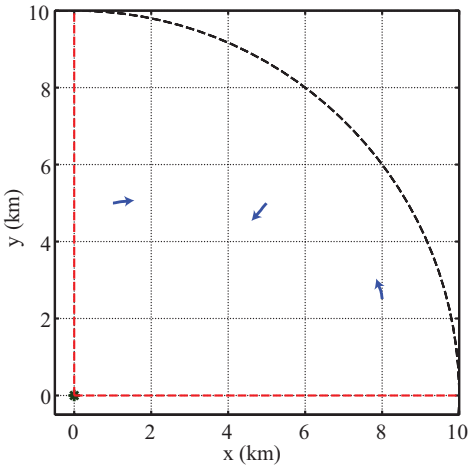

Figure 4.1: The trajectories of the true targets. The radar is at the origin of the axes.

The targets are observed via a radar that provides range and bearing measurements. The measurement noise covariance matrix is $\Sigma_v = \text{diag}[(10\text{ m})^2,\ (0.5\text{ degrees})^2]$.

The radar beam has width of 2 degrees without loss due to the target not being on the boresight of the beam. The probability of detecting a target is calculated using the radar equation and the Swerling I model. Depending on the distance between a target and the radar, the probability of detection is in the range of $[0.8, 0.9]$ for the specific trajectories of the targets. Furthermore, false alarms can arise with rate $\kappa = 3.18 \cdot 10^{-5}\ (\text{rad} \cdot \text{m})^{-1}$, i.e. a clutter measurement is received with probability 0.01 at each time instance.

In order to examine the behavior of the sensor management schemes, it is assumed that the CB-MeMBer filter is initialized with all the correct tracks and one false track. Ideally, the true tracks must be maintained with as good accuracy as possible and the false track should be eliminated. Furthermore, good situation awareness must be achieved, measured by the intrinsic uncertainty in the multitarget threat PDF.

The correct tracks are initialized with $r^{(i)} = 0.8$, with standard deviation of 100 m around the true $x-y$ position and standard deviation of 1 m/s around the true $x-y$ velocities. The false track is initialized with $r^{(i)} = 0.5$, with mean position uniformly random in the sector defined by $[1,9]$ km and $[0.01, 0.9\pi/2]$ rad, standard deviation of 100 m in $x-y$ axes and $x-y$ velocity uniformly random in $[-5,5]$ m/s at each Monte Carlo run.

New tracks are initiated from the measurements of the previous time instance that were not assigned to any existing tracks. The newly created tracks are initialized with $r^{(i)} = 0.5$, standard deviation of 100 m round the measured $x-y$ position and with $x-y$ velocity uniformly random in $[-5,5]$ m/s. The probability of survival of each target is $p_{S,k} = 0.99$ and tracks with $r^{(i)} < 0.005$ are pruned.

Each Bernoulli component (track) is approximated using 2000 particles and the entropy is evaluated using the 50 nearest neighbors of each particle. The integrals in Eq. (4.1), (4.3) and (4.11) are evaluated in a Monte Carlo fashion using particles from the corresponding PDFs. For the random, periodic and PENT sensor management schemes,

100 Monte Carlo simulations were performed. For the entropy-based schemes, 50 Monte Carlo simulations were performed due to computational complexity reasons. For the entropy of the multitarget states PDF it is not clear what is the value of $\bar{K}$. Therefore, two values have been used: $\bar{K}=1$ and $\bar{K}=\mathrm{E}[N]$.

For evaluating the threat, $m_t = m_d = 0.5$, $[t_1, t_{0.5}, t_0] = [0, 50, 10]$ min and $[d_1, d_{0.5}, d_0] = [0, 7.5, 15]$ km were used for both the asset protection and air traffic control contexts. In asset protection, the range between each target and the radar is considered, whereas in air traffic control the range between each pair of targets is considered.

The sensor management results of the various approaches are compared both with respect to the resulting uncertainty in the posterior multitarget threat and with respect to their tracking performance using the Optimal Sub-Pattern Assignment (OSPA) metric, presented in Schuhmacher et al. [2008] and given by:

$$d_{c,p}(A,B) = \left[\frac{1}{n}\left(\min_{\pi\in\Pi_n}\sum_{i=1}^{m} d_c(a_i, b_{\pi(i)})^p + c^p(n-m)\right)\right]^{\frac{1}{p}} \tag{4.13}$$

where $p \geq 1$, $c > 0$, $a, b \in \mathbf{X}$, $d_c(a,b) = \min(c, \|a-b\|)$, Π_n denotes the set of permutations on $\{1,\ldots,n\}$, $A = \{a_1,\ldots,a_m\}$, $B = \{b_1,\ldots,b_n\}$. If $m = n = 0$ then $d_{c,p}(A,B) = d_{c,p}(B,A) = 0$. Eq. (4.13) assumes that $m \leq n$. If $m \geq n$, then $d_{c,p}(A,B) = d_{c,p}(B,A)$. Parameter c represents the cut-off distance and parameter p is the order of the metric and determines its sensitivity to outliers. For intuition purposes, it is common to present separately the cardinality and localization errors:

$$e_{c,p}^{card} = \left(\frac{c^p(n-m)}{n}\right)^{1/p} \tag{4.14}$$

$$e_{c,p}^{loc} = \left(\frac{1}{n}\min_{\pi\in\Pi_n}\sum_{i=1}^{m} d_c(a_i, b_{\pi(i)})^p\right)^{1/p}. \tag{4.15}$$

The OSPA metric is evaluated using the true states of the three targets and the MaM estimator.

4.5.2. THREAT UNCERTAINTY AND TRACKING RESULTS

ASSET PROTECTION

Figure (4.2) shows the entropy of the posterior threat PDF, averaged over 100 Monte Carlo simulations. It can be seen that the proposed threat-based scheme outperforms all the other approaches. Interestingly, in this case, the PENT scheme performs worse than the periodic and random schemes in the long run (keeping in mind though that a myopic optimization scheme is used). The scheme that minimizes the expected cardinality variance has the second best performance.

The OSPA metric, averaged over 100 Monte Carlo simulations, and its corresponding components are shown in Fig. (4.3). It can be seen that the proposed threat-based scheme and the scheme that minimizes the expected cardinality variance outperform all the other approaches. Interestingly, the scheme based on the entropy of the multitarget states with $\bar{K}=1$ has the worst performance. The PENT scheme has slightly

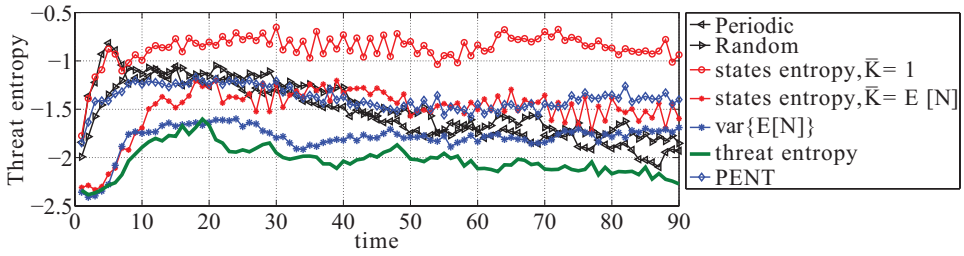

Figure 4.2: Asset protection: The posterior threat entropy, averaged over 100 Monte Carlo runs. The threat-based scheme and the scheme that minimizes the expected cardinality variance have the best performance, the states-based threat scheme has the worst performance and PENT has worse performance than the random and periodic schemes in the long run.

better performance than the random and periodic schemes, contrary to the results in Ristic and Vo [2010] where it performed worse than choosing a random sensing action (albeit in a different experimental setting). One reason for PENT not performing as well as the threat-based approach can be the use of a narrow beam and a myopic optimization scheme that do not allow for observing multiple targets simultaneously or during multiple time steps.

Figure (4.4) shows the MAP estimate of the number of targets, averaged over 100 Monte Carlo simulations. It can be seen that an important reason why the proposed threat-based scheme and the scheme that minimizes the expected cardinality variance outperform the other schemes is their superior performance in estimating the correct number of targets.

AIR TRAFFIC CONTROL

Figure (4.5a) shows the entropy of the posterior threat PDF, averaged over 100 Monte Carlo simulations. It can be seen that the proposed threat-based scheme outperforms all the other approaches. The PENT scheme and the scheme that minimizes the expected cardinality variance have the second best performance.

The OSPA metric, averaged over 100 Monte Carlo simulations is shown in Fig. (4.5b). The scheme that minimizes the expected cardinality variance has the best performance, followed by the threat-based scheme.

Figure (4.5c) shows the MAP estimate of the number of targets, averaged over 100 Monte Carlo simulations. It can be seen again that an important reason why the scheme that minimizes the expected cardinality variance outperforms all other schemes is its superior performance in estimating the correct number of targets. The threat-based scheme has the second best performance, closely followed by PENT.

4.5.3. EXTRACTING RULES BASED ON THE BEHAVIOR OF THE ADAPTIVE APPROACHES

By observing the sensor selections of the adaptive schemes, it was noticed that the state-based entropy scheme observed frequently the track with the highest probability of existence. On the other hand, the PENT, the scheme that minimizes the expected cardinality variance and the threat-based scheme observed frequently the track with the

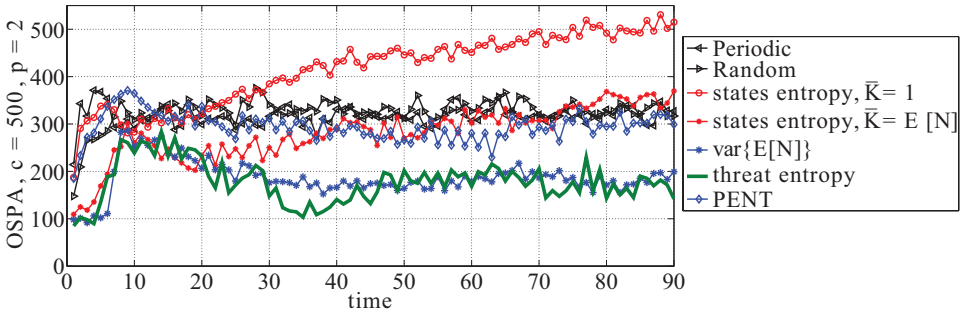

(a) OSPA metric.

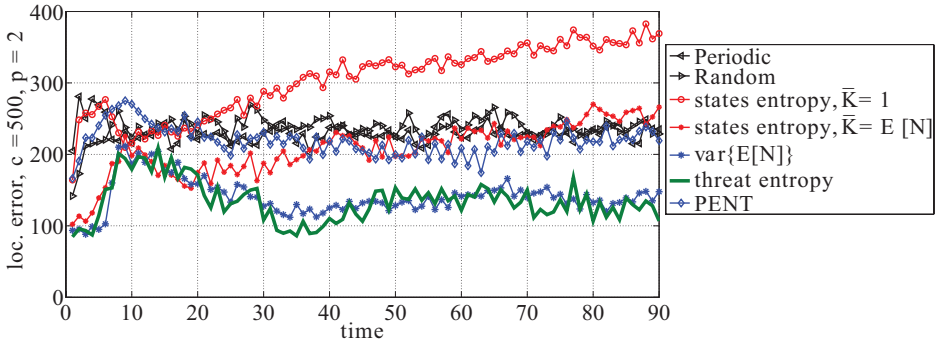

(b) Localization error.

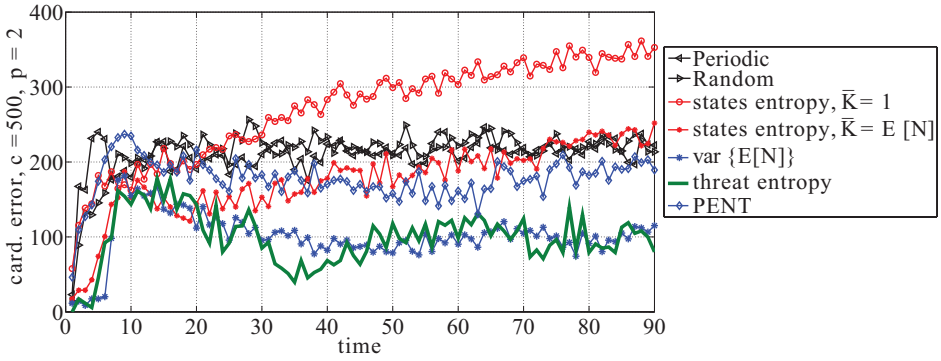

(c) Cardinality error.

Figure 4.3: Asset protection: The OSPA metric and its components, averaged over 100 Monte Carlo runs. The threat-based scheme and the scheme that minimizes the expected cardinality variance have the best performance, the states-based threat scheme has the worst performance and PENT has slightly better performance than the random and periodic schemes.

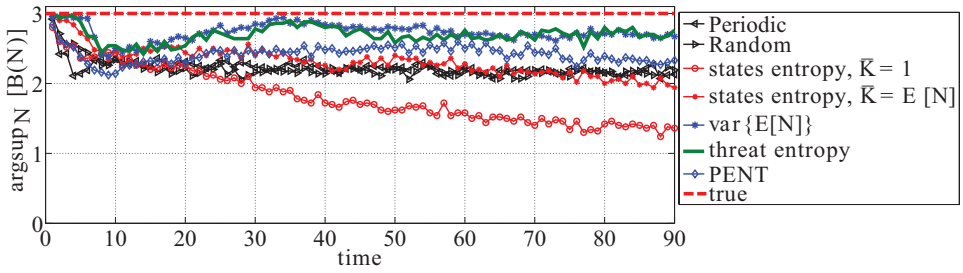

Figure 4.4: Asset protection: The MAP estimate of the number of targets, averaged over 100 Monte Carlo runs. The threat-based scheme and the scheme that minimizes the expected cardinality variance have the best performance, the states-based threat scheme has the worst performance and PENT has slightly better performance than the random and periodic schemes.

lowest probability of existence. In order to gain more intuition, more simulations were performed with two rule-based approaches motivated by the previous observations:

- always observe the track with the highest probability of existence, abbreviated as `MaxProb`; and
- always observe the track with the lowest probability of existence, abbreviated as `MinProb`.

ASSET PROTECTION

Figure 4.6a shows the OSPA metric for the two rule-based methods, PENT, the scheme that minimizes the expected cardinality variance and the threat-based method. Figure 4.6b shows the MAP estimate of the number of targets and Fig. 4.6c shows the entropy of the posterior threat PDF. All results are averaged over 100 Monte Carlo runs.

From these figures, it can be concluded that `MinProb` approach can give results of almost equivalent quality to the results of the best performing approaches. On the other hand, the `MaxProb` approach gives the worst results both in tracking and situation awareness sense. These results serve as an explanation of how the adaptive sensor management schemes work, in the myopic optimization context, and indicate that the `MinProb` approach could be a potential cheap alternative to our proposed method.

AIR TRAFFIC CONTROL

Figure 4.7a shows the OSPA metric for the two rule-based methods, PENT and the threat-based method. Figure 4.7b shows the MAP estimate of the number of targets and Fig. 4.7c shows the entropy of the posterior threat PDF. All results are averaged over 100 Monte Carlo simulations.

From these figures, it can be concluded that `MinProb` approach can give results of better or equivalent quality to the results of the best performing approaches. On the other hand, the `MaxProb` approach gives the worst results both in tracking and situation awareness sense. These results must be treated with caution though since they are based on myopic optimization and on the specific use of filter and threat definition.

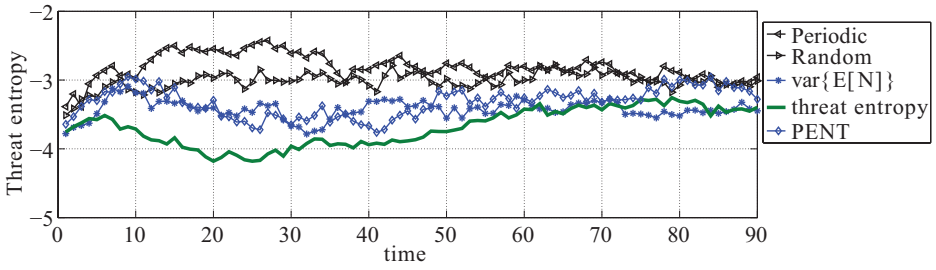

(a) Posterior threat entropy.

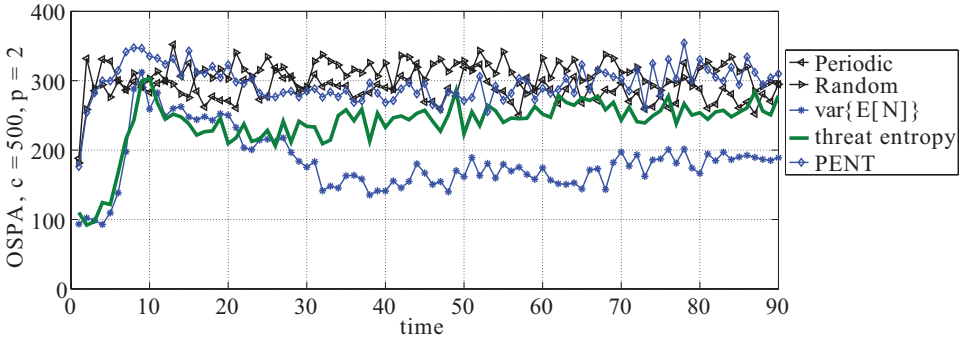

(b) OSPA metric.

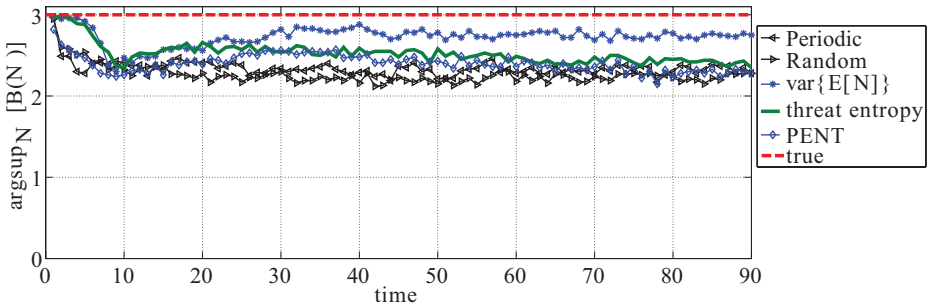

(c) MAP estimate of the number of targets.

Figure 4.5: Air traffic control: Performance of the various approaches, averaged over 100 Monte Carlo runs. The threat-based scheme has the best performance in threat entropy whereas the scheme that minimizes the expected cardinality variance has the best tracking performance.

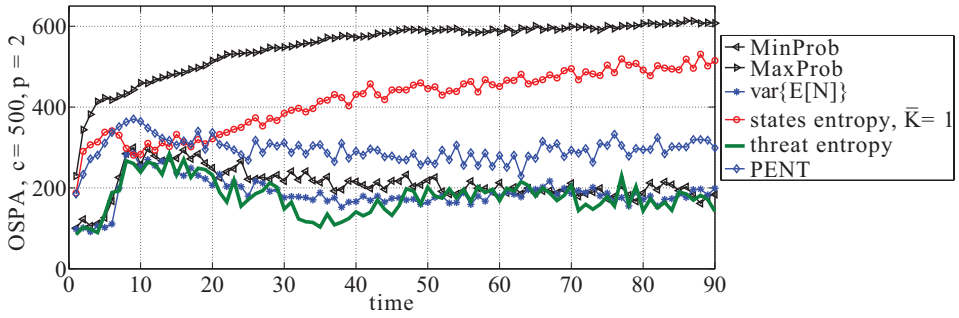

(a) OSPA metric.

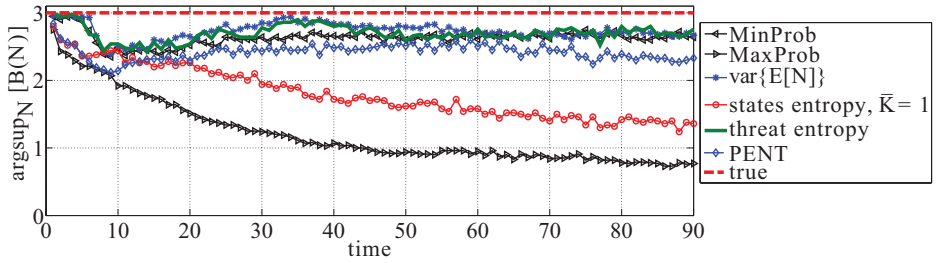

(b) MAP estimate of the number of targets.

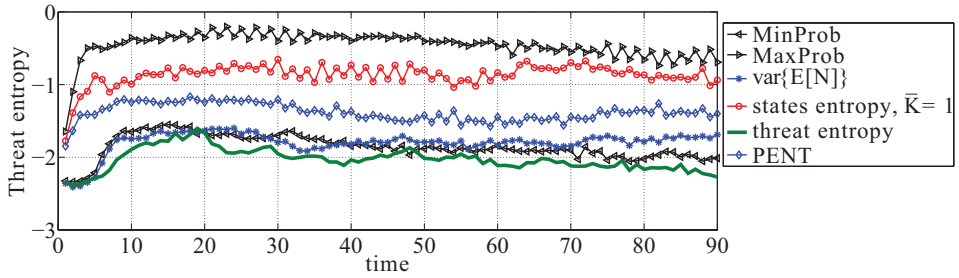

(c) Posterior threat entropy.

Figure 4.6: Asset protection: Performance comparison of the considered criteria averaged over 100 Monte Carlo runs. The `MinProb` approach is almost equivalent to the best performing approaches. On the other hand, the `MaxProb` approach has the worst performance.

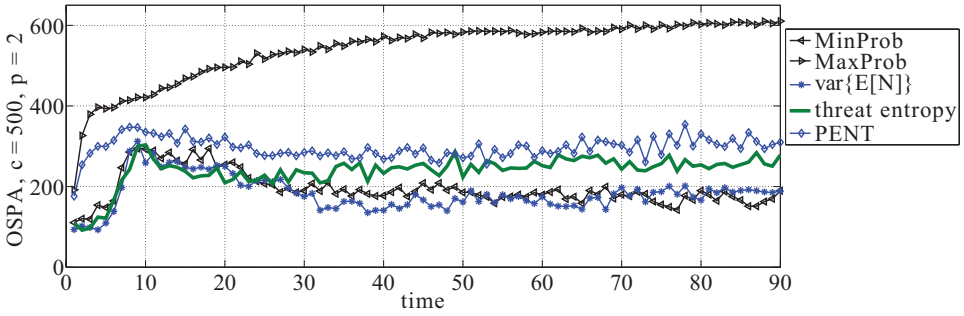

(a) OSPA metric.

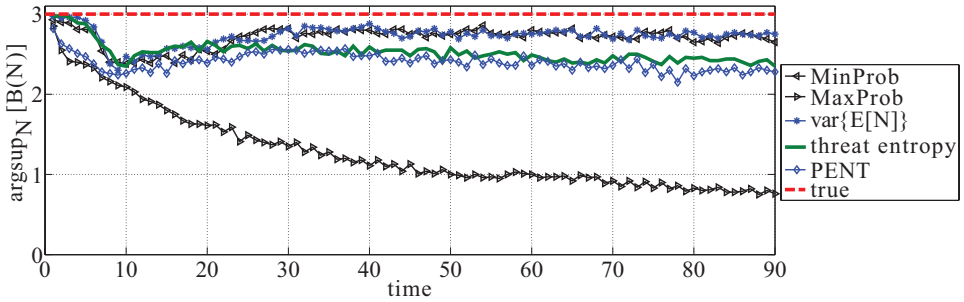

(b) MAP estimate of the number of targets.

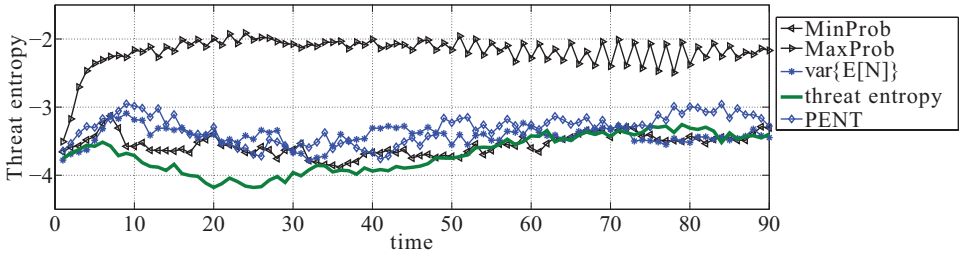

(c) Posterior threat entropy.

Figure 4.7: Air traffic control: Performance comparison of the considered criteria averaged over 100 Monte Carlo runs. The `MinProb` approach is better or equivalent to the threat-based approach and to the scheme that minimizes the expected cardinality variance. On the other hand, the `MaxProb` approach has the worst performance.

4.5.4. VIDEOS

Videos that demonstrate the behavior of various approaches can be found at YouTube, see `http://www.youtube.com/playlist?list=PLE5W2H3_7ZUIXALFQgs19NxA7x0EPYvBn`. Please notice that this playlist is unlisted. It will not appear in search, but anyone with the link can view it.

In all videos:

- blue circles denote the current target positions;
- blue lines denote the target trajectories up to the current time instance;
- red crosses denote the MAP position estimate extracted from each Bernoulli component (track) of the estimated multitarget PDF;
- black diamonds denote the received measurements;
- r's denote the probability of existence of each Bernoulli component (track); and
- green lines denote the radar tracking beam of 2 degrees beamwidth.

The videos show a posteriori estimates and therefore, it might appear that the estimates are outside the radar beam, especially if a missed detection has happened, but this is not the case. The radar beam is always pointed such that it is centered around the predicted MAP position estimate of a target/track.

4.6. SUMMARY

In this chapter, an application of the proposed threat-based approach to radar beam-pointing was presented. The goal was to demonstrate that the proposed, threat-based approach can be used in connection with an advanced signal processing algorithm and with more realistic experimental settings. For this reason, an imperfect detection process was simulated, where the number of targets was unknown, detection uncertainty existed and false alarms could arise.

In the presented application, the beam of an MFR was controlled such that multiple targets could be tracked using measurements resulting from an imperfect detection process. The multitarget filtering problem was solved using a state-of-the-art signal processing algorithm, i.e. a CB-MeMBer filter.

The proposed approach was compared to several resource allocation schemes, both adaptive and naive. By means of simulated examples it was shown that the proposed approach outperformed all other resource allocation schemes in achieving better situation awareness by minimizing the uncertainty in the threat level of the targets. Regarding tracking performance, i.e. *a*) estimating the correct number of targets; and *b*) localizing them; better performance can be potentially achieved by using either the scheme that minimizes the expected cardinality variance or the `MinProb` approach. These two approaches also induce a much lower computational cost than the threat-based approach.

The superior performance of the proposed, threat-based scheme for achieving improved situational awareness was demonstrated in two operationally diverse scenarios: asset protection and air-traffic-control. In this way, it was shown that the proposed approach can be applied in challenging scenarios where state-of-the-art signal processing algorithms must be used.

By observing the behavior of all the compared approaches, two rule-based schemes were extracted. These rule-based schemes provided insight in how the different resource allocation schemes operate and what is the key to achieving good tracking performance in the specific experimental setting. One of the extracted rule-based schemes was shown to perform almost as well as the best performing Bayes-optimal approaches. The key advantage of this rule-based scheme is that it has very low computational complexity, especially when compared to the proposed, threat-based approach.

The specific behavior of the criteria discussed in this chapter is heavily dependent on the behavior of the CB-MeMBer filter. In particular, the CB-MeMBer filter has been reported to produce unstable track existence probabilities even for moderate probability of detection and clutter rate, see the discussion in [Bocquel, 2013, Sec. 5.3]. This might be an explanation of why better tracking performance is achieved by the criteria that favor tracks with lower probability of existence.

5

THREAT-BASED AREA SURVEILLANCE USING AN MFR

The previous chapter presented an application of the proposed, threat-based approach to radar beam-pointing for multitarget tracking. It was assumed that the tracking filter was already initialized with the correct tracks and therefore, it only had to maintain the correct tracks and delete any false ones. In practice, a radar must first search for targets before actually tracking them. Accordingly, this chapter discusses how the proposed approach to resource allocation can be applied to area surveillance, i.e. to adaptively pointing the radar beam such that search for and tracking of multiple targets can be achieved optimally.

Section 5.1 presents the area surveillance problem and explains the search versus tracking trade-off that a resource algorithm must address. Section 5.2 presents the system setup for area surveillance. Section 5.3 explains how the proposed, threat-based approach can be applied to the area surveillance problem. Section 5.4 shows simulated examples where a radar beam is controlled for finding and tracking multiple targets. Finally, Section 5.5 concludes the chapter.

5.1. THE AREA SURVEILLANCE PROBLEM

Wide area surveillance is most commonly performed using radars due to their unique sensing capabilities. Radars can observe objects of interest, also called targets, at very long distances, during day or night and without being severely hindered by unfavorable weather conditions. Area surveillance involves searching for targets and when target detections happen, tracks are initialized and maintained while search is continued.

Multi-Function Radars (MFRs) are a promising alternative to conventional, rotating radars with horn-fed reflector antennas for performing area surveillance. MFRs most commonly employ active phased array technology and digital waveform generators, which allow for adaptive radar-beam pointing strategies. These components offer the ability to steer the beam of an MFR almost instantaneously to a desired direction. In

other words, at each time instance the best radar-beam direction can be selected by a radar resource management algorithm. Adaptive beam-pointing is beneficial when external information about the environment or targets is available and when different operational goals must be taken into account.

The capabilities of MFRs pose significant challenges to radar resource management algorithms. A resource manager must decide at each time instance whether the radar should search for new targets or track an existing one. If the algorithm does not allocate enough resources to searching for targets, several targets might remain undetected and this can result in severe problems both in defence and civilian scenarios. If, on the other hand, the algorithm does not allocate enough resources to maintaining the existing tracks, unreliable track estimates can be produced or, even worse, track loss might happen. Both these problems can result in the radar operator taking decisions with higher operational risk.

The first solution to the aforementioned resource allocation problem was to use rule-based approaches, as also discussed in Blackman and Popoli [1999]. In rule-based approaches, a set of rules is created and tuned according to the operational needs and the radar system characteristics. Such solutions can be very time-efficient and take into account explicitly the operational goals of the radar system but are not optimal in the Bayesian sense and might have unpredictable behavior. For example, a radar operator might set manually a track update rate per target and a track-to-search ratio but the optimality of such parameters is not guaranteed. Instead, their quality is only based on the experience of the operator.

Another approach is to assign priorities to each sensing task (be it search or tracking) and then allocate the radar resources according to these priorities, see Miranda et al. [2006]. In Bolderheij et al. [2005] the priorities (and the radar resources) are assigned according to the risk that is posed to the success of the mission. These approaches, even though they take into account any mission aspects, also suffer from not being Bayes-optimal.

In order to obtain Bayes-optimal solutions that take into account various quantities of interest, one could formulate a weighted sum of these quantities and seek to optimize it. Examples of such quantities are the probability of detecting a target, track accuracy and expected measurement SNR. The disadvantages of this approach are the selection of weights and the mathematically non-meaningful aggregation of non-commensurate quantities.

The latest suggestion in balancing the tasks of search and tracking is based on using information theoretic measures. Accordingly, the information gain when performing search is compared to the information gain when performing a tracking task and the task that provides higher information gain is selected. This approach was suggested in Romero and Goodman [2013] and White et al. [2008]. A disadvantage in both these papers is that a scaling factor is used for trading radar time among search and tracking, thus allowing the user to intervene in resource allocation and make the results non-Bayes-optimal. Nevertheless, even if a scaling factor would not have been used, it is not clear how to take into account different operational requirements when the conditional entropy or the expected KLD are used.

A problem similar to the *search versus tracking* trade-off is also present in robotics. It corresponds to robot-path-planning such that an area is searched for objects or intrud-

ers and such that the detected objects/intruders are tracked, see Cole [2009] for example. In the specific example, the information gain is also used as a means of achieving an optimal trade-off.

In order to address the disadvantages of the aforementioned approaches, the threat-based method presented in Chapter 3 is used. Accordingly, the radar resources are allocated based on the uncertainty in higher-level quantities that depend both on the search and tracking performance of a radar system. In the defense domain, a prominent such quantity is the threat-level of a target. The uncertainty in the threat-level of a target is indicative of the quality of the achieved situation awareness and therefore, if the uncertainty in the threat level of all targets present in a scenario is managed, better situation awareness can be achieved. Moreover, threat can also incorporate the need for performing search for undetected targets. If it can be estimated where undetected targets can be, it can also be estimated what threat they might pose to the mission success. From the discussion above, it follows that multitarget threat can serve as a proxy for balancing the tasks of search and tracking.

5.2. SYSTEM SETUP AND PROBLEM FORMULATION

Consider a scenario where an MFR is tasked with the surveillance of its surrounding area. An MFR can have a narrow beam that can be steered almost instantaneously to a desired direction. The problem that must be tackled is: which sensing mode u_k should the radar use at time instance k? In other words:

- should the radar search for new targets and if yes, towards which direction? or
- should it observe an already detected target and if yes, which one?

The choice of sensing mode also implies that different measurement accuracy is used, i.e. different beamwidth, probability of detection, false alarm rate, range accuracy and bearing accuracy. Other measurements parameters, such as wavelength, beam-width and PRF can also be controlled but are not considered in this case for simplicity reasons.

In this chapter, the search and the multitarget tracking problems are solved by estimating two densities:

a) the *"Detected Targets"* Density (DTD) that is used for estimating the kinematic properties of detected targets; and

b) the *"undetected Targets"* Density (unDTD) that is used for estimating where any undetected targets can be. The estimation of this density is beneficial for determining when and where the radar should search for targets.

These two densities can be estimated recursively based on prior knowledge about and models of the motion of targets, their RCS, the location from which they might enter the surveillance area, the radar sensing parameters etc. Here these two densities are assumed to be decoupled.

For estimating the DTD recursively, a Cardinality-Balanced Multi-target Multi-Bernoulli (CB-MeMBer) filter is selected and the standard assumptions that pertain to it are made, see Vo et al. [2009a]. The reasons behind this selection have been explained in Section 4.1. For updating the DTD recursively, the presence of false alarms and the fact that the

probability of detection can be less tan one are taken into account. For extracting a state estimate from the running CB-MeMBer filter the Marginal Multi-target (MaM) estimator is used, see [Mahler, 2007, pp.497]. The MaM estimator first finds the MAP estimate $\hat{N}_{DTD}$ of the number of tracks and then extracts MAP estimates from the PDFs for the $\hat{N}_{DTD}$ tracks with the highest probability of existence.

For estimating the unDTD recursively, a Probability Hypothesis Density (PHD) filter is used and the standard assumptions that pertain to it are made, see Mahler [2007]. The unDTD is used for estimating where any undetected targets might be, taking into account their motion model, information about where they might appear etc. In this way, adaptive search can be performed, leading to faster detection of targets when external information is available as opposed to using a periodic or random search pattern. The reasoning behind the unDTD is also explained in Section 2.2 and in Katsilieris et al. [2012a]. The use of a PHD filter is a natural extension to multitarget scenarios of the aforementioned work.

In the current chapter, for estimating the unDTD it is assumed that there are *a*) no targets spawned from other targets; *b*) no false alarms; and *c*) no detections. The aforementioned assumptions imply that any received measurements are always used by the running CB-MeMBer filter that estimates the DTD. The PHD filter only estimates where any undetected targets might be.

Due to these assumptions, the prediction step for estimating the unDTD reduces to:

$$D_{k|k-1}(\mathbf{x}) = b_{k|k-1}(\mathbf{x}) + \int p_s(\mathbf{x}') f_{k|k-1}(\mathbf{x}|\mathbf{x}') D_{k-1|k-1}(\mathbf{x}')\, \delta\mathbf{x}' \tag{5.1}$$

where $D_{k|k-1}(\mathbf{x})$ is the predicted probability hypothesis density[1] of unDTD, $b_{k|k-1}(\mathbf{x})$ is the likelihood that a group of new targets with state $\mathbf{x}$ will enter the scene at time k, $p_s(\mathbf{x}')$ is the probability that a target with state $\mathbf{x}'$ at time $k-1$ will survive in time k and $f_{k|k-1}(\mathbf{x}|\mathbf{x}')$ is the single-target Markov transition density (usually given by the motion model of the targets).

Similarly, the update step for estimating the unDTD reduces to

$$D_{k|k}(\mathbf{x}) = [1 - P_D(\mathbf{x})]\, D_{k|k-1}(\mathbf{x}) \tag{5.2}$$

where $P_D(\mathbf{x})$ is the probability of detecting a target with state $\mathbf{x}$. When the likelihood function is equal to $[1 - P_D(\mathbf{x})]$, it is referred to in the literature as *Negative Information*, see Koch [2007]. The SMC implementation of the PHD recursion given by Eq. (5.1) and (5.2) is straightforward and can be found in [Mahler, 2007, Ch. 16.5.2].

A key point is that when using a sensing mode dictated by the resource allocation algorithm both densities are updated. The DTD is updated using the received measurements (if there are any) and the unDTD is always updated assuming that no target has been detected.

For finding the best sensing action, the proposed- threat-based approach to sensor management is used. The proposed approach and its application to search for and tracking of multiple targets is presented in the following Section.

[1] To be precise, $D_{k|k-1}(\mathbf{x})$ is called a *first moment density* or *intensity density*. In other words, *a PHD is not a probability density* since it does not integrate to one but rather to the expected number of targets in $\mathcal{X}$. Also see the discussion in [Mahler, 2007, Ch. 16.1.2.1].

The proposed approach is compared against the standard periodic search-and-track approach and against minimizing the sum of conditional entropies of the DTD and unDTD. The periodic approach amounts to periodically repeating *a*) searching all sectors sequentially; and then *b*) observing all targets sequentially. The sum of conditional entropies of the DTD and unDTD is given by

$$\begin{aligned} u_k &= \arg\min_u \left\{ \int H_{\text{track}}(\mathbf{X}_k|\mathbf{Z}) g_u(\mathbf{Z}|\mathbf{X}_k, u)\, \delta\mathbf{Z} + \int H_{\text{search}}(\mathbf{x}|\mathbf{Z}) g_u(\mathbf{Z}|\mathbf{x}, u)\, \delta\mathbf{Z} \right\} \\ &= \arg\min_u \left\{ \int H_{\text{track}}(\mathbf{X}_k|\mathbf{Z}) g_u(\mathbf{Z}|\mathbf{X}_k, u)\, \delta\mathbf{Z} + H_{\text{search}}(\mathbf{x}|\mathbf{Z}=\emptyset, u) \right\} \end{aligned} \tag{5.3}$$

where

$$u = \left\{ \text{atan2}(\hat{y}^j, \hat{x}^j) \right\} \bigcup \left\{ b^\ell \right\}, \tag{5.4}$$

$\text{atan2}(\hat{y}^j, \hat{x}^j)$ is the four-quadrant inverse tangent function, $\mathbf{Z}$ is the set of measurements collected due to pointing the radar-beam at direction u given by the MAP estimate $\hat{\mathbf{x}}^{(j)} = [\hat{x}^j, \hat{v}_x^j, \hat{y}^j, \hat{v}_y^j]^\intercal$ of the distribution of component $j \in [1, \ldots, N_{DTD}]$ or the axis b^ℓ of sector $\ell \in [1, \ldots, N_S]$ of the surveillance area, $\mathbf{X}_k = \{\mathbf{x}^{(1)}, \ldots, \mathbf{x}^{(N_{DTD})}\}$ is the multitarget state at time k, N_{DTD} is the cardinality of $\mathbf{X}_k$ and $g_u(\mathbf{Z}|\mathbf{X}_k, u)$ is the measurement likelihood, which depends on the sensing mode u.

The expectation in the second term in Eq. (5.3) is trivial and skipped because unDTD is always updated using $1 - P_D(\mathbf{x})$ and therefore, does not depend on the measurement realization. If no tracks have been established, it holds that $H_{\text{track}}(\mathbf{X}_k|\mathbf{Z}) = 0$ and the corresponding term in Eq. (5.3) can be skipped.

The entropy of the DTD has been discussed in Chapter 4. The entropy unDTD is given in Rezaeian and Vo [2000]:

$$H_{\text{search}}(\mathbf{X}) = \text{E}[|\mathbf{X}|](1 + H(p(\mathbf{x}))) \tag{5.5}$$

where $\text{E}[|\mathbf{X}|] = \int D_{k|k}(\mathbf{x}|\mathbf{Z}_{1:k})\, \delta\mathbf{x}$ is the expected number of targets and $p(\mathbf{x})$ is the density that results from dividing the PHD $D_{k|k}(\mathbf{x}|\mathbf{Z}_{1:k})$ by the expected number of targets $\text{E}[|\mathbf{X}|]$.

If the evaluation of the RFS entropies in Eq. (5.3) cannot be done analytically, the entropies can be evaluated numerically by sampling from the corresponding multitarget states PDF/PHD (or using the samples from an SMC implementation) and then using the k-NN method proposed in Ajgl and Šimandl [2011].

The comparison is with respect to the uncertainty in the entropy of the resulting multitarget threat PDF and with respect to their tracking performance. The tracking performance is evaluated using the Optimal Sub-Pattern Assignment (OSPA) metric, see Schuhmacher et al. [2008] and Section 4.5. The OSPA metric is evaluated using the true states of the targets and the MaM estimator.

5.3. THREAT-BASED RADAR BEAM-POINTING FOR AREA SURVEILLANCE

5.3.1. EVALUATION OF THE THREAT LEVEL OF A TARGET

The motivation behind this approach, a longer discussion on how threat can be modeled and several simple examples can be found in Chapter 3.

In this chapter, an asset protection context is considered, i.e. it is assumed that an asset must be protected from hostile targets. The threat that is posed by a target i to asset j depends on how close and how fast the target i can come to asset j. These are measured by the time and range to Closest Point of Approach (CPA), as explained in Chapters 3 and 4.

In order to move from t_{CPA} and r_{CPA} to the threat domain, a simple linear function is utilized[2] $f : \mathscr{X} \longrightarrow \mathscr{T}$ that maps them to the threat domain $\mathscr{T}$. For convenience, threat θ_s is defined to take values in $\theta_s \in [0,1]$, with 0 indicating minimum and 1 indicating maximum threat. Accordingly, it is only necessary to define the points s_0, s_1 where threat becomes equal to 0 and 1 respectively. Then θ_s is given by

$$\theta_s(\mathbf{x}) = \begin{cases} 1 & \text{if } \frac{s-s_0}{s_1-s_0} \geq 1 \\ \frac{s-s_0}{s_1-s_0} & \text{if } s_0 < s < s_1 \\ 0 & \text{if } \frac{s-s_0}{s_1-s_0} \leq 0 \end{cases} \tag{5.6}$$

5

where s represents t_{CPA}, r_{CPA} and s_0, s_1 represent the values of t_{CPA}, r_{CPA} where threat is minimum and maximum respectively.

The two aspects of threat are aggregated using a weighted sum, much like in Chapters 3 and 4.

In the examples considered here, it is assumed that each target has its own threat PDF. Therefore, the cardinality distribution of the multitarget threat variable Θ is the same as the cardinality distribution of the multitarget states variable $\mathbf{X}$. The distribution of each individual threat depends on the distribution of the states of each target (or targets) present in the scenario.

5.3.2. EVALUATION OF THE UNCERTAINTY IN THREAT

UNCERTAINTY IN THE "DETECTED TARGETS" THREAT

When a CB-MeMBer filter is used, the multitarget threat RFS variable Θ is a union of N_{DTD} independent Bernoulli RFSs $\Theta^{(c)}$ with corresponding existence probabilities $r^{(c)} \in [0,1]$ and probability density $p\left(\theta^{(c)}\right)$ defined on $\mathscr{T} = [0,1]$ for $c = 1, \ldots, N_{DTD}$. Accordingly, the multitarget threat Θ is fully described by the corresponding multi-Bernoulli parameter set $\{r^{(c)}, p\left(\theta^{(c)}\right)\}_{c=1,\ldots,N_{DTD}}$, where $p\left(\theta^{(c)}\right) := p\left(\theta^{(c)}(\mathbf{x})\right) : \mathbf{x} \sim p^{(c)}(\mathbf{x})$. The multitarget threat Θ has the same cardinality distribution as the multitarget state RFS $\mathbf{X}$.

The entropy of the multitarget threat can be evaluated using Eq. (4.2), as discussed in Chapter 4. It now has the form:

$$H_{\text{track}}(\Theta) = H(|\Theta|) + \mathrm{E}[H(p_n(\theta))] - \mathrm{E}[\log(|\Theta|!)] - \mathrm{E}[|\Theta|]\log(\bar{K}) \tag{5.7}$$

Due to the proposed definition of the threat space $\mathscr{T} = [0,1]$, it holds that $\bar{K} = 1$. Therefore, the last term in Eq. (5.7) is equal to 0.

[2] More complicated functions, e.g. a sigmoid, can be used if it is deemed necessary by the radar operator.

UNCERTAINTY IN THE "UNDETECTED TARGETS" THREAT

Following the same reasoning, the threat posed by any undetected targets depends on the unDTD, which is estimated using a PHD filter. The threat PHD $D_\theta(\theta)$ is given by

$$D_\theta(\theta) = \lambda p_\theta(\theta(\mathbf{x})) \;\;,\;\; \mathbf{x} \sim p_{\mathbf{x}}(\mathbf{x}) = e^{-\lambda} \prod_{\mathbf{x}\in\mathscr{X}} \lambda p(\mathbf{x}) = e^{-\lambda} \prod_{\mathbf{x}\in\mathscr{X}} D_{\mathbf{x}}(\mathbf{x}) \tag{5.8}$$

where $\lambda = \mathrm{E}[|\Theta|] = \mathrm{E}[|\mathbf{X}|] = \int D_{k|k}(\mathbf{x}|\mathbf{Z}_{1:k})\,\delta\mathbf{x}$ is the expected number of targets and $p_\theta(\theta)$ is the density that results from dividing the threat PHD by the expected number of targets λ. Each target has its own threat level and therefore, the "undetected targets" threat variable Θ has the same cardinality distribution as the "undetected targets" variable $\mathbf{X}$.

The entropy of the "undetected targets" threat PHD is given by Rezaeian and Vo [2000]:

$$H_{\text{search}}(\Theta) = \mathrm{E}[|\Theta|](1 + H(p(\theta(\mathbf{x})))) \tag{5.9}$$

5.3.3. RESOURCE ALLOCATION

Due to the assumption that DTD and unDTD are decoupled, the overall threat is given by the concatenation of the threat posed by any detected and undetected targets. As a consequence, the entropy of the total threat-level is given by the sum of the entropies of these two densities. Accordingly, the index u_k of the sensing action to be performed at time k is given by:

$$\begin{aligned} u_k &= \arg\min_u \left\{ \int H_{\text{track}}(\Theta_{k|k}|\mathbf{Z})\, g_u(\mathbf{Z}|\mathbf{X}_k, u)\,\delta\mathbf{Z} + \int H_{\text{search}}(\Theta_{k|k}|\mathbf{Z})\, g_u(\mathbf{Z}|\mathbf{x}, u)\,\delta\mathbf{Z} \right\} \\ &= \arg\min_u \left\{ \int H_{\text{track}}(\Theta_{k|k}|\mathbf{Z})\, g_u(\mathbf{Z}|\mathbf{X}_k, u)\,\delta\mathbf{Z} + H_{\text{search}}(\Theta_{k|k}|\mathbf{Z} = \emptyset, u) \right\} \end{aligned} \tag{5.10}$$

where

$$u = \left\{ \operatorname{atan2}(\hat{y}^j, \hat{x}^j) \right\} \bigcup \left\{ b^\ell \right\}, \tag{5.11}$$

The expectation in the second term in Eq. (5.10) is trivial and skipped because unDTD is always updated using $1 - P_D(\mathbf{x})$ and therefore, does not depend on the measurement realization. If no tracks have been established, it holds that $H_{\text{track}}(\Theta_{k|k}|\mathbf{Z}) = 0$ and the corresponding term in Eq. (5.10) can be skipped.

If the evaluation of the RFS entropies in Eq. (5.10) cannot be done analytically, the entropies can be evaluated numerically by sampling from the corresponding multitarget states PDF/PHD (or using the samples from an SMC implementation) and then using the k-NN method proposed in Ajgl and Šimandl [2011].

5.4. SIMULATED EXAMPLES

The first set of experiments considers examples where no external information is available about the arrival of targets. This is the simplest experimental setting for demonstrating how the search versus tracking trade-off can be achieved based on tuning the corresponding model parameters and thus avoiding the use of heuristics and scaling factors.

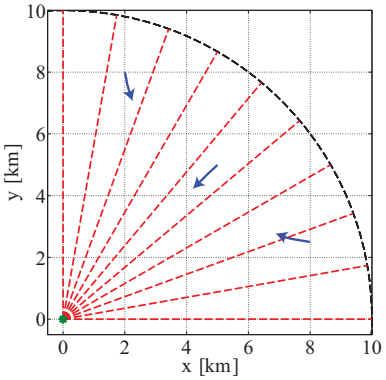

Figure 5.1: Three targets are present and must be found and tracked. The radar is located at the origin of the axes. The surveillance area is divided in 9 sectors of 10 degrees that correspond to the search beam-width of the radar.

Subsequently, a simulated example is shown where external information is available about the arrival of any new targets. In this case, it is demonstrated how external information can be taken into account in a systematic way and how this contributes to better situation awareness and tracking performance.

5.4.1. NO EXTERNAL INFORMATION

EXPERIMENTAL SETUP

Consider a scenario where a radar is tasked with the surveillance of an area defined by $[0,90]$ degrees in bearing and $[0,10]$ km in range, as shown in Fig. 5.1. There exist three targets for the whole duration of the scenario, whose trajectories are also shown in Fig. 5.1.

The radar is set into operation at time $k = 0$ and starts searching for targets. When a target is detected, it must be tracked while the search continues for other undetected targets. The duration of the scenario is 150 time instances and 50 Monte Carlo runs are performed.

The true target parameters are: *Target 1*: initial position $[2,8]$ km and initial velocity $[1,-6]$ m/s; *Target 2*: initial position $[5,5]$ km and initial velocity $[-5,-5]$ m/s; and *Target 3*: initial position $[8,2.5]$ km and initial velocity $[-6,1]$ m/s.

The targets follow a nearly constant velocity model with noise covariance matrix:

$$\Sigma_w = \begin{bmatrix} \sigma_x^2 T^3/3 & \sigma_x^2 T^2/2 & 0 & 0 \\ \sigma_x^2 T^2/2 & \sigma_x^2 T & 0 & 0 \\ 0 & 0 & \sigma_y^2 T^3/3 & \sigma_y^2 T^2/2 \\ 0 & 0 & \sigma_y^2 T^2/2 & \sigma_y^2 T \end{bmatrix} \tag{5.12}$$

where $T = 1$ sec and $\sigma_x^2 = \sigma_y^2 = 0.3$ (m/s)^2. All targets have RCS $= 10$ m^2.

For evaluating the threat $m_t = m_r = 0.5$, $[t_1 \;\; t_0] = [0 \;\; 100]$ min and $[r_1 \;\; r_0] = [0 \;\; 15]$ km are used.

The radar provides range and bearing measurements according to u_k. The index u_k of the selected sensing mode contains information about the beam direction and

the sensing mode (search or tracking). The corresponding sensing parameters for each mode are given in 5.4.1.1.1 and 5.4.1.1.2. The main differences between a search and a track beam are that a track beam has smaller beamwidth but higher probability of detection and better range accuracy.

The parameters for the implementation of CB-MeMBer and PHD filters are given in 5.4.1.1.3. The multitarget threat entropy is evaluated using the 50 nearest neighbors of each particle and the k-NN approach presented in Ajgl and Šimandl [2011]. Due to computational complexity reasons, only 25 nearest neighbors of each particle are used for evaluating the multitarget states entropy.

5.4.1.1.1 Search mode parameters A search beam has width of 10 degrees without loss due to the target not being on the boresight of the beam. The direction of a search beam can be one of the axes of the sectors resulting from dividing the surveillance area by 10 degrees, i.e. one of $\{5, 15, \ldots, 85\}$ degrees. The measurement noise covariance matrix is $\Sigma_v = \text{diag}[(20\text{ m})^2,\ (3\text{ degrees})^2]$ and it is ensured that a measurement always falls within the beamwidth. The probability of detecting a target is calculated using the radar equation and the Swerling I model, resulting in probability of detection in range of $[0.7777, 0.7994]$ for the specific trajectories of the targets. The probability of detection outside the radar beam is assumed to be zero. Furthermore, false alarms can arise with rate $\kappa = 5.73 \cdot 10^{-7}\ (\text{rad} \cdot \text{m})^{-1}$, i.e. a clutter measurement is received with probability 0.0001 at each time instance.

5.4.1.1.2 Tracking mode parameters A track beam has width of 2 degrees without loss due to the target not being on the boresight of the beam. The direction of a track beam is defined by the radar location and the MAP estimate $\hat{\mathbf{x}}^{(j)} = [\hat{x}^j, \hat{v}_x^j, \hat{y}^j, \hat{v}_y^j]^\intercal$ of the target to be observed. The measurement noise covariance matrix is defined as $\Sigma_v = \text{diag}[(10\text{ m})^2,\ (0.5\text{ degrees})^2]$ and it is ensured that a measurement always falls within the beamwidth. The probability of detecting a target is calculated using the radar equation and the Swerling I model, resulting in probability of detection in range of $[0.9123, 0.9161]$ for the specific trajectories of the targets. The probability of detection outside the radar beam is assumed to be zero. Furthermore, false alarms can arise with rate $\kappa = 2.87 \cdot 10^{-7}\ (\text{rad} \cdot \text{m})^{-1}$, i.e. a clutter measurement is received with probability 0.0001 at each time instance. The presence of false alarms and the probability of detection being less than one imply that the probability of confirming a track is less than one. Furthermore, the problem of deciding which measurements are false alarms and which are target-originated is solve by the CB-MeMBer over time.

5.4.1.1.3 Filtering parameters Irrespective of the chosen sensing mode u_k, any measurement that is received is only used for updating the DTD. The unDTD is always updated using $1 - P_D(\mathbf{x})$.

At time $k = 0$ the CB-MeMBer filter has no Bernoulli components (tracks) because no target has been detected yet and it is assumed that there is no external knowledge about any existing targets. New tracks are initiated from measurements of the previous time instance that were not assigned to any existing tracks (if there are any). The newly created tracks are initialized with $r^{(i)} = 0.5$, standard deviation of 100 m round the measured $x-y$ position and with $x-y$ velocity uniformly random in $[-7, 1]$ m/s. The targets'

motion is modeled using a nearly constant velocity model with noise covariance matrix $\Sigma = 2\Sigma_w$. Notice that the tracking model does not match perfectly the true motion model of the targets in order to pose an extra challenge to the radar resource management algorithm. The probability of survival of each target is $p_{S,k} = 0.99$ and tracks with $r^{(i)} < 0.005$ are pruned. Each Bernoulli component (track) is approximated using 2000 particles. Resampling is performed after every update step.

The PHD filter is initialized with three different expected number of targets $N_{0|0}$ and with $50 \cdot 10^3$ particles uniformly distributed in the surveillance area with $x-y$ velocities uniformly random in $[-7,1]$ m/s. This represents the time instance when the radar is turned on and when there is no prior information about any existing targets. The targets' motion is modeled using a nearly constant velocity model with noise covariance matrix $\Sigma = 2\Sigma_w$. New targets are assumed to be born at each time instance at *a*) the border of the surveillance area, with $x-y$ velocities uniformly random in $[-7,1]$ m/s and with three different expected cardinalities using 2000 particles, modeling newly-arrived targets; and *b*) uniformly in the surveillance area, with $x-y$ velocities uniformly random in $[-7,1]$ m/s and with three different expected cardinalities using 2000 particles, modeling pop-up targets. The probability of survival is $p_s(\mathbf{x}') = 0.99$. Multinomial resampling is performed when the number of particles is higher than $75 \cdot 10^3$ or when the efficient number of particles is smaller than $10 \cdot 10^3$.

Three cases are considered:

Low expected number of undetected targets: the PHD filter is initialized with $N_{0|0} = 0.5$, newborn targets are modeled at the border of the surveillance area with expected cardinality 0.05 and at the whole surveillance area with expected cardinality 0.005;

Medium expected number of undetected targets: the PHD filter is initialized with $N_{0|0} = 2$, newborn targets are modeled at the border of the surveillance area with expected cardinality 0.1 and at the whole surveillance area with expected cardinality 0.01; and

High expected number of undetected targets: the PHD filter is initialized with $N_{0|0} = 5$, newborn targets are modeled at the border of the surveillance area with expected cardinality 0.5 and at the whole surveillance area with expected cardinality 0.05.

THREAT UNCERTAINTY AND TRACKING RESULTS

By averaging the sensor selections over 50 Monte Carlo runs it was noticed that:

Low expected number of undetected targets: the proposed threat-based approach uses **84.4**% of the time instances a search beam and in the remaining **15.6**% it uses a tracking beam for observing a target. The corresponding percentages for periodic search & tracking are 72.9% and 27.1% respectively. The minimization of the entropy of the DTD and unDTD leads to using a search beam 98.6% of time instances and in only 1.4% a tracking beam;

Medium expected number of undetected targets: the proposed threat-based approach uses **86.1**% of the time instances a search beam and in the remaining **13.9**% it uses a tracking beam for observing a target. This means that the threat-based approach now assigns more time to searching because more targets are expected to be found. The corresponding percentages for periodic search & tracking are 72.8% and 27.2% respectively. The minimization of the entropy of the DTD and unDTD leads to using a search beam 99.6% of time instances and in only 0.4% a tracking beam;

High expected number of undetected targets: the proposed threat-based approach

uses **91**% of the time instances a search beam and in the remaining **9**% it uses a tracking beam for observing a target. This means that the threat-based approach assigns now even more time to searching because even more targets are expected to be found. The corresponding percentages for periodic search & tracking are 72.81% and 27.18% respectively. The minimization of the entropy of the DTD and unDTD leads to using a search beam 100% of time instances;
From the aforementioned percentages it can be concluded that the proposed threat-based approach can take into account knowledge about the expected number of undetected targets and adapts accordingly the resource allocation to tracking and search functions. The periodic approach does not demonstrate any adaptive resource allocation and the minimization of the entropy of the DTD and unDTD gives minimal control on the search-to-track time ratio. The behavior of the minimization of the entropy of the DTD and unDTD can be explained by the fact that these two entropies are disproportionate because they measure the uncertainty of two completely different densities.

The maximum number of tracks that is maintained when estimating the DTD is also examined. By looking at all the Monte Carlo runs it can be observed that:
Low expected number of undetected targets: the proposed threat-based approach maintains a maximum of 6 tracks whereas the periodic approach maintains up to 8 tracks and the states-based approach up to 6;
Medium expected number of undetected targets: the proposed threat-based approach maintains a maximum of 7 tracks whereas the periodic approach maintains up to 8 tracks and the states-based approach up to 6; and
High expected number of undetected targets: the proposed threat-based approach maintains a maximum of 6 tracks whereas the periodic approach maintains up to 8 tracks and the states-based approach up to 6.
It can be concluded that the adaptive approaches have better performance in rejecting false alarms. This results in faster computation times at the update step of the DTD and this happens because the computational complexity of the CB-MeMBer filter scales exponentially with the number of components/tracks.

Figures 5.2a through 5.2c show the entropy of the posterior threat PDF, averaged over 50 Monte Carlo runs. It can be seen that the proposed, threat-based approach always results in lower uncertainty in the multitarget threat PDF.

Figures 5.3a through 5.5c show the OSPA metric and its components for $c = 250$ and $p = 2$, averaged over 50 Monte Carlo runs. The proposed approach results in lower OSPA values, especially due to lower cardinality error. This can also be noticed in Fig. 5.6a through 5.6c, where the estimated number of targets is shown, averaged over 50 Monte Carlo runs.

Figures 5.7a through 5.7c show the search time instances per sector. It can be seen that the proposed approach devotes less time in sectors where targets are located, i.e. first in sectors 2,5,8 and then in sector 3 instead of 2. This can be explained by the behavior of CB-MeMBer filter that can have unstable behavior when updating the track existence probabilities, also see the discussion in [Bocquel, 2013, Sec. 5.3].

Figures 5.8a through 5.8c show the expected number of undetected targets, averaged over 50 Monte Carlo runs, for the two compared approaches. It can be noticed that the proposed approach reaches a higher steady-state value even though more search actions are performed. The key difference is that the search actions are not evenly dis-

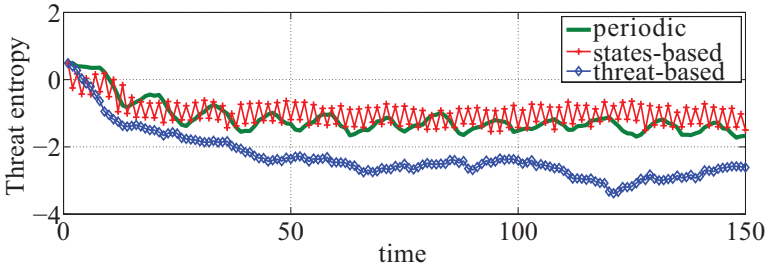

(a) Low expected number of undetected targets.

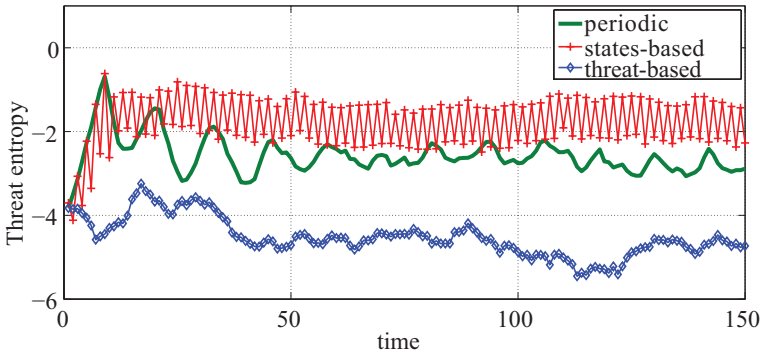

(b) Medium expected number of undetected targets.

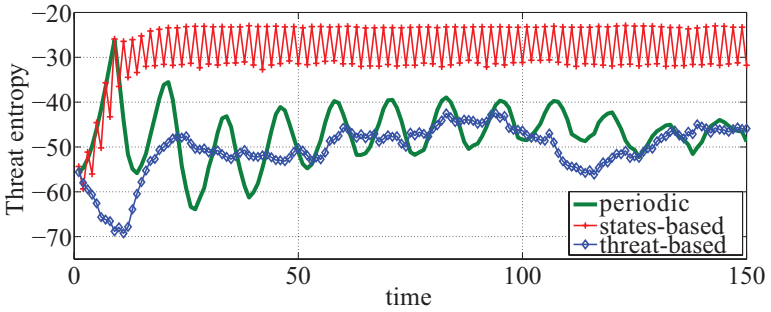

(c) High expected number of undetected targets.

Figure 5.2: The posterior entropy of the estimated multitarget threat pdf, averaged over 50 Monte Carlo runs. The proposed approach results in lower uncertainty in threat than the other approaches.

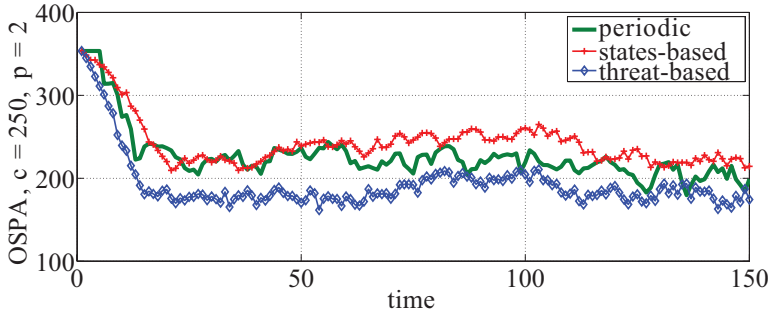

(a) Low expected number of undetected targets.

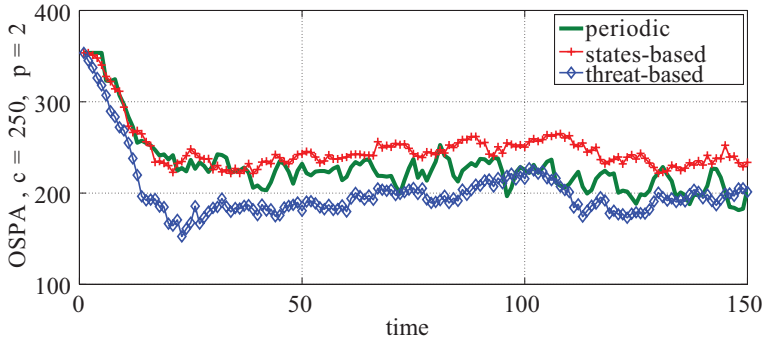

(b) Medium expected number of undetected targets.

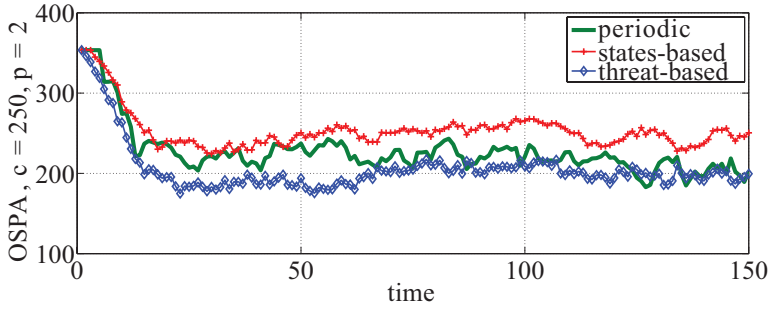

(c) High expected number of undetected targets.

Figure 5.3: The OSPA metric, averaged over 50 Monte Carlo runs. The threat-based scheme has the best performance.

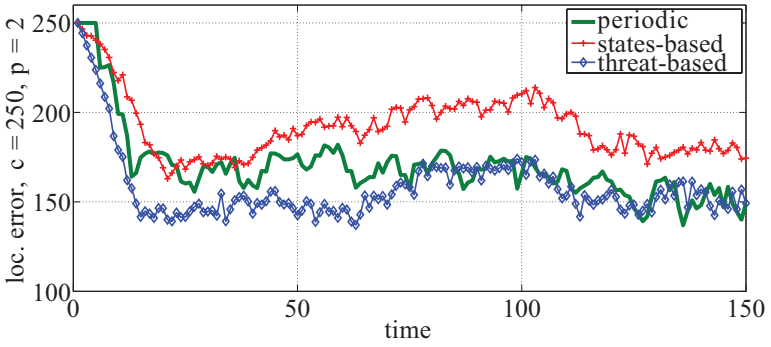

(a) Low expected number of undetected targets.

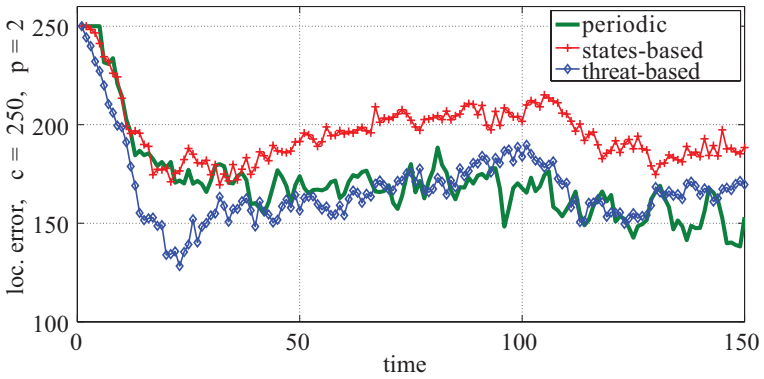

(b) Medium expected number of undetected targets.

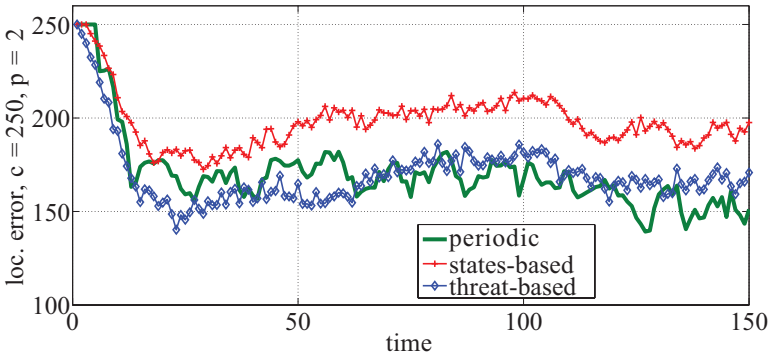

(c) High expected number of undetected targets.

Figure 5.4: The localization error, averaged over 50 Monte Carlo runs. The threat-based scheme has similar performance to periodic search and tracking.

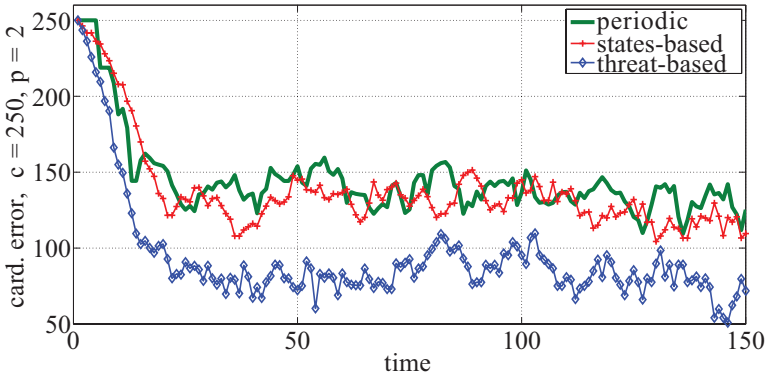

(a) Low expected number of undetected targets.

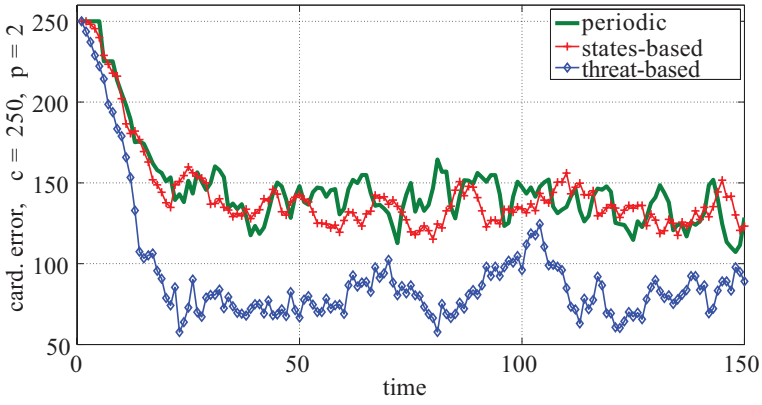

(b) Medium expected number of undetected targets.

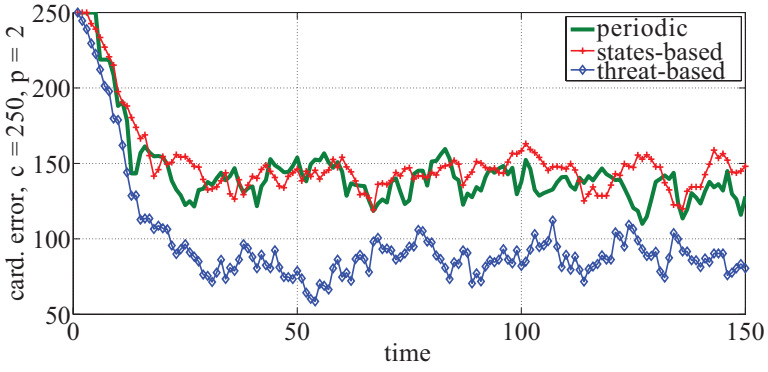

(c) High expected number of undetected targets.

Figure 5.5: The cardinality error, averaged over 50 Monte Carlo runs. The threat-based scheme has the best performance.

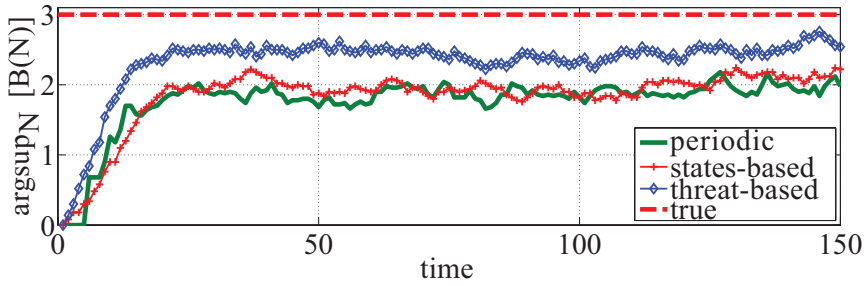

(a) Low expected number of undetected targets.

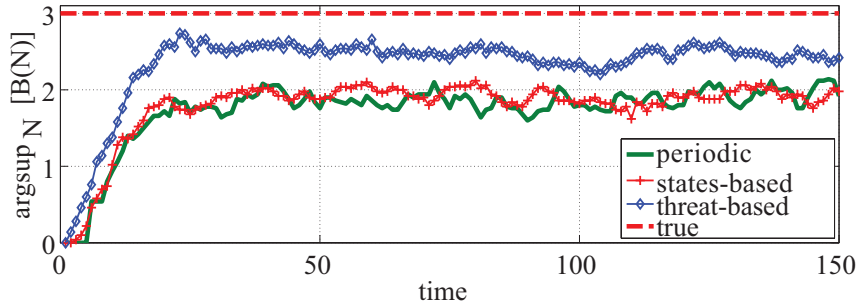

(b) Medium expected number of undetected targets.

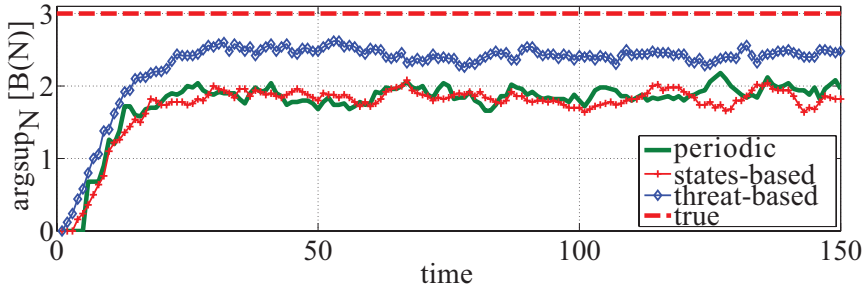

(c) High expected number of undetected targets.

Figure 5.6: The MAP estimate of number of detected targets in the considered scenario, averaged over 50 Monte Carlo runs. The proposed approach results in a better estimate.

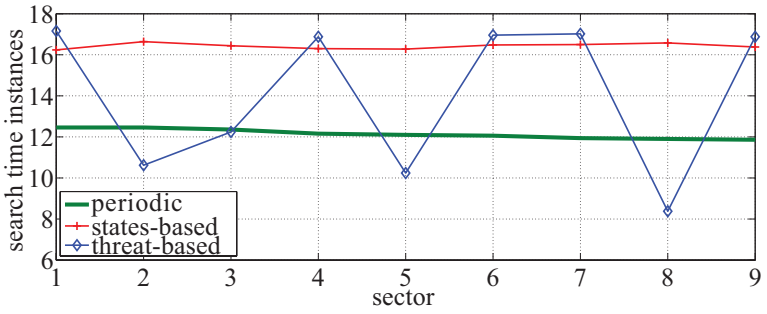

(a) Low expected number of undetected targets.

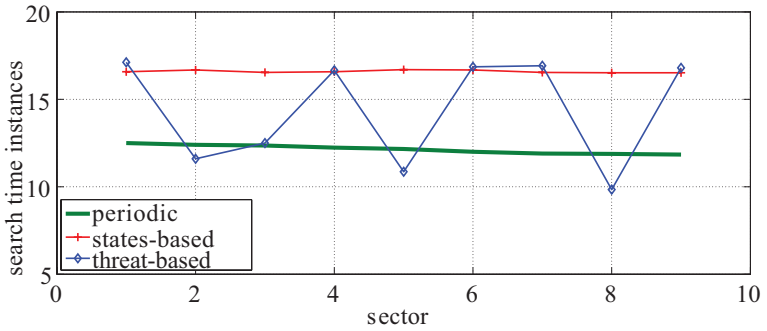

(b) Medium expected number of undetected targets.

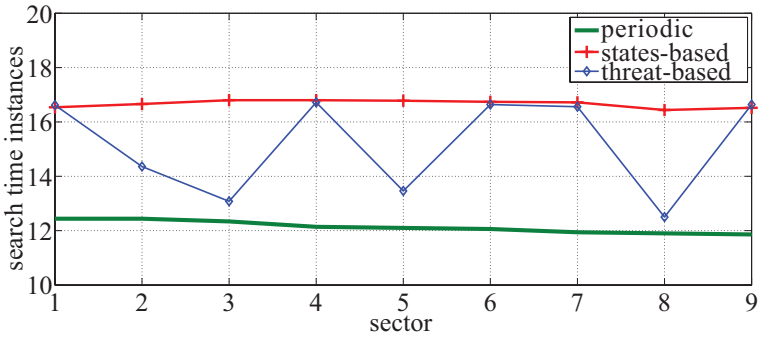

(c) High expected number of undetected targets.

Figure 5.7: The time instances of search per sector. The proposed approach spends less time in sectors where targets are located, which can be attributed to the behavior of CB-MeMBer filter.

tributed among all sectors.

The argument that the behavior of the proposed approach is heavily affected by the selection of CB-MeMBer filter can also be justified by looking at the performance of periodic search and tracking. In Fig. 5.2 through 5.8 it can be seen that as targets are detected and components are added in CB-MeMBer filter, oscillations appear in the corresponding curves. This also implies that the main component of uncertainty is the estimated DTD and especially its cardinality.

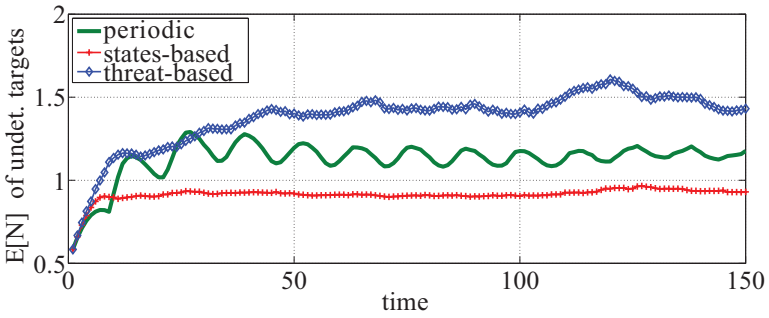

(a) Low expected number of undetected targets.

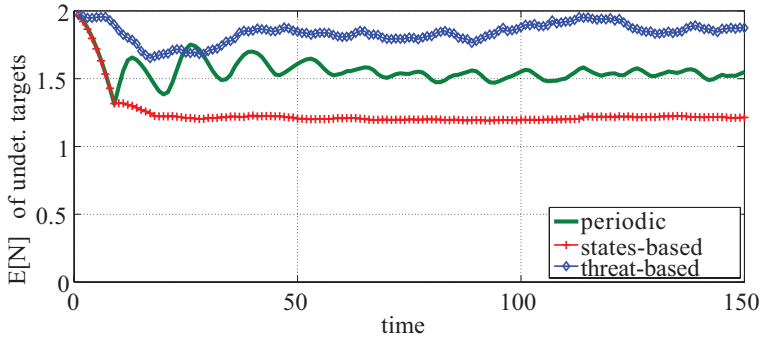

(b) Medium expected number of undetected targets.

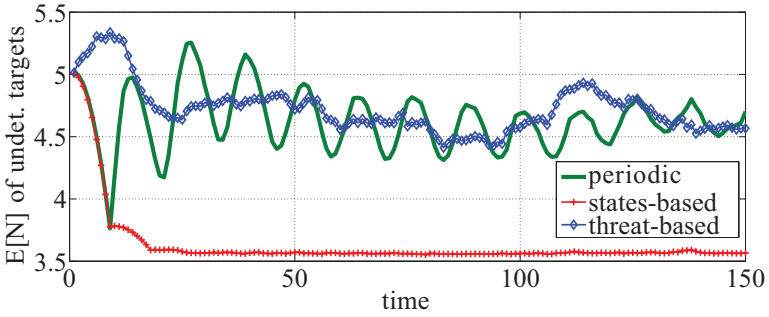

(c) High expected number of undetected targets

Figure 5.8: The expected number of undetected targets, averaged over 50 Monte Carlo runs. The proposed approach may result in a higher steady-state value even though more time is dedicated to searching for targets when compared to periodic search-and-track. This happens because the search actions are not evenly distributed among all sectors.

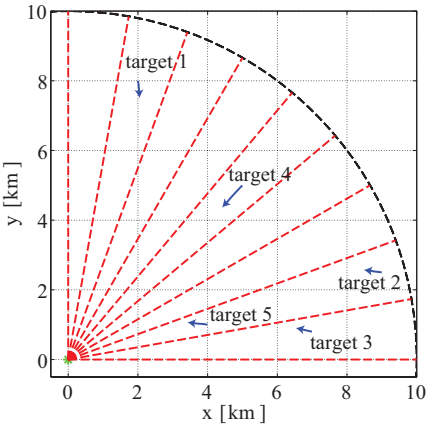

Figure 5.9: The geometry of the considered scenario. Five targets in total but not simultaneously are present and must be found and tracked. The radar is located at the origin of the axes and targets appear and disappear during the scenario. The surveillance area is divided in 9 sectors of 10 degrees that correspond to the search beam-width of the radar.

5.4.2. TAKING INTO ACCOUNT EXTERNAL INFORMATION

Let us assume now that it is known that more targets arrive from directions in [0,20] degrees, i.e., from the two first sectors using a counter-clockwise direction. The trajectories of five targets in such a scenario are shown in Figure 5.9. The duration of the scenario is 200 time instances. Each target exists for a limited amount of time and there is detection uncertainty:

Target 1: from $t = 1$ until $t = 79$. The resulting probability of detection is in the range of $[0.7777,\ 0.7818]$ for a search and in $[0.9125,\ 0.9132]$ for a tracking beam;

Target 2: from $t = 1$ until $t = 90$. The resulting probability of detection is in the range of $[0.768,\ 0.7721]$ for a search and in $[0.9111,\ 0.9117]$ for a tracking beam;

Target 3: from $t = 80$ until $t = 150$. The resulting probability of detection is in the range of $[0.7888,\ 0.7931]$ for a search and in $[0.9143,\ 0.915]$ for a tracking beam;

Target 4: from $t = 91$ until $t = 200$. The resulting probability of detection is in the range of $[0.7885,\ 0.7969]$ for a search and in $[0.9143,\ 0.9157]$ for a tracking beam; and

Target 5: from $t = 91$ until $t = 200$. The resulting probability of detection is in the range of $[0.8195,\ 0.8261]$ for a search and in $[0.9199,\ 0.9212]$ for a tracking beam.

The only difference from the experimental settings in the previous section is that now the external information about targets arriving more often in the specific two sectors is taken into account. The PHD filter is now initialized with $N_{0|0} = 2$. New targets are assumed to be born at each time instance at *a*) the border of the surveillance area, with $x-y$ velocities uniformly random in $[-7,1]$ m/s and with expected cardinality 0.1 using 2000 particles, modeling newly-arrived targets; *b*) uniformly in the surveillance area, with $x-y$ velocities uniformly random in $[-7,1]$ m/s and with expected cardinality 0.01

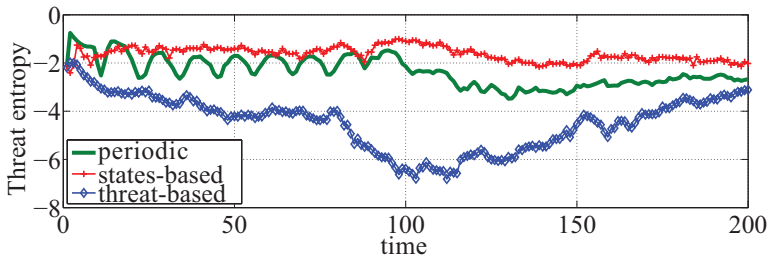

Figure 5.10: The posterior entropy of the estimated multitarget threat pdf, averaged over 50 Monte Carlo runs. The proposed approach results in the lowest uncertainty.

using 2000 particles, modeling pop-up targets; and *c*) uniformly in the first two sectors, with $x-y$ velocities uniformly random in $[-7,1]$ m/s and with expected cardinality 0.005 using 2000 particles, modeling pop-up targets in the first two sectors.

By averaging the sensor selections over 50 Monte Carlo runs it was noticed that the proposed threat-based approach uses 88.21% of the time instances a search beam and in the remaining 11.73% it uses a tracking beam for observing a target. The corresponding percentages for periodic search & tracking are 76.39% and 23.61% respectively. When using the states-based entropy, the corresponding percentages for periodic search & tracking are 99.13% and 0.84% respectively.

The maximum number of tracks that is maintained when estimating the DTD is examined again. By looking at all Monte Carlo runs it can be observed that the adaptive (threat- and states-based entropy) approaches maintain a maximum of 7 tracks. The periodic approach maintains up to 9 tracks. It can be concluded that the adaptive approaches have better performance in rejecting false alarms. Furthermore, this results in faster computation times at the update step of the DTD.

Figure 5.10 shows the entropy of the posterior threat PDF, averaged over 50 Monte Carlo runs. It can be seen that the proposed, threat-based approach results in lower uncertainty in the multitarget threat PDF.

Figures 5.11a through 5.11c show the OSPA metric and its components for $c = 250$ and $p = 2$, averaged over 50 Monte Carlo runs. The proposed approach results in lower OSPA values, especially due to lower cardinality error. This can also be noticed in Fig. 5.12, where the estimated number of targets is shown, averaged over 50 Monte Carlo runs.

Figure 5.13 shows the search time instances per sector. It can be seen that both adaptive approaches devote more time than the periodic search in the first two sectors where more targets are expected to be found. It can also be noticed that when using the threat-based approach, sector two receives less attention than sector one, contrary to the behavior of the states-based approach. This can be explained by: *a*) the "leakage" of particles to sectors 1 and 3; and *b*) the specific behavior of the CB-MeMBer filter regarding the update of track existence probabilities, also discussed in the previous set of experiments.

Figure 5.14 shows the expected number of undetected targets, averaged over 50 Monte Carlo runs, for the two compared approaches. It can be noticed that the proposed approach reaches the highest steady-state value even though more search actions are per-

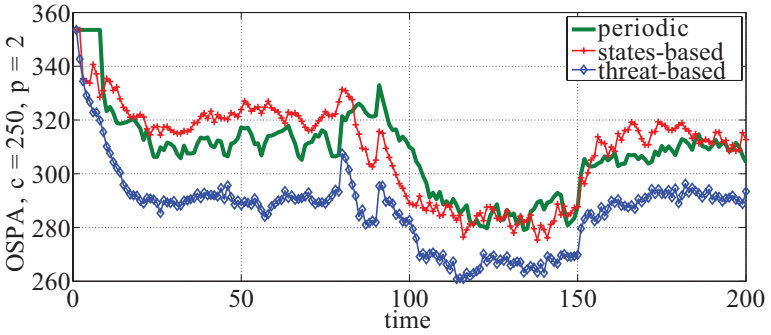

(a) OSPA metric.

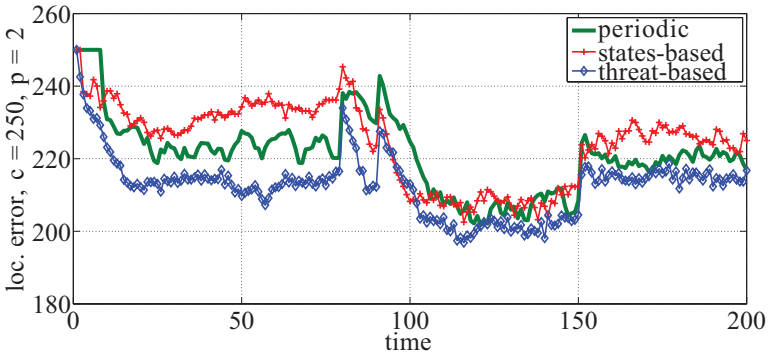

(b) Localization component.

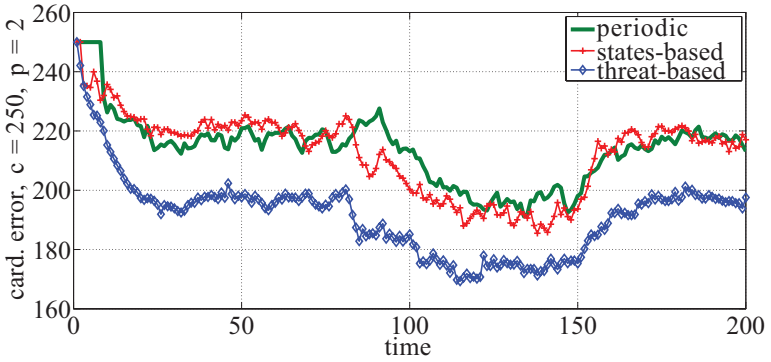

(c) Cardinality component.

Figure 5.11: The OSPA metric and its component, averaged over 50 Monte Carlo runs. The threat-based scheme has the best performance.

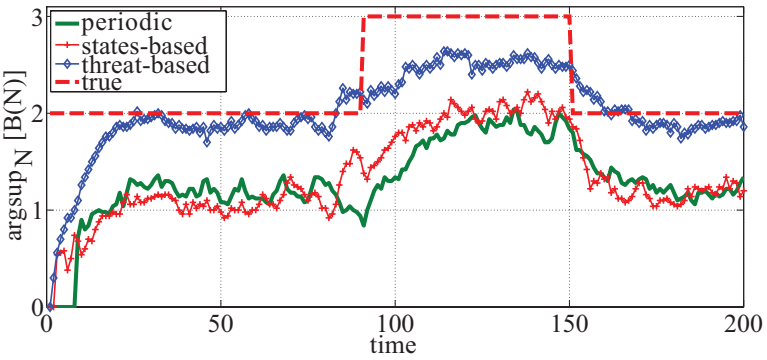

Figure 5.12: The MAP estimate of number of detected targets in the considered scenario, averaged over 50 Monte Carlo runs. The proposed approach provides the most accurate estimate.

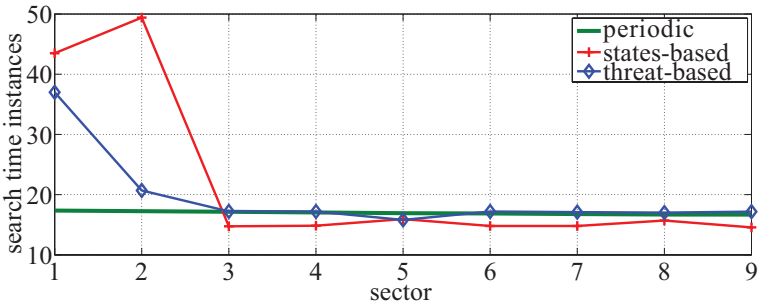

Figure 5.13: The time instances of search per sector. The adaptive approaches spend more time in the two sectors where more targets are expected to be found.

formed when compared to the periodic approach. The key difference is that the search actions are not evenly distributed among all sectors. The states-based approach attains the lowest steady-state value because it almost exclusively uses search beams.

5.5. SUMMARY

In this chapter, an application of the proposed, threat-based approach was presented for performing area surveillance. The proposed approach controlled an agile radar-beam such that multiple targets could be detected and tracked. The goal was to demonstrate that the proposed, threat-based approach can be used with state-of-the-art signal processing algorithms for producing Bayes-optimal allocation of radar resources such that multiple target can be detected and tracked.

The multitarget filtering problem was solved using a CB-MeMBer filter. A PHD filter was used for estimating where any undetected targets could be and therefore, where the radar should search for any undetected targets. The proposed algorithm managed the uncertainty in the threat that is posed both by the detected and any undetected targets in the considered scenarios.

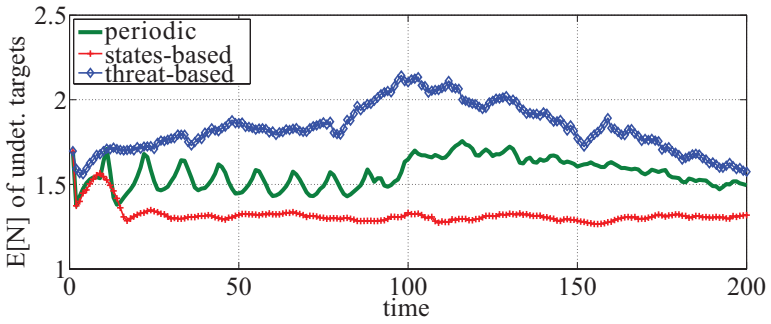

Figure 5.14: The expected number of undetected targets, averaged over 50 Monte Carlo runs. The proposed approach results in a higher steady-state value even though more time is dedicated to searching for targets when compared to the periodic approach.

Via simulated examples it was shown that the proposed algorithm managed to detect all targets, maintained the tracks for the whole duration of the scenario and suppressed any false tracks. The proposed approach outperformed periodic resource allocation and allocating resources based on the entropy of the DTD and unDTD in: *a*) achieving lower uncertainty in the threat-level of all targets; *b*) estimating the correct number of targets present in the considered scenario; *c*) localizing the detected targets; and *d*) maintaining less tracks, thus lowering the computation time at the update step.

Moreover, it was demonstrated that the proposed, threat-based resource allocation scheme can achieve a resource trade-off among search for and tracking of multiple targets only by tuning model parameters used in the filters. In the presented examples, any information available about the number and the location of undetected targets was incorporated in the models used for estimating the unDTD. The incorporation of external information lead to adaptive allocation of radar-time among the search for and tracking of multiple targets. Such external information can be intelligence about the strategy of incoming targets, historical traffic data and even map-data that describe the location of airports.

The model-based incorporation of external information when performing adaptive area surveillance is a major advantage over the existing resource allocation schemes. Ad-hoc solutions, such as scaling factors (that control the track/search time ratio), are completely avoided. In other words, the proposed approach results in the first model-based and Bayes-optimal solution to balancing the tasks of searching for and tracking of multiple targets while taking into account the operational context.

6

CONCLUSIONS

This chapter concludes this dissertation by summarizing the results achieved and providing suggestions for future research.

6.1. CONCLUDING REMARKS

Radar resource management is a necessary component of modern, efficient radar systems. It is used for allocating the limited radar resources such that the operational goal of a radar system, e.g. asset protection or air-traffic-control, is achieved. The construction of such resource management algorithms is a daunting task, also inhibited by changes in operational goals depending on the mission at hand. In this thesis, I have explored the existing solutions to radar resource management, compared their performance, determined their shortcomings, and proposed a new method for addressing the disadvantages of the existing solutions.

In Chapter 2, I analyzed and compared the performances of task-based and information-driven sensor management approaches based on two case-studies. Using the first case-study, I showed that task-based and information-driven objective functions can result in similar sensor selections when the estimated PDF is multimodal and there exists a sensing option that can eliminate the multiple modes. Using the second case-study, I found a practical explanation of an information theoretic sensor management criterion when performing search for an object/target. The results of these case studies were reported in Katsilieris et al. [2012b,a]. This similarity (and in certain cases equivalence) is both unexpected and important. It is unexpected because the compared criteria are fundamentally different and important because a practical explanation is found for an information theoretic criterion.

In a comparison presented in Chapter 2, both these and the other existing approaches to sensor management have been found to lack the combination of three essential properties: *Bayes-optimal* allocation of resources *among diverse tasks* while *taking into account explicitly the user-needs* within a given operational context. This combination is of special importance when a set of tasks must be executed in different operational contexts. A typical example is the use of an MFR for detecting and tracking aircrafts.

Why would the same trade-off between search and tracking be optimal when performing asset-defense and when performing air-traffic-control? Rephrasing this conclusion using JDL terminology, it is extremely difficult (or even impossible) to formulate an optimization problem for controlling a multi-functional system, in this case an MFR, using objective functions based on Level 0/1 quantities.

To deal with the shortcomings of sensor management approaches that are based on JDL Level 0/1 quantities, I proposed in Chapter 3 a systematic method for modeling mathematically Level 2/3 quantities that are directly related to the operational goal of the radar system (or the platform that carries it). The key idea behind the proposed approach is that radar resources can be allocated such that the uncertainty in higher-level quantities, such as the threat-level of a target, is managed. Accordingly, I explain how objective functions can be formulated for controlling an agile sensor in operational contexts as diverse as asset defence and traffic control. The proposed approach is motivated by the threat assessment process, which is an integral part of defense missions. The novelty of the proposed method lies in managing the uncertainty in threat-level instead of *a*) allocating resources according to threat-level; or *b*) managing the uncertainty in the states' PDF of a target.

The feasibility and flexibility of the proposed approach were demonstrated in Chapter 3 via simple but illustrating simulated examples. The main difference in the presented examples is the way that threat is modeled. By changing the mathematical definition of threat according to the operational context, different resource allocations can be obtained. These results were also reported in Katsilieris et al. [2014, 2015a].

In Chapter 4, I showed that the proposed approach can also be used for tracking multiple targets in complicated experimental settings. Detection uncertainty in the measurement process was taken into account and a state-of-the-art signal processing algorithm, i.e. a CB-MeMBer filter, was used. I also showed that the proposed approach outperforms several existing approaches by achieving both better situational awareness and better tracking performance. This was demonstrated in two diverse operational contexts: asset-protection and air-traffic-control. Furthermore, by observing the behavior of the compared criteria, two rule-based schemes were defined that can be used for explaining the behavior of the compared criteria. One of these rule-based schemes performed almost as well as the proposed approach, albeit at a much lower computational cost. These results were also published in Katsilieris et al. [2015a].

In Chapter 5, I proposed using a density that describes where any undetected targets can be (denoted as unDTD). This density is updated sequentially and allows for model-based inclusion of information regarding target appearance and detection uncertainty among others. As a result, I showed that the approach proposed in Chapter 3 can now be used for solving the challenging problem of area surveillance while taking into account the operational context. In area surveillance the diverse tasks of searching for and tracking of multiple targets must be combined. The combination of the unDTD with the density describing the states of the detected targets is a novel idea that plays a crucial role in allocating the resources of an MFR adaptively among its search and tracking functions. Furthermore, the proposed approach does not use heuristics and scaling factors (that control the track/search time ratio). Therefore, it results in Bayes-optimal resource allocation between search and tracking while taking into account any external information that might be available. Moreover, I showed via simulated examples that

the threat-based approach outperforms both the periodic search-and-track approach and the approach that minimizes the intrinsic uncertainty in the two aforementioned densities. The proposed approach achieved both better situational awareness and better tracking performance. These results were also reported in Katsilieris et al. [2015b].

In summary, the advantages of the threat-based approach to sensor management, which I have proposed in this thesis, are:

- it manages the uncertainty in higher-level quantities that describe exactly what the user is interested in instead of managing the uncertainty in quantities that are relevant to what the user needs;
- no heuristics are used and therefore, the resulting resource allocation is always Bayes-optimal;
- it demonstrates adaptive behavior by taking into account any external information about target existence and arrival by tuning the corresponding model parameters; and more importantly
- it can also adapt to the operational context at hand, as shown in the presented examples where it was applied to diverse scenarios such as asset-protection and air-traffic-control.

In practice, the proposed method can be used in applications where agile sensors or sensor suites, such as MFRs or robots equipped with cameras, must perform complex tasks. A typical such application involves the combination of search for and tracking of multiple objects of interest, e.g. aircrafts or intruders. The proposed method can enhance the reconfigurability of such systems in two ways. First, by allowing a user to take into account in a model-based manner any available external information. Such external information can be provided by historical data, maps and even from intelligence sources. Secondly, a user can also select the aspects of threat that are of interest in a specific operational context. Therefore, the resulting resource allocations are also optimal with respect to a considered operational context.

The proposed method has certain limitations. The main challenge when applying the proposed, threat-based approach is the mathematical definition of threat in different contexts. Even though I have presented several interesting aspects of threat in two diverse contexts, it might be quite challenging to create such functions in other contexts that are not discussed in this thesis. Another limitation of this method is that, as seen in Chapter 3, depending on the mathematical definition of threat the proposed approach might not result in better performance than the existing approaches. This can be attributed to the myopic optimization schemes that are used, as discussed in Chapter 3. A way to address this issue is to use non-myopic optimization, such as OLFC schemes, but this might be infeasible due to the high computational complexity of the chosen signal processing algorithm and the chosen measure of uncertainty. I encountered the specific problem when I conducted experiments with low probability of detection or high false alarm rate using a CB-MeMBer filter and measuring the uncertainty in multitarget threat via its entropy.

Except for the threat-based approach and its applications, I achieved additional results during two research visits to the following institutes:

(a) Fraunhofer FKIE: I merged the research that I reported in Section 2.2 with the research of Dr. Alexander Charlish, reported in Charlish et al. [2011], in order to create an algorithm for online radar surveillance control. The results of this collaboration are discussed in Appendix A and were published in Katsilieris et al. [2012c].

(b) NATO-STO CMRE: I developed an algorithm that detects the spoofing of AIS messages. The algorithm compares the received position report with the information obtained by a radar system and determines, using a sequential probability ratio test, whether the AIS report is trustworthy or spoofed. The significance of the AIS spoofing detection problem and the results of this collaboration are discussed in Appendix B and were published in Katsilieris et al. [2013].

6.2. SUGGESTIONS FOR FUTURE RESEARCH

Resource management is a problem found in many domains besides radar target tracking. Such domains are robotics, wireless communications and medical imaging to name a few. Therefore, it is possible to extend the presented research both by addressing challenges within the radar domain and by exploring its application to other domains.

An outline of possible extensions to the presented approach to resource managements follows.

- More aspects of threat can be taken into account, possibly after interviewing sensor operators from different domains. Threat is a context-sensitive quantity and therefore, it is subject to a specific operational context where a sensor is used. In this way, a library of threat definitions could be compiled and operators could select the aspects of interests in a given operational context.

- The results presented in Chapters 4 and 5 depend heavily on the behavior of the specific signal processing algorithms that are used (PHD and CB-MeMBer filters). It would be of interest to test the performance of the proposed threat-based approach in connection with other signal processing algorithms, such as the one presented in Bocquel [2013].

- As seen in Chapter 3, if the tracking accuracy is not taken into account explicitly as an aspect of threat, practical problems might appear. It can lead, for example, to track loss because even though the radar system has minimized the uncertainty in the threat-level of a target, the tracking accuracy has decreased in levels that do not allow the tracking of the said target. For this reason, it is of interest to develop threat definitions that take into account the tracking accuracy.

- The threat definitions presented in this thesis do not take into account the target classification problem, e.g. estimating the *vessel-type* of a target. The proposed approach offers the possibility to take the classification problem into account by defining class conditional threat definitions and it would be of interest to explore such an extension.

- The proposed approach was not compared to the PENTI scheme proposed by Mahler in Mahler [2004], which also tries to improve the situational awareness

by taking into account the tactical significance of the targets present in a given scenario. It is of interest to implement the PENTI scheme using quantities of a running CB-MeMBer filter in order to compare its performance with the approach presented in this thesis.

- In Chapter 5, only an asset-protection scenario was presented. It would be of interest to also consider an air-traffic-control scenario. In such scenario, the two densities would interact when evaluating the multitarget threat PDF and therefore, the multitarget threat PDF would not have two decoupled components anymore. This would pose an added challenge when evaluating the uncertainty in the multitarget threat PDF, for instance via its entropy.

- In this thesis, the use of the estimated threat PDF was not considered in the context of decision making when actions must be taken. In other words, an operator might consider performing a series of actions based on the estimate of the threat-level of a target and its corresponding uncertainty. An interesting question that arises then is how the decision process can be also taken into account when selecting the best sensing action.

- The proposed approach can result in a very high computational load due to the combinatorial complexity of the entropy evaluation algorithm and of the chosen signal processing algorithm (in this thesis a CB-MeMBer filter). Therefore, methods to reduce the computational complexity are needed if the proposed approach is to be used in a system with real-time requirements.

- It would be of interest to apply the threat-based approach in robotics applications where autonomous robots are used for detecting dangerous objects (e.g. mines), intruders or search for survivors. In this context, threat is still an important higher-level quantity, relevant to the mission of the robots and interesting results can be obtained if the proposed approach is used for planning the trajectories for autonomous robots.

Appendices

A

MERGING THE 'UNDETECTED TARGET' DENSITY WITH CDAPS

This work was performed in collaboration with Dr. Alexander Charlish during my research visit to Fraunhofer FKIE, Bonn, Germany. The results were also published in Katsilieris et al. [2012c].

Section A.1 motivates the problem of online control for radar surveillance. Section A.2 formulates the parameter selection problem. Section A.3 describes the proposed solution of applying CDAPS based on the 'undetected target' density. Section A.4 describes the generation of surveillance performance measures from the 'undetected target' density, which is critical for the interface to the CDAPS algorithm. Section A.5 analyzes the simulated results and Section A.6 summarizes this work.

A.1. MOTIVATION

MFRs are subject to increasing appeal due to their ability to configure nearly instantaneously an array of radar parameters, subject to the requirements of different radar functions. This includes the ability to control an agile beam, which enables a dynamic time-energy resource allocation. Consequently, MFRs are able to maintain a large number of individual tasks, which support a variety of differing radar functions such as target tracking, surveillance and weapon guidance. The automated control and management of such sensors, given that the resources available for the numerous tasks are finite, remains a significant challenge.

The majority of literature on MFR resource management is focused on the control and scheduling of tracking tasks, and various solutions have been presented with local optimization, see for example van Keuk and Blackman [1993]; Koch [1999]; Boers et al. [2005], or consideration of the global optimization, as in Hansen et al. [2006]. However, much less consideration has been given towards the surveillance function, which is often implemented using a periodic search or simple rule based approaches. Such surveillance control schemes are unable to generate behavior that adapts to changes in

the environment or operational requirements and so do not fully exploit the hardware potential.

Recently, a number of works have addressed the problem of surveillance control for multifunction radars. In Bolderheij and Van Genderen [2004] the track and search functions of an MFR are scheduled according to a threat-based criterion. For scheduling surveillance tasks, the authors use ghost targets that dictate volume or horizon search instead of tracking tasks. In White et al. [2008] the authors use a user-defined *search-to-track* ratio. Accordingly, the sensor manager schedules the corresponding tasks of the radar. For performing surveillance, an estimate of the spatial density of previously undetected targets is utilized. The sensing action that maximizes the expected number of newly detected targets is chosen whenever a search function is scheduled. In Matthiesen [2010] an a priori probability distribution of the target to be detected is specified by a set of discrete target position probabilities corresponding to each search beam. The proposed method suggests making the next look in the search cell that will provide the maximum value of the incremental search energy and S/N payoff ratios for all cells and that will maximize the duty factor of each cell. Despite the successes of these previous works, resource is allocated myopically in general, without direct consideration of the finite resource constraint.

In Charlish et al. [2011] the Continuous Double Auction Parameter Selection (CDAPS) algorithm is introduced and demonstrated on the long-range surveillance function. CDAPS utilizes a market mechanism to find the global optimum parameter selection, in terms of utility maximization, given the global finite resource constraint. However, in Charlish et al. [2011], the CDAPS algorithm is applied using a simple model of the cumulative detection range with assumed expected target parameters. In Katsilieris et al. [2012a] a particle filter is proposed to estimate a probability density of the undetected target location in the surveillance volume. This probability density, as it depends on the received data, is a better basis for resource allocation than the simple model used in Charlish et al. [2011]. The undetected target location has also been proposed for surveillance control in Williams [2011] using a multi-target Poisson density and a (quasi) Newton method. In contrast, this paper utilizes a single target density of the undetected target location and applies the CDAPS algorithm. Additionally, this method is compared to the two myopic management criteria proposed in Katsilieris et al. [2012a], being the maximum expected KLD and maximum expected probability of detecting a target.

A.2. PROBLEM FORMULATION

Consider an MFR that performs surveillance along with its other tasks (target tracking, weapon guidance etc.). The considered problem amounts to finding the surveillance parameters $\mathbf{u}_i^{opt}$ for each sector i that maximizes a surveillance criterion J_i given a global resource constraint r_{max}:

$$\mathbf{u}^{opt} = \arg\max_{\mathbf{u}} \mathbf{J}(\mathbf{x}_k, \mathbf{Z}_{1:k-1}, \mathbf{z}, \mathbf{u}) \tag{A.1}$$

$$\text{subject to} \sum_{i=1}^{N_S} r_i(\mathbf{u}_i) \leq r_{max} \tag{A.2}$$

where

- $k = 1,2,\ldots$ is the time index;
- $i = 1,2,\ldots,N_S$ is the sector index;
- $\mathbf{x}_k \in \mathbb{R}^{N_s}$ is the state vector of the target at time k;
- $\mathbf{u} = [\mathbf{u}_1,\ldots,\mathbf{u}_{N_s}] \in \mathscr{U}$ is a generic parameter selection across all sectors and $\mathscr{U} \in \mathbb{R}^{N_u}$ is the set of all the available surveillance parameters;
- $\mathbf{z} \in \mathbb{R}^{N_z}$ is the simulated measurement using $\mathbf{u}$ and $\mathbf{Z}_{1:k-1} = \{\mathbf{z}_1,\ldots,\mathbf{z}_{k-1}\}$ is the measurement history up to and including time $k-1$;
- $\mathbf{u}^{opt} = [\mathbf{u}_1^{opt},\ldots,\mathbf{u}_{N_s}^{opt}] \in \mathscr{U}$ is the optimal parameter selection across all sectors;
- $\mathbf{J} = [J_1,\ldots,J_{N_S}]$ is the vector of the criteria to be optimized;
- $r_i(\mathbf{u}_i)$ is the resource loading per sector i due to the surveillance parameters $\mathbf{u}_i$ expressed as percentage throughout; and
- r_{max} is the global resource constraint expressed as percentage throughout

This is a challenging multiobjective, constrained optimization problem.

A.3. PROPOSED SOLUTION

The proposed solution is to allocate the finite resource available for surveillance using the CDAPS algorithm, using information extracted from the estimated probability density of the undetected target.

A.3.1. CONTINUOUS DOUBLE AUCTION PARAMETER SELECTION (CDAPS)

The CDAPS algorithm has been developed in order to solve multi-objective constrained optimization problems in an efficient way, see Charlish [2011]. The CDAPS algorithm is an agent based approach to optimization where distributed agents, each representing single tasks, produce the global optimum resource allocation under a global resource constraint. The optimum is defined in terms of maximization of utility, where utility functions can be defined for each task, which map from task quality to utility space. The optimization is performed using a continuous double auction, where each agent is able to buy or sell resource, given the performance of its represented task.

In this paper, each agent represents the task of surveillance of a given sector and the surveillance parameters are the dwell time τ_c and the revisit interval t_f.

A full description of the CDAPS algorithm can be found in Charlish [2011] and the algorithm is demonstrated for radar surveillance function in Charlish et al. [2011] and the active tracking function in Charlish et al. [2012]. The CDAPS algorithm requires that the resource loading, task quality and utility from each potential parameter selection can be calculated. The method of extracting these from the 'undetected target' PDF is described in Sec. A.4.

CDAPS tackles the multi-objective constrained optimization problem by assuming that each criterion J_i can be mapped to a concave utility function V_i of the resource and requiring that the sum of the individual utility functions V_i be maximized. The

problem described by Eq. (A.1) and (A.2) is now simplified to a concave, single objective, constrained optimization problem:

$$\mathbf{u}^{opt} = \arg\max_{\mathbf{u}} \left[\sum_{i=1}^{N_S} V_i(\mathbf{u}) \right] \tag{A.3}$$

$$\text{subject to} \sum_{i=1}^{N_S} r_i(\mathbf{u}_i) \leq r_{max} \tag{A.4}$$

As a concave maximization problem can be formulated as a convex minimization problem, convex optimization theory can be applied. In addition, as the possible parameter selections will be discrete, the solution is optimal for the given discrete parameter set, but only near optimal in contrast to continuous parameter selections.

A.3.2. ESTIMATING THE 'UNDETECTED TARGET' DENSITY

The CDAPS algorithm is able to find the global optimum resource allocation; however, this allocation is only as good as the performance model or estimate it is based upon. Therefore, it is desirable to incorporate as much information as possible, such as prior information or information from previous measurements, into the performance estimate. This can be achieved by the recursive estimation of a PDF that describes the location of the undetected target. This methodology along with a particle filter implementation have been presented in Katsilieris et al. [2012a].

The input of the algorithm presented in Katsilieris et al. [2012a] is the density and the chosen sensing action at time $k-1$. First, the prediction step is performed using the Chapman-Kolmogorov equation in order to obtain the predictive density:

$$p(\mathbf{x}_k|\mathbf{u}_{k-1}) = \int p(\mathbf{x}_k|\mathbf{x}_{k-1}) \cdot p(\mathbf{x}_{k-1}|\mathbf{U}_{1:k-1})\, \mathrm{d}\mathbf{x}_{k-1} \tag{A.5}$$

where $p(\mathbf{x}_k|\mathbf{x}_{k-1})$ is determined by the kinematic model of the target (in this paper a constant velocity model is assumed) and $\mathbf{U}_{1:k-1}$ is the parameter selection history.

Then the predictive density is updated using negative information, see Koch [2007], and Bayes' rule:

$$p(\mathbf{x}_k|\mathbf{U}_{1:k}) = \frac{p(\mathbf{x}_k|\mathbf{U}_{1:k-1}) \cdot [1 - P_D(\mathbf{x}_k, \mathbf{u}_k)]}{\mathscr{C}} \tag{A.6}$$

$$\text{where } \mathscr{C} = \int p(\mathbf{x}_k|\mathbf{U}_{1:k-1}) \cdot [1 - P_D(\mathbf{x}_k, \mathbf{u}_k)]\, \mathrm{d}\mathbf{x}_k$$

The output updated density $p(\mathbf{x}_k|\mathbf{u}_k)$ at time k can be used to assess the performance of different sensing actions, as described in Sec. A.4.2.

A.4. SURVEILLANCE PERFORMANCE

The CDAPS algorithm requires that the resource loading and utility can be calculated for each potential parameter selection. The parameters under control considered in this paper are the revisit interval t_f and the dwell length τ_c of each sector. Modern radar systems allow for other parameters to be controlled, such as the waveform bandwidth

and pulse repetition frequency, however the revisit interval and dwell length are critical assuming maximum duty factor and waveform bandwidth operation. The proposed method can be readily extended to include additional parameter dimensions.

This section details how the resource loading, task quality and utility can be extracted from the probability density of the undetected target.

A.4.1. RESOURCE LOADING

The resource loading of each parameter selection for any sector, expressed as percentage throughout, is given by:

$$r^{j,l} = \frac{\tau_c^j}{t_f^l} \tag{A.7}$$

where $j = 1,\ldots,N_{\tau_c}$ is the dwell length index and $l = 1,\ldots,N_{t_f}$ is the revisit interval index.

A.4.2. TASK QUALITY

The task quality that is achieved, for a given parameter selection, is calculated using the output of the particle filter, which is the density $p(\mathbf{x}_k|\mathbf{u}_k)$. To produce this density, the filter is propagated over period of time N_k using the parameter selection $\mathbf{u}_{i,k}^{j,l}$.

An intuitive criterion was chosen as the task quality for performing search, being the maximum cumulative probability of detecting a target at each sector i:

$$J_i = \sum_{k=1}^{N_k} \left[\int P_D(\mathbf{x}_k, \mathbf{u}_{i,k}^{j,l}) \cdot p(\mathbf{x}_k|\mathbf{U}_{1:k-1}) \, \mathrm{d}\mathbf{x}_k \right] \tag{A.8}$$

where $P_D(\mathbf{x}_k, \mathbf{u}_{i,k}^{j,l})$ is the probability of detecting a target with states $\mathbf{x}_k$ if the parameters $\mathbf{u}_{i,k}^{j,l}$ are chosen and $p(\mathbf{x}_k|\mathbf{U}_{1:k-1})$ is the predictive probability density function of the target states at time k.

The length of the simulation time used can affect the task quality values calculated for each possible sensing action. As this is the input to the CDAPS algorithm, the simulation time N_k also affects the parameter selection, which is discussed further in Sec. A.5.1.

A.4.3. UTILITY

A utility function is required which maps task quality into utility. In this case an exponential utility function was chosen, which is a function of the cumulative probability of detecting a target:

$$V_i = 1 - \exp[-\alpha \cdot J_i] \tag{A.9}$$

and α is a sensitivity parameter. This utility function is chosen relatively arbitrarily, except for maintaining concavity. In practice, this utility function can be adapted to suit the requirement of the represented task.

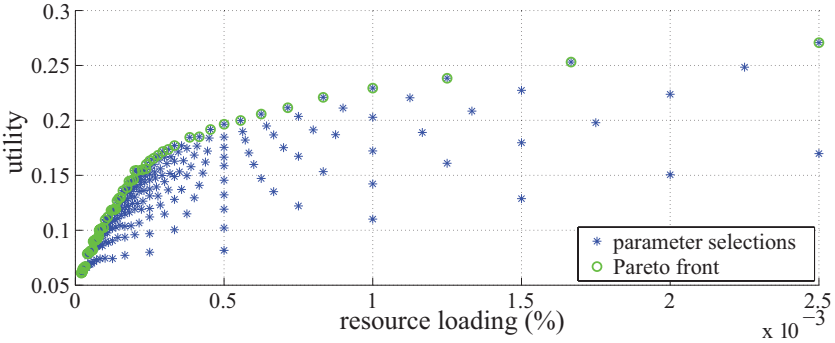

Figure A.1: Each point in the graph (of the $N_{\tau_c} \times N_{t_f}$ in total) represents how much utility is gained and how much resource loading is exerted by all possible combinations of parameters. The optimal points, also known as the *Pareto front*, are highlighted.

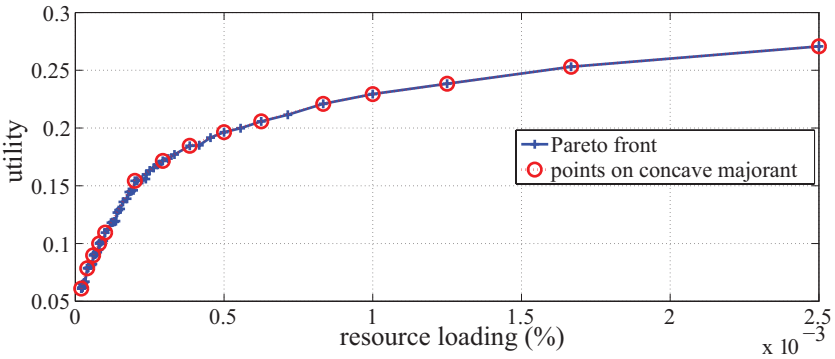

Figure A.2: After extracting the Pareto front from Fig. A.1, the points that lie on a concave majorant are selected and passed to the corresponding agent in the CDAPS algorithm.

A.4.4. RESOURCE-UTILITY SPACE

The CDAPS algorithm uses the resource and utility values of potential parameters selections. Figure A.1 shows an example where the N_j points for a sector are plotted in the utility vs resource loading space. As it can be seen, there are some points that have a larger utility value for the same resource as other points. These better points are known as the *Pareto front* in the literature and they can be extracted easily, using for example the Matlab code given in Cao [2008].

Because a discrete set of parameter selections is used, the Pareto front will not always be strictly concave. In order to solve this problem, the points that do not lie on a strictly concave majorant are removed and only the remaining points will be passed to the corresponding agent in the CDAPS algorithm, see Fig. A.2.

A.5. SIMULATIONS

In the simulations, the following dwell lengths and revisit intervals are considered:

$$\tau_c = [0.2, 0.4, \ldots, 2] \text{ msec} \tag{A.10}$$

$$t_f = [0.4, 0.8, \ldots, 10] \text{ sec} \tag{A.11}$$

for simulation times of

$$\begin{aligned} N_k &= [1,3,5,10,15,20,25] \cdot \max(t_f) \\ &= [10,30,50,100,150,200,250] \text{ sec} \end{aligned} \tag{A.12}$$

and the sensitivity parameter is set as $\alpha = 0.1$.

The density is initialized at $k = 0$ by uniformly distributing the particles in a disk of 300 km radius. The velocities v_x and v_y are chosen such that the radial speed of the targets is uniformly distributed in [0, 400] m/s and they move towards the radar. This initialization process resembles the real life scenario of the moment when the radar is turned on and there is no information about the targets location, meaning that targets might be anywhere. A constant velocity model is used with $b_x = b_y = 2$ $(\text{m/s}^2)^2$ as the power spectral densities of the acceleration noise in the $x-y$ direction. Furthermore, target birth is modeled at the border of the field of view of the radar by means of replacing a fixed percentage of particles with new ones at the border during the resampling process.

The aforementioned parameters are tested in a scenario where an MFR has to perform surveillance of 8 sectors of 10×10 degrees. Using a $b_w = 1.5°$ beamwidth and $0.8 b_w$ spacing means that there are 81 beam positions per sector. Therefore, the total resource utilization percentage for given combinations of $\tau_c^{j_i}$ and $t_f^{l_i}$ per sector will be:

$$r = \sum_{i=1}^{N_S} \frac{\tau_c^{j_i}}{t_f^{l_i}} \cdot 81 \cdot 100\% \tag{A.13}$$

and a global resource constraint of $r_{max} = 10\%$ is imposed.

The standard radar range equation can be used to calculate the SNR. Realistic radar parameters are used according to standard texts such as Blackman and Popoli [1999]; Skolnik [2002] to give an instrumented range of 300 km for a target with RCS = 1 m^2.

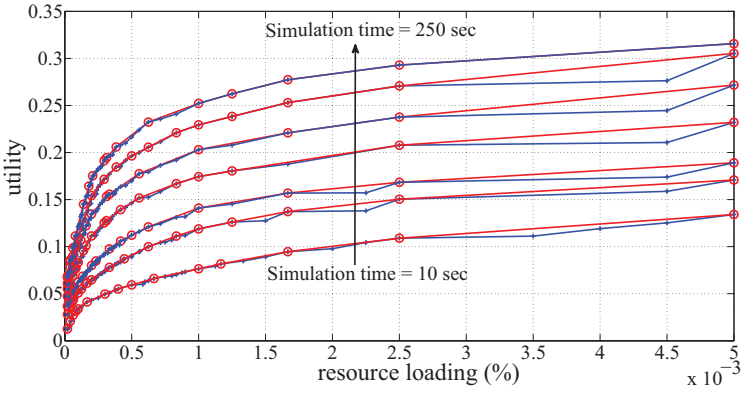

Figure A.3: The procedure explained in Fig. A.2 is demonstrated for varying simulation times. It can be observed that changing the length of the simulation time greatly changes the task utility.

The probability of detection can then be calculated assuming a Swerling 1 target and a probability of false alarm P_{FA}:

$$P_D = P_{FA}^{\left(\frac{1}{1+SNR}\right)} \tag{A.14}$$

Although the selection of parameters affects the performance of the radar, the conclusions that will be drawn are relevant over a range of possible parameter choices.

A.5.1. EFFECT OF SIMULATION TIME

The first step is to assess the effect of the simulation time N_k needed to evaluate the utility of each parameter selection. As this evaluation of the utility, extracted from the particle filter, is passed to the CDAPS algorithm, it can greatly affect the resulting parameter selection.

Figure A.3 shows the different resource utility curves that are passed to the CDAPS algorithm for the various simulation times. It can be seen that changing the length of the simulation time greatly changes the task utility. The reason for this great variation is that when the simulation time is short, it is only evaluating over the initialization stage of the particle filter. In this stage, it is necessary to detect targets close to the radar; however, for the longer simulation times these close-in targets have already been detected and the algorithm focuses on detecting the distant targets.

A scenario where there is no external information, much like in [Katsilieris et al., 2012a, Subsec.V-A], is used to produce the optimal parameter selections chosen by CDAPS for each value of N_k, as shown in Table A.1. It can be seen that shorter simulation times result in a short dwell length and short revisit interval, whereas longer simulation times result in longer dwell lengths and revisit intervals. This is intuitive, as the shorter simulation time, which is evaluated over the initialization stage, is required to detect many targets close to the radar. However, the steady selection, which is observed for longer simulation times, needs to detect targets far away from the radar.

Table A.1: The optimal dwell lengths and revisit times for different simulation times

method	Sim. time (sec)	revisit int. (sec)	dwell length (msec)	resource (%)
1)	10	1.2(a) & 2(b)	0.2	9
2)	10	1.4	0.2	9.26
3)	30	3.6(a) & 4.8(b)	0.6	9
4)	50	6	0.8	8.64
5)	100	10	1.4	9.07
6)	150	10	1.2(a) & 1.6(b)	9
7)	150	10	1.4	9.07
8)	200	10	1(a) & 2(b)	9
9)	200	10	1.4	9.07
10)	250	10	1.4	9.07

A.5.2. PERFORMANCE EVALUATION

An assessment of the surveillance performance is generated in a scenario where the MFR has to detect 300 targets that have RCS = 1 m^2 and move following a constant velocity model. The initial velocities of all the targets are chosen such that the radial speed of the targets is uniformly distributed in $[0,\ 400]$ m/s and they move towards the radar. The azimuth of the targets is uniformly distributed in $[0, 2\pi)$ radians. Furthermore, the targets are divided into 3 groups according to their initial distance to the radar:

- Group 1: 100 targets with initial range in $[0, 50]$ km;
- Group 2: 100 targets with initial range in $(50, 100]$ km; and
- Group 3: 100 targets with initial range in $(100, 300]$ km.

The aforementioned parameter selections are compared with performing periodic search such that a probability of detection of 0.7 at 10 km is achieved[1] for a target with RCS = 1 m^2, assuming the Swerling I model and false alarm rate of $P_{FA} = 1.4 \cdot 10^{-9}$. This requirement results in revisit time of 8 sec and dwell length of 1 msec.

The parameter selections are also compared to performing myopic search every 2 sec using the two criteria[2] discussed in Katsilieris et al. [2012a] for choosing the sector to be searched and the optimal dwell length. The revisit interval for each sector can then be derived indirectly.

We performed 100 Monte Carlo runs. Each run was terminated either when all targets had been detected or when 20 minutes of radar surveillance had passed. The results are reported in Tables A.2 and A.3.

In Tables A.2 and A.3 it can be observed that longer revisit intervals and longer dwell times result in detecting targets at long distances faster and with higher probability. On

[1] This probability of detection can appear to be low for the considered distance. However, it happens due to the selected radar parameters and does not affect qualitatively the conclusions that will be drawn.

[2] The criteria are the maximum expected probability of detecting a target and the maximum expected Kullback-Leibler divergence between the posterior and the predictive “undetected target" density.

Table A.2: Comparison results of various methods for surveillance - Part 1

Method	Avg. number of detected targets	Avg. percentage of detected targets (%)	Variance of detected targets percentage
1a)	269.32	89.77	21.67
1b)	268.09	89.36	22.35
2)	268.68	89.56	22.97
3a)	281.91	93.97	14.18
3b)	281.65	93.88	14.01
4)	285.2	95.07	12.36
5)	290.59	96.86	10.22
6a)	288.54	96.18	12.90
6b)	290.87	96.96	6.36
7)	293.01	97.67	6.17
8a)	287.37	95.79	8.76
8b)	290.89	96.96	8.14
9)	295.34	98.45	4.61
10)	291.43	97.14	6.17
E[P_D]	293.72	97.91	5.52
E[KLD]	293.37	97.79	7.57
Periodic	287.9	95.97	9.44

the other hand, short revisit intervals and dwell times result in fast detection of targets that are close to the radar.

These results can be explained by the fact that for short simulation times, detection of targets at short ranges is favored over detection of targets at long ranges. On the other hand, if long simulation times are used then the density reaches a steady-state condition where targets are expected to be only at long distances from the radar and long dwell times are needed for their detection. Consequently, long revisit intervals are also chosen in order to satisfy the resource constraint. The aforementioned results demonstrate the importance of the simulation time due to its connection to the ranges that targets are expected to be found.

The myopic criteria do not offer the flexibility of adapting the resource consumption according to where any undetected targets might be. Because they are myopic, they always choose the longest dwell time and therefore their performance depends only on the search period that the user sets.

The periodic search, designed such that a certain probability of detection is achieved, produced results that lie between the results obtained for simulation times of 50 and 100 seconds. This is intuitive since the revisit interval and dwell time of the periodic search also lie between the corresponding selections chosen by the CDAPS algorithm.

A.6. SUMMARY

A novel algorithm for selecting surveillance parameters of an MFR has been presented. The presented algorithm extracts resource utility measures for a number of surveillance sectors from a density of the undetected target location. These resource utility measures are used to allocate the finite radar resource using the Continuous Double Auction Pa-

Table A.3: Comparison results of various methods for surveillance - Part 2

Method	Group 1 avg. number of detected targets (%)	Group 1 avg. time until detection (sec)	Group 2 avg. number of detected targets (%)	Group 2 avg. time until detection (sec)	Group 3 avg. number of detected targets (%)	Group 3 avg. time until detection (sec)
1a)	100	1.59	100	3.83	69.32	216.78
1b)	100	2.45	100	6.13	68.09	235.63
2)	100	1.77	100	4.50	68.68	224.95
3a)	100	3.67	100	7.26	81.91	161.31
3b)	100	4.76	100	9.37	81.65	171.92
4)	100	5.85	100	10.64	85.2	158.84
5)	100	11.15	100	17.53	90.59	138.63
6a)	100	11.22	100	18.31	88.54	153.67
6b)	100	11.18	100	17.21	90.87	129.11
7)	100	10.75	100	17.29	93.01	130.74
8a)	100	11.38	100	18.93	87.37	164.56
8b)	100	10.94	100	17.74	90.89	126.49
9)	100	10.82	100	16.24	95.34	107.00
10)	100	10.91	100	17.59	91.43	140.32
E[P_D]	100	18.74	100	27.43	93.72	142.11
E[KLD]	100	18.30	100	26.66	93.37	141.82
Periodic	100	8.39	100	14.62	87.9	135.4

rameter Selection algorithm.

As a first step in evaluating the performance of the presented algorithm, the effect of simulation time of the “undetected target" density on the parameter selection was studied. The results show that for short simulation times the joint algorithm chooses parameters that are suited for detecting quickly targets close to the radar. On the other hand, for long simulation times the joint algorithm chooses parameters that are suited for detecting targets that are far away from the radar.

In the future, we would like to get a better insight into the benefits of using non-myopic, adaptive methods instead of myopic or naive methods, such as periodic scanning, for performing surveillance. Towards this goal, the algorithm can be extended to include external information, such as map information about airports, and be tested in such scenarios.

Another aspect of the algorithm that needs to be tested is its ability to select the best parameters online, as the operational requirements change. For this reason, it can be tested in scenarios where the targets are expected to be found at different places as the time passes by. In these cases, the best parameters will have to be re-evaluated every few time instances.

The surveillance criterion J_i is an important part of the algorithm and it has to be chosen according to the operational requirements. For this reason, selecting the most suitable surveillance criterion is an important research topic.

It would also be of interest to include more parameters in the optimization procedure (e.g., waveform bandwidth) in order to create an even more realistic model.

B

AIS SPOOFING DETECTION USING RADAR INFORMATION

This work was performed in collaboration with Dr. Paolo Braca during my research visit to NATO-STO CMRE (formerly known as NURC), La Spezia, Italy. The results were also published in Katsilieris et al. [2013].

Section B.1 motivates the problem of detecting whether an AIS report is spoofed or not. The problem is formulated in Section B.2, the proposed solution is developed in Sections B.3 and B.4. Simulations and experimental results are presented in Section B.5. Finally, the work is summarized in Section B.6.

B.1. MOTIVATION

Maritime situational awareness, which includes accurate knowledge of moving vessel location, has increased the focus on the development of data fusion algorithms. These algorithms can fuse data from several heterogeneous systems in order to provide a better perception of the activity close to the shores of a nation. For example, data from coastal radars, the AIS, video and infrared surveillance systems and SAR systems can be fused. A goal of these systems, in addition to tracking the present vessels, is to introduce some sort of intelligence in the surveillance systems to automatically identify possibly suspicious (also called anomalous) behavior. Some example applications include the deviation of vessels from known shipping lanes, the *rendez-vous* of vessels at sea, the motion of fast moving vessels close to the shore, methods to automatically detect the switching-off of an AIS transponder and others. Some examples from the relevant bibliography are Ristic et al. [2008]; Lane et al. [2010]; Guerriero et al. [2010]; Kowalska and Peel [2012]; Vespe et al. [2012].

A common characteristic among the given examples is that they rely on the high accuracy of AIS reports in order to derive training patterns or the “ground truth" for the motion of vessels. An often hidden assumption is that AIS reports are trustworthy. This paper is based on the assumption that AIS reports can be falsified (or *spoofed*) as

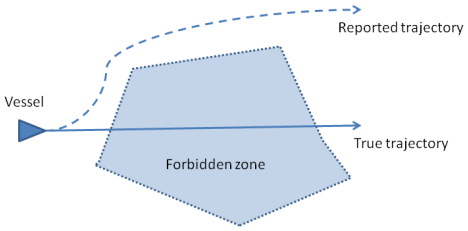

(a) Example 1: A vessel reports a different trajectory from the one that it is actually following. For instance, a fishing boat could violate a no-fishing zone.

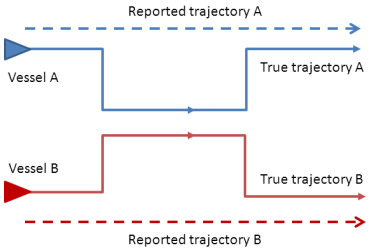

(b) Example 2: Two vessels meet in the sea for an illegal transaction and report a different trajectory in order to conceal their *rendez-vous*.

Figure B.1: Two examples where AIS spoofing can be of interest.

suggested in Teleplan Globe AS [2012]; CNS Systems [2012]. The trustworthiness of AIS reports depends on the willingness of the crew of a ship to report their true data.

Fig. B.1a shows an example of interest for this problem. Consider an area that specific types of vessels are not supposed to enter, *e.g.*, an area where fishing is not allowed. In this case, a fishing boat could enter the no-fishing zone, following the trajectory denoted by the solid line, while reporting that it is bypassing it, reporting the trajectory denoted by the dashed line. Fig. B.1b shows an example where two vessels meet but try to conceal their actions by reporting false trajectories.

This paper addresses the problem of determining whether the AIS data received from a vessel are trustworthy or not by using information from additional sensors. The proposed methodology uses radar measurements and prior information from the corresponding tracking system. In the case that the AIS data are indeed trustworthy, they can be safely used in the data fusion algorithms, *e.g.*, for enhancing the tracking accuracy. If the AIS data are estimated to be spoofed, then their fusion with other data can be avoided and an anomaly can be flagged to the operator of the surveillance system.

B.2. PROBLEM FORMULATION

As explained in the introduction, the considered problem amounts to determining whether the AIS data transmitted by a vessel is spoofed or not by using measurements from any available radar and the predicted vessel position according to the tracking system of the radar.

First, some notation will be introduced. Subsequently, the fundamental assumptions will be stated and finally, the problem will be posed in the statistical hypothesis testing framework.

B.2.1. NOTATION

The following notation is used:

- the two-dimensional true target position in Cartesian coordinates will be denoted as $\mathbf{x}_0$, the predicted target position as $\mathbf{x}$ and the AIS reported position as $\mathbf{x}_{AIS}$;

- there is a number of K radars measuring the position of the target at each time instance i and the measurement of each radar is denoted as $\mathbf{z}_j(i), j \in [1,\dots,K]$. From now on, the time index will be suppressed. The radar measurements are usually expressed in polar coordinates, *i.e.*, target range r, bearing θ and possibly target range rate $\dot{r}$. For simplicity reasons, the cartesian system will be used for the radar measurements with corresponding transformation of the measurement covariance matrix.
- $\mathcal{N}(\mathbf{x};\mu,\Sigma)$ denotes the two-dimensional Gaussian PDF:

$$\mathcal{N}(\mathbf{x};\mu,\Sigma) = \frac{1}{(2\pi)\sqrt{|\Sigma|}} e^{-\frac{1}{2}(\mathbf{x}-\mu)^T\Sigma^{-1}(\mathbf{x}-\mu)} \tag{B.1}$$

- The symbol ~ stands for “is distributed according to".

B.2.2. ASSUMPTIONS

For formulating and tackling the problem at hand, the following assumptions are made:

- Zero false alarm rate at the detector of the radar tracker is assumed because in practice most radar systems operate at low false alarm rate regimes.
- The *a priori* information on the vessel position is a Gaussian with mean $\mathbf{x}_0$ and covariance matrix $\Sigma_{\mathbf{x}}$: $\mathbf{x} \sim \mathcal{N}(\mathbf{x}_0, \Sigma_{\mathbf{x}})$. This represents the predicted position of the vessel according to the tracking system at the same time instance as the radar measurements and the AIS contact are received.
- The measurement from the kth radar is $\mathbf{z}_k = \mathbf{x}_0 + \mathbf{w}_k$, where $\mathbf{w}_k$ is additive Gaussian noise with zero mean and covariance matrix Σ_R: $\mathbf{z}_k \sim \mathcal{N}(\mathbf{x}_0, \Sigma_R)$. Furthermore, it is assumed that the measurements are conditionally independent form radar to radar.
- The trustworthy AIS data $\mathbf{x}_{AIS}$ follow a Gaussian distribution with mean $\mathbf{x}_0$ and covariance matrix Σ_{AIS}. When the AIS data are spoofed, it is assumed that an arbitrary bias $\mathbf{d} = [d_x, d_y]^T$ is added to the true position of the vessel, *i.e.*, the mean is now $\mathbf{x}_0 + \mathbf{d}$.
- Perfect reception of AIS reports is assumed. In other words, the transmitted AIS reports are always received by the corresponding tracking system.
- Typically, it holds that the elements of Σ_{AIS} are smaller than the elements of Σ_R.
- Only the single-target case is considered. This approximation is valid in multitarget scenarios when there is a perfect data association scheme or when the targets are sufficiently separated and the single-target case can be reconstructed. In the maritime domain, this approximation is valid when the vessels are outside from a port, which is the case where the AIS spoofing is of interest.
- The mathematical derivation of the joint likelihood of the radar measurements and AIS contacts is done for the static case, *i.e.*, in a snapshot time. When the sequential detection of spoofing is considered, the measurements are correlated in

time, as discussed in Bar-Shalom et al. [2011], but they are approximated to be independent. The validity of this approximation is demonstrated by three examples using real and simulated data.

Note that the assumptions of Gaussian prior and Gaussian measurement noise are very common in the target tracking context, see for example Bar-Shalom et al. [2011].

B.2.3. STATISTICAL HYPOTHESIS TESTING OF AIS SPOOFING

The AIS spoofing detection problem can be formed as a statistical hypothesis testing problem:

- $H_0 : (\mathbf{z}, \mathbf{x}_{AIS}) \sim p(\mathbf{z}, \mathbf{x}_{AIS}|H_0)$ is the *simple* null hypothesis that the AIS data are trustworthy, versus
- $H_1 : (\mathbf{z}, \mathbf{x}_{AIS}) \sim p_{\mathbf{d}}(\mathbf{z}, \mathbf{x}_{AIS}|H_1)$ is the *composite* alternative hypothesis that the AIS data are spoofed,

where $p_{\mathbf{d}}(\mathbf{z}, \mathbf{x}_{AIS}|H_1)$ is the joint distribution of the radar measurements and AIS contacts, parameterized by the spoofing distance $\mathbf{d}$, and $p(\mathbf{z}, \mathbf{x}_{AIS}|H_0)$ is the joint distribution of the radar measurements and trustworthy AIS contacts.

In testing H_0 versus H_1 there are two types of error that can be made: H_0 can be falsely rejected or H_1 can be falsely rejected. The first type of error is called a *false alarm*, meaning that trustworthy AIS data are classified as spoofed, and the false alarm probability is denoted as P_{FA}. The second type of error is called a *missed detection* and it means that the spoofing of the AIS data has not been detected. The missed detection probability P_{MD} is equal to 1 minus the probability of detection, or $P_{MD} = 1 - P_D$.

During the design process of the test for H_0 versus H_1, one has to find a good trade-off between the two error probabilities, since one error can become arbitrarily small at the expense of the other error becoming unacceptably large. It is very common in the radar community to follow the Neyman-Pearson paradigm, as described in Poor [1994]. Accordingly, a low upper bound on the false alarm probability is set and the miss detection probability is minimized, or equivalently the detection probability is maximized. For a better discussion on the fundamentals of hypothesis testing see Poor [1994]; Kay [1998].

B.3. SINGLE SAMPLE DETECTORS

As a first step, the expression for the clairvoyant[1] Likelihood Ratio Test (LRT) is derived for the case of one radar and K radars. Subsequently, the generalized version of the likelihood ratio test is introduced in order to deal with the unknown spoofing distance.

B.3.1. CLAIRVOYANT LIKELIHOOD RATIO TEST

In the beginning, the PDFs of receiving a given radar measurement and a given AIS report under each hypothesis need to be calculated.

The radar measurements and the AIS data are conditionally independent given $\mathbf{x}$:

[1] The *clairvoyant* test is an ideal test that knows the true spoofing distance but not whether the data are spoofed.

$$p(\mathbf{z},\mathbf{x}_{AIS}|H_i) = \int_{-\infty}^{\infty} p(\mathbf{z}|\mathbf{x})\ p(\mathbf{x}_{AIS}|H_i,\mathbf{x})\ p(\mathbf{x})\,\mathrm{d}\mathbf{x} \tag{B.2}$$

where $i = 0, 1$.

The integral in Eq. (B.2) can be evaluated analytically in the case of Gaussian measurements and prior because the product of two Gaussian PDFs is an unormalized Gaussian, see Petersen and Pedersen [2012]:

$$\mathcal{N}(\mathbf{x};\mu_1,\Sigma_1)\cdot\mathcal{N}(\mathbf{x};\mu_2,\Sigma_2) = \alpha\ \mathcal{N}(\mathbf{x};\mu_3,\Sigma_3) \tag{B.3}$$

where

$$\alpha = \mathcal{N}(\mu_1;\mu_2,\Sigma_1+\Sigma_2) = \mathcal{N}(\mu_2;\mu_1,\Sigma_1+\Sigma_2) \tag{B.4}$$

$$\Sigma_3 = \left(\Sigma_1^{-1}+\Sigma_2^{-1}\right)^{-1}\ ,\ \mu_3 = \Sigma_3\left(\Sigma_1^{-1}\mu_1+\Sigma_2^{-1}\mu_2\right) \tag{B.5}$$

Accordingly, the clairvoyant LRT is

$$\Lambda(\mathbf{z},\mathbf{x}_{AIS},\mathbf{d}) = \frac{\mathcal{N}(\mathbf{z};\mathbf{x}_{AIS}-\mathbf{d},\Sigma_R+\Sigma_{AIS})}{\mathcal{N}(\mathbf{z};\mathbf{x}_{AIS},\Sigma_R+\Sigma_{AIS})} \times \frac{\mathcal{N}(\mathbf{x}_0;\mu_1(\mathbf{z},\mathbf{x}_{AIS})-\Delta\mathbf{d},\Sigma_1+\Sigma_{\mathbf{x}})}{\mathcal{N}(\mathbf{x}_0;\mu_1(\mathbf{z},\mathbf{x}_{AIS}),\Sigma_1+\Sigma_{\mathbf{x}})} \gtrless \tau \tag{B.6}$$

where

$$\Sigma_1 = (\Sigma_R^{-1}+\Sigma_{AIS}^{-1})^{-1} \tag{B.7}$$

$$\mu_1(\mathbf{z},\mathbf{x}_{AIS}) = \Sigma_1(\Sigma_R^{-1}\mathbf{z}+\Sigma_{AIS}^{-1}\mathbf{x}_{AIS}) \tag{B.8}$$

$$\Delta = (\Sigma_{AIS}\Sigma_R^{-1}+I_{2\times 2})^{-1} \tag{B.9}$$

In the case of Gaussian measurements and prior, an analytic formula for Eq. (B.6) can be found, see Section B.7.

The LRT can also be generalized to address the case where measurements from several radars are available. The multi-radar likelihood $p(\mathbf{z}|\mathbf{x}_0)$ in the case of Gaussian measurements is evaluated in Section B.8. It can be seen, see Section B.8, that in the case where measurements from similar radars are available, the measurements can be easily aggregated and the LRT has the same form as in Eq. (B.6).

Eq. (B.6) is interesting for one more reason. The expected value of the logarithm of Eq. (B.6) under H_1, *i.e.*, $E[\log(\Lambda(\mathbf{z},\mathbf{x}_{AIS},\mathbf{d}))|H_1]$ is equal to the KLD between the nominator and the denominator, see [Cover and Thomas, 2006, Theorem 11.8.1]. In other words, it measures how much the two hypotheses are disjoint. This expression can also be evaluated analytically, see Section B.7. In the simulations it is shown that the hypotheses become more disjoint as the spoofing distance increases, which is a desirable property.

B.3.2. GENERALIZED LIKELIHOOD RATIO TEST

In practice, the spoofing distance $\mathbf{d}$ is not known to the system and therefore, the generalized version of the LRT (from now on called G-LRT) can be used.

The Generalized Likelihood Ratio Test (G-LRT) is one of the most powerful tools available for solving composite hypothesis testing problems, such as the problem at hand, where the spoofing distance is not known. For a better discussion on the G-LRT see Kay [1998].

When using the G-LRT, one first needs to find the estimate $\hat{\mathbf{d}}$ that maximizes the likelihood under H_1

$$\hat{\mathbf{d}} = \underset{|\mathbf{d}|>|\mathbf{d}_{min}|}{\arg\max} \left[\mathcal{N}(\mathbf{z}; \mathbf{x}_{AIS} - \mathbf{d}, \Sigma_R + \Sigma_{AIS}) \times \mathcal{N}(\mathbf{x}_0; \mu_1(\mathbf{z}, \mathbf{x}_{AIS}) - \Delta\mathbf{d}, \Sigma_1 + \Sigma_{\mathbf{x}}) \right] \tag{B.10}$$

and then use it in Eq. (B.6) or in the corresponding analytic expression shown in Section B.7.

During the likelihood maximization process, where $\hat{\mathbf{d}}$ is evaluated, a minimum distance $\mathbf{d}_{min}$ is set. If the estimated spoofing distance $\hat{\mathbf{d}}$ has a smaller value than $\mathbf{d}_{min}$ then it is assumed that the vessel is not spoofing. The determination of $\mathbf{d}_{min}$ is important for the performance of the G-LRT and depends on the accuracy of the radar measurements, the AIS data and the prior information. In other words, it depends on $\Sigma_{\mathbf{x}}$, Σ_R and Σ_{AIS}. For instance, if the accuracy is poor, then setting $\mathbf{d}_{min}$ to a small value results in an increased false alarm probability. On the other hand, if the accuracy is good, then setting $\mathbf{d}_{min}$ to a large value results in an increased miss detection probability.

B.4. SEQUENTIAL DETECTION OF AIS SPOOFING

In the previous subsections, one-sample solutions for the problem at hand were developed. As their name suggests, they make a decision about the trustworthiness of AIS data using one radar measurement and one AIS report. This approach can also be generalized to using a larger, fixed number of samples and is suitable for applications where the number of observations is known in advance and no new observations can be made.

In the case studied in this paper, new observations are periodically available according to the radar scanning period and the frequency of AIS reports. Subsequently, it can be noticed that the problem of AIS spoofing detection would ideally be dealt online, as new observations are received and one would like to make a decision with certain error probabilities as fast as possible.

Given the aforementioned discussion, the sequential version of the aforementioned LRTs, from now on called Sequential Likelihood Ratio Test (SLRT), is a more appropriate solution. An SLRT has the property that, in general, it requires a smaller expected number of observations than the fixed number of observations needed by the corresponding fixed sample size test in order to achieve the same error probabilities, see the discussion in Wald [1945].

The sequential version of the previously described tests has the general form:

$$\log B < \sum_{i=1}^{N} \log\left[\Lambda(\mathbf{z}(i), \mathbf{x}_{AIS}(i), \hat{\mathbf{d}})\right] < \log A \tag{B.11}$$

$$B \geqslant \frac{1-P_D}{1-P_{FA}} \ , \ A \leqslant \frac{P_D}{P_{FA}} \tag{B.12}$$

The test is terminated at *stopping time* N when $\sum_{i=1}^{N} \log\left[\Lambda(\mathbf{z}(i), \mathbf{x}_{AIS}(i), \hat{\mathbf{d}})\right]$ exceeds one of the two thresholds or a maximum allowed time has elapsed. In practice, the equalities are used in (B.12). For a better description of the SLRTs, see Wald [1945].

Wald's approximations can be used for finding the lower and upper thresholds $-\alpha, h$ for desired error probabilities $P_{FA}, 1-P_D$ under each hypothesis, see Basseville and Nikiforov [1993]:

$$-\alpha \approx \log\left(\frac{1-P_D}{1-P_{FA}}\right) < 0 \ , \ h \approx \log\left(\frac{P_D}{P_{FA}}\right) > 0 \tag{B.13}$$

Wald's approximations can also be used together with the calculated expected value of the LRTs under the two hypotheses in order to derive the expected number of necessary samples under each hypothesis, see Basseville and Nikiforov [1993]:

$$E[N|H_0] = \frac{(1-P_{FA})\log\left(\frac{1-P_{FA}}{1-P_D}\right) - P_{FA}\log\left(\frac{P_D}{P_{FA}}\right)}{E[\log(\Lambda)|H_0]} \tag{B.14}$$

$$E[N|H_1] = \frac{(P_D)\log\left(\frac{P_D}{P_{FA}}\right) - (1-P_D)\log\left(\frac{1-P_{FA}}{1-P_D}\right)}{E[\log(\Lambda)|H_1]} \tag{B.15}$$

In the case where a fixed value $\hat{\mathbf{d}}$ is used for all sampling times $i = 1, \ldots, N$, an analytic expression for the expected value of the LRT $E[\log(\Lambda)|H_0], E[\log(\Lambda)|H_1]$ under H_0 and H_1 respectively can be found, see Section B.7.

It should be pointed out that formulas (B.11) through (B.15) are exact only in the static case, where the vessel is not moving and the spoofing distance is constant and known. The reason for the formulas to not be exact in the dynamic case is that the predicted positions of the vessel at every time instance are correlated across time. The correlation is introduced by the motion model used for performing the prediction step in the tracking system. The motion model typically has the form:

$$\mathbf{x}(i) = \mathbf{f}(\mathbf{x}(i-1), \mathbf{v}(i)) \tag{B.16}$$

where it can be seen that the state of the target at time instance i is predicted using the state of the vessel at the time instance $(i-1)$ and some noise $\mathbf{v}(i)$. A typical example of a motion model is the *nearly constant velocity model*, presented in Li and Jilkov [2003].

In the next section it is shown that formulas (B.11) through (B.15) are good approximations in the case of a moving vessel as long as the spoofing distance is constant. If the vessel is moving and the spoofing distance is increasing then fewer samples are needed.

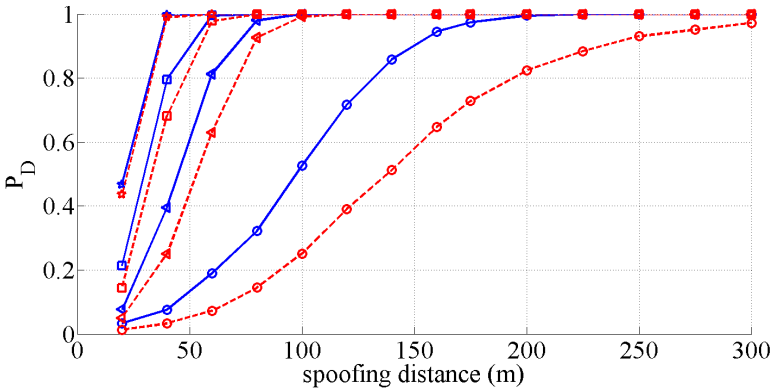

Figure B.2: The probability of detection at different distances using one measurement from a varying number of radars and for $P_{FA} = 0.01$. The C-LRT is denoted by solid blue and the G-LRT by dashed red line. The $\circ$ denotes the use of one, the ∇ of three, the $\square$ of five and the $\star$ of ten radars.

B.5. EXPERIMENTAL RESULTS

In subsection B.5.1, the test statistics for one-sample LRTs are simulated in order to demonstrate the effect of the spoofing distance and the number of radars on the performance of the various tests. Similarly, the test statistics for the SLRTs are simulated in subsection B.5.2. Finally, in subsection B.5.3, the SLRTs are applied to real and simulated data in order to verify the validity of the assumptions and approximations made in the previous sections.

B.5.1. SINGLE SAMPLE LOG-LIKELIHOOD RATIO TESTS

As a first step, it is demonstrated that the generalized LRT has performance that gets close to the performance of the clairvoyant LRT as the spoofing distance and the number of radars increase. This demonstrates two things: *a*) the benefit of using measurements from more than one radars; and *b*) that as the spoofing distance increases, the two hypotheses become more disjoint and therefore, it is easier to detect the spoofing behavior. The latter phenomenon manifests itself faster when measurements from more radars are used.

The settings for the following simulations are $\mathbf{x}_0 = [10^3,\ 10^3]^T$ m, $\Sigma_{\mathbf{x}} = \text{diag}(70^2, 70^2)$ m^2, $\Sigma_R = \text{diag}(50^2, 50^2)$ m^2, $\Sigma_{AIS} = \text{diag}(5^2, 5^2)$ m^2. The spoofing distance is varied as $d_x = [20, 40, \ldots, 160, 175, 200, \ldots, 300]$, $d_y = 0$ m. The minimum distance $\mathbf{d}_{min}$ for the G-LRT is set to 85 m and the grid points are located in increments of 20 meters in the x and y directions. The statistics are evaluated over 10^4 Monte Carlo runs.

Figure B.2 shows the resulting probability of detection at each value of the spoofing distance for the two tests for varying number of radars and for $P_{FA} = 0.01$ using data in a single time interval. Figure B.3 shows the corresponding Receiver Operating Characteristic (ROC) curves for $\mathbf{d} = [40, 0]$ m. It can be noticed that the performance of the G-LRT becomes equivalent to the performance of the Clairvoyant Likelihood Ratio Test (C-LRT) as the spoofing distance and the number of radars increase.

Figures B.4 and B.5 show how the expected values of the two tests vary under H_1

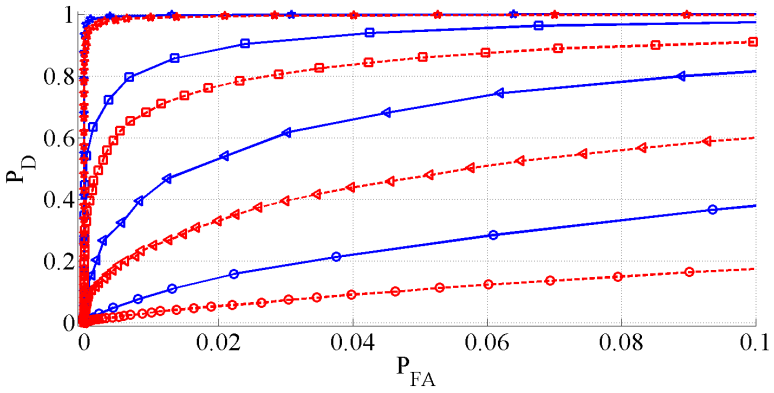

Figure B.3: ROC curves for the two tests for varying number of radars. The spoofing distance is 40 meters in the x direction. The C-LRT is denoted by solid blue and the G-LRT by dashed red line. The $\circ$ denotes the use of one, the ∇ of three, the $\square$ of five and the $\star$ of ten radars.

and H_0 respectively. The settings for these simulations remain the same. As expected, the longer the spoofing distance and the larger the number of radars that are used, the higher the expected value of the tests under H_1 and therefore, the easier it is to detect the spoofing behavior. In other words, the KLD between the two hypotheses increases and therefore they become more disjoint. It can also be noticed that due to the specific choice of $\mathbf{d}_{min}$, the G-LRT has a negative expected value under H_1 for spoofing distances shorter than 30 to 60 meters, depending on the number of radars used. Using a lower $\mathbf{d}_{min}$ would make the expected value positive at the expense of the expected value of the G-LRT under H_0, which would have smaller absolute value. This effect becomes important when the sequential LRT is used because as the expected value under each hypothesis becomes lower, the corresponding termination time of the test becomes longer for reaching a conclusion with the same error probabilities.

Again, as the number of radars increases under H_1, the G-LRT becomes equivalent to the C-LRT. On the other hand, under H_0 the G-LRT has constant performance that depends on the number of radars.

B.5.2. SEQUENTIAL LOG-LIKELIHOOD RATIO TEST STATISTICS

Using the same settings and fixing the spoofing distance at $\mathbf{d} = [80, 80]^T$ m, the thresholds can be varied such that the two tests have the same probability of false alarm. In this way, one can see how long it takes to reach a conclusion with a given probability of detection.

Figure B.6 shows the probability of detection versus the expected termination time of each test. For these simulations, one radar is used and the probability of false alarm is fixed at $P_{FA} = 10^{-5}$. The results are evaluated over 10^5 Monte Carlo runs. It can be observed that in this case Wald's approximations are not accurate enough because the expected values of the LRTs are too large compared to the evaluated thresholds.

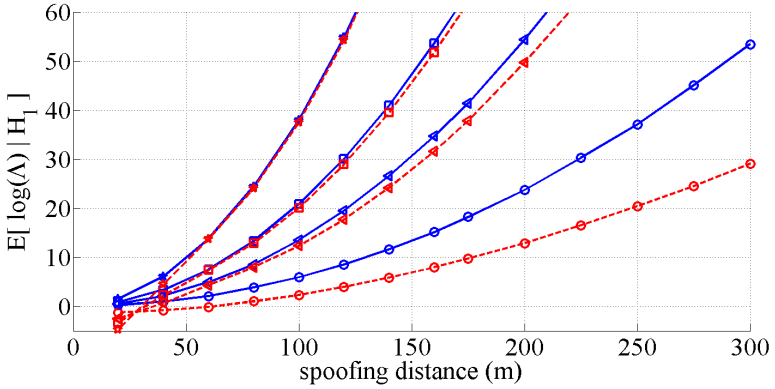

Figure B.4: The performance of the two LRTs under H_1 for varying number of radars. As the spoofing distance and the number of radars increases, the expected value of the tests under H_1 also increases and makes the spoofing detection easier. The C-LRT is denoted by solid blue and the G-LRT by dashed red line. The ∘ denotes the use of one, the ∇ of three, the □ of five and the ⋆ of ten radars.

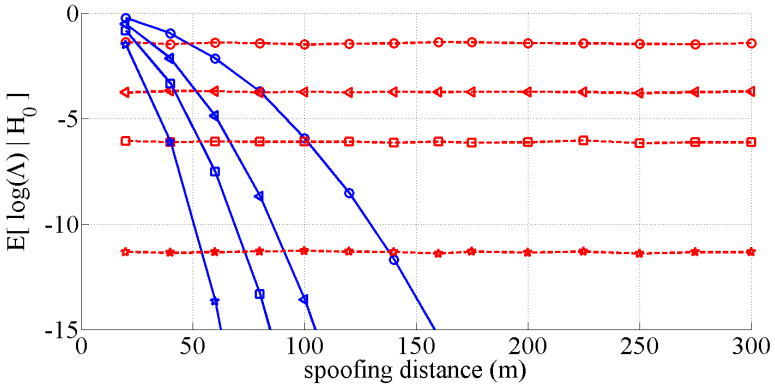

Figure B.5: The performance of the two LRTs under H_0 for varying number of radars. The C-LRT is denoted by solid blue and the G-LRT by dashed red line. The ∘ denotes the use of one, the ∇ of three, the □ of five and the ⋆ of ten radars.

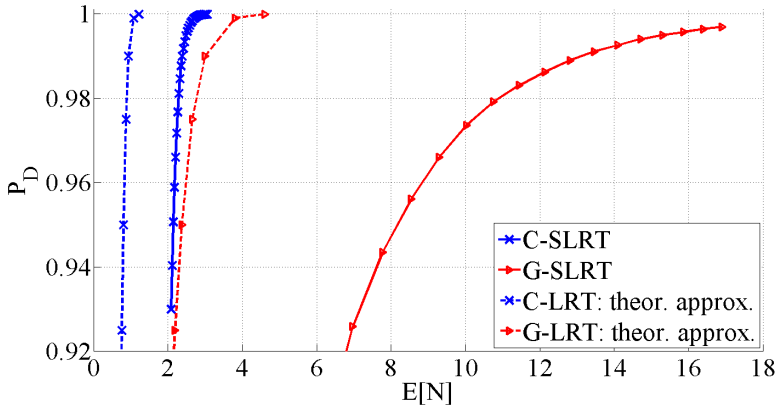

Figure B.6: The probability of detection of the different tests using one radar as a function of the expected number of necessary samples. The false alarm probability is fixed to $P_{FA} = 10^{-5}$.

Table B.1: Necessary number of samples per example such that $P_D = 0.95$ and $P_{FA} = 10^{-5}$

	Example					
	I		II		III	
Test	$E[N]$	N	$E[N]$	N	$E[N]$	N
C-SLRT	2	2	2	2	2	2
G-SLRT	8	22	8	21	8	24

B.5.3. EXPERIMENTS WITH REAL AND SIMULATED DATA

In this subsection, the validity of the most important approximations is checked. In other words, it is shown that the developed SLRTs are valid approximations and can be used in a dynamic case where the vessel is moving.

The SLRTs are applied to the real data collected from two targets, shown in Fig. B.7, B.8 and B.9. In these scenarios, the two example vessels are sailing in open sea while being observed by a third vessel. The third vessel is recording the radar measurements and uses these measurements for tracking them. Furthermore, it registers their trustworthy AIS reports. The spoofed AIS data are simulated for the purposes of this work.

The thresholds for the two SLRTs are chosen such that the probability of detection and the false alarm probability is $P_D = 0.95$ and $P_{FA} = 10^{-5}$ respectively. Subsequently, the termination time of each SLRT is evaluated and compared to the expected number shown in Fig. B.6 in order to validate our assumptions and approximations.

The results are summarized in Table B.1. In all examples, the SLRTs detect the correct behavior of the target.

In the second example, it can be observed that when the vessel tries to report a fake trajectory by increasing the spoofing distance, it is even easier to detect the spoofing behavior. This is a direct consequence of the fact that the two hypotheses become more disjoint as the spoofing distance increases.

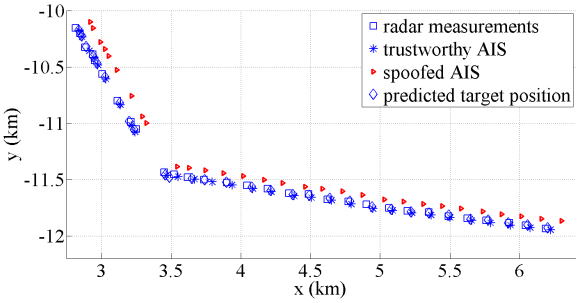

Figure B.7: Example I: Maneuvering target. The collected AIS data are trustworthy and the spoofing is simulated by adding 80 meters in both x and y directions.

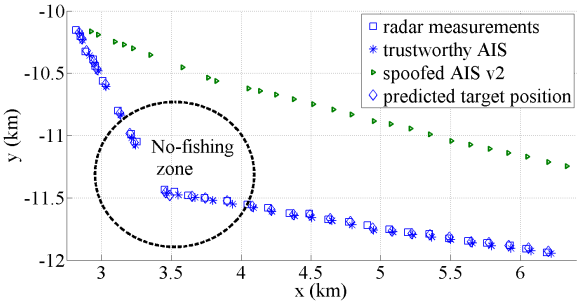

Figure B.8: Example II: The maneuvering target from Example I now spoofs its transmitted AIS data such that it appears that it is not entering a forbidden zone.

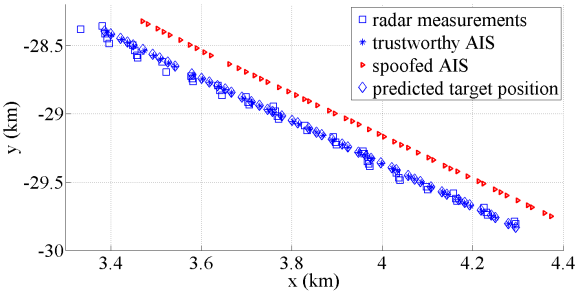

Figure B.9: Example III: A target moving in a straight line. The collected AIS data are trustworthy and the spoofing is simulated by adding 80 meters in both x and y directions.

B.6. SUMMARY

The problem of detecting whether a vessel is transmitting spoofed AIS data was formulated in the context of hypothesis testing. For this scenario, the spoofing distance and the number of radars were varied in order to obtain the corresponding ROC curves and the expected number of necessary samples for making a correct decision. The proposed solution was successfully demonstrated using real data with simulated spoofing.

There are also several other problems pertaining to the AIS data transmission, reception and exploitation. Rather than spoofing, vessels could simply turn off their AIS transmitters, possibly periodically, in order to hinder the surveillance systems and their operators from detecting illicit activities. Furthermore, a varying AIS reception probability, for instance due to weather conditions, would further complicate the AIS spoofing detection process, as described in Guerriero et al. [2010]. It would be of interest to study these effects in the context of the solution proposed in the current paper.

Another interesting topic for future research would be to extend the current work such that it can address scenarios with multiple targets. In such cases, collaborative spoofing, for instance swapping of identities, can pose further difficulties in addition to the obvious radar-to-AIS association problem.

B.7. DERIVATION OF THE CLAIRVOYANT LOG-LRT

The analytic expression of the clairvoyant log-LRT can be found as follows:

$$\begin{aligned} p(\mathbf{z},\mathbf{x}_{AIS}|H_0) &= \int_{\mathbb{R}^2} \mathcal{N}(\mathbf{z};\mathbf{x},\Sigma_R)\,\mathcal{N}(\mathbf{x}_{AIS};\mathbf{x},\Sigma_{AIS})\,\mathcal{N}(\mathbf{x};\mathbf{x}_0,\Sigma_{\mathbf{x}})\,\mathrm{d}\mathbf{x} \\ &= \int_{\mathbb{R}^2} \mathcal{N}(\mathbf{x};\mathbf{z},\Sigma_R)\,\mathcal{N}(\mathbf{x};\mathbf{x}_{AIS},\Sigma_{AIS})\,\mathcal{N}(\mathbf{x};\mathbf{x}_0,\Sigma_{\mathbf{x}})\,\mathrm{d}\mathbf{x} \\ &= \mathcal{N}(\mathbf{z};\mathbf{x}_{AIS},\Sigma_R+\Sigma_{AIS})\,\mathcal{N}(\mathbf{x}_0;\mu_1(\mathbf{z},\mathbf{x}_{AIS}),\Sigma_1+\Sigma_{\mathbf{x}}) \\ &\quad \times \int_{\mathbb{R}^2} \mathcal{N}(\mathbf{x};\mu^*,\Sigma^*)\,\mathrm{d}\mathbf{x} \\ &= \mathcal{N}(\mathbf{z};\mathbf{x}_{AIS},\Sigma_R+\Sigma_{AIS})\,\mathcal{N}(\mathbf{x}_0;\mu_1(\mathbf{z},\mathbf{x}_{AIS}),\Sigma_1+\Sigma_{\mathbf{x}}) \end{aligned} \tag{B.17}$$

where $\mathcal{N}(\mathbf{z};\mathbf{x}_{AIS},\Sigma_R+\Sigma_{AIS})$ comes from:

$$\mathcal{N}(\mathbf{x};\mathbf{z},\Sigma_R)\mathcal{N}(\mathbf{x};\mathbf{x}_{AIS},\Sigma_{AIS}) = \mathcal{N}(\mathbf{z};\mathbf{x}_{AIS},\Sigma_R+\Sigma_{AIS})\,\mathcal{N}\left(\mathbf{x};\mu_1(\mathbf{z},\mathbf{x}_{AIS}),\Sigma_1\right) \tag{B.18}$$

with

$$\Sigma_1 = (\Sigma_R^{-1}+\Sigma_{AIS}^{-1})^{-1} \tag{B.19}$$

$$\mu_1(\mathbf{z},\mathbf{x}) = \Sigma_1(\Sigma_R^{-1}\mathbf{z}+\Sigma_{AIS}^{-1}\mathbf{x}_{AIS}) \tag{B.20}$$

and $\mathcal{N}(\mathbf{x}_0;\mu_1(\mathbf{z},\mathbf{x}),\Sigma_1+\Sigma_{\mathbf{x}})$ comes from the following multiplication:

$$\mathcal{N}\left(\mathbf{x};\mu_1(\mathbf{z},\mathbf{x}_{AIS}),\Sigma_1\right)\,\mathcal{N}(\mathbf{x};\mathbf{x}_0,\Sigma_{\mathbf{x}}) = \mathcal{N}(\mathbf{x}_0;\mu_1(\mathbf{z},\mathbf{x}_{AIS}),\Sigma_1+\Sigma_{\mathbf{x}})\,\mathcal{N}(\mathbf{x};\mu^*,\Sigma^*) \tag{B.21}$$

and μ^*, Σ^* do not need to be calculated.

Setting $\mathbf{x}_{AIS} = \mathbf{x}_{AIS} - \mathbf{d}$, it holds that under H_1:

$$p(\mathbf{z}, \mathbf{x}_{AIS}|H_1) = \mathcal{N}(\mathbf{z}; \mathbf{x}_{AIS} - \mathbf{d}, \Sigma_R + \Sigma_{AIS}) \times \mathcal{N}(\mathbf{x}_0; \mu_1(\mathbf{z}, \mathbf{x}_{AIS}) - \Delta\mathbf{d}, \Sigma_1 + \Sigma_{\mathbf{x}}) \tag{B.22}$$

where

$$\Delta = (\Sigma_{AIS}\Sigma_R^{-1} + I_{2\times 2})^{-1} \tag{B.23}$$

Then, the log-LRT is

$$\begin{aligned}
\log\Lambda(\mathbf{z}, \mathbf{x}_{AIS}, \mathbf{d}) &= \log\left(\frac{p(\mathbf{z}, \mathbf{x}_{AIS}|H_1)}{p(\mathbf{z}, \mathbf{x}_{AIS}|H_0)}\right) \\
&= -(\mathbf{x}_{AIS} - \mathbf{z} - \mathbf{d})^T(\Sigma_R + \Sigma_{AIS})^{-1}(\mathbf{x}_{AIS} - \mathbf{z} - \mathbf{d}) \\
&\quad + (\mathbf{x}_{AIS} - \mathbf{z})^T(\Sigma_R + \Sigma_{AIS})^{-1}(\mathbf{x}_{AIS} - \mathbf{z}) \\
&\quad - (\mathbf{x}_0 - \mu_1(\mathbf{z}, \mathbf{x}_{AIS}) + \Delta\mathbf{d})^T(\Sigma_1 + \Sigma_{\mathbf{x}})^{-1}(\mathbf{x}_0 - \mu_1(\mathbf{z}, \mathbf{x}_{AIS}) + \Delta\mathbf{d}) \\
&\quad + (\mathbf{x}_0 - \mu_1(\mathbf{z}, \mathbf{x}_{AIS}))^T(\Sigma_1 + \Sigma_{\mathbf{x}})^{-1}(\mathbf{x}_0 - \mu_1(\mathbf{z}, \mathbf{x}_{AIS}))
\end{aligned} \tag{B.24}$$

Setting

$$A = (\Sigma_R + \Sigma_{AIS})^{-1}\ , \qquad B = (\Sigma_1 + \Sigma_{\mathbf{x}})^{-1} \tag{B.25}$$

$$\mathbf{v} = \mathbf{x}_{AIS} - \mathbf{z}\ , \qquad \mathbf{w} = \mathbf{x}_0 - \mu_1(\mathbf{z}, \mathbf{x}_{AIS}) \tag{B.26}$$

the log-likelihood ratio test has the form

$$\begin{aligned}
\log\Lambda(\mathbf{z}, \mathbf{x}_{AIS}, \mathbf{d}) &= [a_{xx}d_x(2v_x - d_x) - b_{xx}(\Delta\mathbf{d})_x(2w_x + (\Delta\mathbf{d})_x)] \\
&\quad + \left[a_{yy}d_y(2v_y - d_y) - b_{yy}(\Delta\mathbf{d})_y(2w_y + (\Delta\mathbf{d})_y)\right] \\
&\quad + (a_{xy} + a_{yx})\left[v_y d_x + v_x d_y - d_x d_y\right] \\
&\quad - (b_{xy} + b_{yx})\left[w_y(\Delta\mathbf{d})_x + w_x(\Delta\mathbf{d})_y + (\Delta\mathbf{d})_x(\Delta\mathbf{d})_y\right]
\end{aligned} \tag{B.27}$$

where: a_{ij} are the elements of matrix A, b_{ij} the elements of matrix B, v_i the elements of vector $\mathbf{v}$, w_i the elements of vector $\mathbf{w}$ and $(\Delta\mathbf{d})_i$ are the elements of vector $\Delta\mathbf{d}$.

Given the fact that

$$E[\mathbf{v}|H_0] = [0,0]\ ,\ E[\mathbf{v}|H_1] = \mathbf{d} \tag{B.28}$$

$$E[\mathbf{w}|H_0] = [0,0]\ ,\ E[\mathbf{w}|H_1] = \Delta\mathbf{d} \tag{B.29}$$

the expected value of the log-LRT under the two hypotheses can be evaluated:

$$E[\log\Lambda(\mathbf{z},\mathbf{x}_{AIS})|H_0] = -\left[a_{xx}(\hat{d}_x)^2 + b_{xx}(\Delta\hat{\mathbf{d}})_x^2\right] - \left[a_{yy}(\hat{d}_y)^2 + b_{yy}(\Delta\hat{\mathbf{d}})_y^2\right] - (a_{xy}+a_{yx})\hat{d}_x\hat{d}_y - (b_{xy}+b_{yx})(\Delta\hat{\mathbf{d}})_x(\Delta\hat{\mathbf{d}})_y \tag{B.30}$$

$$\begin{aligned} E[\log\Lambda(\mathbf{z},\mathbf{x}_{AIS},\mathbf{d})|H_1] = &\left[a_{xx}\hat{d}_x(2d_x-\hat{d}_x) - b_{xx}(\Delta\hat{\mathbf{d}})_x(2(\Delta\mathbf{d})_x + (\Delta\hat{\mathbf{d}})_x)\right] \\ &+ \left[a_{yy}\hat{d}_y(2d_y-\hat{d}_y) - b_{yy}(\Delta\hat{\mathbf{d}})_y(2(\Delta\mathbf{d})_y + (\Delta\hat{\mathbf{d}})_y)\right] \\ &+ (a_{xy}+a_{yx})\left[d_y\hat{d}_x + d_x\hat{d}_y - \hat{d}_x\hat{d}_y\right] \\ &- (b_{xy}+b_{yx})\left[(\Delta\mathbf{d})_y(\Delta\hat{\mathbf{d}})_x + (\Delta\mathbf{d})_x(\Delta\hat{\mathbf{d}})_y + (\Delta\hat{\mathbf{d}})_x(\Delta\hat{\mathbf{d}})_y\right] \end{aligned} \tag{B.31}$$

where d_i are the elements of the true spoofing distance vector, $\hat{d}_i$ are the elements of the spoofing distance vector used in the log-LRT and $(\Delta\hat{\mathbf{d}})_i$ are the elements of vector $\Delta\hat{\mathbf{d}}$.

B.8. MULTI-RADAR LIKELIHOOD

When measurements from K radars are available, the multi-radar likelihood is:

$$p([\mathbf{z}_1,\ldots,\mathbf{z}_K],\mathbf{x}_{AIS}|H_i) = \int \prod_{k=1}^{K}\{p(\mathbf{z}_k|\mathbf{x})\}\; p(\mathbf{x}_{AIS}|H_i,\mathbf{x})\; p(\mathbf{x})\,\mathrm{d}\mathbf{x} \tag{B.32}$$

where $i = 0, 1$.

If the measurements of each radar follow a Gaussian distribution and all have the same covariance matrix then using Eq. (B.3-B.5) it holds that:

$$\prod_{k=1}^{K}\{p(\mathbf{z}_k|\mathbf{x})\} = \prod_{k=1}^{K}\{\mathcal{N}(\mathbf{z}_k;\mathbf{x},\Sigma_R)\} = \epsilon\;\mathcal{N}(\mathbf{z}';\mathbf{x},\Sigma'_R) \tag{B.33}$$

with

$$\mathbf{z}' = \frac{1}{K}\sum_{k=1}^{K}(\mathbf{z}_k), \qquad \Sigma'_R = \frac{1}{K}\Sigma_R, \qquad \epsilon = \prod_{k=2}^{K}\left[\mathcal{N}\left(\mathbf{z}_k;\mathbf{z}'_{k-1},\left(\frac{k}{k-1}\right)\Sigma_R\right)\right] \tag{B.34}$$

Therefore, the LRT has the same form as in the case of one sensor (see Eq. B.27) with the differences that *a*) the arithmetic mean of the measurements of all radars is used as a single measurement; and *b*) the common measurement covariance matrix divided by the number of radars K is used as new measurement covariance matrix.

C

THE CB-MEMBER FILTER

In this appendix, the Cardinality-Balanced Multi-target Multi-Bernoulli (CB-MeMBer) filter is discussed. The discussion draws heavily from Mahler [2007] and Vo et al. [2009b].

Section C.1 presents the Bernoulli and multi-Bernoulli RFSs and describes the major assumptions made by the CB-MeMBer filter. Section C.2 describes the CB-MeMBer filter recursion and its SMC implementation. Finally, Section C.3 explains how an estimate can be extracted from the estimated posterior multi-Bernoulli distribution.

C.1. BERNOULLI AND MULTI-BERNOULLI RFSS

The key assumption behind the CB-MeMBer filter is that the multi-target posterior density is a multi-object multi-Bernoulli process. A Bernoulli RFS $\mathbf{X}$ on $\mathscr{X}$ has probability r of being a singleton whose PDF is $p(\mathbf{x})$ defined on $\mathscr{X}$ and probability $1-r$ of being empty. The cardinality distribution of a Bernoulli RFS is a Bernoulli distribution with parameter r and the PDF of a Bernoulli RFS is

$$p(\mathbf{X}) = \begin{cases} 1-r & \text{if } \mathbf{X} = \emptyset \\ r \cdot p(\mathbf{x}) & \text{if } \mathbf{X} = \{\mathbf{x}\}. \end{cases} \tag{C.1}$$

Accordingly, a multi-Bernoulli RFS $\mathbf{X}$ on $\mathscr{X}$ is the union of N independent Bernoulli RFSs $\mathbf{X}^{(i)}$ with corresponding existence probability $r^{(i)}$ and PDF $p^{(i)}(\mathbf{x})$, $i = 1, \ldots, N$. In other words, $\mathbf{X} = \bigcup_{i=1}^{N} \mathbf{X}^{(i)}$. A multi-Bernoulli RFS is completely described by the parameter set $\{(r^{(i)}, p^{(i)})\}_{i=1}^{N}$. Its cardinality distribution is given by the multi-Bernoulli distribution, see [Mahler, 2007, pp.369]. The probability density of a multi-Bernoulli RFS $\mathbf{X}$ is given by

$$p(\emptyset) = \prod_{i=1}^{N} \left(1 - r^{(i)}\right) \tag{C.2}$$

$$p(\mathbf{X}) = p(\emptyset) \sum_{1 \le i_1 \ne \ldots \ne i_n \le N} \prod_{j=1}^{n} \frac{r^{(i_j)} p^{(i_j)}(\mathbf{x}_j)}{1 - r^{(i_j)}}. \tag{C.3}$$

Assume that at time k there are $N(k)$ targets present, each taking values in $\mathscr{X} \subseteq \mathbb{R}^{n_x}$ and $M(k)$ measurements, each taking values in $\mathscr{Z} \subseteq \mathbb{R}^{n_z}$. Following the RFS approach, the finite sets of targets and measurements are treated as the multitarget state and the multitarget measurement respectively:

$$\mathbf{X}_k = \{\mathbf{x}_{k,1}, \ldots, \mathbf{x}_{k,N(k)}\} \tag{C.4}$$

$$\mathbf{Z}_k = \{\mathbf{z}_{k,1}, \ldots, \mathbf{z}_{k,M(k)}\}. \tag{C.5}$$

Given the multitarget state $\mathbf{X}_{k-1}$ at time $k-1$, each element $\mathbf{X}_{k-1,i} \in \mathbf{X}_{k-1}$ either continues to exist at time k with probability $p_{S,k}(\mathbf{x}_{k-1})$ and moves to a new state $\mathbf{x}_k$ with probability density $f(\mathbf{x}_k|\mathbf{x}_{k-1})$, or dies with probability $1 - p_{S,k}(\mathbf{x}_{k-1})$. The probability $p_{S,k}(\mathbf{x}_{k-1})$ is also called survival probability and is used for modeling target disappearance from the scenario. The probability density $f(\mathbf{x}_k|\mathbf{x}_{k-1})$ is usually defined according to the motion model of the targets. Furthermore, new targets might enter the scenario. This is modeled by the new (multi-)Bernoulli RFS Γ_k. The RFS modeling the predicted multi-target state $\mathbf{X}_k$ is given by

$$\mathbf{X}_k = \left[\bigcup_{\mathbf{x}_{k-1} \in \mathbf{X}_{k-1}} S_{k|k-1}(\mathbf{x}_{k-1}) \right] \bigcup \Gamma_k \tag{C.6}$$

assuming that the RFSs constituting the union in Eq. (C.6) are mutually independent and that $S_{k|k-1}(\mathbf{x}_{k-1})$ is a Bernoulli RFS with parameters $r = p_{S,k}(\mathbf{x}_{k-1})$ and $p(\cdot) = f(\cdot|\mathbf{x}_{k-1})$. The RFS $\mathbf{X}_k$ is a multi-Bernoulli RFS conditional on $\mathbf{X}_{k-1}$ and Eq. (C.6) represents the predicted PDF of the RFS $\mathbf{X}_k$ at time k, taking into account the motion of existing targets, the arrival of new targets and the possible disappearance of existing ones.

Depending on the radar beam pointing, a given target $\mathbf{x}_k \in \mathbf{X}_k$ is either detected with probability $p_{D,k}(\mathbf{x}_k)$ and generates a measurement $\mathbf{z}_k$ whose likelihood is $g_k(\mathbf{z}_k|\mathbf{x}_k)$, or missed with probability $1 - p_{D,k}(\mathbf{x}_k)$. In other words, each measurement is a Bernoulli RFS $\Theta_k(\mathbf{x}_k)$ with parameters $r = p_{D,k}(\mathbf{x}_k)$ and $p(\cdot) = g_k(\cdot|\mathbf{x}_k)$. In addition to the target-originated measurements, the sensor produces a set of false alarms (or clutter) that are modeled as a Poisson RFS C_k with intensity function $\kappa_k(\cdot)$. Thus, the measurement RFS $\mathbf{Z}_k$ is given by

$$\mathbf{Z}_k = \left[\bigcup_{\mathbf{x}_k \in \mathbf{X}_k} \Theta_k(\mathbf{x}_k) \right] \bigcup C_k. \tag{C.7}$$

Assuming that the RFSs constituting the union in Eq. (C.7) are independent of one another, the target-originated measurements in (C.7) form a multi-Bernoulli RFS $\mathbf{Z}_k$.

C.2. SMC IMPLEMENTATION OF THE CB-MEMBER FILTER

For the sake of brevity, only the SMC implementation of the CB-MeMBer filter is presented, also see Vo et al. [2009a]. Suppose that at time $k-1$ the multi-Bernoulli posterior multitarget density is given and that the $p_{k-1}^{(i)}(\mathbf{x})$ of each Bernoulli component $\mathbf{X}^{(i)}$ is approximated by a set of K weighted particles:

$$p_{k-1}^{(i)}(\mathbf{x}) = \sum_{i=1}^{K} w_{k-1}^{(i,j)} \delta_{\mathbf{x}_{k-1}^{(i,j)}}(\mathbf{x}). \tag{C.8}$$

Given the proposal densities $q_k^{(i)}(\mathbf{x}_k|\mathbf{x}_{k-1}, \mathbf{Z}_{1:k}) = f_k^{(i)}(\mathbf{x}_k|\mathbf{x}_{k-1})$ (motion model) and $b_k^{(i)}(\cdot|\mathbf{Z}_{1:k-1})$ (target birth), the predicted multitarget density

$$p_{k|k-1} = \left\{\left(r_{P,k|k-1}^{(i)}, p_{P,k|k-1}^{(i)}\right)\right\}_{i=1}^{N(k-1)} \bigcup \left\{\left(r_{\Gamma,k}^{(i)}, p_{\Gamma,k}^{(i)}\right)\right\}_{i=1}^{N_\Gamma(k)} \tag{C.9}$$

can be found using:

$$r_{P,k|k-1}^{(i)} = r_{k-1}^{(i)} \sum_{j=1}^{K} w_{k-1}^{(i,j)} p_{S,k}\left(\mathbf{x}_{k-1}^{(i,j)}\right) \tag{C.10}$$

$$p_{P,k|k-1}^{(i)}(\mathbf{x}) = \sum_{j=1}^{K} \tilde{w}_{P,k|k-1}^{(i,j)} \delta_{\mathbf{x}_{P,k|k-1}^{(i,j)}}(\mathbf{x}) \tag{C.11}$$

$$r_{\Gamma,k}^{(i)} : \text{given by the birth model} \tag{C.12}$$

$$p_{\Gamma,k}^{(i)}(\mathbf{x}) = \sum_{j=1}^{K_\Gamma} \tilde{w}_{\Gamma,k}^{(i,j)} \delta_{\Gamma,\mathbf{x}_k^{(i,j)}}(\mathbf{x}) \tag{C.13}$$

where

$$\mathbf{x}_{P,k|k-1}^{(i,j)} \sim f_k^{(i)}(\mathbf{x}_k|\mathbf{x}_{k-1}) \,,\ j = 1, \ldots, K \tag{C.14}$$

$$w_{P,k|k-1}^{(i,j)} = w_{k-1}^{(i,j)} p_{S,k}\left(\mathbf{x}_{k-1}^{(i,j)}\right) \tag{C.15}$$

$$\tilde{w}_{P,k|k-1}^{(i,j)} = w_{P,k|k-1}^{(i,j)} \Big/ \left(\sum_{j=1}^{L} w_{P,k|k-1}^{(i,j)}\right) \tag{C.16}$$

$$x_{\Gamma,k}^{(i,j)} \sim b_k^{(i)}(\cdot|\mathbf{Z}_{1:k-1}) \,,\ j = 1, \ldots, K_\Gamma \tag{C.17}$$

$$w_{\Gamma,k}^{(i,j)} = \frac{p_{\Gamma,k}\left(\mathbf{x}_{\Gamma,k}^{(i,j)}\right)}{b_k^{(i)}\left(\mathbf{x}_{\Gamma,k}^{(i,j)}|\mathbf{Z}_{1:k-1}\right)} \tag{C.18}$$

$$\tilde{w}_{\Gamma,k}^{(i,j)} = w_{\Gamma,k}^{(i,j)} \Big/ \left(\sum_{j=1}^{K_\Gamma} w_{\Gamma,k}^{(i,j)}\right) \tag{C.19}$$

Now assume that at time k the predicted multi-Bernoulli multitarget density is given and that the $p_{k|k-1}^{(i)}(\mathbf{x})$ of each Bernoulli component (i) is approximated by a set of K

weighted particles:

$$p^{(i)}_{k|k-1}(\mathbf{x}) = \sum_{i=1}^{K} w^{(i,j)}_{k|k-1}\delta_{\mathbf{x}^{(i,j)}_k}(\mathbf{x}). \tag{C.20}$$

Then, given a set of measurements $\mathbf{Z}_k$, the multi-Bernoulli approximation of the updated multitarget density

$$p_k = \left\{\left(r^{(i)}_{L,k}, p^{(i)}_{L,k}\right)\right\}_{i=1}^{N(k|k-1)} \bigcup \left\{\left(r^{(i)}_{U,k}(\mathbf{z}), p^{(i)}_{U,k}(\cdot;\mathbf{z})\right)\right\}_{\mathbf{z}\in\mathbf{Z}_k} \tag{C.21}$$

can be found using:

$$r^{(i)}_{L,k} = r^{(i)}_{k|k-1}\frac{1-\varrho^{(i)}_{L,k}}{1-r^{(i)}_{k|k-1}\varrho^{(i)}_{L,k}} \tag{C.22}$$

$$p^{(i)}_{L,k}(\mathbf{x}) = \sum_{j=1}^{K} \tilde{w}^{(i,j)}_{L,k}\delta_{\mathbf{x}^{(i,j)}_k}(\mathbf{x}) \tag{C.23}$$

$$r^{(i)}_{U,k}(\mathbf{z}) = \frac{\sum_{i=1}^{M}\frac{r^{(i)}_{k|k-1}\left(1-r^{(i)}_{k|k-1}\right)\varrho^{(i)}_{U,k}(\mathbf{z})}{\left(1-r^{(i)}_{k|k-1}\varrho^{(i)}_{L,k}\right)^2}}{\kappa_k(\mathbf{z}) + \sum_{i=1}^{M}\frac{r^{(i)}_{k|k-1}\varrho^{(i)}_{U,k}(\mathbf{z})}{1-r^{(i)}_{k|k-1}\varrho^{(i)}_{L,k}}} \tag{C.24}$$

$$p^{(i)}_{U,k}(\mathbf{x};\mathbf{z}) = \sum_{i=1}^{M}\sum_{j=1}^{K} \tilde{w}^{(i,j)}_{U,k}(\mathbf{z})\delta_{\mathbf{x}^{(i,j)}_k}(\mathbf{x}) \tag{C.25}$$

where

$$\varrho^{(i)}_{L,k} = \sum_{j=1}^{K} w^{(i,j)}_{k|k-1} p_{D,k}\left(\mathbf{x}^{(i,j)}_k\right) \tag{C.26}$$

$$w^{(i,j)}_{L,k} = w^{(i,j)}_{k|k-1}\left(1-p_{D,k}\left(\mathbf{x}^{(i,j)}_k\right)\right) \tag{C.27}$$

$$\tilde{w}^{(i,j)}_{L,k} = w^{(i,j)}_{L,k}\Big/\left(\sum_{j=1}^{K} w^{(i,j)}_{L,k}\right) \tag{C.28}$$

$$\psi_{k,\mathbf{z}}\left(\mathbf{x}^{(i,j)}_k\right) = g_k(\mathbf{z}|\mathbf{x}_k)p_{D,k}\left(\mathbf{x}^{(i,j)}_k\right) \tag{C.29}$$

$$\varrho^{(i)}_{U,k}(z) = \sum_{j=1}^{K} w^{(i,j)}_{k|k-1}\psi_{k,z}\left(\mathbf{x}^{(i,j)}_k\right) \tag{C.30}$$

$$w^{(i,j)}_{U,k}(\mathbf{z}) = w^{(i,j)}_{k|k-1}\frac{r^{(i)}_{k|k-1}}{1-r^{(i)}_{k|k-1}}\psi_{k,\mathbf{z}}\left(\mathbf{x}^{(i,j)}_k\right) \tag{C.31}$$

$$\tilde{w}^{(i,j)}_{U,k}(\mathbf{z}) = w^{(i,j)}_{U,k}(\mathbf{z})\Big/\left(\sum_{i=1}^{M}\sum_{j=1}^{K} w^{(i,j)}_{U,k}(\mathbf{z})\right) \tag{C.32}$$

Because the number of Bernoulli components grows without bound due to the birth terms and the measurement update, track management techniques such as pruning and merging must be applied, see Vo et al. [2009a].

C.3. STATE ESTIMATE EXTRACTION

The main advantage of the CB-MeMBer filter over the (C)PHD filter is the intuitive way of extracting state estimates. One can estimate first the mean or mode of the number of targets and subsequently extract individual state estimates from the corresponding posterior spatial densities. The evaluation of state estimates for a CB-MeMBer filter is, therefore, more robust and (potentially) less computationally expensive than for a (C)PHD.

The two most common options are the expected (or mean) estimate and the MAP estimate. The expected number of targets is given by

$$\bar{N} = \sum_{i=1}^{N} r^{(i)}. \tag{C.33}$$

The MAP estimate of the number of targets is given by

$$\begin{aligned} \hat{N} &= \arg\sup_{n} \left\{ B_{r_1,\ldots,r_N}(n) \right\} \\ &= \arg\sup_{n} \left\{ \left[\prod_{i=1}^{N} \left(1 - r^{(i)}\right) \right] \left[\sum_{1 \le i_1 \le \ldots \le i_n \le N} \left(\frac{r^{(i_1)}}{1 - r^{(i_1)}} \cdots \frac{r^{(i_n)}}{1 - r^{(i_n)}} \right) \right] \right\} \end{aligned} \tag{C.34}$$

see [Mahler, 2007, pp.369].

Given our preferred estimate $\bar{N}$ of the number of targets, a state estimate can be extracted from the spatial distributions of the $\bar{N}$ Bernoulli components with the highest probability of existence $r^{(i)}$. Assuming that a weighted-sample approximation of $p^{(i)}(\mathbf{x})$ is available in the form $\{\mathbf{x}_j, w_j\}_{j=1}^{L}$, the mean estimate is given by

$$\bar{\mathbf{x}} = \sum_{j=1}^{L} \left(\mathbf{x}_j \cdot w_j \right). \tag{C.35}$$

Unfortunately, there is no analytic method for extracting a MAP estimate from an arbitrary density, of which there is available only a weighted-sample approximation. For this reason, first the density is estimated, using any of the kernel density estimation methods that are available, and then the point for which it attains its maximum is found. The kernel density estimation software that implement the algorithm presented in Kristan et al. [2011] is used in this thesis.

Using the MAP estimate, first of the number of targets and subsequently of the corresponding spatial PDFs, corresponds to the Marginal Multi-target (MaM) estimator, introduced in [Mahler, 2007, pp.497]. The MaM estimator is Bayes optimal but it is not known if it is statistically consistent.

Another option is the Joint Multitarget (JoM) estimator, introduced in [Mahler, 2007, pp.498]. First, the argmax estimate for each cardinality $n = 1, \ldots, N(k)$ is determined:

$$\hat{\mathbf{X}}_n = \arg\sup_{\mathbf{x}_1,\ldots,\mathbf{x}_n} p(\{\mathbf{x}_1, \ldots, \mathbf{x}_n\}|\mathbf{Z}) \tag{C.36}$$

and then the JoM estimate will be

$$\hat{\mathbf{X}} = \hat{\mathbf{X}}_j \ , \ \ j = \arg\sup_{n} \left[p(\hat{\mathbf{X}}_n|\mathbf{Z}) \cdot \frac{c^n}{n!} \right] \tag{C.37}$$

or in more compact form

$$\hat{\mathbf{X}} = \underset{n,\mathbf{x}_1,\ldots,\mathbf{x}_n}{\arg\sup} \left[p(\{\mathbf{x}_1,\ldots,\mathbf{x}_n\}|\mathbf{Z}) \cdot \frac{c^n}{n!} \right] \tag{C.38}$$

where c is a fixed constant. The JoM estimator is Bayes optimal and statistically consistent. For very small values of c, the JoM estimator is a limiting case of the MAP estimator on a discrete multitarget space, see [Mahler, 2007, pp.499].

BIBLIOGRAPHY

J. Ajgl and Miroslav Šimandl. Differential entropy estimation by particles. In *Proceedings of the 18th IFAC World Congress*, volume 18, pages 11991–11996, 2011. doi: 10.3182/20110828-6-IT-1002.01404.

Edson Hiroshi Aoki. *Characterization of uncertainty in Bayesian estimation using sequential Monte Carlo methods*. PhD thesis, University of Twente, Enschede, October 2013.

Edson Hiroshi Aoki, Arunabha Bagchi, Pranab Mandal, and Yvo Boers. A theoretical look at information-driven sensor management criteria. In *Proceedings of the 14th International Conference on Information Fusion*, volume 1, pages 1180–1187, 2011.

Jason Matthew Aughenbaugh and Brian R. La Cour. Metric selection for information theoretic sensor management. In *Proceedings of the 11th International Conference on Information Fusion*, pages 1961–1968, 2008.

Jason Matthew Aughenbaugh and Brian R. LaCour. Sensor management for particle filter tracking. *IEEE Transactions on Aerospace and Electronic Systems*, 47(1):503–523, January 2011.

Yaakov Bar-Shalom and Xiao-Rong Li. *Multitarget-Multisensor tracking: principles and techniques*. YBS publishing, 1995. ISBN 0-9648312-0-1.

Yaakov Bar-Shalom, Peter Willet, and Xin Tian. *Tracking and Data Fusion: A Handbook of Algorithms*. YBS publishing, 2011. ISBN 978-0964831278.

Frederic Barbaresco. Radar resources optimization by adaptive search domains priority assignment based on most threatening trajectories computation. In *Proceedings of the 10th International Conference on Information Fusion*, pages 1–8, 2007.

Michele Basseville and Igor V. Nikiforov. *Detection of Abrupt Changes: Theory and Application*. Prentice-Hall, Inc., 1993. URL http://people.irisa.fr/Michele.Basseville/kniga/kniga.pdf.

James O. Berger. *Statistical decision theory: Foundations, concepts, and methods*. Springer Series in Statistics. Springer, 1980. ISBN 3-540-90471-9.

Iwo Bialynicki-Birula. Rényi entropy and the uncertainty relations. In *Foundations of Probability and Physics*. American Institute of Physics, 2007. URL http://www.cft.edu.pl/~birula/publ/RenyiEntr.pdf.

Samuel Blackman and Robert Popoli. *Design and Analysis of Modern Tracking Systems*. Artech House, 1999.

Erik Blasch, J. Salerno, I. Kadar, K. Hintz, J. Biermann, and S. Das. Resource management coordination with level 2/3 fusion issues and challenges [Panel Report]. *Aerospace and Electronic Systems Magazine, IEEE*, 23(3):32–46, 2008. ISSN 0885-8985. doi: 10.1109/MAES.2008.4476103.

Melanie Bocquel. *Random finite sets in multi-target tracking - efficient sequential MCMC implementation*. PhD thesis, University of Twente, Enschede, October 2013.

Yvo Boers and Hans Driessen. A particle filter multi target track before detect application. In *Proceedings of IEE Radar, Sonar and Navigation*, pages 351–357, 2004.

Yvo Boers, Hans Driessen, and Jitse Zwaga. Adaptive MFR parameter control: fixed vs. variable probabilities of detection. In *Proceedings of Signal and Data Processing of Small Targets*, pages 2–6, 2005.

Yvo Boers, Hans Driessen, and Linda Schipper. Particle filter based sensor selection in binary sensor networks. In *Proceedings of the 11th International Conference on Information Fusion*, pages 1–7, 2008.

Yvo Boers, Hans Driessen, Arunabgha Bagchi, and Pranab Mandal. Particle filter based entropy. In *Proceedings of the 13th International Conference on Information Fusion*, pages 1–8, 2010.

F. Bolderheij, F.G.J. Absil, and P. van Genderen. A risk-based object-oriented approach to sensor management. In *Proceedings of the 8th International Conference on Information Fusion*, volume 1, page 8, 2005.

Fok Bolderheij. *Mission-Driven sensor management analysis, design, implementation and simulation*. PhD thesis, Electrical Engineering, Mathematics and Computer Science, Delft University of Technology, 2007.

Fok Bolderheij and Piet Van Genderen. Mission driven sensor management. In *Proceedings of the 7th International Conference on Information Fusion*, 2004.

L.A.M. Bush, A.J. Wang, and B.C. Williams. Risk-based sensing in support of adjustable autonomy. In *IEEE Aerospace Conference*, pages 1–18, 2012. doi: 10.1109/AERO.2012.6187312.

J.M.K. Butler. *Tracking and control in multi-function radar*. PhD thesis, University College London (UCL), 1998.

Yi Cao. Identification of the Pareto front from a set of points, July 2008. URL http://www.mathworks.de/matlabcentral/fileexchange/17251-pareto-front.

David A. Castañón, Ron Mahler, Kenneth J. Hintz, Jim Reich, Ivan Kadar, M. Farooq, T. Kirubarajan, R. Tharmarasa, T. Sathyan, and A. Sinha. Issues in resource management with applications to real-world problems. *Proc. SPIE*, 6235:62351O–62351O–55, 2006. doi: 10.1117/12.694899. URL http://dx.doi.org/10.1117/12.694899.

Alexander Charlish. *Autonomous agents for multi-function radar resource management*. PhD thesis, University College London (UCL), 2011.

Alexander Charlish, K. Woodbridge, and H. Griffiths. Agent based multifunction radar surveillance control. In *Proceedings of the IEEE Radar Conference (RADAR)*, volume 1, pages 824 – 829, 2011.

Alexander Charlish, K. Woodbridge, and H. Griffiths. Multi-target tracking control using Continuous Double Auction Parameter Selection. In *Information Fusion (FUSION), 2012 15th International Conference on*, pages 1269–1276, July 2012.

Remi Chou, Yvo Boers, Martin Podt, and Matthieu Geist. Performance evaluation for particle filters. In *Proceedings of the 14th International Conference on Information Fusion*, pages 1882–1888, 2011.

CNS Systems. SENTINEL Surveillance and Secure Information System, dec 2012. URL http://www.cns.se/virtupload/content/5/CNSS_11_1667_E_Sentinel.pdf.

David T. Cole. *A Cooperative UAS Architecture for Information-Theoretic Search and Track*. PhD thesis, Australian Centre for Field Robotics, School of Aerospace, Mechanical and Mechatronic Engineering, The University of Sydney, 2009.

Thomas M. Cover and Joy A. Thomas. *Elements of Information Theory*. John Wiley & Sons, Inc., 2006.

John M. Danskin. A helicopter versus submarine search game. *Operations Research*, 16 (3):509–517, 1968.

Arnaud Doucet, B.N. Vo, C. Andrieu, and M. Davy. Particle filtering for multi-target tracking and sensor management. In *Proceedings of the 5th International Conference on Information Fusion*, pages 474–481, 2002.

M. Flint, E. Fernandez-Gaucherand, and M. Polycarpou. Cooperative control for UAV's searching risky environments for targets. In *Proceedings of the 42nd IEEE Conference on Decision and Control (CDC)*, volume 4, page 3567, 2003.

Brian P. Gerkey, Sebastian Thrun, and Geoff Gordon. Visibility-based pursuit-evasion with limited field of view. In *International Journal of Robotics Research*, pages 20–27, 2004.

B.F. Gore and K.M. Corker. A systems engineering approach to behavioral predictions of an advanced air traffic management concept. In *Digital Avionics Systems Conference, 2000. Proceedings. DASC. The 19th*, volume 1, pages 4B3/1–4B3/8 vol.1, 2000. doi: 10.1109/DASC.2000.886949.

Amirali K. Gostar, R. Hoseinnezhad, and A Bab-Hadiashar. Multi-Bernoulli sensor control for multi-target tracking. In *Intelligent Sensors, Sensor Networks and Information Processing, 2013 IEEE Eighth International Conference on*, pages 312–317, April 2013a. doi: 10.1109/ISSNIP.2013.6529808.

Amirali K. Gostar, R. Hoseinnezhad, and A Bab-Hadiashar. Robust Multi-Bernoulli sensor selection for multi-target tracking in sensor networks. *Signal Processing Letters, IEEE*, 20(12):1167–1170, Dec 2013b. ISSN 1070-9908. doi: 10.1109/LSP.2013.2283735.

Amirali K. Gostar, R. Hoseinnezhad, A Bab-Hadiashar, and Ba-Tuong Vo. Control of sensor with unknown clutter and detection profile using Multi-Bernoulli filter. In *Information Fusion (FUSION), 2013 16th International Conference on*, pages 1021–1028, July 2013c.

Amirali K. Gostar, R. Hoseinnezhad, and A. Bab-Hadiashar. Sensor control for multi-object tracking using labeled Multi-Bernoulli filter. In *Information Fusion (FUSION), 2014 17th International Conference on*, pages 1–8, July 2014.

Marco Guerriero, Stefano Coraluppi, Craig Carthel, and Peter Willett. Analysis of AIS Intermittency and Vessel Characterization using a Hidden Markov Model. In *Informatik 2010: Service Science - Neue Perspektiven für die Informatik, Beiträge der 40. Jahrestagung der Gesellschaft für Informatik e.V. (GI), Band 2. 5th German Workshop SDF 2010 - Sensor Data Fusion: Trends, Solutions, Applications*, 2010.

Jeffery Hansen, Ragunathan Rajkumar, J. Lehoczky, and S. Ghosh. Resource management for radar tracking. In *IEEE International Radar Conference*, pages 140–147, Verona, NY., May 2006.

Alfred O. Hero and D. Cochran. Sensor management: Past, present, and future. *Sensors Journal, IEEE*, 11(12):3064–3075, 2011. ISSN 1530-437X. doi: 10.1109/JSEN.2011.2167964.

Hung Gia Hoang. Control of a mobile sensor for multi-target tracking using multi-target/object Multi-Bernoulli filter. In *Control, Automation and Information Sciences (ICCAIS), 2012 International Conference on*, pages 7–12, Nov 2012. doi: 10.1109/ICCAIS.2012.6466635.

Hung Gia Hoang and Ba-Tuong Vo. Sensor management for multi-target tracking via Multi-Bernoulli filtering. *Automatica*, 50 (4):1135–1142, 2014. doi: 10.1016/j.automatica.2014.02.007.

Xiao-Li Hu, T.B. Schon, and L. Ljung. A basic convergence result for particle filtering. *IEEE Transactions on Signal Processing*, 56(4):1337 –1348, april 2008.

Marco Huber. *Probabilistic Framework for Sensor Management*. PhD thesis, Intelligent Sensor-Actuator-Systems Laboratory, Universität Karlsruhe, 2009. URL http://digbib.ubka.uni-karlsruhe.de/volltexte/1000012224.

Mike Kalandros. Covariance control for multisensor systems. *IEEE Transactions on Aerospace and Electronic Systems*, 38(4):1138 – 1157, oct 2002.

M. R. Kastelein. Implicit maneuver coordination: Issues and potential solutions. In *Digital Avionics Systems Conference (DASC), 2012 IEEE/AIAA 31st*, pages 2B5–1–2B5–11, Oct 2012. doi: 10.1109/DASC.2012.6382285.

Fotios Katsilieris and Yvo Boers. Optimal search: a practical interpretation of information-driven sensor management. Memorandum 1979, Department of Applied Mathematics, University of Twente, Enschede, March 2012.

Fotios Katsilieris, Yvo Boers, and Hans Driessen. Optimal search: a practical interpretation of information-driven sensor management. In *Proceedings of the 15th International Conference on Information Fusion*, pages 439–446, 2012a.

Fotios Katsilieris, Yvo Boers, and Hans Driessen. Sensor management for PRF selection in the track-before-detect context. In *Proceedings of the IEEE Radar Conference*, pages 360–365, 2012b.

Fotios Katsilieris, Alexander Charlish, and Yvo Boers. Towards an online, adaptive algorithm for radar surveillance control. In *Future Security - Security Research Conference 2012: Sensor Data Fusion Workshop (Future Security 2012 - Sensor Data Fusion Workshop)*, Bonn, Germany, sep 2012c.

Fotios Katsilieris, Paolo Braca, and Stefano Coraluppi. Detection of malicious AIS position spoofing by exploiting radar information. In *Proceedings of the 16th International Conference on Information Fusion*, pages 1196–1203, 2013.

Fotios Katsilieris, Hans Driessen, and Alexander Yarovoy. Radar resource management for improved situational awareness, 2014. URL http://homepage.tudelft.nl/k5w32/pubs/Katsilieris_radar14_v04.pdf. Accepted for publication to the International Radar Conference 2014, Lille, France.

Fotios Katsilieris, Hans Driessen, and Alexander Yarovoy. Threat-based sensor management for target tracking, 2015a. URL http://homepage.tudelft.nl/k5w32/pubs/Katsilieris_threat_based_SM_paper_v07.pdf. Under review for the IEEE Transactions on Aerospace and Electronic Systems.

Fotios Katsilieris, Hans Driessen, and Alexander Yarovoy. Adaptive radar beam-pointing for area surveillance, 2015b. To be submitted to the IEEE Transactions on Aerospace and Electronic Systems.

Steven Kay. *Fundamentals of Statistical Signal Processing, Volume II: Detection Theory*. Prentice Hall, 1998. ISBN 978-0135041352.

Wolfgang Koch. On adaptive parameter control for phased-array tracking. In *Proceedings of Signal and Data Processing of Small Targets*, 1999.

Wolfgang Koch. On exploiting 'negative' sensor evidence for target tracking and sensor data fusion. *Information Fusion*, 8(1):28–39, 2007.

Bernard O. Koopman. The Theory of Search. III. The Optimum Distribution of Searching Effort. *Operations Research*, 5(5):613–626, Oct. 1957. URL http://www.jstor.org/stable/167462.

K. Kowalska and L. Peel. Maritime anomaly detection using Gaussian process active learning. In *15th International Conference on Information Fusion*, pages 1164 –1171, july 2012.

Thomas M. Kratzke and John R. Frost. Search and rescue optimal planning system. In *Proceedings of the 13th International Conference on Information Fusion*, volume 1, pages 1–9, 2010.

Christopher Kreucher, Keith Kastella, and Alfred O. Hero III. *Signal processing*, volume 85/2005, chapter Sensor management using an active sensing approach, pages 607–624. Elsevier, 2005a.

Cristopher Kreucher, Keith Kastella, and Alfred O. Hero III. A comparison of task driven and information driven sensor management for target tracking. In *Proceedings of IEEE CDC*, pages 4004–4009, 2005b.

Vikram Krishnamurthy and Robert J. Evans. Hidden Markov model multiarm bandits: a methodology for beam scheduling in multitarget tracking. *IEEE Transactions on Signal Processing*, 49(12):2893 –2908, dec 2001. ISSN 1053-587X. doi: 10.1109/78.969499.

Matej Kristan, Aleš Leonardis, and Danijel Skočaj. Multivariate online kernel density estimation with Gaussian kernels. *Pattern Recogn.*, 44(10-11):2630–2642, oct 2011. ISSN 0031-3203. doi: 10.1016/j.patcog.2011.03.019. URL http://dx.doi.org/10.1016/j.patcog.2011.03.019.

R.O. Lane, D.A. Nevell, S.D. Hayward, and T.W. Beaney. Maritime anomaly detection and threat assessment. In *13th International Conference on Information Fusion*, pages 1 –8, july 2010.

X. Rong Li and Vesselin P. Jilkov. Survey of maneuvering target tracking. *IEEE Transactions on Aerospace and Electronics Systems*, 39:1333–1400, 2003.

James Llinas, Christopher Bowman, Galina Rogova, Alan Steinberg, Ed Waltz, and Frank White. Revisiting the JDL Data Fusion Model II. In *In P. Svensson and J. Schubert (Eds.), Proceedings of the 7th International Conference on Information Fusion*, pages 1218–1230, 2004.

Ronald Mahler. Objective functions for Bayesian control-theoretic sensor management, 1: multitarget first-moment approximation. In *Proceedings of the IEEE Aerospace Conference*, volume 4, pages 1905–1923, 2003. doi: 10.1109/AERO.2003.1235121.

Ronald Mahler. *Multitarget sensor management of dispersed mobile sensors*, chapter 12, pages 239–310. 2004. doi: 10.1142/9789812796592_0012. URL http://www.worldscientific.com/doi/abs/10.1142/9789812796592_0012.

Ronald P. S. Mahler. *Statistical Multisource-Multitarget Information Fusion*. Artech House, 2007. ISBN 978-1596930926.

Ronald P. S. Mahler and Tim R. Zajic. Probabilistic objective functions for sensor management. *Proc. SPIE*, 5429:233–244, 2004. doi: 10.1117/12.543530. URL http://dx.doi.org/10.1117/12.543530.

James Manyika and Hugh Durrant-Whyte. *Data Fusion and Sensor Management: A Decentralized Information-Theoretic Approach*. Prentice Hall PTR, 1995. ISBN 0133031322.

D.J. Matthiesen. Efficient beam scanning, energy allocation, and time allocation for search and detection. In *IEEE International Symposium on Phased Array Systems and Technology (ARRAY)*, pages 361 –368, oct. 2010.

Sergio Miranda, Chris Baker, Karl Woodbridge, and Hugh Griffiths. Knowledge-based resource management for multifunction radar. *IEEE Signal Processing Magazine*, pages 66–76, January 2006.

M. Nilsson, J. van Laere, T. Ziemke, and J. Edlund. Extracting rules from expert operators to support situation awareness in maritime surveillance. In *Information Fusion, 2008 11th International Conference on*, pages 1–8, June 2008.

Dimitri Papageorgiou and Maxim Raykin. A risk-based approach to sensor resource management. In PanosM. Pardalos, Robert Murphey, Don Grundel, and MichaelJ. Hirsch, editors, *Advances in Cooperative Control and Optimization*, volume 369 of *Lecture Notes in Control and Information Sciences*, pages 129–144. Springer Berlin Heidelberg, 2007. ISBN 978-3-540-74354-5. doi: 10.1007/978-3-540-74356-9_8. URL http://dx.doi.org/10.1007/978-3-540-74356-9_8.

K. B. Petersen and M. S. Pedersen. The matrix cookbook, nov 2012. URL http://www2.imm.dtu.dk/pubdb/p.php?3274. Version 20121115.

H. Vincent Poor. *An Introduction to Signal Detection and Estimation; 2nd edition*. Springer, 1994. ISBN 978-0387941738.

Mohammad Rezaeian and Ba-Ngu Vo. The entropy of random finite sets, 2000. URL www.researchgate.net/.

Branko Ristic and Ba-Ngu Vo. Sensor control for multi-object state-space estimation using random finite sets. *Automatica*, 46(11):1812 – 1818, 2010. ISSN 0005-1098. doi: http://dx.doi.org/10.1016/j.automatica.2010.06.045. URL http://www.sciencedirect.com/science/article/pii/S0005109810002955.

Branko Ristic, Sanjeev Arulampalam, and Neil Gordon. *Beyond the Kalman filter*. Artech House, 2004.

Branko Ristic, B. La Scala, M. Morelande, and N. Gordon. Statistical analysis of motion patterns in AIS data: Anomaly detection and motion prediction. In *Information Fusion, 2008 11th International Conference on*, pages 1 –7, 30 2008-july 3 2008.

M. Riveiro and G. Falkman. Supporting the analytical reasoning process in maritime anomaly detection: Evaluation and experimental design. In *Information Visualisation (IV), 2010 14th International Conference*, pages 170–178, July 2010. doi: 10.1109/IV.2010.34.

Harland Romberg. A game theoretic approach to search. *AIAA Guidance, Navigation, and Control Conference and Exhibit*, 1:1, 2000.

R.A. Romero and N.A. Goodman. Cognitive radar network: Cooperative adaptive beamsteering for integrated search-and-track application. *Aerospace and Electronic Systems, IEEE Transactions on*, 49(2):915–931, 2013. ISSN 0018-9251. doi: 10.1109/TAES.2013.6494389.

J.N. Roux and J.H. van Vuuren. Threat evaluation and weapon assignment decision support: A review of the state of the art. *ORiON*, 23(2):151–187, 2007. ISSN 2224-0004. URL http://orion.journals.ac.za/pub/article/view/54.

Jean Roy, Stephane Paradis, and Mohamad Allouche. Threat evaluation for impact assessment in situation analysis systems, 2002. URL http://dx.doi.org/10.1117/12.477618.

Dominic Schuhmacher, Ba-Tuong Vo, and Ba-Ngu Vo. A consistent metric for performance evaluation of multi-object filters. *Signal Processing, IEEE Transactions on*, 56 (8):3447–3457, 2008. ISSN 1053-587X. doi: 10.1109/TSP.2008.920469.

Merrill Ivan Skolnik. *Introduction to Radar Systems*. McGraw-Hill Science/Engineering/Math, 3 edition, 2002. ISBN 978-0072881387.

Alan N. Steinberg and Christopher L. Bowman. Rethinking the JDL data fusion levels. In *National Symposium on Sensor and Data Fusion (NSSDF)*, pages 1–6, June 2004.

L.D. Stone, C.M. Keller, T.M. Kratzke, and J.P. Strumpfer. Search analysis for the underwater wreckage of Air France Flight 447. In *Proceedings of the 14th International Conference on Information Fusion*, volume 1, pages 1–8, 2011.

I. Suzuki and M. Yamashita. Searching for a mobile intruder in a polygonal region. *SIAM Journal on Computing*, 21(5):863–888, 1992.

Teleplan Globe AS. MARIA Warship AIS Module, dec 2012. URL http://www.teleplanglobe.com/index.php/products/maria.

T. van Erven and P. Harremos. Rényi Divergence and Kullback-Leibler Divergence. *Information Theory, IEEE Transactions on*, 60(7):3797–3820, July 2014. ISSN 0018-9448. doi: 10.1109/TIT.2014.2320500.

G. van Keuk and S.S. Blackman. On phased-array radar tracking and parameter control. *IEEE Transactions on Aerospace and Electronic Systems*, 29(1):186 –194, jan 1993.

Ph. Vanheeghe, E. Duflos, P.E. Dumont, and V. Nimier. Sensor management with respect to danger level of targets. In *Proceedings of the 40th lEEE Conference on Decision and Control*, volume 1, pages 4439–4444, 2001.

Michele Vespe, Ingrid Visentini, Karna Bryan, and Paolo Braca. Unsupervised learning of maritime traffic patterns for anomaly detection. In *9th IET Data Fusion Target Tracking Conference (DF TT 2012): Algorithms Applications*, pages 1 –5, may 2012. doi: 10.1049/cp.2012.0414.

Ba-Ngu Vo and Wing-Kin Ma. The Gaussian mixture probability hypothesis density filter. *Signal Processing, IEEE Transactions on*, 54(11):4091–4104, Nov 2006. ISSN 1053-587X. doi: 10.1109/TSP.2006.881190.

Ba-Ngu Vo, Sumeetpal Singh, and Arnaud Doucet. Sequential Monte Carlo implementation of the PHD filter for multi-target tracking. In *Proceedings of the Sixth International Conference of Information Fusion*, volume 2, pages 792–799, 2003. doi: 10.1109/ICIF.2003.177320.

Ba-Tuong Vo, Ba-Ngu Vo, and Antonio Cantoni. Analytic implementations of the cardinalized probability hypothesis density filter. *Signal Processing, IEEE Transactions on*, 55(7):3553–3567, 2007. ISSN 1053-587X. doi: 10.1109/TSP.2007.894241.

Ba-Tuong Vo, Ba-Ngu Vo, and A. Cantoni. The cardinality balanced multi-target multi-Bernoulli filter and its implementations. *IEEE Transactions on Signal Processing*, 57 (2):409 –423, feb. 2009a. ISSN 1053-587X. doi: 10.1109/TSP.2008.2007924.

Ba-Tuong Vo, Ba-Ngu Vo, and Antonio Cantoni. The cardinality balanced multi-target multi-Bernoulli filter and its implementations. *Signal Processing, IEEE Transactions on*, 57(2):409–423, 2009b. ISSN 1053-587X. doi: 10.1109/TSP.2008.2007924.

Abraham Wald. Sequential tests of statistical hypotheses. *The Annals of Mathematical Statistics*, 16(2):117–186, June 1945. URL http://www.jstor.org/stable/2235829.

K. White, J. Williams, and P. Hoffensetz. Radar sensor management for detection and tracking. In *Proceedings of the 11th International Conference on Information Fusion*, pages 1–8, 2008.

Jason L. Williams. Search theory approaches to radar resource allocation. In *Proceedings of the 7th U.S./Australia Joint Workshop on Defense Applications of Signal Processing (DASP)*, 2011.

Johannes Wintenby and Vikram Krishnamurthy *IEEE Fellow*. Hierarchical resource management in adaptive airborne surveillance radars. In *IEEE Transactions on AES*, volume 42, pages 401–420, 2006.

Chun Yang, L. Kaplan, and Erik Blasch. Performance measures of covariance and information matrices in resource management for target state estimation. *IEEE Transactions on Aerospace and Electronic Systems*, 48(3):2594–2613, 2012. ISSN 0018-9251. doi: 10.1109/TAES.2012.6237611.

Jitse H. Zwaga, Yvo Boers, and Hans Driessen. On tracking performance constrained MFR parameter control. In *Proceedings of the 6th International Conference on Information Fusion*, volume 1, pages 712–718, 2003.

SUMMARY

Radars have gained increased popularity as sensing devices due to their unique capability to sense objects of interest at very long distances and without being severely limited by weather conditions. Advances in technology have led to the possibility of choosing the sensing parameters of a radar in order to further improve its performance. Especially in the class of active phased array radars, the control of the agile beam is of paramount importance. By controlling the radar beam improved estimation results can be achieved leading to better situation awareness.

In the literature, several approaches to sensor (including radar) management can be found. These can be roughly grouped into: *a*) rule-based or heuristics; *b*) task-based; *c*) information-driven; and *d*) risk/threat-based. These approaches are compared in this thesis and it is found that there is not a single approach that is both Bayes-optimal and takes into account explicitly the user requirements in different operational contexts.

In order to overcome the challenges with the existing approaches, this thesis proposes managing the uncertainty in higher-level quantities (as per the JDL model) that are directly of interest to the operator and directly related to the operational goal of the radar system. The proposed approach is motivated by the threat assessment process, which is an integral part of defence missions. Accordingly, a prominent example of a commonly used higher-level quantity is the threat-level of a target.

The key advantage of the proposed approach is that it results in Bayes-optimal sensor control that also takes into account the operational context in a model-based manner. In other words: *a*) a radar operator can select the aspects of threat that are relevant to the operational context at hand; and *b*) external information about the arrival of targets and other scenario parameters can be included when defining the models used in the signal processing algorithms, leading to context-adaptive sensor management.

The proposed approach is initially used in simple tracking examples in order to demonstrate its potential and flexibility. Subsequently, it is used for controlling an agile radar beam such that multiple targets can be tracked while taking into account detection uncertainty and presence of spurious measurements. In these examples, a state-of-the art signal processing algorithm is used, i.e. a CB-MeMBer filter. Finally, the proposed approach is used for area surveillance, i.e. for detection and tracking of multiple targets while taking into account detection uncertainty and presence of spurious measurements. In this context, a density that estimates where any undetected targets might be (denoted as unDTD) plays a key role in balancing the search-to-track time ratio.

The presented examples have been drawn both from the civilian and the military domain. From the civilian domain, air-traffic-control examples are shown where threat is modeled based on how fast and how close to each other two aircrafts might come. From the defence domain, asset protection examples are shown where threat is modeled based on how fast and how close to an asset of interest a target might come. Furthermore, the deviation from expected trajectories has been modeled because it can be of interest for anomaly detection purposes.

The proposed approach has outperformed all the other approaches in the simulated examples presented in this thesis in achieving lower uncertainty in the threat-level of all targets. In all examples, the proposed approach has outperformed naïve approaches, such as periodic or random selection of sensing actions, in *a*) estimating the correct number of targets present in the considered scenarios; *b*) localizing the detected targets; and *c*) maintaining less tracks, thus lowering the computation time at the update step. When only tracking of targets is considered, the proposed approach was only outperformed in tracking accuracy by a scheme that minimizes the expected variance of the estimated number of targets present in the considered scenario and by a derived rule-based scheme.

The main challenge when implementing the proposed approach is the mathematical description of threat. Several interesting aspects of threat have been modeled in this thesis but there are even more to be modeled. Taking into account non-measurable aspects of threat poses an added challenge. Other challenges that might be encountered are *a*) lower tracking accuracy; and *b*) higher computational complexity, when compared to other sensor management schemes.

The presented research can be extended both within the radar domain and by exploring its application to other domains. Two prominent extensions of interest within the radar domain are: *a*) taking more aspects of threat into account; and *b*) addressing the target classification problem. Robotics applications, such as autonomous robot path-planning, offer a promising alternative domain for applying the proposed method.

(NL) SAMENVATTING

De populariteit van radars als sensoren is mede ontstaan vanwege hun unieke vermogen om belangrijke objecten over zeer lange afstanden op te sporen zonder daarbij door weersomstandigheden ernstig te worden beperkt. De technologische vooruitgang heeft geleid tot een toegenomen keuzevrijheid in de parameters van een radar, hetgeen de prestaties verder kan verbeteren. Vooral in de klasse van *active phased array radars*, is de besturing van de *agile beam* van groot belang. Door de besturing van de radarbundel kunnen verbeterde schattingsresultaten behaald worden die tot een beter beeld van de actuele situatie (situational awareness) kunnen leiden.

In de literatuur zijn verschillende aanpakken van sensorbesturing (waaronder radar) gevonden. Deze kunnen grofweg worden onderverdeeld in: *a*) regel-gebaseerd of heuristieken; *b*) taak-gericht; *c*) informatie-gestuurd; en *d*) risico/bedreiging-gebaseerd. Deze aanpakken worden in dit proefschrift vergeleken en het blijkt dat er in de literatuur geen enkele methode wordt beschreven, die zowel Bayes-optimaal is en tevens expliciet rekening houdt met de behoeften van de gebruikers in de verschillende operationele contexten.

Om de problemen met de bestaande methodes te overwinnen, stelt dit proefschrift voor om de onzekerheid te beheersen in grootheden die gedefinieerd zijn op een hoger niveau (volgens het JDL model), en die direct van belang zijn voor de gebruiker en direct gerelateerd zijn aan het operationele doel van het radarsysteem. De voorgestelde aanpak is ingegeven door het dreigingsbeoordelingsproces (alternatief: het proces dat het dreigingsniveau beoordeelt) dat een integraal onderdeel van defensiemissies is. Het dreigingsniveau van een doel is een bekend voorbeeld van een veelgebruikte hogerniveau grootheid.

Het belangrijkste voordeel van de voorgestelde aanpak is dat het resulteert in een Bayes-optimale sensorbesturing die op een model-matige manier ook rekening houdt met de operationele context. Met andere woorden: *a*) een radaroperator kan de aspecten van bedreiging selecteren die bij de huidige operationele context relevant zijn; en *b*) externe informatie over de komst van de doelen en andere scenarioparameters kunnen worden opgenomen bij het definiëren van de modellen van de signaalverwerkingsalgoritmen, wat leidt tot context-adaptieve sensorbesturing.

Om het potentieel en de flexibiliteit aan te tonen wordt de voorgestelde aanpak in eerste instantie gebruikt in eenvoudige voorbeelden van het volgen van objecten. Vervolgens wordt de aanpak voor het besturen van een agile radarbundel gebruikt zodat meerdere doelen kunnen worden gevolgd, met inachtneming van de detectieonzekerheid en de aanwezigheid van valse metingen. In deze voorbeelden wordt een CB-MeMBer filter gebruikt, hetgeen een state-of-the-art signaalverwerkingsalgoritme is. Tenslotte is de voorgestelde aanpak voor gebiedsbewaking gebruikt, dat wil zeggen voor het detecteren en het volgen van meerdere doelen, met inachtneming van de detectieonzekerheid en de aanwezigheid van valse metingen. In deze context, speelt een kansdichtheidsschatting van onopgemerkte doelen (aangeduid als unDTD) een belangrijke

rol bij het (automatisch) instellen van de verhouding tussen de tijd die besteed wordt aan search en track.

De gepresenteerde voorbeelden zijn uit zowel het civiele als het militaire domein. Uit het civiele domein zijn luchtverkeerscontrolevoorbeelden getoond waar de dreiging is gemodelleerd op basis van hoe snel en hoe dicht twee vliegtuigen bij elkaar zouden kunnen komen. Uit het defensiedomein zijn voorbeelden van bezits-bescherming getoond waar de dreiging is gemodelleerd op basis van hoe snel en hoe dicht een doel bij een belangrijk bezit zou kunnen komen. Bovendien is de afwijking ten opzichte van verwachte trajectoriën gemodelleerd, omdat dit van belang kan zijn voor anomaliedetectie-doeleinden.

De voorgestelde aanpak heeft beter gepresteerd dan alle andere benaderingen in de gesimuleerde voorbeelden in dit proefschrift in het bereiken van lagere onzekerheid in het dreigingsniveau van alle doelen. De voorgestelde aanpak heeft naïeve benaderingen, zoals periodieke of willekeurige selectie van sensing acties, in alle voorbeelden overtroffen in *a*) het schatten van het juiste aantal doelen in de beschouwde scenario's; *b*) het lokaliseren van de gedetecteerde doelen; en *c*) het handhaven van minder tracks, met als gevolg het verlagen van de rekentijd bij de update-stap. Wanneer alleen het volgen van de doelen wordt beschouwd, is de voorgestelde aanpak alleen in volgnauwkeurigheid overtroffen door een regeling die de verwachte variantie minimaliseert van het geschatte aantal doelen dat aanwezig is in het beschouwde scenario en door een afgeleide regel-gebaseerd systeem.

De belangrijkste uitdaging bij de uitvoering van de voorgestelde aanpak is de wiskundige beschrijving van het dreigingsniveau. Verschillende interessante aspecten van het dreigingsniveau zijn in dit proefschrift gemodelleerd, maar nog meer zouden moeten worden gemodelleerd. Rekening houden met de niet-meetbare aspecten van het dreigingsniveau vormt een extra uitdaging. Andere uitdagingen die zouden kunnen optreden in vergelijking met andere sensorbesturing aanpakken, zijn: *a*) lagere trackingsnauwkeurigheid; en *b*) hogere rekenkundigecomplexiteit.

Het gepresenteerde onderzoek kan worden voortgezet verlengd zowel binnen het radar domein en door het verkennen van toepassing op andere domeinen. Twee prominente uitbreidingen die van belang zijn binnen het radar domein zijn: *a*) het houden rekening met meer aspecten van het dreigingsniveau; en *b*) de classificatie van doelen. Robotica toepassingen zoals autonome robot path-planning, bieden een veelbelovend alternatief domein voor toepassing van de voorgestelde aanpak.

(GR) ΠΕΡΙΛΗΨΗ

Τα ραντάρ έχουν αποκτήσει αυξημένη δημοτικότητα ως συσκευές ανίχνευσης λόγω της μοναδικής ικανότητάς τους να ανιχνεύουν αντικείμενα ενδιαφέροντος σε πολύ μεγάλες αποστάσεις και χωρίς να περιορίζονται σημαντικά από τις καιρικές συνθήκες. Η τεχνολογική πρόοδος έχει δημιουργήσει την δυνατότητα να ελέγχονται οι παράμετροι ενός ραντάρ με σκοπό την περαιτέρω βελτίωση των επιδόσεων του. Ειδικά στην κατηγορία των ραντάρ ενεργής ηλεκτρονικής σάρωσης, ο έλεγχος της ευέλικτης ακτίνας τους είναι υψίστης σημασίας. Βελτιωμένα αποτελέσματα εκτίμησης μπορούν να επιτευχθούν ελέγχοντας την ακτίνας ενός ραντάρ, το οποίο οδηγεί σε καλύτερη επίγνωση της επικρατούσας κατάστασης.

Στη βιβλιογραφία μπορούν να βρεθούν διάφορες προσεγγίσεις για την διαχείριση αισθητήρων (συμπεριλαμβανομένων των ραντάρ). Αυτές μπορούν να ομαδοποιηθούν χονδρικά ως εξής: α′) ομάδες κανόνων, β′) βελτιστοποίηση παραμέτρων σχετικών με το έργο του αισθητήρα, γ′) διαχείριση αβεβαιότητας στο πλαίσιο της θεωρίας πληροφορίας, και δ′) σύμφωνα με τους κίνδυνους/απειλές. Οι προσεγγίσεις αυτές συγκρίνονται σε αυτή τη διατριβή και διαπιστώνεται ότι δεν υπάρχει μία ενιαία προσέγγιση που να είναι τόσο Bayes-βέλτιστη όσο και να λαμβάνει ρητά υπόψη τις απαιτήσεις των χρηστών σε διάφορα επιχειρησιακά περιβάλλοντα.

Προκειμένου να ξεπεραστούν οι προκλήσεις με τις υπάρχουσες προσεγγίσεις, σε αυτή τη διατριβή προτείνεται η διαχείριση της αβεβαιότητας σε ποσότητες υψηλότερου επιπέδου (κατά το μοντέλο JDL) που είναι άμεσα ενδιαφέρουσες για τον χειριστή και σχετίζονται άμεσα με τον επιχειρησιακό στόχο του ραντάρ. Η προτεινόμενη προσέγγιση είναι εμπνευσμένη από τη διαδικασία εκτίμησης-αξιολόγησης απειλών, η οποία αποτελεί αναπόσπαστο μέρος των αποστολών άμυνας. Κατά συνέπεια, ένα προεξέχον παράδειγμα χρησιμοποιούμενης ποσότητα υψηλότερου επιπέδου είναι το επίπεδο απειλής ενός στόχου.

Το βασικό πλεονέκτημα της προτεινόμενης προσέγγισης είναι ότι οδηγεί σε Bayes-βέλτιστο έλεγχο του αισθητήρα και λαμβάνει επίσης υπόψη το επιχειρησιακό πλαίσιο λειτουργίας με ένα πλήρως μοντελοποιημένο τρόπο. Με άλλα λόγια: α′) ένας χειριστής ραντάρ μπορεί να επιλέξει τις πτυχές της απειλής που είναι σχετικές με το επιχειρησιακό πλαίσιο και β′) εξωτερικές πληροφορίες σχετικά με την άφιξη στόχων και άλλων παραμέτρων σεναρίου μπορούν να συμπεριληφθούν κατά τον καθορισμό των μοντέλων που χρησιμοποιούνται στους αλγορίθμους επεξεργασίας σήματος, το οποίο οδηγεί σε διαχείριση αισθητήρα που είναι προσαρμοστική ως προς το επιχειρησιακό πλαίσιο.

Η προτεινόμενη προσέγγιση χρησιμοποιείται αρχικά σε απλά παραδείγματα εντοπισμού στόχων, προκειμένου να αποδειχθούν οι δυνατότητες και η ευελιξία της. Στη συνέχεια χρησιμοποιείται για τον έλεγχο μιας ευκίνητης ακτίνας ραντάρ, έτσι ώστε να παρακολουθούνται πολλαπλοί στόχοι, λαμβάνοντας παράλληλα υπόψη την αβεβαιότητα ανίχνευσης και την παρουσία παρασιτικών μετρήσεων. Σε αυτά τα παραδείγματα, χρησιμοποιείται ένας αλγόριθμος επεξεργασίας σήματος τελευταίας τεχνολογίας, δηλαδή

ένα φίλτρο CB-MeMBer. Τέλος, η προτεινόμενη προσέγγιση χρησιμοποιείται για επιτήρηση περιοχής, δηλαδή για την ανίχνευση και παρακολούθηση πολλαπλών στόχων, λαμβάνοντας υπόψη την αβεβαιότητα ανίχνευσης και την παρουσία παρασιτικών μετρήσεων. Σε αυτό το πλαίσιο, μια συνάρτηση πυκνότητας πιθανότητας, που υπολογίζει που θα μπορούσαν να βρεθούν απαρατήρητοι στόχοι (συμβολίζεται ως unDTD), διαδραματίζει καίριο ρόλο στην εξισορρόπηση της αναλογίας του χρόνου αναζήτησης προς χρόνου παρακολούθησης.

Παραδείγματα παρουσιάζονται τόσο από τον πολιτικό όσο και από τον στρατιωτικό τομέα. Από τον πολιτικό τομέα παρουσιάζονται παραδείγματα ελέγχου εναέριας κυκλοφορίας όπου η απειλή εξαρτάται από το πόσο γρήγορα και πόσο κοντά μπορούν να βρεθούν δύο αεροσκάφη. Από τον τομέα της άμυνας παρουσιάζονται παραδείγματα προστασίας μονάδων όπου η απειλή διαμορφώνεται με βάση το πόσο γρήγορα και πόσο κοντά σε μία μονάδα μπορεί να πλησιάσει ένας στόχος. Επιπλέον, η απόκλιση από μια αναμενόμενη πορεία έχει μοντελοποιηθεί επειδή μπορεί να παρουσιάζει ενδιαφέρον για σκοπούς ανίχνευσης ανώμαλης συμπεριφοράς.

Η προτεινόμενη προσέγγιση έχει καλύτερες επιδόσεις από όλες τις άλλες προσεγγίσεις στα προσομοιωμένα παραδείγματα που παρουσιάζονται σε αυτή τη διατριβή σε σχέση με την επίτευξη χαμηλότερης αβεβαιότητας στο επίπεδο απειλής όλων των στόχων. Σε όλα τα παραδείγματα, η προτεινόμενη προσέγγιση έχει καλύτερες επιδόσεις από απλοϊκές μεθόδους, όπως περιοδική ή τυχαία επιλογή παραμέτρων μετρήσεως, α′) στην εκτίμηση του σωστού αριθμού στόχων που υπάρχουν στα εξεταζόμενα σενάρια, β′) στον εντοπισμό των στόχων που έχουν ανιχνευτεί και γ′) στη διατήρηση λιγότερων τροχιών στόχων, μειώνοντας έτσι τον χρόνο υπολογισμού του βήματος ενημέρωσης. Όσον αφορά την παρακολούθηση στόχων, οι μόνες μέθοδοι που παρέχουν μεγαλύτερη ακρίβεια παρακολούθησης είναι μία μέθοδος που ελαχιστοποιεί τη αναμενόμενη διακύμανση του εκτιμόμενου αριθμού στόχων οι οποίοι είναι παρώντες σε ένα σενάριο και μία μέθοδος που βασίζεται σε κανόνες.

Η κύρια πρόκληση κατά την υλοποίηση της προτεινόμενης προσέγγισης είναι η μαθηματική περιγραφή της απειλής. Σε αυτή τη διατριβή έχουν μοντελοποιηθεί αρκετές ενδιαφέρουσες πτυχές της απειλής αλλά υπάρχουν ακόμα περισσότερες προς μοντελοποίηση. Το πως να ληφθούν υπόψη μη μετρήσιμα στοιχεία της απειλής αποτελεί μια πρόσθετη πρόκληση. Άλλες προκλήσεις που μπορεί να προκύψουν είναι: α′) η μικρότερη ακρίβεια εντοπισμού, και β′) η υψηλότερη υπολογιστική πολυπλοκότητα, όταν συγκρίνεται με άλλους αλγόριθμους διαχείρισης αισθητήρων.

Η παρουσιαζόμενη έρευνα μπορεί να επεκταθεί τόσο μέσα στον τομέα των ραντάρ όσο και εξερευνώντας την εφαρμογή της σε άλλους τομείς. Δύο εξέχουσες επεκτάσεις στον τομέα των ραντάρ είναι οι εξής: α′) πως να ληφθούν υπόψη περισσότερες πτυχές της απειλής, και β′) η αντιμετώπιση του προβλήματος της ταξινόμησης στόχων. Ρομποτικές εφαρμογές, όπως ο σχεδιασμός διαδρομών για αυτόνομα ρομπότ, προσφέρουν έναν πολλά υποσχόμενο εναλλακτικό τομέα για την εφαρμογή της προτεινόμενης μεθόδου.

CURRICULUM VITÆ

Fotios KATSILIERIS

Born in Amarousio, Attica, Greece on 28-12-1983.
E-mail: Fotios.Katsilieris@gmail.com

EDUCATION

1998–2001	4o Enieo Likio (4th High school) Neas Ionias, Nea Ionia, Attica, Greece
2001–2006	Diploma in Electrical and Computer Engineering, University of Patras, Patras, Greece
2007–2009	MSc in Systems, Control and Robotics, Royal Institute of Technology (KTH), Stockholm, Sweden *MSc Thesis:* Search and Secure Using Mobile Robots. *Supervisor:* Prof. dr. K. H. Johansson
2011–2013	PhD candidate, University of Twente, Enschede, the Netherlands
2013–2015	PhD. Electrical Engineering, Mathematics and Computer Science Delft University of Technology, Delft, the Netherlands *Thesis:* Sensor management for surveillance and tracking: An operational perspective. *Promotor:* Prof. DSc. A. Yarovoy *Co-promotor:* dr. J. N. Driessen

EMPLOYMENT

2007–2007	Sales Engineer, IL.VIO.KAT., Athens, Greece
2009–2009	Research Engineer, Royal Institute of Technology (KTH), Stockholm, Sweden
2010–2013	Marie Curie Early Stage Researcher, Thales Nederland B.V., Hengelo, the Netherlands Research visits to Fraunhofer FKIE and NATO-STO CMRE.

List of Publications

8. **Fotios Katsilieris, Hans Driessen, and Alexander Yarovoy**, *Adaptive radar beam-pointing for area surveillance*, to be submitted to the IEEE Transactions on Aerospace and Electronic Systems.

7. **Fotios Katsilieris, Hans Driessen, and Alexander Yarovoy**, *Threat-based sensor management for target tracking*, Submitted to the IEEE Transactions on Aerospace and Electronic Systems.

6. **Fotios Katsilieris, Hans Driessen, and Alexander Yarovoy**, *Radar resource management for improved situational awareness*, Accepted for publication to the International Radar Conference, Lille, France, 2014.

5. **Fotios Katsilieris, Paolo Braca, and Stefano Coraluppi**, *Detection of malicious AIS position spoofing by exploiting radar information*, In Proceedings of the 16th International Conference on Information Fusion, pages 1–7, 2013.

4. **Fotios Katsilieris, Alexander Charlish, and Yvo Boers**, *Towards an online, adaptive algorithm for radar surveillance control*, In Future Security - Security Research Conference 2012: Sensor Data Fusion Workshop, Bonn, Germany, 2012.

3. **Fotios Katsilieris, Yvo Boers, and Hans Driessen**, *Optimal search: a practical interpretation of information-driven sensor management*, In Proceedings of the 15th International Conference on Information Fusion, pages 439–446, 2012.

2. **Fotios Katsilieris, Yvo Boers, and Hans Driessen**, *Sensor management for PRF selection in the track-before-detect context*, In Proceedings of the IEEE Radar Conference, pages 360–365, 2012.

1. **Fotios Katsilieris, Magnus Lindhe, Dimos V. Dimarogonas, Petter Ögren, and Karl Henrik Johansson**, *Demonstration of multi-robot search and secure*, IEEE International Conference on Robotics and Automation (ICRA2010) Workshop: Search and Pursuit/Evasion in the Physical World: Efficiency, Scalability, and Guarantees, 2010.